# Experimental and Theoretical Evaluation of Progressive Collapse Capacity of Reinforced Concrete Framed Structures

## KAMAL DARWEESH IBRAHIM ALOGLA

School of Computing, Science and Engineering

College of science and Technology

University of Salford, Salford, UK

Submitted in Partial Fulfilment of the Requirements of the Degree of

Doctor of Philosophy, March 2017

## *Table of Contents*

## *List of Figures*

# *List of Tables*

## *Acknowledgement*

# *Declaration*

I declare that this thesis has been composed solely by myself and that it has not been submitted, in whole or in part, in any previous application for a degree. Except where states otherwise by reference or acknowledgment, the work presented is entirely my own.

The data presented in this thesis was obtained in an experiment carried out by myself. Data analysis and interpretation are entirely by own work.

KAMAL ALOGLA

Parts of this work have been published as follows:

## *List of Publications*

1- Alogla, K., L. Weekes, and L. Augusthus-Nelson, *A new mitigation scheme to resist progressive collapse of RC structures.* Construction and Building Materials, 2016. **125**: p. 533-545.

2- Alogla, K., Weekes, L. & Augusthus Nelson, L. 2017. *Theoretical assessment of progressive collapse capacity of reinforced concrete structures*. Magazine of Concrete Research, 69 (3)**,** 145-162.

3- Alogla, K., L. Weekes, and L. Augusthus-Nelson, *Progressive collapse resisting mechanisms of reinforced concrete structures.* Proceedings of the 5th International Conference on Integrity, Reliability and Failure. , 2016: p. 479-480.

4- Alogla, K., L. Weekes, and L. Augusthus-Nelson, *Progressive collapse resisting mechanisms of reinforced concrete structures.* First International Conference for Students on Applied Engineering 2016 (ICSAE_2016).

5- Alogla, K. and L. Weekes,  *Numerical analysis of reinforced concrete structures in the event of progressive collapse*. CSE 2017 Annual PGR Symposium ( CSE-PGSym 17).

6- Alogla, K. and L. Weekes,  *Modified Steel Reinforcement to Mitigate Progressive Collapse in RC Structures*. Salford Postgraduate Annual Research Conference (SPARC 2017).

## *List of Abbreviation*

| | |
|---|---|
| ACI | American Concrete Institute |
| AD | Approved Document |
| AEM | Applied Element Method |
| APM | Alternate Path Method |
| ASCE | American Society of Civil Engineers |
| ASTM | American Standard for Testing Material |
| BRR | Bottom Reinforcement Ration |
| BS | British Standard |
| BSI | British Standards Institution |
| CAA | Compressive Arch Action |
| CEB | Comité Euro-International du Béton (Euro-International Concrete Committee) |
| CFRP | Carbon Fibre Reinforced Polymer |
| CMA | Compressive Membrane Action |
| CRS | Column Removal Scenario |
| CTA | Catenary Action |
| DCR | Demand Capacity Ratios |
| DIF | Dynamic Increase Factor |
| D.L. | Dead Load |
| DLAF | Dynamic Load Amplification Factor |
| DoD | Department of Defence |
| EC2 | European Code 2 |
| ELS | Extreme Loading for Structures. |
| FE | Finite Element |
| FIP | Fédération Int. de la Précontrainte (International Federation of Pre-stressing) |
| GSA | General service Administration. |
| IMF | Intermediate Moment Frame |
| LDVT | Linear Differential Variable Transformers |

| | |
|---|---|
| L.L. | Live Load |
| LSP | Linear Static Procedure |
| MJD | Middle joint Displacement |
| NDP | Nonlinear Dynamic Procedure |
| NIST | National Institute of Standards and Technology |
| NSP | Nonlinear Static Procedure |
| RC | Reinforced Concrete |
| SDOF | Single Degree of Freedom |
| SLR | Specific Local Resistance Method |
| SMF | Special Moment Frame |
| TF | Tie Force |
| TMA | Tensile Membrane Action |
| TRR | Top Reinforcement Ratio |
| UFC | Unified Facilities Criteria |
| UKAS | United Kingdom Accreditation Service |

# *List of Notations*

| | |
|---|---|
| $a_1$ | The arching depth. |
| $A_s$ , $A'_s$ | Area of tensile and compression reinforcement, respectively. |
| $A_s^{bottom}$ , $A_s^{top}$ | Area of reinforcement at bottom and top of the beam section, respectively |
| $b$ | Width of a beam. |
| $\beta$ | Ratio of the depth of the equivalent rectangular stress block to the neutral axis depth. |
| $c'$ , $c$ | The compression depth zone at section 1 and 2, respectively. |
| $c_m$ , $c_e$ | Neutral axis depth at the middle joint interface and at the beam end, respectively. |
| $C_{cm}$ , $C_{ce}$ | Concrete compressive force acting at the beam end and the middle joint interface, respectively. |
| $C_{se}$ , $C_{sm}$ | Steel compressive force acting at the beam end and the middle joint interface, respectively. |
| $d$ | Effective depth of a beam section. |
| $d_i$ | Effective depth of a beam section at each step of $\delta_i$. |
| $d_m$ | Modified effective depth of a beam section. |
| $d_b$ | Diameter of a reinforcing bar. |
| $d'$ | Distance from the extreme compression fibre of concrete to the centroid of compression reinforcement. |
| $E_c$ | Elastic modulus of concrete. |
| $E_s$ | Elastic modulus of steel reinforcement. |
| $E_h$ | Hardening modulus of reinforcement. |
| $F_t$ | Load for the calculation of the tie force. |
| $f_0$ | Bar stress at the joint centre acting as a boundary. |
| $f'_c$ | Concrete compressive cylinder strength. |
| $f_s$ | Steel reinforcement stress. |
| $f_y$ , $f_u$ | Yield strength and ultimate tensile strength of reinforcement. |
| $g_k$ | Dead load. |

| | |
|---|---|
| $G$ | Shear modulus. |
| $h$ | Depth of a beam section. |
| $K$ | Stiffness of axial restraints. |
| $L$ | Net span length of a one-bay beam. |
| $L_c$ | Combined total load. |
| $L_j$ | Joint width. |
| $L_s$ | Floor to ceiling height. |
| $l_e$ , $l_m$ | Crack width at the beam end and middle joint interfaces, respectively. |
| $l_{fs}$ | Propagation length of the bar stress. |
| $l_p$ | Plastic hinge length. |
| $l_y$ | Length of plastic steel reinforcement. |
| $M_e$ , $M_m$ | Bending moments acting on the beam end and on the joint interface, respectively. |
| $n_0$ | Number of storeys in a building. |
| $N_e$ , $N_m$ | Axial force at the end and middle of the beam section, respectively |
| $P$ | Progressive collapse resistance of sub-assemblages (or applied load). |
| $P_{com}$ , $P_{cat}$ | Applied load at CAA and catenary action, respectively. |
| $P_f$ | Calculated flexural capacity based on plastic hinge mechanism. |
| $Q$ | The imposed load. |
| $S$ | Snow load. |
| $T'$ , $T$ | The steel tensile forces at section 1 and 2, respectively. |
| $u$ | The axial movement of the lateral restraints. |
| $V$ | Shear force at a middle joint interface. |
| $V_m$, $V_e$ | Shear force at a middle joint interface and beam end respectively. |
| $w_f$ | Total floor load. |
| $W$ | Wind load. |
| $z$ | The distance from the point of maximum moment to the point of zero moment. |

$\delta$                Beam deflection or displacement at the middle joint.

$\delta_D$             The deflection at which the onset of catenary action.

$\delta_{FT}$ , $\delta_{FB}$       The deflections at which top and bottom fracture, respectively.

$\Delta L$             Axial extension of the beam.

$\varepsilon_{cu}$             Ultimate compressive strain of concrete.

$\varepsilon'_s$             Strain of compression reinforcement.

$\varepsilon_{se}, \varepsilon_{sm}$       Strain of tension reinforcement at the beam end and at the middle joint, respectively.

$\varepsilon_y$             Yield strain of steel reinforcement.

$\varepsilon_u$             Ultimate tensile strain of steel.

$\theta$               Rotation of the beam section.

$\theta_i$              Rotation of the beam section at each value of $\delta_i$.

$\tau_E$             Average elastic bond strength for a bar in tension.

$\tau_Y$             Average inelastic bond strength for a bar in tension.

$\varphi$              The angle of the tensile action line at catenary action correspond the second bar fracture.

# *Abstract*

Progressive collapse is a situation when local failure is followed by collapse of adjoining members, which in turn causes global collapse, threatening life. Local failure of a vertical load carrying member, can be caused by abnormal loading such as explosion, bombing, sudden vehicle impact and design errors.

The design of structures against progressive collapse has not been an integral part of structural design. It is difficult to predict the structural behaviour of building members during progressive collapse because of the dynamic nature of the event and the limited experimental tests conducted to understand the nature of progressive collapse. An experimental program comprising eight reinforced concrete (RC) beam-column sub-assemblages is presented to investigate the structural behaviour and progressive collapse resistance of RC frame members subjected to column removal scenario (CRS). The specimens were tested under quasi-static loading.

Mitigation of progressive collapse has become a primary concern of engineers in recent years. A new mitigation scheme is proposed in this study to increase the resistance of RC beams against progressive collapse using modified detailing of reinforcement. The effect of the proposed scheme on the structural behaviour of sub-assemblages is investigated through testing some of the specimens with modified detailing. The test results showed that the proposed scheme was able and efficient to increase progressive collapse capacity.

A finite element (FE) model was developed using the software package ANSYS in order to numerically simulate the structural behaviour of RC beam-column sub-assemblages under CRS. A macro-model based approach was used in the analysis using beam elements and a series of non-linear springs to capture the real behaviour of structural members associated with the redistribution of loads under CRS. Numerical results were compared with those obtained from the experimental program, and showed a good agreement.

An analytical model was developed to predict the structural behaviour of RC structures under CRS. The development of the model equations was based on the concepts of equilibrium, compatibility, and material properties. Steel bar fracture and the reduction in the effective beam depth due to concrete crushing were included in the model. The model was validated by comparing the results with the experimental results. The comparison shows that the model was able to capture the structural behaviour of RC beams under CRS. A parametric study was conducted to investigate the effect of different factors on the progressive collapse capacity.

## 1. CHAPTER ONE    INTRODUCTION

## 1.1 GENERAL

Concrete frame structures are very common, perhaps one of the most common type of construction for modern buildings. As the name suggests, this type of building is formed of a frame, or skeleton of concrete, usually reinforced with steel rebar. Horizontal members of this frame are called beams, and vertical members are called columns.

Columns are the most important members, as they are the primary load-carrying element of the building. The damage of a beam in a building usually affects only one floor, but damage to a column could collapse the entire building.

Nowadays, concrete is widely used in high-rise buildings. A major advantage of concrete construction for high-rise buildings is the material's inherent properties of strength and mass heaviness, which creates lateral stiffness, or resistance to horizontal movement. Occupants of concrete towers are less able to perceive building motion than occupants of comparable tall buildings with non-concrete structural systems such as steel. As a result, concrete has become the material of choice for many tall, slim towers (Buildings & Structures, 2014).

In the conventional design of RC structures, the designer usually takes into account the dead loads of the structure, live loads, and the characteristics of the location of the structure, seismic, and climate-related loads such as wind and snow loads.  While the majority of structures experience the conventional type of loads during their lifetimes, some of them could be subjected to abnormal loadings which they were not explicitly designed for.

Characteristically, abnormal loads usually act over a relatively short period of time in comparison with ordinary design loads. Abnormal loading conditions, such as blast, gas explosions, vehicle impact, support failure, in addition, design and construction errors are all possible actions. All these loads and inertial effects due to rate of loading become important which may cause the loss of one or more load bearing elements which could trigger progressive collapse.

## 1.2 PROGRESSIVE COLLAPSE BACKGROUND

## 1.2.1 DEFINITIONS AND CAUSES

Progressive collapse of building structures is initiated when one or more vertical load carrying members, such as columns or walls, are removed. Once a column or a wall is removed due to abnormal loading, the building's weight (gravity load) transfers to adjacent columns or walls in the structure. If these columns or walls are not adequate to resist and redistribute the additional gravity load, that part of the structure collapses. The vertical load carrying elements of the structure continue to collapse until the additional loading is stabilized. As a result, a large part of the structure may collapse, causing greater damage to the structure than the initial impact.

Progressive collapse can be defined as the collapse of all or a large part of a structure caused by the failure or damage of a relatively small part of the structure. There are many definitions provided by some guidelines such as General Services Administration GSA (2003) and American Society of Civil Engineers (ASCE, 2005).

The definition provided by General Services Administration is "Progressive collapse is a situation where local failure of a primary structural component leads to the collapse of adjoining members which, in turn, leads to additional collapse.", while the definition of (ASCE, 2005) is "The spread of local damage, from an initiating event, from element to element resulting, eventually, in the collapse of an entire structure or a disproportionately large part of it". From an analytical point of view, progressive collapse occurs when a structure has its load pattern or boundary conditions changed so that other structural elements are loaded beyond their capacity and consequently fail (Krauthammer et al., 2002).

(Abedi and Parke, 1996) Defined progressive collapse in braced domes as the widespread propagation of local instability, initiated by member or node instability, to a portion of a structure.

(Allen, 1972) defined progressive collapse as a situation where the local failure of a primary structural component(s) leads to the collapse of adjoining members, which in turn leads to additional collapse. Thus, the extent of collapse is disproportionate to the original cause. In other words, progressive collapse is a chain reaction of failures following damage to a relatively small portion of a structure.

## 1.2.2 EXAMPLES

Some of the more famous examples of progressive collapse phenomena include the collapse of the World Trade Centre (2001) towers due to terrorist attack, the bombing of the Murrah Federal Building (1995) in Oklahoma City, and the collapse of the Ronan Point (1968) building due to a gas explosion. The following gives examples pertaining to reinforced concrete (precast or cast-in-place) structures:

## 1.2.2.1 RONAN POINT

The earliest and most famous examples of progressive collapse are the collapse of the Ronan Point apartment building in 1968 in the U.K., Figure 1-1. An accidental explosion caused by a gas leak blew out one of the precast wall panels on the 18th floor triggering the collapse of the upper floors.

This failure was followed by the lower ones due to the additional dead load of the fallen upper floors, thus the impact loading on the 18th floor initiated a second phase of collapse, failure of the 18th floor and progressing in the lower floors until it reached the ground. While the initial damage due to the gas explosion was only on the 18th floor, at the end, the entire corner of the building collapsed.

Four people were killed in the incident, and seventeen were injured. Figure 1-1 shows the final state of the Ronan Point apartment building after the collapse.

The building was a precast concrete wall and floor system with the floors being supported directly by the walls. However, the connections between the walls and floors did not provide any alternate load path for load redistribution leading to the progressive collapse of the structure (NIST, 2007)

Figure 1-1 Ronan Point collapse (Nair, 2004)

## 1.2.2.2 MURRAH BUILDING

Another progressive collapse tragedy is the collapse of the Alfred P. Murrah federal office building in Oklahoma City on April 19, 1995, which was damaged by a bomb, Figure 1-2. The collapse of Murrah federal office building was initiated from the loss of support from first-floor columns leading to the catastrophic failure of a transfer girder between G16 and G24 as shown in Figure 1-3. 168 people were killed in the incident, and more than 500 were injured (Corley et al., 1998).

The Alfred P. Murrah building was a nine-storey reinforced concrete moment frame structure with shear walls, Figure 1-2(a). Different from the upper floors, there was a transfer girder at the third floor level in the north side of the building. Due to the blast, three exterior columns that supported the transfer girder on the third floor were destroyed.

With the loss of these columns, the transfer girder at the third floor collapsed causing the progressive collapse of the upper storeys. Corley et al. pointed out that most of the devastation was due to progressive collapse rather than direct effects of the explosion. Ninety percent of the 168 people who died in the Murrah building were killed by falling debris; therefore, limiting the collapse of the structure could have saved those lives (Corley et.al., 1998).

Murrah Building before collapse          Murrah Building after collapse

(FEMA(277), 1996)                     (Encyclopaedia Britannica, 2012)

Figure 1-2 Murrah Building before and after collapse
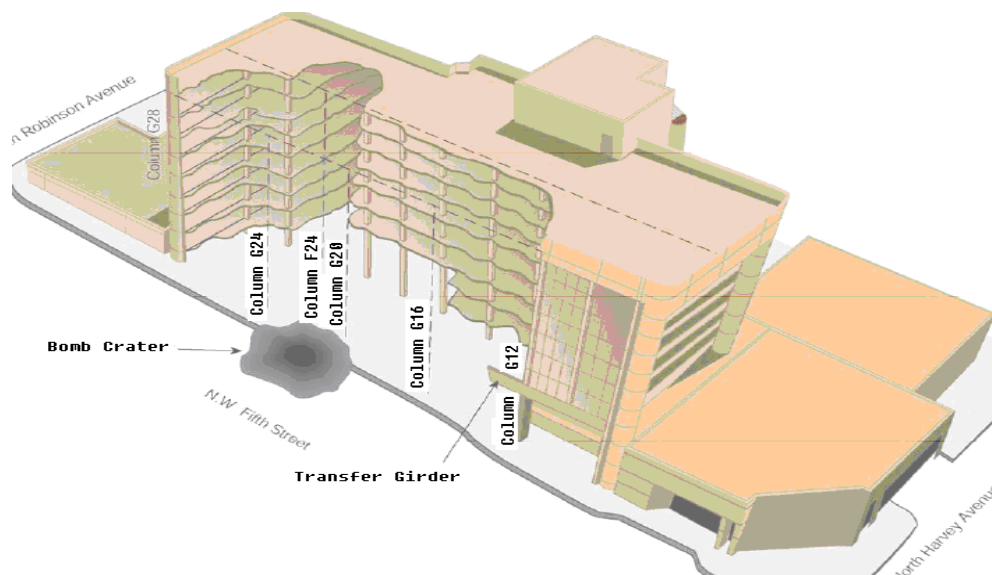


Figure 1-3 Murrah Building Sketch after collapse (Corley et.al., 1998)

The above mentioned extreme events brought the problem of progressive collapse to the attention of the international structural community. In the UK, after partial collapse of Ronan Point, which is a landmark of progressive collapses in recent history that triggered code changes, the government's report revealed a number of deficiencies in the building regulations as there was no Code of Practice relating specifically to large concrete panel construction, and there was no Regulation or Code that took into account the possibility of progressive collapse. Thus the need for progressive collapse requirements to be included in standards and regulations has become very important.

The Workshop on Progressive collapse of Building Structures (Breen, 1975) concluded that if the Ronan Point had been designed in accordance with CEB - FIP Bulletin No. 60 (1967) "Recommendations for the Design and Construction of Large-panel Structures", the disproportionate collapse might have not occurred. The workshop proposed "The absolute necessity of effectively joining the various components of the structure together in order to obviate any possible tendency for it to behave like a house of cards".

## 1.3 STANDARDS, CODES AND GUIDELINES

To mitigate progressive collapse, efforts are directed at both code provisions and research work. Since the Ronan Point collapse event, design considerations to improve the integrity, robustness, and ability of structures to resist progressive collapse have been incorporated into building codes. After the Alfred P. Murrah federal building event, more specific structural analysis has been required for buildings with a certain level of protection in design guidelines. In this section, progressive collapse requirements in codes and guidelines will be presented.

Before presenting the codes and guidelines requirements, it is useful to look at the main approaches to mitigate progressive collapse utilized by current codes, standards and guidelines. These approaches can be classified into two main categories, direct design approach and indirect design approach. Each of these approaches is described as follows:

## 1.3.1 INDIRECT DESIGN APPROACH

The indirect design approach attempts to mitigate progressive collapse through the provision of minimum levels of strength, continuity, redundancy and ductility; it relies on an integrated system of tie forces so that a structure has an inherent resistance to progressive collapse. The examples of this approach are to improve joint connections by special detailing, to improve redundancy, and to provide more ductility to a structure. However, additional structural analysis beyond those considered in typical building design is not required.

The indirect design approach is generally integrated into most building codes and standards since it can create a redundant structure that will perform under any conditions and improve overall structural response. For example, the UK design code (BSI, BS5950-1 2000) gives the requirement under section 2.4.5 of structural integrity that "All buildings should be effectively tied together at each principal floor level, and a specific factored tensile force should be resisted by all horizontal members".

## 1.3.2 DIRECT DESIGN APPROACH

In contrast to the measures pertaining to the indirect design approach, which is characterised by an absence of detailed procedures, the direct design approach explicitly considers the resistance of a structure to progressive collapse during the design process. Additional structural analysis must be performed for loading conditions not considered in typical building design including cases where bearing members are removed from the structural model, and designing important bearing members (key elements) to resist extra abnormal loading conditions.

There are two direct design methods: the specific local resistance method and the alternate load path method. The specific local resistance method seeks to provide strength to be able to resist progressive collapse. The alternate load path method seeks to provide alternative load paths to absorb localized damage and resist progressive collapse.

## 1.3.2.1 SPECIFIC LOCAL RESISTANCE METHOD (SLR)

The specific local resistance method requires that a critical structural element is able to resist abnormal loading, so the designer should explicitly design critical vertical load bearing elements to resist the design level threat, such as blast pressures. In other words, this method, which is also referred to as "key element design ", provides sufficient strength to resist an abnormal load by ensuring all load-bearing elements remain intact and in place.

## 1.3.2.2 ALTERNATIVE PATH METHOD (APM)

In the alternate load path method, the designer localizes response by designing the structure to carry loads by means of an alternate path in the event of the loss of a primary load bearing component. The alternate load path method provides a formal check of the capability of the structural system to resist the removal of specific elements, such as a column at the building perimeter. The method does not require characterization of the threat causing loss of the element, and is, therefore, a threat independent approach.

Depending on the analytical method used to implement the alternate load path method, the results may not provide an accurate representation of actual performance in the event of a damaging event. The method may be viewed as a tool to ensure redundancy in the gravity load resisting system rather than a simulation of structural response after initial damage (NIST 2007).

## 1.3.3 BRITISH STANDARDS

On November 15, 1968, after the partial collapse of the Ronan Point building, which is considered to be the watershed event initiating interest in the topic of progressive collapse, the U.K. Ministry of Housing and Local Government issued "Standards to Avoid Progressive Collapse – Large Panel Construction", which listed two methods:

A) Provide alternate paths of support to carry the load, assuming the removal of a critical section of the load bearing walls.

B) Provide a form of construction of such stiffness and continuity so as to ensure the stability of the building against forces liable to damage the load supporting members.

The standards also specified an accidental static pressure of 34 kN/m$^2$ (or 5 psi, a town-gas explosion of average intensity), and derived minimum tie forces. These standards became part of the Fifth Amendment that the British Parliament approved in April 1970 as part of mandatory Building Regulations that required consideration of progressive collapse for buildings taller than five storeys.

Provisions for structural ties entered the British Standards in 1974. These provisions, with certain modifications that put less emphasis on explosions and more on ductile performance, are still in use today in the U.K. The notional removal of an essential structural element should cause only local collapse 70 $m^2$ (750 ft$^2$) or 15 % of the plan area of the storey, Figure 1-4, whichever is the lesser, and buildings should be designed for an accidental pressure of 34 kN/m$^2$ or 5 psi acting simultaneously with dead and imposed loads (NIST 2007).
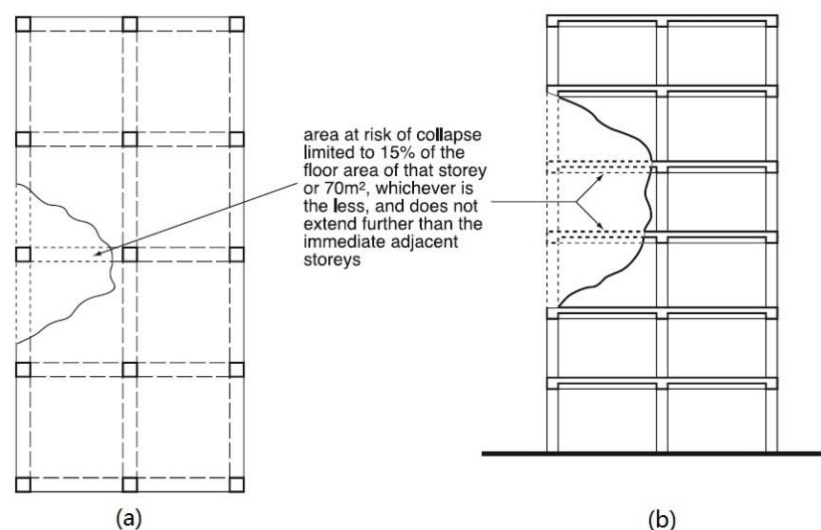


Figure 1-4 Recommended limit of the admissible damage a) Plan b) Section (Minister 2004)

The new building regulations for England and Wales were published in 2004. The Section A3 of the Approved Document A (AD A) (Minister, 2004) deals with the requirement for disproportionate collapse. The new regulations classify all buildings into four categories, that is, class 1, class 2A, class 2B and class 3, based on the number of storeys, building type, and occupancy, Table 1-1. All buildings, regardless of the number of storeys, are required to have effective horizontal and vertical ties. The approach to satisfying the requirement for each class can be summarized as follows:

a) For buildings in Consequences Class 1: Provided a building has been designed and constructed in accordance with the rules given in (AD A), and/or appropriate codes of practice for satisfying stability in normal use, no further specific consideration is necessary with regard to accidental actions from unidentified causes.

b) For buildings in Consequences Class 2A (Lower Risk Group): In addition to the recommended strategies for Consequences Class 1, it is necessary to use effective horizontal ties, or effective anchorage of suspended floors to walls, as described in the Standards (BS 8110-1:1997).

c) For buildings in Consequences Class 2B (Upper-Risk Group): In addition to the recommended strategies for Consequences Class 1, the provision of:
- horizontal ties, as defined (BS 8110-1:1997) for framed and load-bearing wall construction together with vertical ties, in all supporting columns and walls should be provided, or alternatively,
- the building should be checked to ensure that upon the notional removal of each supporting column and each beam supporting a column, or any nominal section of load-bearing wall (one at a time in each storey of the building) the building remains stable and that any damage must be localized to the smaller of 15% of the floor area or (70 m$^2$), and does not extend further than the immediate adjacent storeys, Figure 1-4.

Where the notional removal of such columns and sections of walls would result in an extent of damage in excess of the agreed limit, or other such limit specified, then such elements should be designed as a "key element", which should be capable of sustaining an accidental design loading of 34 kN/m$^2$ applied in the horizontal and vertical direction (in one direction at a time) to the member and any attached components (e. g. cladding etc.) having regard to the ultimate strength of such components and their connections.

Table 1-1: Building classes

| Classes | Example of categorization of building type and occupancy |
|---|---|
| Class 1 | - Single occupancy houses not exceeding 4 storeys.<br>- Agricultural buildings.<br>- Buildings into which people rarely go, provided no part of the building is closer to another building, or area where people do go, than a distance of 1.5 times the building height. |
| Class 2A<br>Lower Risk<br>Group | -5 storey single occupancy houses.<br>- Hotels not exceeding 4 storeys.<br>-Flats, apartments, and other residential buildings not exceeding 4 storeys.<br>-Offices not exceeding 4 storeys.<br>-Industrial buildings not exceeding 3 storeys.<br>-Retailing premises not exceeding 3 storeys of less than 2000 m2 floor area in each storey.<br>-Single storey educational buildings<br>-All buildings not exceeding two storeys to which the public are admitted and which contain floor areas not exceeding 2000 $m^2$ at each storey. |
| Class 2B<br>Upper Risk<br>Group | -Hotels, flats, apartments and other residential buildings greater than 4 storeys but not exceeding 15 storeys.<br>-Educational buildings greater than the single storey but not exceeding 15 storeys.<br>-Retailing premises greater than 3 storeys but not exceeding 15 storeys.<br>-Hospitals not exceeding 3 storeys.<br>-Offices greater than 4 storeys but not exceeding 15 storeys.<br>-All buildings to which the public are admitted and which contain floor areas exceeding 2000 $m^2$ but not exceeding 5000 $m^2$ at each storey.<br>-Car parking not exceeding 6 storeys. |
| Class 3 | -All buildings defined above as Class 2 Lower and Upper Consequences Class that exceed the limits on area and number of the storey.<br>-All buildings to which members of the public are admitted in significant numbers.<br>-Stadia accommodating more than 5000 spectators Buildings containing hazardous substances and /or processes. |

The document does not suggest the load that should be used in the analysis of the structure after the removal of a vertical load bearing element. However, BS 8110-1:1997 Clause 2.4.3.2 gives the loads to be considered in case of taking an exceptional load or localized damage:

- 1.05 of the dead load
- One-third of the wind load
- For buildings used predominantly for storage or industrial purposes or when the imposed loads are permanent, 100% of the imposed load or, for other buildings, one-third of the imposed load.

Therefore, the equation of the load combination can be written as:

$$L_c = 1.05\,G + Q + 0.35\,W \quad \text{For buildings where imposed loads are permanent} \quad (1\text{-}1)$$

$$L_c = 1.05\,G + 0.35\,Q + 0.35\,W \qquad \text{For other buildings} \hspace{3cm} (1\text{-}2)$$

Where:

$L_c$, is the combination of total load.

$G$ , is the dead load

$Q$ , is the imposed load

$W$, is the wind load

    d) For buildings in Consequences Class 3: A systematic risk assessment of the building should be undertaken taking into account both foreseeable and unforeseeable hazards. Critical situations or design should be selected to reflect the conditions that can reasonably be foreseen as possible during the life of the building. Unfortunately, this guidance gives the designer little assistance and no references are provided.

AD A refers to BS 8110-1:1997 as an appropriate standard for the details of ties and key elements (where required). BS 8110-1: 1997 defines four kinds of ties:

a) Peripheral ties

b) Internal ties

c) Horizontal ties to column and walls

d) Vertical ties

British Standard also stated that the tying requirements can be met by using reinforcement provided for other purposes. Figure 1-5 shows some kinds of these ties.

## PERIPHERAL TIES IN FLOORS

At each floor and roof level, an effectively continuous tie should be provided within 1.2 m of the floor edge or within the perimeter wall. The peripheral tie should be able to resist a tensile force ($F_t$) in kN of the lesser of $P$ and 60, where $P$ is:

$$P = (20 + 4n_0) \tag{1 - 3}$$

Where
$n_0$, is the number of storeys in the structure.

## INTERNAL TIES IN FLOORS

At each floor and roof level, internal ties should be provided in two directions approximately at right angles. The internal ties may be spread evenly in slabs or may be grouped at walls or other positions, with maximum spacing not greater than $1.5L_r$. If located in walls, the reinforcement should be within 0.5 m of the top or bottom of the floor slabs. In each direction the tie needs to be able to resist a force, which should be taken as:

$$F_{tie.int} = \frac{(g_k + q_k)}{7.5}\left(\frac{L_r}{5}\right)F_t \qquad F_{tie.int} \geq F_t \tag{1 - 4}$$

Where
$(g_k + q_k)$ = characteristic dead and imposed floor loads in (kN/m²)
$L_r$ = greater of the distances (in m) between centres of the columns, frames or walls supporting any two adjacent floor spans in the direction of the tie under consideration
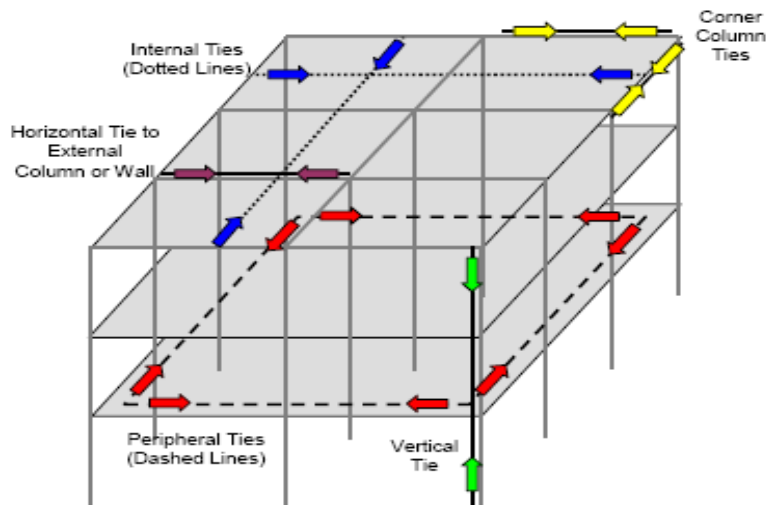


Figure 1-5 System of tie forces

**HORIZONTAL TIES TO COLUMNS AND WALLS**

Each external column and, if the peripheral ties are not located within the wall, every meter length of external wall carrying vertical load should be tied horizontally into the structure at each floor and roof level with a tie capable of developing a force in (kN) equal to the greater of:

a) 2.0 $F_t$ [or $\left(\frac{L_s}{2.5}\right) F_t$ if less, where $L_s$ is the floor to ceiling height (in meters)]; or

b) 3% of the total design ultimate vertical load carried by the column or wall at that level

Corner columns should be tied into the structure at each floor and roof level in each of two directions.

**VERTICAL TIES TO COLUMNS AND WALLS**

Each column and each wall carrying vertical load should be tied continuously from the lowest to the highest level. The tie should be capable of resisting a tensile force equal to the maximum design ultimate dead and imposed load received by the column or wall from any one storey.

## 1.3.4 GENERAL SERVICES ADMINISTRATION (GSA)

The U.S. General Services Administration (GSA) guideline, entitled "Progressive collapse analysis and design guidelines for new federal office buildings and major modernization projects", was specifically prepared for reducing or assessing the potential for progressive collapse of new or existing buildings. The latest version of these guidelines was released in June 2003.

The objective of the guidelines is not necessarily to prevent collapse initiation from a specific cause. It is to prevent or mitigate the potential for progressive collapse after having an initial damage as a result of an abnormal loading. The GSA provides a threat independent approach to mitigate the potential for progressive collapse.

The GSA guideline has a detailed exemption process for evaluating if the risk of a structure experiencing progressive collapse is low enough that a detailed progressive collapse assessment is not required. The exemption process takes into account many factors such as the use of the building, the number of storeys, the type of the structure (reinforced concrete, steel structure, etc.), the level of protection, seismic zone, etc. Structures that are evaluated to be exempt are not required for further considerations. Otherwise, non-exempt structures are subjected to a rigorous progressive collapse resistance assessment.

The GSA (2003) recommends that a structure is analysed by instantaneously removing a column from specific locations of the structure, the middle of the traverse side of the building, near the middle of the longitudinal side of the building, and at the corner of the building, Figure 1-6. GSA guideline allows the analysis of the structure either statically or dynamically and using either a linear analysis for buildings of 10 storeys or less or using a nonlinear analysis for buildings of more than 10 storeys.
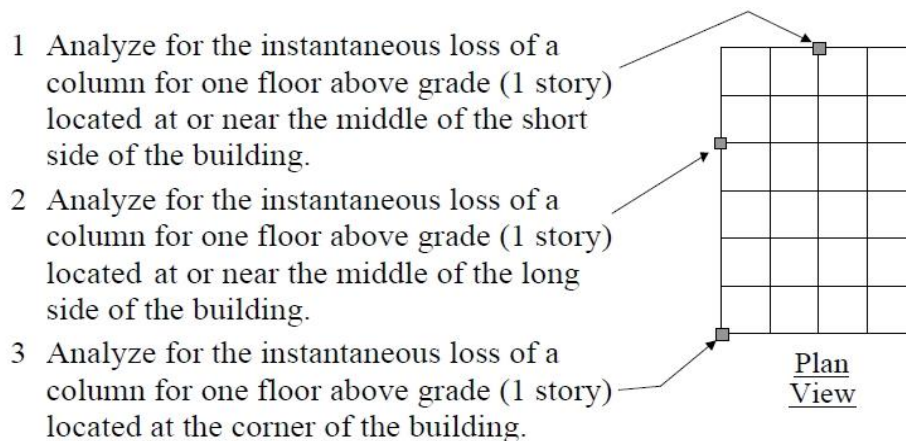


Figure 1-6 Exterior Column Removal Process for A Typical Framed Structure (GSA 2003)

When a static analysis procedure (either linear or nonlinear) is used the structure is required to be analysed for the following vertical load combination:

$$Load = 2.0(DL + 0.25LL) \qquad\qquad (1 - 5)$$

When a dynamic analysis procedure (either linear or nonlinear) is used the structure is required to be analysed for the following vertical load combination:

$$Load = (DL + 0.25LL) \qquad\qquad (1 - 6)$$

Where, *DL* is dead load and *LL* is live load

The coefficient of 2.0 in the load combination to be used in the static analysis procedure accounts for the dynamic effects in the static analysis. Structural collapse resulting from the instantaneous removal of a primary vertical support should be limited to the smaller of:

For exterior considerations

1. The structural bays directly associated with the instantaneously removed vertical member in the floor level directly above the instantaneously removed vertical member. Or

2. 1800 ft² (167 m²) at the floor level directly above the instantaneously removed vertical member.

For interior Considerations

1. The structural bays directly associated with the instantaneously removed vertical member, or

2. 3,600 ft² (334 m²) at the floor level directly above the instantaneously removed vertical member.

## ACCEPTANCE CRITERIA

GSA uses an approach which identifies the magnitude and distribution of potential demands on both the primary and secondary structural elements for quantifying collapse areas. The magnitude and distribution of these demands will be indicated by Demand-Capacity Ratios (*DCR*), which can be calculated as follows:

$$DCR = Q_{ud}/Q_{ce} \qquad\qquad (1 - 7)$$

Where,

$Q_{ud}$ = Acting force (demand) determined in component or connection/joint (moment, axial force, shear, and possible combined forces)

$Q_{ce}$ = Expected ultimate, un-factored capacity of the component and/or connection/joint (moment, axial force, shear and possible combined forces)

Using the DCR criteria of the linear elastic approach, structural elements, and connections that have DCR values that exceed the following allowable values are considered to be severely damaged or collapsed.

The allowable DCR values for primary and secondary structural elements are:

• DCR <  2.0 for typical structural configurations (Facilities that have a relatively simple layout)

• DCR < 1.5 for atypical structural configurations (i.e., buildings often contain distinguishing structural features or details).

The step-by-step procedure for conducting the linear elastic, static analysis follows:

**Step 1** Remove a vertical support from the location being considered and conduct a linear-static analysis of the structure. The load combination is $2(DL + 0.25LL)$.

**Step 2** Determine which members and connections have DCR values that exceed the acceptance criteria. If the DCR for any member end connection is exceeded based upon shear force, the member is to be considered a failed member. In addition, if the flexural DCR values for both ends of a member or its connections, as well as the span itself, are exceeded, the member is to be considered a failed member. Failed members should be removed from the model, and all dead and live loads associated with failed members should be redistributed to other members in adjacent bays.

**Step 3** For a member or connection whose DCR ratio exceeds the applicable flexural DCR values place a hinge at the member end or connection to release the moment. This hinge should be located at the centre of flexural yielding for the member or connection. Use rigid offsets and/or stub members from the connecting member as needed to model the hinge in the proper location. For yielding at the end of a member, the centre of flexural yielding should not be taken to be more than $1/2$ the depth of the member from the face of the intersecting member, which is usually a column, Figure 1-7.

**Step 4** At each inserted hinge apply equal-but-opposite moments to the stub/offset and member end to each side of the hinge. The magnitude of the moments should equal the expected flexural strength of the moment or connection, and the direction of the moments should be consistent with the direction of the moments in the analysis performed in **Step 1.**

**Step 5** Re-run the analysis and repeat **Steps 1** through **4**. Continue this process until no DCR values are exceeded. If moments have been re-distributed throughout the entire building and DCR values are still exceeded in areas outside of the allowable collapse region, the structure will be considered to have a high potential for progressive collapse.
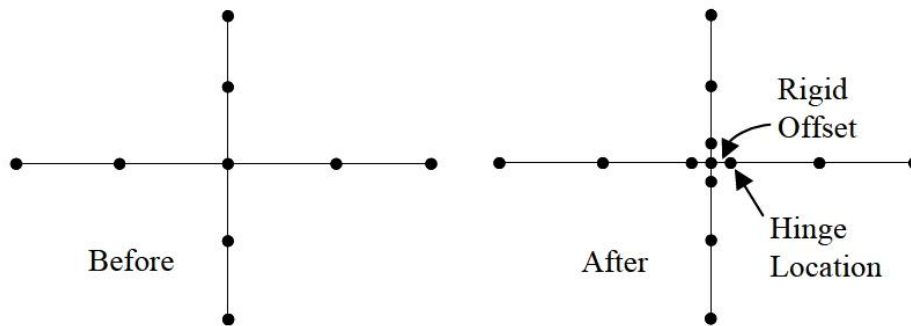
Figure 1-7 Rigid offset placement (GSA 2003)

### 1.3.5 AMERICAN DEPARTMENT OF DEFENSE (DOD: 2005)

The Department of Defence introduced the first Unified Facilities Criteria (UFC) (DoD, 2005) for Design of Buildings to Resist Progressive Collapse in 2005. This document is updated in 2010 including significant changes. The document provides the design requirements necessary to reduce the potential of progressive collapse for new and existing buildings that experience localized structural damage as a result of accidental events.

Three design approaches are considered in the document to design new and existing structures to resist progressive collapse; Tie Forces, Alternate Path Method and Enhanced Local Resistance, which depends on the required level of protection for the facility.

### 1.3.5.1 TIE FORCES APPROACH

As described in the British Standard, the tie forces method prescribes a tensile force capacity of the floor or roof system, to allow the transfer of load from the damaged portion of the structure to the undamaged portion, by providing the continuity and ductility, which play the key roles in the redistribution of the loads over a damaged region. The approach categorizes the ties to be provided in the structure into three categories, Figure 1-8:

1. Longitudinal and Transverse Ties.
2. Peripheral Ties.
3. Vertical Ties.

The following floor load is to be used in the calculation of the required tie strengths:

$$w_f = 1.2DL + 0.5LL \qquad\qquad (1\text{-}8)$$

Where

$w_f$ is floor load in (lb/ft$^2$ or kN/m$^2$), $DL$ and $LL$ are dead and live load, respectively

## 1- Longitudinal and Transverse Ties

The following formula is used to calculate the required tie strength for the longitudinal or transverse ties for framed structures as well as for load bearing wall structures:

$$F_i = 3\, w_f\, L_1 \tag{1-9}$$

Where

$F_i$ is the required tie strength (lb/ft. or kN/m), $w_f$ is the floor load and $L_1$ is the greater of the distances between the centres of the columns, frames, or walls supporting any two adjacent floor spaces in the direction under consideration (ft. or m).

## 2- Peripheral Ties

The following formula is used to calculate the required peripheral tie strength for framed structures as well as for load bearing wall structures:

$$F_P = 6\, w_f\, L_1 L_p \tag{1-10}$$

Where

$w_f$ is floor load, $L_1$ is the greater of the distances between the centres of the columns, frames, or walls at the perimeter of the building in the direction under consideration (for exterior peripheral ties) or the length of the bay in which the opening is located, in the direction under consideration (for peripheral ties at openings), and $L_p$ is 3.3ft (1.0 m).

## 3- Vertical Ties

The vertical tie must have design strength in tension equal to the largest vertical load received by the column or wall from any one storey. Each column and load-bearing wall shall be tied continuously from the roof level down to the first column- or wall-supported floor above the foundation, i.e., the vertical ties are not required to extend to the foundation.

In the case that the structural elements cannot provide the required tie strength, the elements and connections should be redesigned or retrofitted in order to develop the required tie force. For the vertical ties, however, if any structural element or connection fails to provide vertical required tie strength, redesigning is not required if it can be proven that the structure is capable of bridging over this deficient element using the Alternate Path Method.
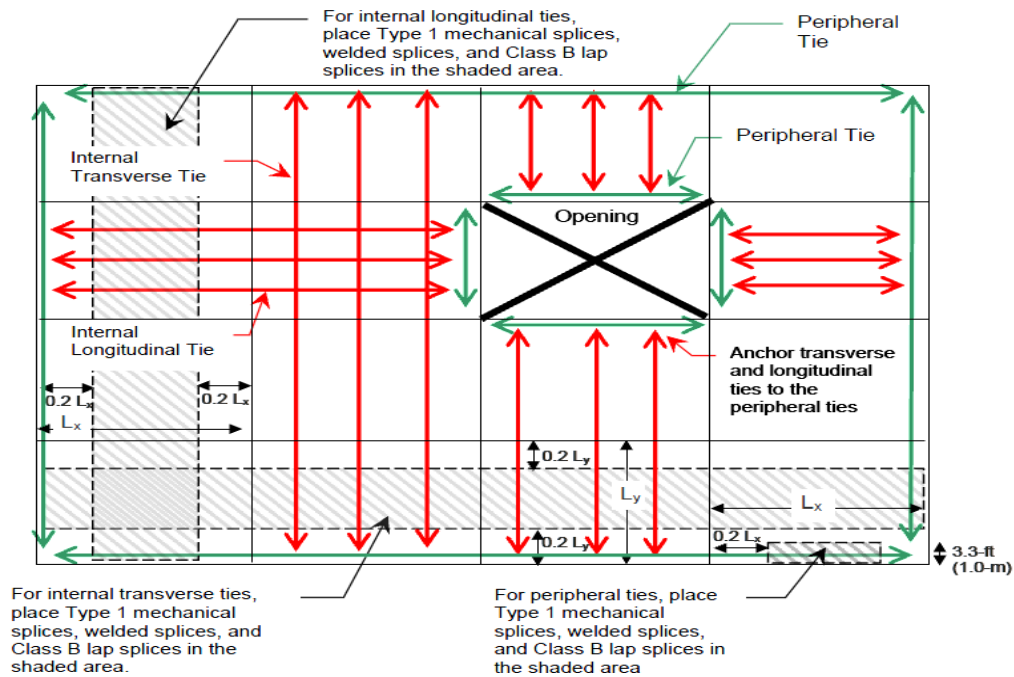
Figure 1-8 Locations and Interruptions of ties (UFC 2009)

## 1.3.5.2 ALTERNATE PATH METHOD (APM)

The second approach is based on the alternate path method, in which the building should bridge across a removed element. UFC allows the structure to be analysed after removing bearing element by using three analysis procedures:

Linear Static (LSP), Nonlinear Static (NSP) and Nonlinear Dynamic (NDP). The load combinations that should be used are as follows:

- For Linear, Non-Linear Static Analysis

$$G_s = 2.0\,[1.2\,DL + (0.5\,LL \text{ or } 0.2\,S)] \tag{1-11}$$

To be applied at the bays adjacent to the removed element, and at all floors above the removed element.

$$G = 1.2\,DL + (0.5\,LL \text{ or } 0.2\,S) \quad \text{To those bays not loaded with } G_s \tag{1-12}$$

Where

$G_s$ , $G$ = Increased gravity loads for Linear Static Analysis (lb/ft$^2$ or kN/m$^2$)

$DL$ = Dead load including façade loads (lb/ft$^2$ or kN/m$^2$)

$LL$ = Live load (lb/ft$^2$ or kN/m$^2$)

$S$ = Snow load (lb/ft$^2$ or kN/m$^2$)

- For Non-Linear dynamic analysis

$$G_D = 1.2\,DL + (0.5\,LL\ or\ 0.2\,S) \qquad \text{To be applied for the entire structure} \qquad (1\text{-}13)$$

Where

$G_D$ = Gravity loads for Nonlinear Dynamic Analysis (lb/ft$^2$ or kN/m$^2$)

It can be seen that the vertical load prescribed for a static analysis is twice the vertical load recommended for a dynamic analysis to allow for dynamic effects.

## ACCEPTANCE CRITERIA

The DOD adopted an approach similar to that used by GSA to evaluate the magnitude and distribution of potential progressive collapse for a building. The magnitude and distribution of these demands will be indicated by (DCR), which can be calculated using equation (1-7).

As mentioned before three analysis procedures are suggested in UFC for Design of Buildings to Resist Progressive Collapse; Linear Static Analysis Procedure, Nonlinear Static Analysis Procedure, and Nonlinear Dynamic Analysis Procedure.

If the primary elements and components meet the acceptance criteria for the corresponding procedure, then the building satisfies the progressive collapse requirements, otherwise, it must be redesigned or retrofitted.

## 1.3.5.3 ENHANCED LOCAL RESISTANCE

In the Enhanced Local Resistance approach, the shear and flexural capacity of the perimeter columns and walls are increased to provide additional protection by reducing the probability and extent of the initial damage. The Enhanced Local Resistance approach is required along with other approaches (e.g. Tie Forces, Alternate Path).

## 1.4  MOTIVATION AND RESEARCH SIGNIFICANCE

The study of progressive collapse, although it has intermittently been a subject of interest in the academic and industrial structural engineering communities for several decades, has gained a heightened interest from not only engineers but also from the general public and government institutions (Almusallam et al., 2010).

Recently, progressive collapse has become an issue of increasing importance because of escalation in terrorist activities worldwide. Therefore, interest in this phenomenon has increased. Current building codes provide general guidelines to prevent progressive collapse based on redundancy, integrity, continuity, and ductility. Progressive collapse is typically not considered in the conventional structural design process, although it is a devastating failure which may cause a huge loss of lives.

The significant loss of lives in the event of progressive collapse introduces important questions. One question is whether existing buildings have adequate capacity to resist progressive collapse. The second question is whether available design guidelines are sufficiently clear for the engineer to design new buildings against progressive collapse. Researchers may need to develop a new and innovative robust structural systems that are economical and do not interfere significantly with the functionality of the building. The success of the structural system is gauged by its capacity of minimising loss of lives (Mohamed, 2006).

Therefore, one of the goals of this research is to propose a new scheme to prevent or reduce the potential of progressive collapse. It cannot be assumed that progressive collapse can be totally prevented, so the aim of proposed scheme is to mitigate progressive collapse, not necessarily to prevent it.

Experimental data are essential for practices in progressive collapse prevention (Ellingwood et al., 2009). Currently, limited experimental data is available to date to calibrate the critical parameters used to define the strength properties of structural components in nonlinear analysis modelling or to validate numerical simulation results.

Therefore, one of the goals of this research is to better understand the resistance mechanisms of RC buildings against progressive collapse. The ultimate goal is to contribute to a set of guidelines on how to best resist progressive collapse.

One of the most effective load-carrying mechanisms for a structure following the loss of vertical load-bearing elements is for the beam and connection to develop catenary action. In catenary action, a beam or a system of beams deflects and develops plastic hinges at locations along the beam, such that it acts like a cable carrying its load in tension.

This requires a connection first to develop a plastic hinge and then simultaneously, have enough capacity to carry large tensile forces. In other words, it is critical that the primary structural elements, such as girders and beams must be capable of spanning two full spans after the loss of a column. This requires that both beam-to-beam structural continuity across the removed column, and deform well beyond the elastic limit without experiencing structural collapse.

All conclusions, analysis, and recommendations of previous studies are focussed on determining how to prevent the failure of the continuous beam when column loss occurs. With this idea in mind, it can be seen that establishing modified detailing of bar reinforcements in RC beams would be the ideal way to prevent or mitigate progressive collapse in RC structures through providing steel bars strategically placed in the beam section to absorb the released energy, and other steel bars to control the development of plastic hinges at specific locations to develop catenary action properly and effectively.

## 1.5 RESEARCH OBJECTIVES

In order to reduce the potential of progressive collapse, detailed behaviour of a structural system is needed when a structural load carrying member is damaged. Two main objectives of this research intend to be established.

Firstly, to better understand the collapse resistance mechanisms of RC buildings under CRS. The effect of these resistance mechanisms needs to be studied because they are often not considered in the analysis and design, although there is an evidence of their effectiveness, but there is a lack of understanding regarding how to determine their capacities. Secondly, is to propose a new mitigation scheme to prevent or at least reduce the potential of progressive collapse of RC buildings in case of column failure or loss, by providing the RC beams with modified reinforcing details. The objectives of the research can be summarised into the points below:

- Contribute to expanding the available experimental and analytical data on membrane action of RC beams and progressive collapse resistance of RC buildings.

- Enhance the understanding of the mechanisms of compressive and tensile membrane action of RC beams at the local level.

- Provide a better understanding of the mechanism of dynamic load redistribution and progressive collapse resistance of RC buildings at the global level.

- Investigate the effect of the modified proposed reinforcement detailing of RC beams on structural behaviour and structural capacity to resist progressive collapse.

- Develop a beam-column joint model that can represent and simulate structural behaviour through finite-element analysis, in which beams and columns are modelled using fibre elements (line elements).

- Develop an analytical model to predict the load-carrying capacity of a beam at the CAA and catenary action stage.

## 1.6 SCOPE OF WORK

The current proposed study is mainly concerned with RC frames, beams and joints without considering the effect from slabs and transverse beams. Therefore, the membrane action of RC slabs and transverse beams is outside the scope of current work, and the columns adjacent to the removed one are assumed to be able to sustain the increased axial loads and transfer the lateral loads from the two-bay beam after load redistribution.

In addition, the threat which may cause the initial damage is not considered in this study, therefore, the investigation of specific threads such as blast, vehicle impact, etc. and their effect on the structural behaviour is outside of the scope of this study.

In the experimental work, the size effect of specimens will not be of concern in this work although the specimens are one-half scale, this is because that one-quarter scale is regarded as the minimum scale for joint specimens fabricated with conventional deformed bars and aggregate concrete mix (Abrams, 1987), and shear behaviour is not dominant under CRS.

## 2. CHAPTER TWO   LITERATURE REVIEW

## 2.1 GENERAL

To mitigate progressive collapse, efforts are directed at both code provisions and research work. In general code provisions, structural integrity reinforcement is required to improve redundancy and ductility in structures. To achieve continuity in structural components, tie forces are required to tie the elements together so they act as one unit. When one of the critical load bearing elements is damaged or removed, connecting spans deflect until rotational capacity provided by the adjacent beams or slabs is exhausted. Then, the catenary action may allow the beam to carry vertical loads at large displacements. This behaviour is defined as "CATENARY ACTION".

- CATENARY ACTION

  Catenary action is considered as the last line of defence for a structure to mitigate progressive collapse when a load bearing element is removed or damaged. The beam above a removed column undergoes three stages or mechanisms i.e. flexural action, compressive arch action (CAA) and catenary action (Orton 2007). Initially, all beams mobilise flexural action, which they are designed for and they are able to sustain the design load. When a column is removed, the span of the beam increases and in most cases leads to larger deflections occurring in the remaining beam system. Compressive arch action, which enhances the flexural strength at critical sections, can be mobilised in the presence of axial compression provided by strong lateral restraints.

  At large deflections, catenary action can be mobilised. (Orton, 2007) discovered that catenary action will not begin until the beam has reached a deflection equal to the depth of the beam. This is due to the fact that the beam remains in axial compression until tension forces are mobilised. Furthermore, the design and steel detailing of a RC beam must ensure enough ductility so that the beam can reach catenary action without fracture of all the steel bars. Therefore, catenary action is an in-plane force that resists vertical loads by mobilising axial tension throughout the beam.

  Previous research indicates that development of catenary action depends on many factors such as large deformation, stiff lateral restraints from surrounding elements and the resistance of the beam under investigation. Furthermore, the resistance of the beam depends on, beam geometry, material properties and reinforcement detailing, which plays a fundamental role in the ductility, continuity and ultimate strength of structural members and connections for reinforced concrete structures. Figure 2-1shows the layout of catenary action forces.

However there are very few previous studies on catenary action of reinforced concrete beams and most of the experimental studies are concerned with catenary action of steel beams at ambient and elevated temperatures and under column loss scenarios ((Byfield et al., 2007); (Byfield and Paramasivam, 2007)  (Izzuddin, 2005);(Yin and Wang, 2005)).

In this chapter, the very limited tests on RC frames under column loss scenarios, numerical works and approaches to mitigate progressive collapse will be presented. It should be mentioned that most of the experimental tests on concrete structures were implemented under quasi-static load despite the fact that the redistribution of loads after column loss is dynamic in nature. The reason for that is because static tests can provide more details and insight towards the development of different structural load resisting mechanisms.
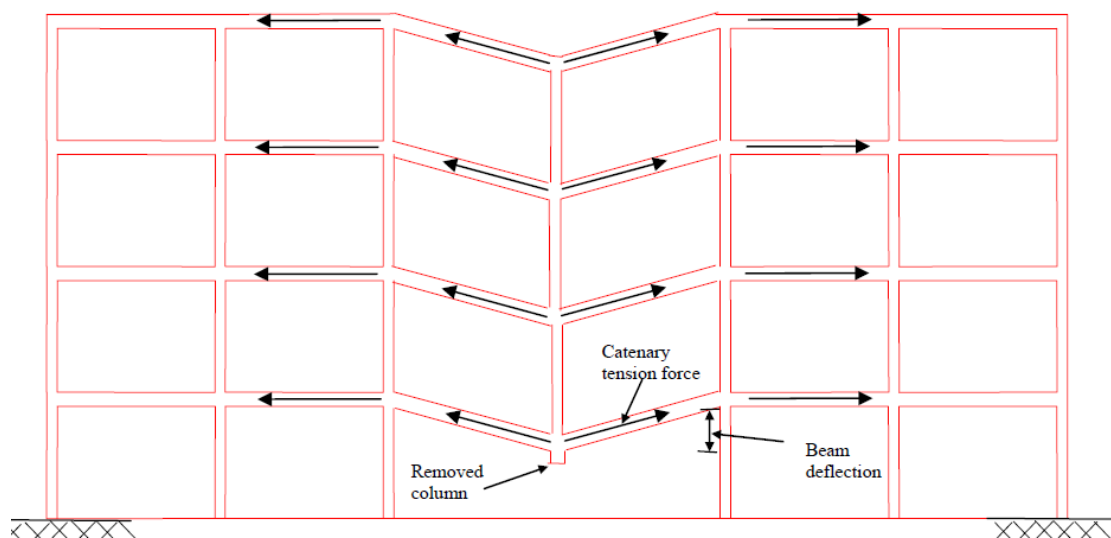
Figure 2-1 Catenary tension force (Orton 2007)

## 2.2 EXPERIMENTAL STUDIES:

In this section, the very limited tests on RC frames and beams under column loss scenarios will be reviewed, focusing on studies concerned with catenary action.

### 2.2.1 Regan (1975)

One of earliest works was reported by (Regan, 1975) at Imperial College in London. As shown in Figure 2-2. Regan conducted tests on precast floor strips ranging from 14 in. (356 mm) to 28 in. (711 mm) wide and 18 ft. (5.5 m) long with a central joint at the 'lost support' between two 9 ft (2.75 m) spans. The specimens comprised a 2 in. (50 mm) thick precast panel and a 2 in. (50 mm) thick cast-in-place topping. Details of the ties between the panels varied according to the specimens' width. Specimens were loaded with hydraulic jacks.

For almost all the tests, there was an initial compressive arch phase, which was "snapped through" and was followed by a catenary action phase. The majority of the beams failed by tearing out of the bottom bars near the supports at a deflection of 5 to 7% of the double span length (test #5 in Figure 2-3). However, some specimens were able to yield in flexure at the supports before tearing out of the bottom bars. In these cases, the catenary loads were much higher and the ultimate deflection was near 10% of the span length (test #3 in Figure 2-3). The beams eventually failed by fracture of the end rebar due to large rotation at the support. For most tests, catenary action started at around 6 to 7 in (150 to 175 mm) of displacement, which is slightly greater than the beam depth 4 in. (100 mm).

The tests also included two specimens that were loaded by sandbags and the central support suddenly pulled out. For one test, the specimen did not fail, but the deflections were 50% greater than for the same load applied to an identical specimen that was loaded with hydraulic jacks. Another specimen failed, although the total weight was only 56% of the ultimate load reached in the hydraulically loaded test.

Due to insufficient anchorage and poor continuity of specimens, not all of them could develop catenary action successfully. Based on the tests results, Regan concluded that "successful development of a catenary action requires that the members in question possess not only tensile strength but also ductility, which largely depends on the detailing of the longitudinal steel bar reinforcement."
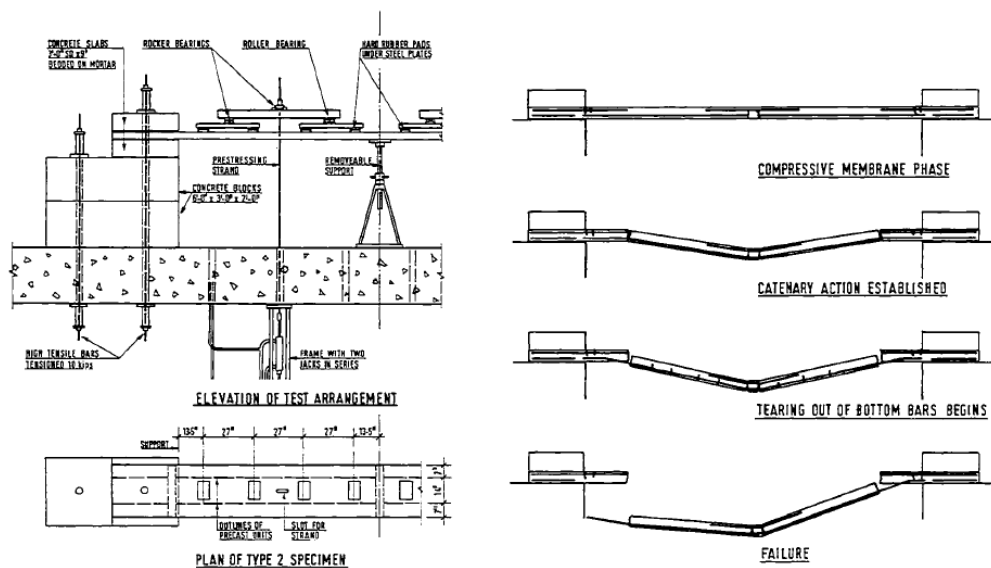


Figure 2-2 Catenary action tests of precast floor strips (Regan 1975)
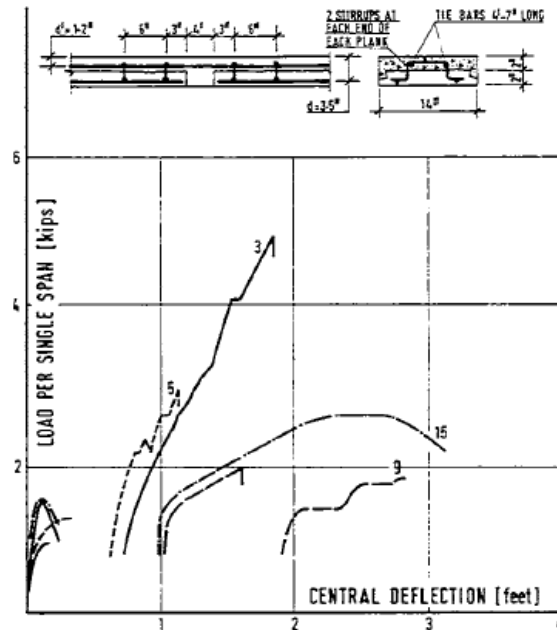
Figure 2-3 Results of catenary tests of precast floor strips (Regan, 1975)

## 2.2.2 Sasani and Kropelnicki (2007)

Experimental and analytical research on the topic of progressive collapse was conducted by Sasani. In 2007, (Sasani and Kropelnicki, 2007) carried out an experimental program to evaluate the behaviour of a continuous perimeter beam in a reinforced concrete frame. He tested a 3/8 scaled RC perimeter beam under a middle CRS. The specimen was designed in accordance with (ACI-318, 2002), which specifies integrity requirements. In order to investigate the behaviour of that beam analytically, they also implemented a detailed finite element model using the ANSYS software package.

The actual dimensions of the beam were 13 ft. 8¼ in. (4170 mm) long, 12 in. (300 mm) width, and 20 in. (500 mm) depth. In order to examine the effects of splices on the development of catenary action in beams and progressive collapse of structures, the longitudinal reinforcements were spliced, Figure 2-4. Loading was applied by displacement control at the mid-span, and then vertical deflection versus applied load was plotted as shown in Figure 2-5.

From Figure 2-5, and the test results, it was observed that the two bottom bars fractured at vertical displacements of about 6.0 in.(150mm) and 7.5 in.(190mm). Figure 2-6. In addition, they found that catenary action developed in the top reinforcement following the bar fractures by satisfying the integrity requirements of (ACI-318, 2002), and no indication of splice failure was observed.

27
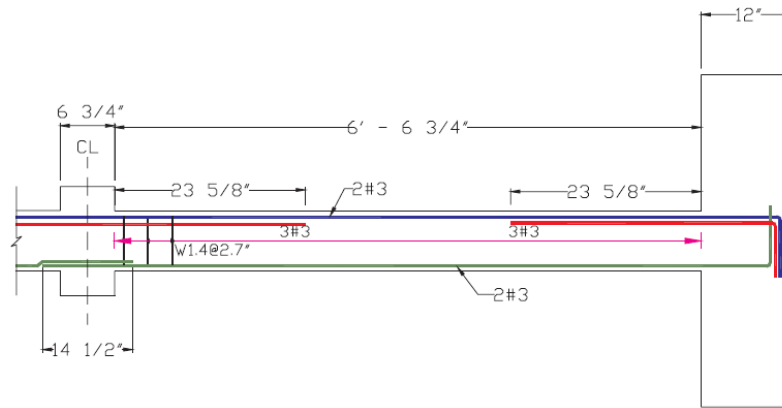
Figure 2-4 Detailing of the test beam (Sasani and Kropelnicki 2007)
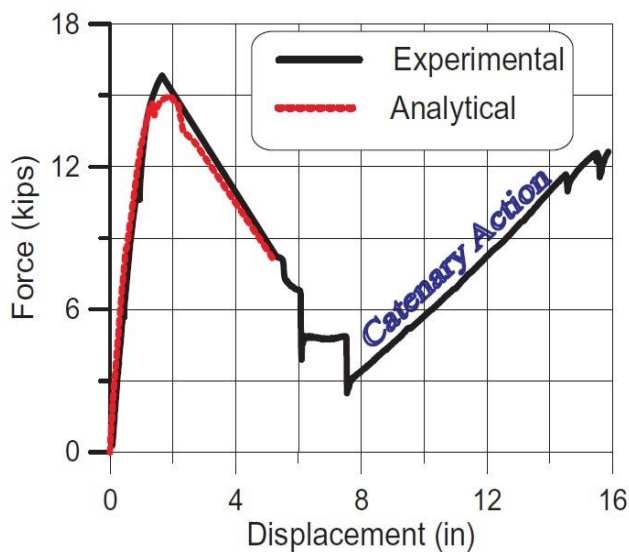


Figure 2-5 Force–displacement relationships          Figure 2-6 Bar fracture
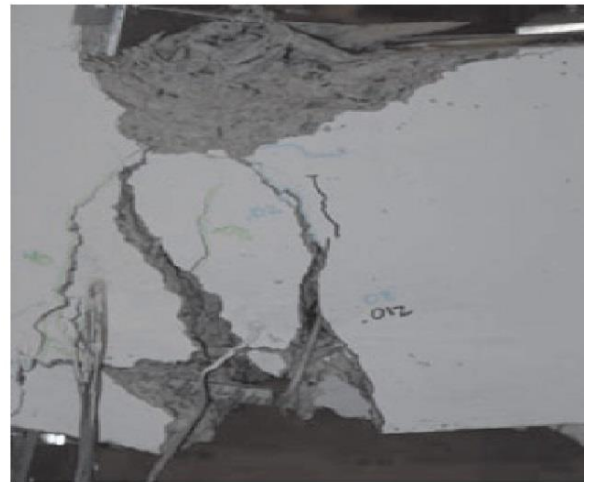
## 2.2.3 Yi et al (2008)

In 2008, (Yi et al., 2008) tested a one-third scaled specimen of four bays and lower three-storey RC frame extracted from a building of a four-bay, eight-storey RC frame structure, as shown in Figure 2-7, designed in accordance with the concrete design code of China, which is similar to ACI 318-02. The dimensions of beam section were 200 mm in depth and 100 mm width, and the cross-section of columns was 200 mm by 200 mm.

The experiment was conducted statically, the gravity load was applied by servo-hydraulic actuator to the upper floors, and the CRS was simulated by unloading a mechanical jacking system in a displacement-controlled manner. The main purpose of the testing was to observe the force-deformation response in the simulated failing column which was located at the centre of the lower storey.

The test results indicated that the beam above the removed column experienced three phases, i.e. elastic, plastic and catenary action as shown from the relationship between vertical displacement and middle column load as shown in Figure 2-8. Yi et al concluded that from the experimentally recorded results and the analytical approximations, that the failure load computed on the basis of a plastic mechanism is approximately 70% of the estimated capacity of the catenary mechanism.

Also, they concluded that the failure of the RC frame resulting from column removal was controlled by the fracture of steel bars, different from the collapse of normal limit state for beam bending, which is controlled either by crushing of concrete in compression zone or shear failure.
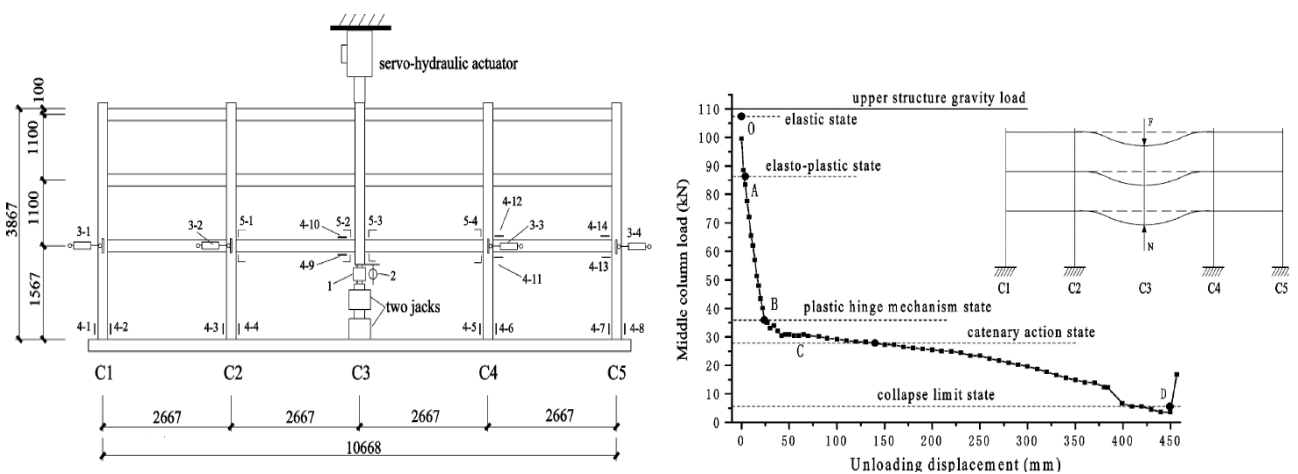
Figure 2-7: Specimen dimensions (Yi et al. 2008)   Figure 2-8: Middle col. load vs. deflection

## 2.2.4 Wei-Jian and Qing-Feng 2008

In 2008,(Wei-jian, 2008) tested five half scaled specimens to investigate the effect of steel reinforcement ratio, steel grade, steel type and loading rate on the resistance capacity of RC structures against progressive collapse.

The specimens were RC beam-column sub-structure with various steel detailing and steel type, designed and detailed according to the Chinese design Code (GB50010-2008). Figure 2-9 shows specimen details. Both ends of the specimens were pin-connected. The load was applied on the top of the middle column using a hydraulic actuator with displacement control until the failure of the specimen. Figure 2-10 shows the test setup used.

The behaviour of the specimens was monitored by recording applied loads, vertical displacement and horizontal displacement of the supports and steel strains at sections near the supports.

From the test results, it was found that as the steel ratio increased, the ultimate load capacity of the specimens proportionally increased. As the steel grade decreased, the ultimate deformation of the specimens increased and the load capacity decreased. The specimens reinforced with round steel bars were much better than the specimens reinforced with ribbed steel bars in forming the catenary action mechanism since the round steel bars deformed more evenly and had larger elongation than the ribbed steel bars.

They concluded that the development of catenary action is strongly related to uniform elongation and strength of the steel, and the whole deformation process of the beam-column structure experienced all stages of elastic deformation, plastic deformation stage and catenary action.
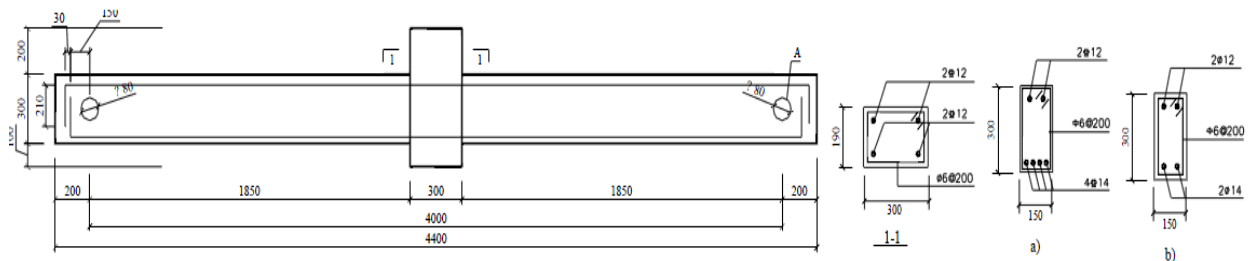


Figure 2-9 Specimens Detail (Wei-jian and Qing-feng 2008)



Figure 2-10 Photograph of test setup (Wei-jian and Qing-feng 2008)

## 2.2.5 Su et al. (2009)

In 2009, (Su et al., 2009) tested twelve one-third-scale frame sub-assemblages to investigate their capacity to resist progressive collapse. Each specimen represented a two-bay beam and three column stub, as shown in Figure 2-11.  The specimens were restrained longitudinally against axial deformation to study the effect of CAA on the capacity of the beam against progressive collapse.

The specimens were divided into three groups to study the effect of the following parameters: 1) Flexural reinforcement ratio (group A), 2) Beam span to depth ratio (group B), and 3) Rate of loading (group C). A servo-controlled actuator was used to simulate gravity loading by applying a downward displacement at the middle column stub.

The behaviour of the specimens is monitored by recording the following readings, the vertical load P, horizontal reaction N, and vertical displacement at the centre column stub. For each group, the vertical load P and horizontal reaction N versus centre deflection to depth ratio ($\delta/h$) were plotted as shown in Figures 2-12, 2-13 and 2-14.

From the test results, it was concluded that the axial restraint enhanced the CAA, and increased loading capacity by 50 to 160% of the capacity estimated without considering axial restraint. In addition, the increase of beam span-depth ratio and the increase of flexural reinforcement ratio caused a decrease in the effect of the CAA. The effect of loading rate can be neglected.
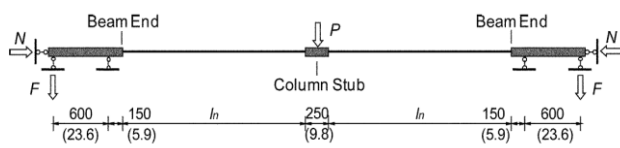


Figure 2-11 Schematic of the specimen
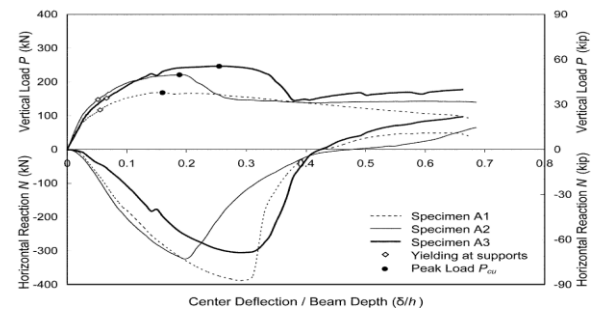


Figure 2-12 P and N versus ($\delta/h$) for group A
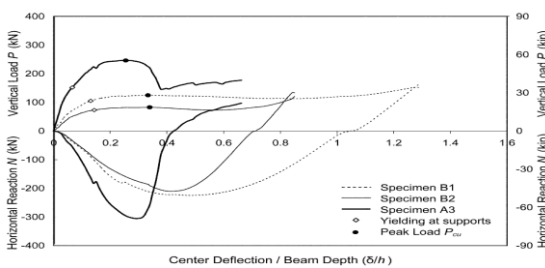


Figure 2-13 P and N versus ($\delta/h$) for group B
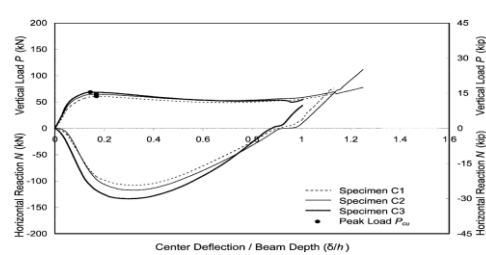


Figure 2-14 P and N versus ($\delta/h$) for group C

## 2.2.6 H. Choi and J. Kim (2010)

In 2010, (Choi and Kim, 2010) tested four sub-assemblages to investigate their structural capacity against progressive collapse. The specimens were one-third scale of two-bay and three column stubs sub-assemblages, which were designed as a part of five and eight-storey RC moment-resisting frames with and without seismic load according to the ACI 318-2005.

The specimen dimensions and reinforcement detailing is shown in Figure 2-15. The gravity load was applied by using a hydraulic actuator. The force-displacement relationship is plotted as shown in Figure 2-16.

From the test results, they observed that at failure, plastic hinges were developed at the ends of the beam associated with flexural cracks and crushing of the concrete, and specimens with low concrete strength failed to develop catenary action due to joint failure. In addition, they noticed from the force-middle joint displacement (MJD) relationship that the capacities of sub-assemblages designed for seismic load were larger than the capacities of the specimens designed without considering seismic load by about 200%.

They concluded that development of catenary action was significantly affected by concrete strength and anchorage detailing of reinforcement. RC frame structures seismically designed might have inherent resistance against progressive collapse while structures with low concrete strength might be susceptible to progressive collapse even if they were seismically designed.
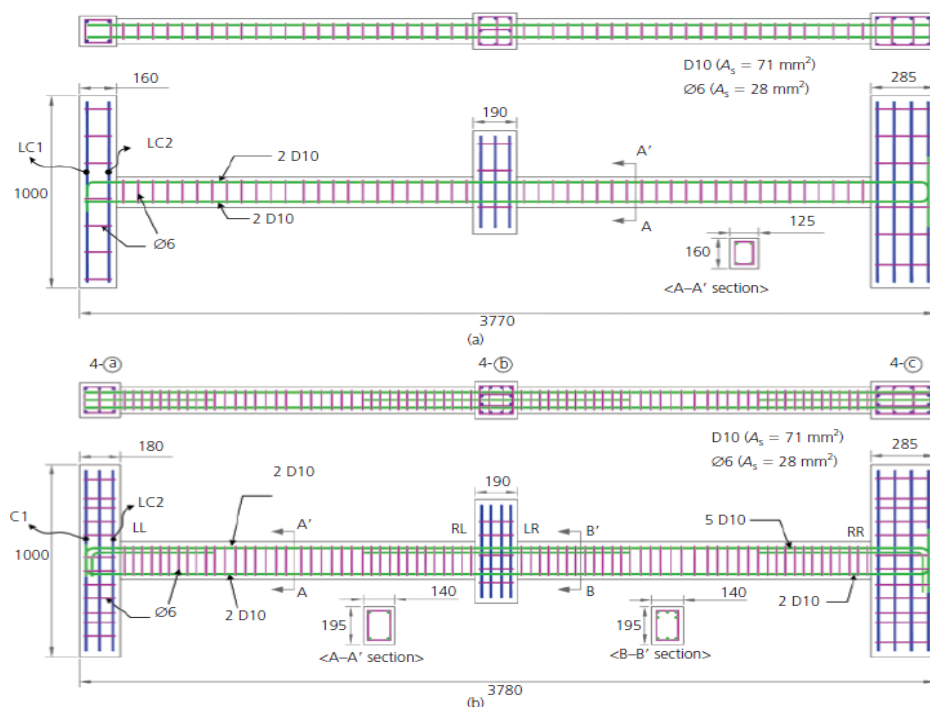


Figure 2-15 Detailing of 8-Storey Specimens. a) without seismic load, b) with a seismic load
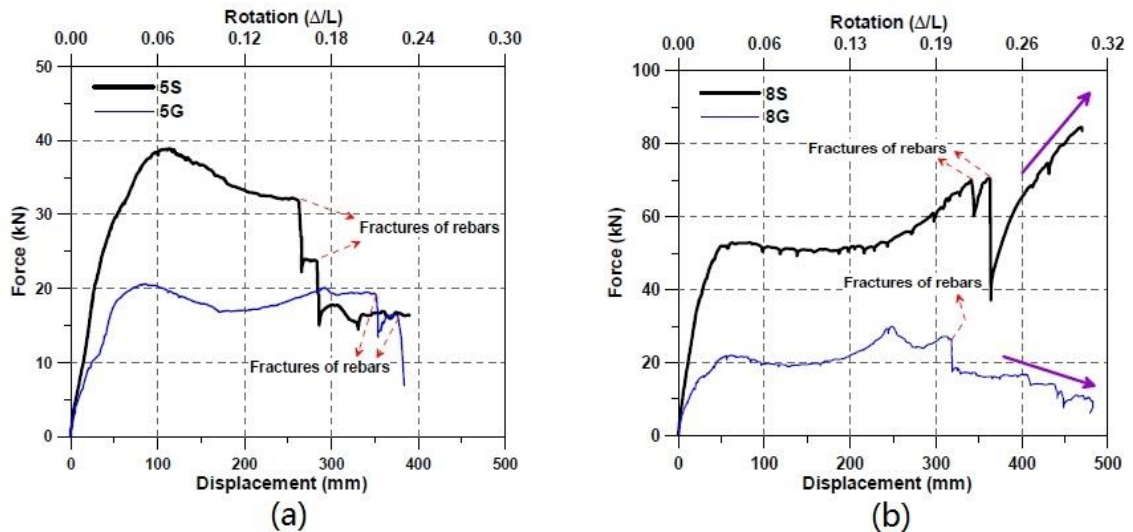
Figure 2-16: Force- MJD Relationship a) 5-storey, b) 8-storey (H. Choi and J. Kim 2010)

## 2.2.7 Sadek et al. (2011)

In 2011, (Sadek et al., 2011) carried out an experimental and computational program of work to investigate the performance of RC structures under CRS. The experimental program comprised of testing two full-scale sub-assemblages. Each assembly contained two-bay beams and three column stubs representing a part of the second floor of a 10-storey building designed and detailed in accordance with ACI 318-02. One specimen was designed without considering seismic load (IMF), and the other one was designed with seismic load consideration (SMF), the dimensions and reinforcement detailing is shown in Figure 2-17.

The gravity load was simulated by applying a controlled downward displacement at the centre column until failure using four hydraulic rams.

The computational program comprised of creating detailed and reduced finite element models to capture the response aspects of the same specimens tested in the experimental program and comparing the results. The main objective of the study was to simulate the behaviour and failure modes of structures under CRS, including the development of catenary action.

From the test results, they observed that the behaviour of both specimens (IMF) and (SMF) was similar, wherein a catenary action was developed preceded by flexural behaviour, which allowed the specimen to carry a higher load. At the end of the flexural phase, the load decreased due to the crushing of the concrete in the compression zone of the beam section adjacent to the centre column.

At the catenary action phase, the load increased as vertical displacement increases, the specimens reached their maximum load at a vertical displacement of 1090mm, 1220mm for (IMF) and (SMF) respectively. At this stage, the load dropped to approximately half of its maximum value, followed by further bar rupture, which causing specimen failure, Figures 2-18 and 2-19. In the comparison between the specimens, it was noticed that the failure displacements were fairly similar.

The maximum load of the (SMF) specimen was 2.25 times higher than that of (IMF) specimen. However, it was concluded that buildings designed without considering seismic loading are more vulnerable to progressive collapse. The computational program, in which detailed and reduced finite element models were created, showed a good agreement with the experimental program, which provided a modelling approach to represent the behaviour and failure modes of the assemblies under CRS.
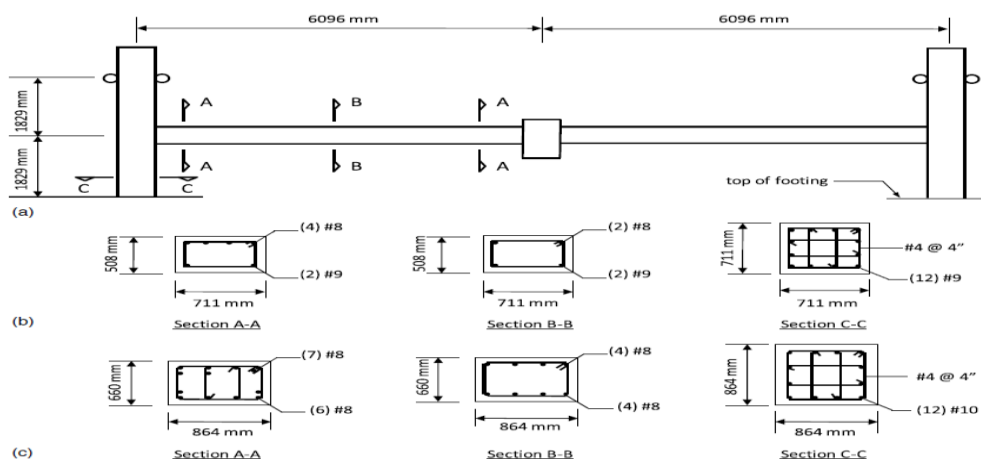


Figure 2-17 (a) Schematic of assemblies; (b) IMF; (c) SMF (Sadek et al. 2011
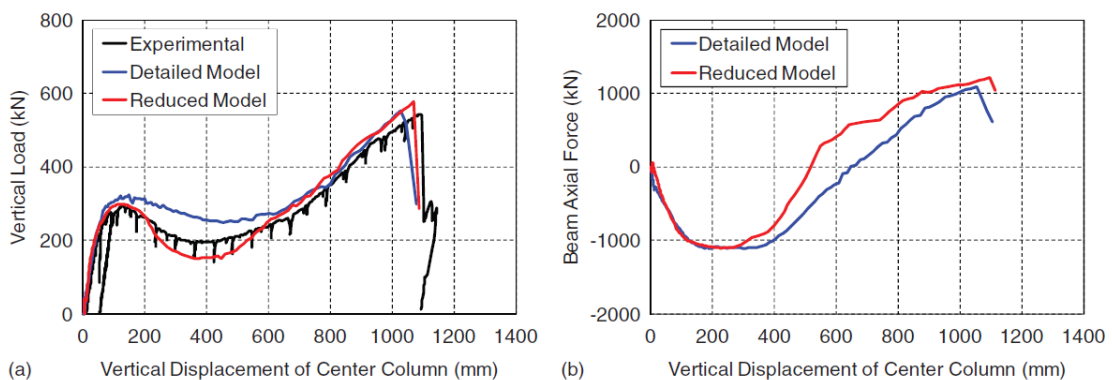


Figure 2-18 IMF Assembly: (a) Vertical load; (b) Axial Force vs. MJD (Sadek et al. 2011)
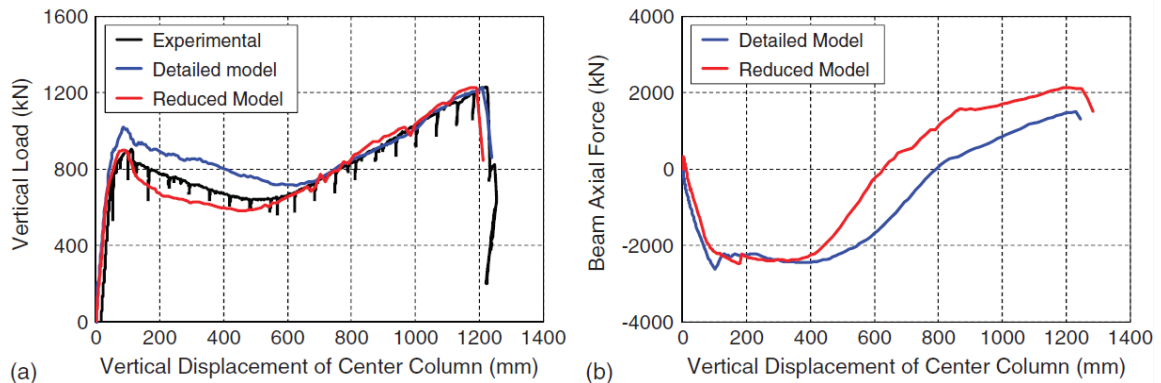
Figure 2-19 SMF Assembly: (a) Vertical load; (b) Axial Force vs. MJD (Sadek et al. 2011)

## 2.2.8 Tian and Su (2011)

In 2011, (Tian and Su, 2011) carried out an experimental study comprising four sub-assemblages to investigate the dynamic response of reinforced concrete beams under CRS. The specimens were half-scale comprising of two-span beam and three column stubs, extracted from an eight-bay, four-storey building designed and detailed in accordance with ACI 318-08. Figure 2-20 shows the dimensions of the specimens.

Two of specimens (D1, D2) were designed to resist seismic loads to investigate the effect of the compressive arch action on resistance capacity of RC structures against progressive collapse. Specimens (D3, D4) were designed according to the alternate load path approach in order to redistribute the loads, and sustain the redistributed internal forces under sudden column removal. All specimens were axially restrained except specimen D1.

Gravity loads were simulated by stacking and anchoring mass blocks made of concrete and cast iron into three locations as shown in Figure 2-21. Sudden column removal was simulated by quickly releasing the supporting force at the middle of the specimens. Each specimen was subjected to multiple tests by using different gravity loads, starting from a lower level of gravity load.

The maximum deflection at the centre column stub was restrained to protect the equipment, and provide safety during fast dynamic loading tests, for this reason, catenary action was not examined. The time-deflection history was recorded at the centre column stub for lower loading as shown in Figure 2-22.
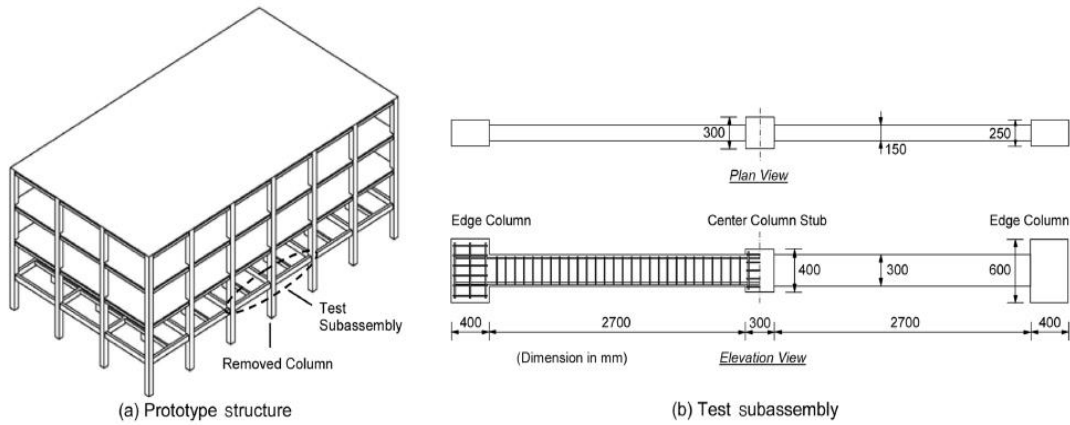
Figure 2-20 Prototype structure and test subassembly configuration (Tian and Su 2011)
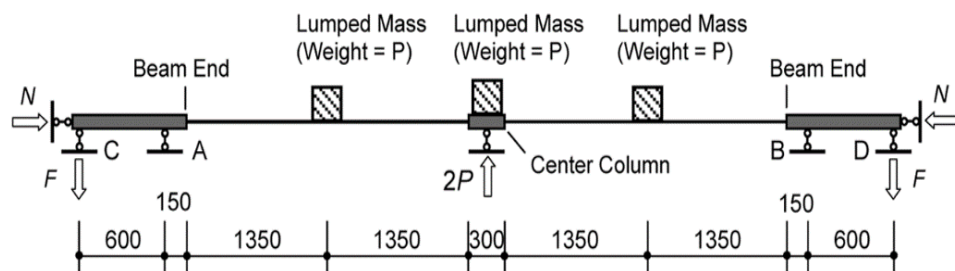


Figure 2-21 Gravity loads layout (Tian and Su 2011)
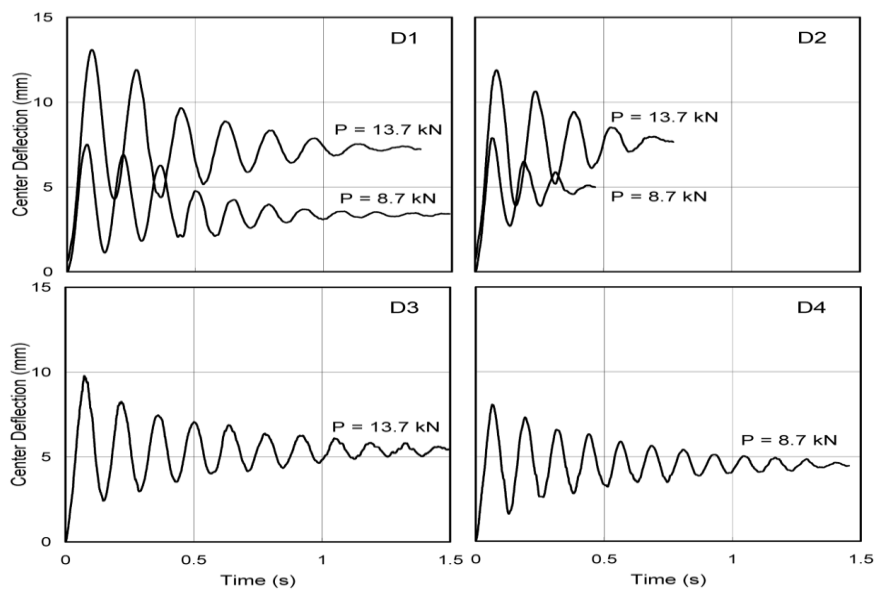


Figure 2-22 Centre deflection-time history at lower loads (Tian and Su 2011)

From the test results, it was observed that the maximum deflection occurred between 0.007 and 0.27 sec, and the dynamic wave ended at a steady-state within 2 seconds. In addition, it was noticed that the flexural crack occurred in the specimens even at the lowest load level causing a horizontal compressive force along the beam.

It was concluded that the compressive arch action increases the load-carrying capacity by more than 60% of the capacity without considering the effect of compressive arch action for specimens with a moderate reinforcement ratio, while it was less than 20% for specimens with high reinforcement ratio. On the other hand, the performance of specimen D2 showed that a seismically detailed beam possesses inherent progressive collapse resistance. In addition, they concluded that the effect of dynamic impact decreases with the increase of load levels.

### 2.2.9 Yu and Tan (2013)

In 2013, (Yu and Tan, 2013) tested eight RC sub-assemblages, consisting of two-bay beams and three column stubs to investigate the effect of the following parameters, 1) Top and bottom reinforcement ratios through joints (BRR) and (TRR), 2) Beam span-to-depth ratio on the structural behaviour of RC assemblies under CRS. The specimens were designed and detailed in accordance with ACI 318-05, with seismic and non-seismic detailing. Due to symmetry Figure 2-23 shows dimensions and schematic half of the specimen. In order to study the effect of beam span-to-depth ratios, the length ($L_n$) of two of the specimens were 2150mm and 1550mm and for the rest of the specimens was 2750mm.

Gravity load was simulated by applying a concentrated force at the top of the middle column stub using a hydraulic actuator at a controlled displacement rate of 0.1mm/s until the failure of the specimens. Horizontal reactions and vertical loads were recorded and plotted versus vertical displacement at the middle column stub as shown in Figures 2-24 and 2-25.
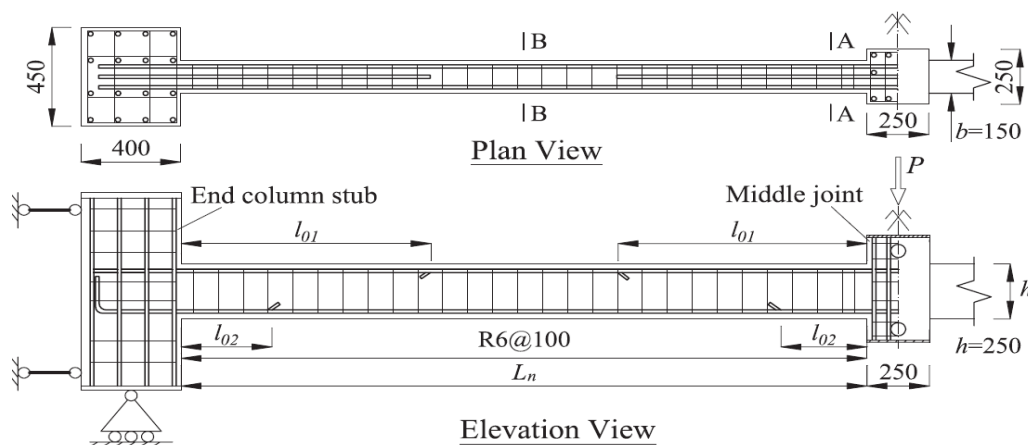


Figure 2-23 Dimension and Detailing specimens (unit: mm). (Yu and Tan 2012)
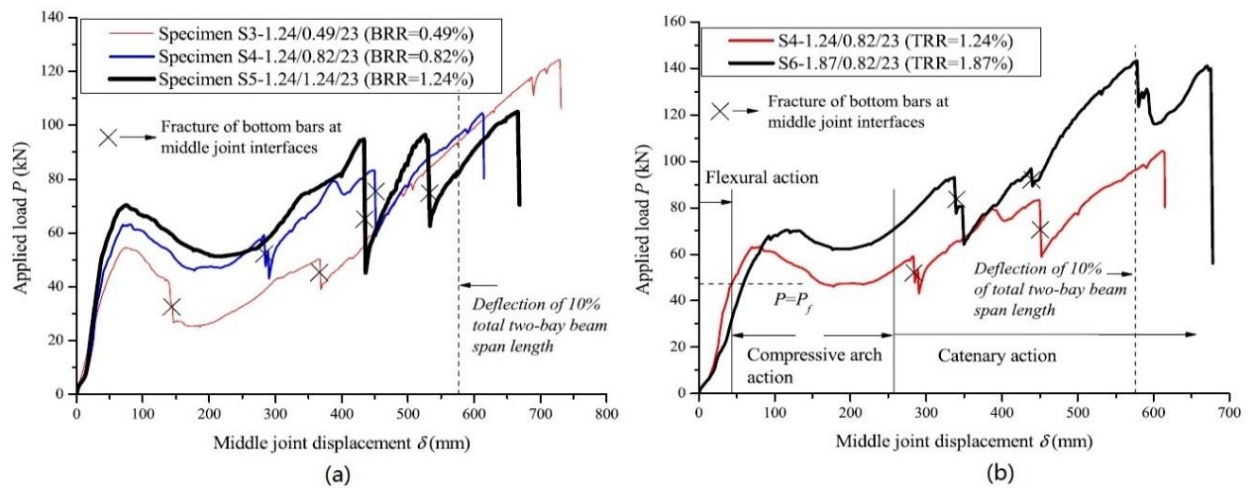
Figure 2-24 Load- MJD (a) Effect of (BRR); (b) Effect of (TRR) (Yu and Tan 2013)
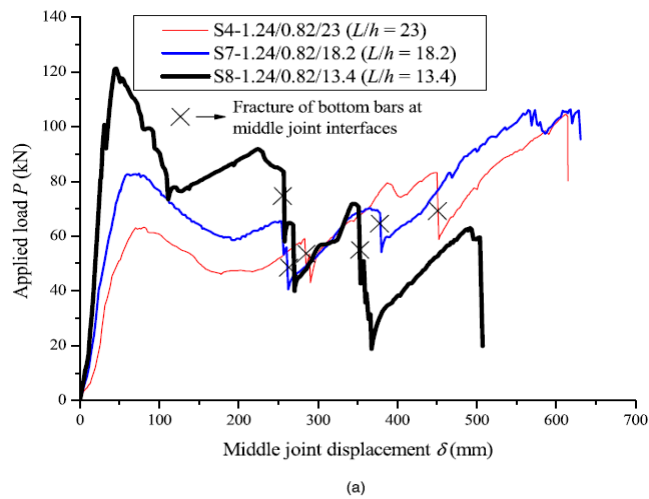


Figure 2-25 Effect of beam span- depth (a) load-MJD; (b) horizontal reaction-MJD

From the test results, they observed that the catenary action in most specimens was mobilised at a displacement equal to the beam depth, and bar fracture has a great effect on the axial tension force developed during the catenary action phase. Moreover, premature bar fracture can be caused by strain concentration of bars at column stub and middle joint interfaces, but it was difficult to predict the vertical displacement at middle joint corresponding to bar fracture.

It was concluded that the increase of beam span-to-depth ratio can significantly decrease the structural resistance during the compressive arch phase, and increases the structural resistance during catenary action. The CAA can increase the structural resistance with a low longitudinal reinforcement ratio. Symmetric longitudinal reinforcement detailing seems more favourable in the catenary action. This is because that the catenary action can be developed at smaller MJD.

Finally, it was pointed out, that all specimens failed at end column stub and middle joint interfaces, this was due to the strain concentration at these interfaces, therefore, measures should be taken to reduce this strain concentration.

## 2.2.10 Yu et.al (2014)

In 2014, (Yu et al., 2014) carried out an experimental study on three half-scale RC sub-assemblages to investigate the behaviour of reinforced concrete beams under dynamic redistribution of the loads after losing a column caused by contact detonation. Test results were compared with the results of quasi-static tests conducted by the same researcher in 2013. Three specimens (SD1, SD2, SD3) comprised of two-bay beams and three column stubs were designed and detailed without considering seismic loading in accordance with ACI 318-05. Due to symmetry, the geometric, dimensions and the detailing of one-half specimen are shown in Figure 2-26.

Gravity load was simulated by applying a concentrated load on the top of the middle column stub using two concrete blocks and a steel transfer frame. CRS was simulated by placing and detonating an explosive charge near the bottom of the middle column stub. Middle joint displacement, bar strains at critical sections, and horizontal reaction forces were recorded and plotted versus time as shown in Figures 2-27, 2-28 and 2-29.
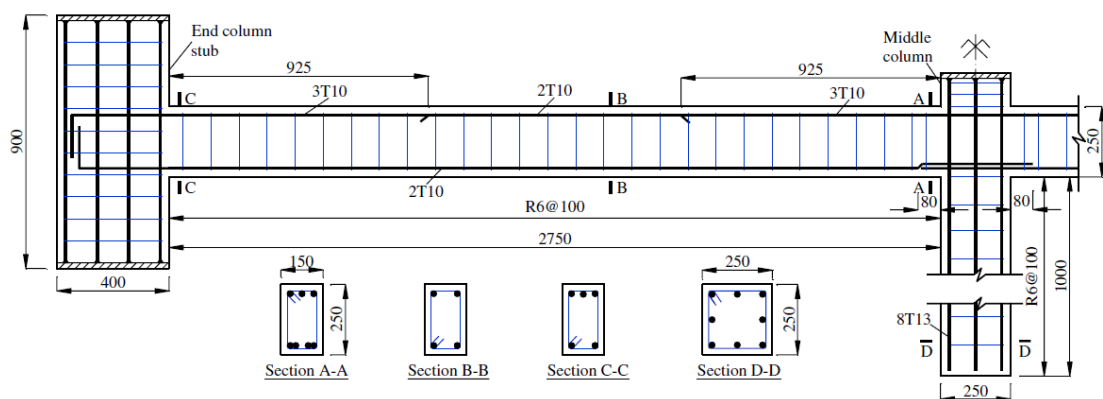


Figure 2-26 Specimen detailing, (unit: mm) (Yu et al 2014)
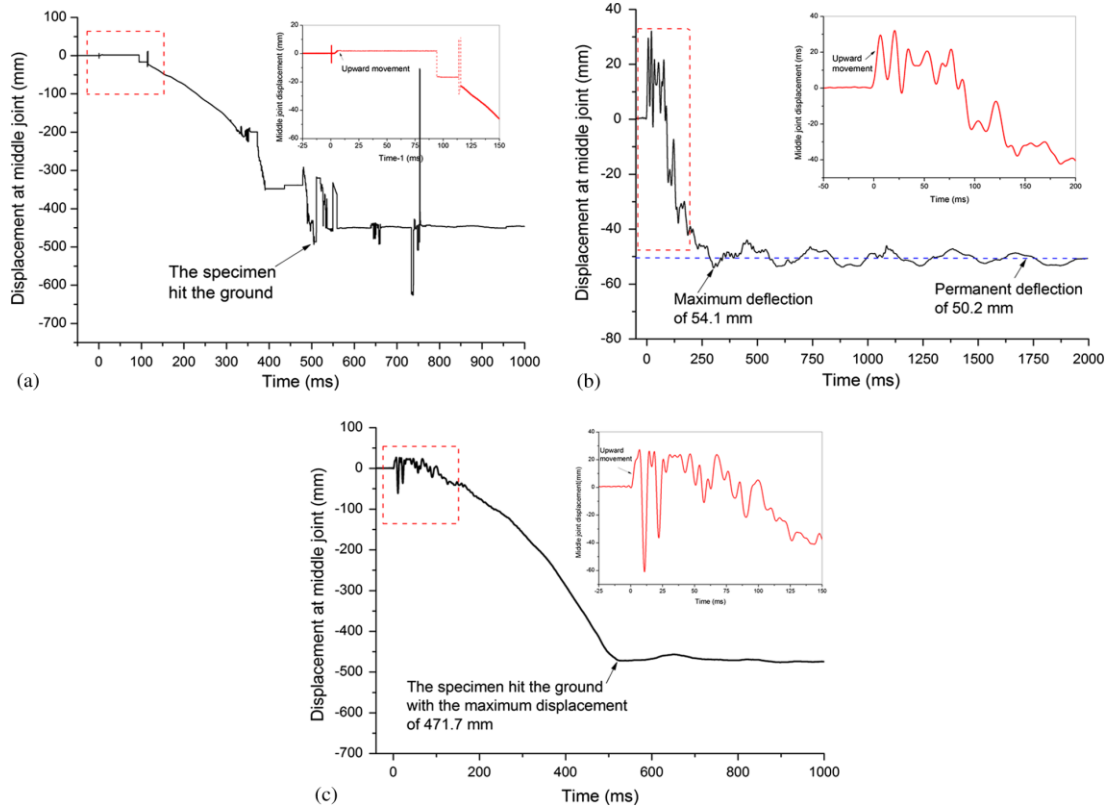
Figure 2-27 Time histories of middle joint displacements a) SD-1, b) SD-2, c) SD-3
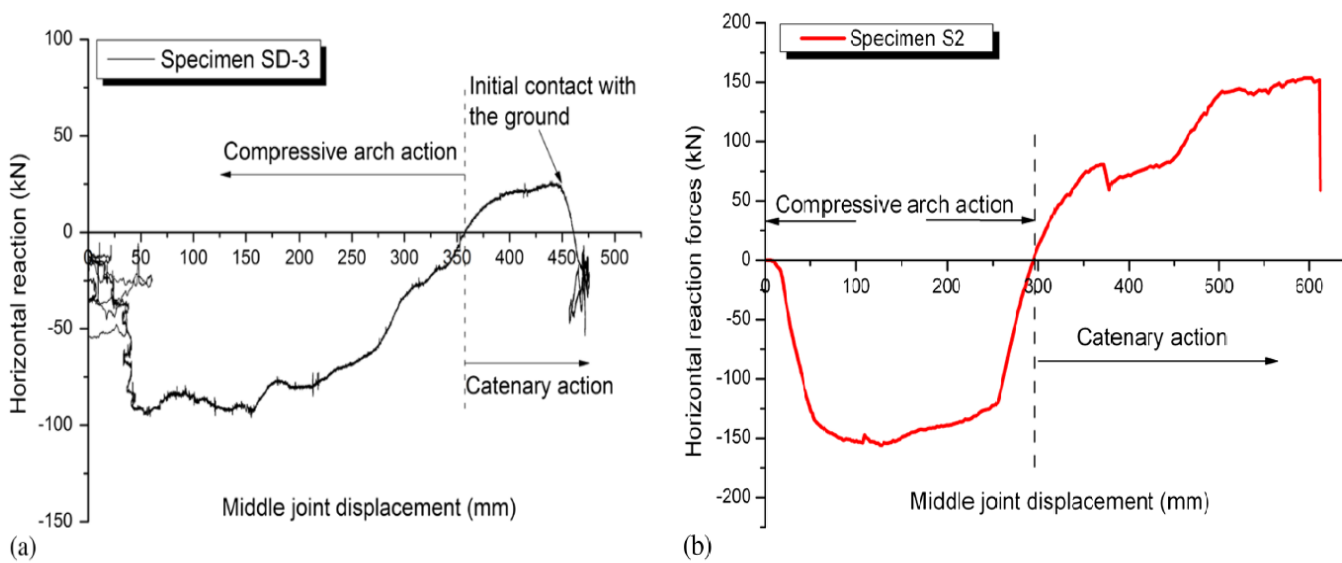


Figure 2-28 horizontal reaction versus MJD (a) in dynamic tests; (b) in static test
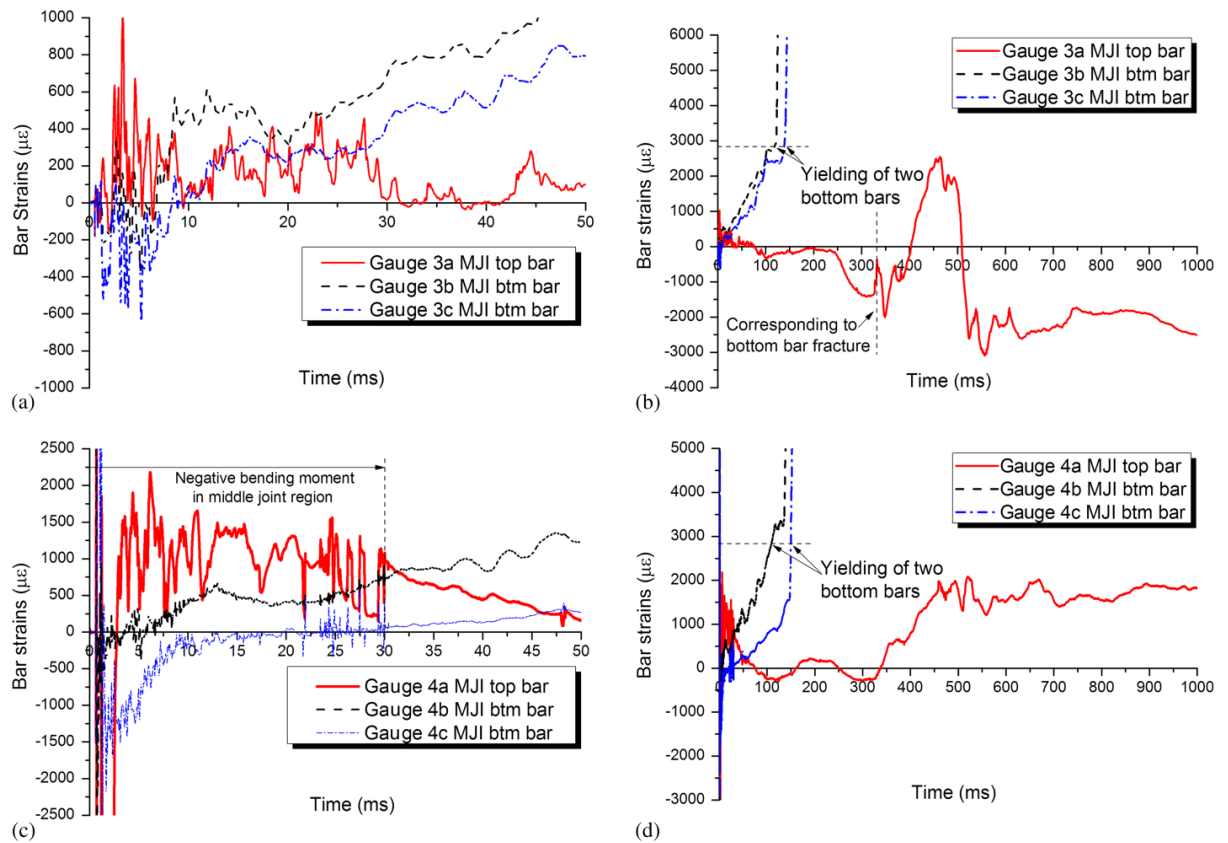
Figure 2-29 Time histories of bar strains at the middle joint interfaces of SD-1(Yu et al 2014)

From the test results, Yu et al observed that the middle column joint moved upward within the first few milliseconds due to explosion shock, after that, it moved downward under the effect of dead load, CAA and catenary action was sequentially developed. Specimens SD-1 and SD-3 moved downward until the residual middle column hit the ground.

Catenary action was not mobilised in specimen SD-2 due to the dead load applied being half of the ultimate capacity for the same specimen in the quasi-static test. Compared with quasi-static tests, the crack patterns and local failure modes, such as bar fracture and crushing of concrete during the dynamic tests were similar.

It was concluded that the dynamic load amplification factor (DLAF) calculated through this study take into account the initial damage caused by contact detonation, while (DLAF) calculated through the energy equilibrium approach proposed by Izzuddin et al. (2008) does not consider any initial damage at the onset of the progressive collapse, which leads to underestimating (DLAF) and further overestimate progressive collapse resistance.

### 2.2.11 Pour et al. (2015)

(Pour et al., 2015) tested six 2/5th scaled RC beam assemblages with different concrete compressive strengths, and two different longitudinal steel reinforcement arrangements. The longitudinal bar arrangement (samples with two or three longitudinal bars) and compressive strength of concrete were the main variables. The load was applied as a monotonically increasing displacement at the centre stub. Figure 2-30 shows the geometry and specimen dimensions.
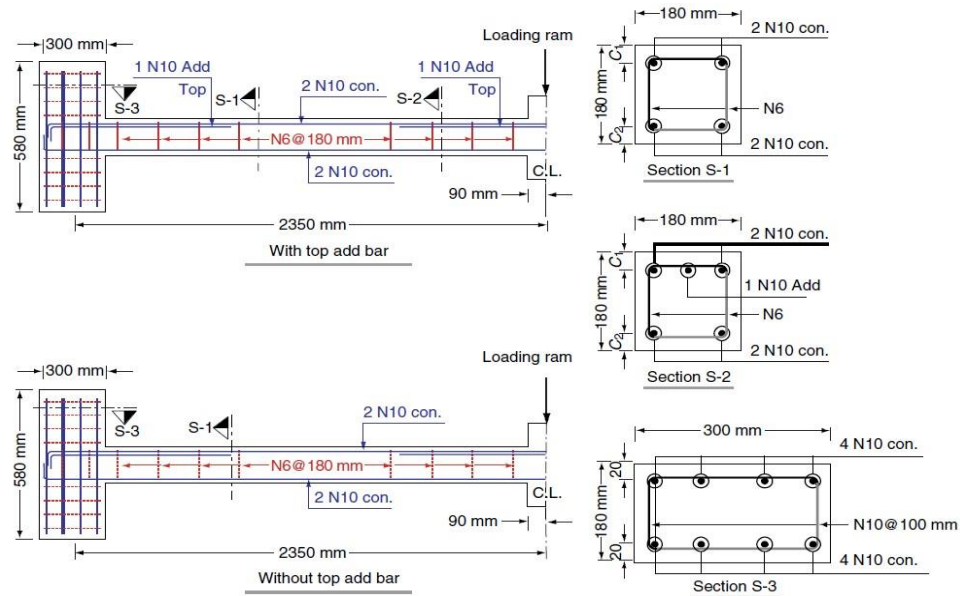


Figure 2-30 Specimen detailing (Pour et al. 2015)

Figure 2-31 shows the comparison between the test results of the specimens. They concluded that the concrete strength has a fairly significant effect on the peak capacity which is directly attributed to the development of CAA. The longitudinal reinforcing ratio significantly increases the peak load capacity at catenary action, while, the reinforcing ratio had a negligible effect on the loading capacity provided by the compressive arch action.
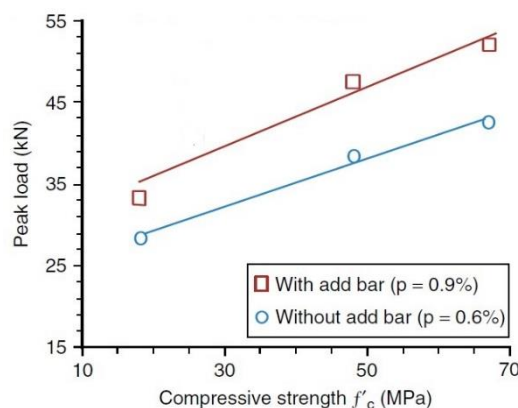


Figure 2-31 Experimental peak loads vs. concrete compressive strength (Pour et al. 2015)

## 2.2.12 Ahmadi et al. 2016

(Ahmadi et al., 2016) carried out a test on one specimen of $3/10^{th}$ scale to investigate the progressive collapse behaviour of reinforced concrete (RC) structures and the effect of specimen size on the test results. Test results were compared with results of a full-scale specimen tested by Sadek et al. (2011). Figure 2-32 shows the comparison between the full and reduced scale specimen.
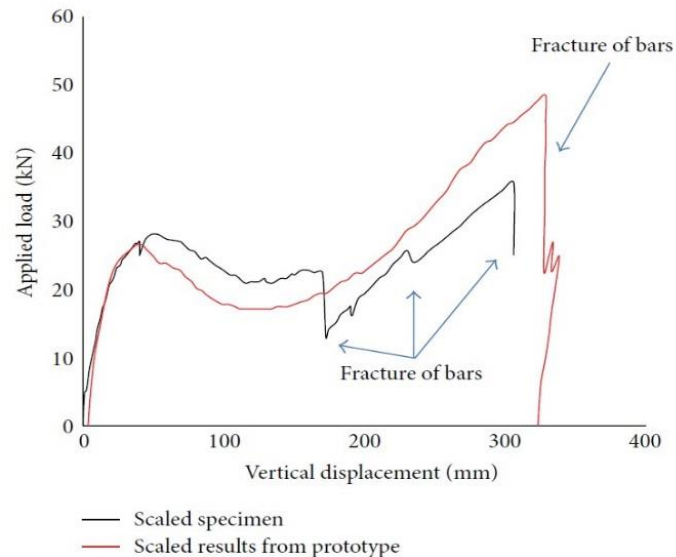


Figure 2-32 Comparison of results from scaled specimen and scaled results from prototype.

Ahmadi et al. found that the scaled specimen accurately predicted the structural behaviour of RC specimen in progressive collapse event. The number of cracks in the full-scale specimen was more than the scaled specimen.

## 2.2.13 Ren et al. (2016)

(Ren et al., 2016) tested seven one-third scale specimens to investigate the effect of section dimension and seismic detailing on the progressive collapse resisting capacity. Five beam–slab specimens and two continuous-beam specimens without slabs, were tested under a middle CRS. The specimens were tested by applying the load statically using two hydraulic actuators.

As can be seen from Figure 2-33, which shows the structural behaviour of all specimens, the general trend of the behaviour of both beams and slabs were similar. RC slabs can significantly increase the resisting capacity at both CAA and catenary action. The progressive collapse capacity at CAA was mainly affected by the beam depth, slab width and seismic reinforcement in the beams. The resistance at catenary action stage relied mainly on the area of the continuous reinforcement of the whole section.
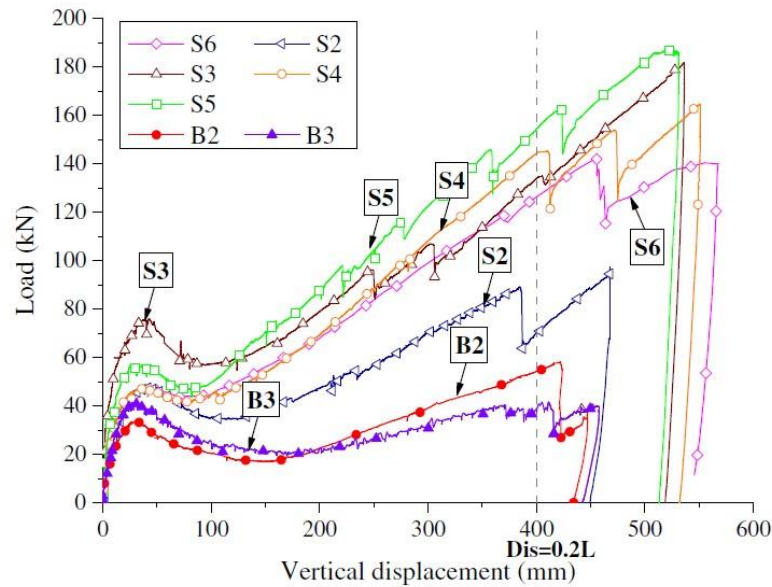
Figure 2-33 Load–displacement curves of all specimens (Ren et al. 2016)

## 2.3 NUMERICAL STUDIES:

In this section, computational, proposed models to simulate specimens under CRS and numerical studies will be reviewed focusing on studies investigating catenary action and its effect on the structural resistance to mitigate progressive collapse.

### 2.3.1 Lowes et al. (2003)

(Lowes et al., 2003a) developed a beam-column joint model (Macro-Model) to represent the response of RC beam-column joints under reversed cyclic loading. The configuration of the model includes four external nodes and four internal ones as shown in Figure 2-34.

In terms of components in the joint model, eight zero length bar-slip components are used to simulate the stiffness and strength loss due to anchorage failure of beam and column longitudinal reinforcement embedded within the joint. Four interface-shear components with zero length are used to simulate the loss of shear-transfer capacity due to shear transfer failure at the beam-joint and the column-joint interfaces.

Constitutive relationships are developed to define the load-deformation response of the joint model on the basis of material, geometric, and design parameters.

Comparison of simulated and observed response for a series of beam-column joint building sub-assemblages indicates that the proposed model represents well the fundamental characteristics of response for joints subjected to moderate shear demands.

44

Due to its capability to capture various mechanisms, macro-model was modified and used by researchers to simulate the response of RC beam-column joints in sub-assemblages under the CRS.
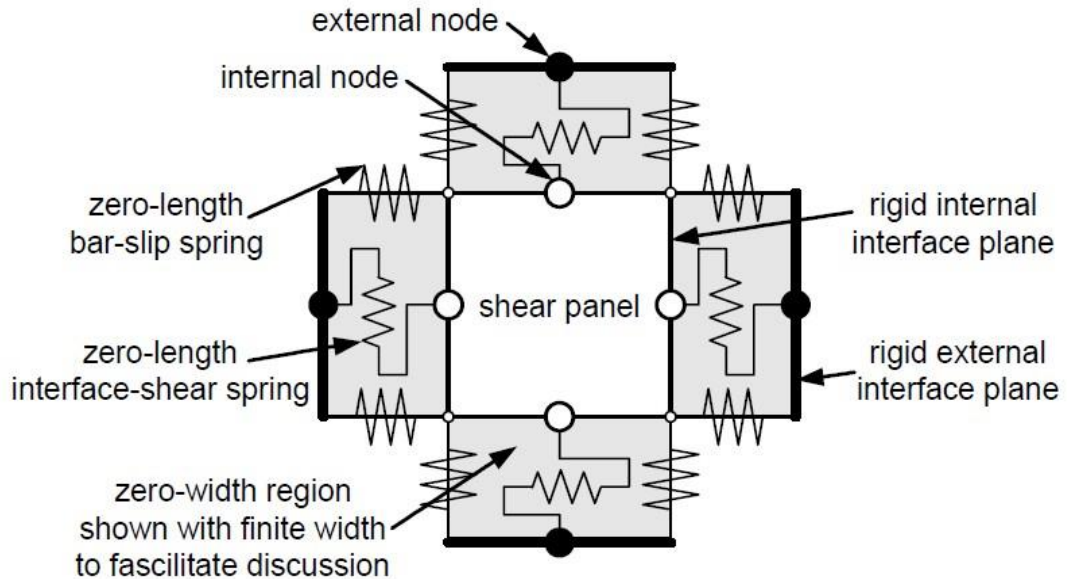


Figure 2-34 Components of the beam-column joint model Lowes et al. (2003)

## 2.3.2 Izzuddin et al (2008)

(Izzuddin et al., 2008) suggested a simplified approach to assess progressive collapse in multi-storey buildings subjected to sudden CRS. In this approach the structure is divided into different sub-levels of structural idealisation and the whole structural response for the building can be obtained from assembling the structural responses of these sub-levels.

The main steps of this approach are 1) Determination of nonlinear static response for each level considering the material and geometric non-linearity. 2) Determination of the pseudo-static response at each floor level. Izzuddin suggested that the pseudo-static response can be obtained from an energy conservation approach.

For a structure to resist progressive collapse in the event of column removal, this approach requires that the work done by the external loads due to gravity equals the energy absorbed by the structure. Figure 2-35 shows the calculation of the pseudo-static curve.

Izzuddin stated that the pseudo-static response can be used as a measure of robustness, which accounts for combined influence of energy absorption capacity, redundancy and ductility on the overall system level. In this approach, the effect of damping was neglected because the event of progressive collapse occurs in a very short time and the damping consumes little energy. The accuracy of this approach has been validated by (Tsai, 2010).
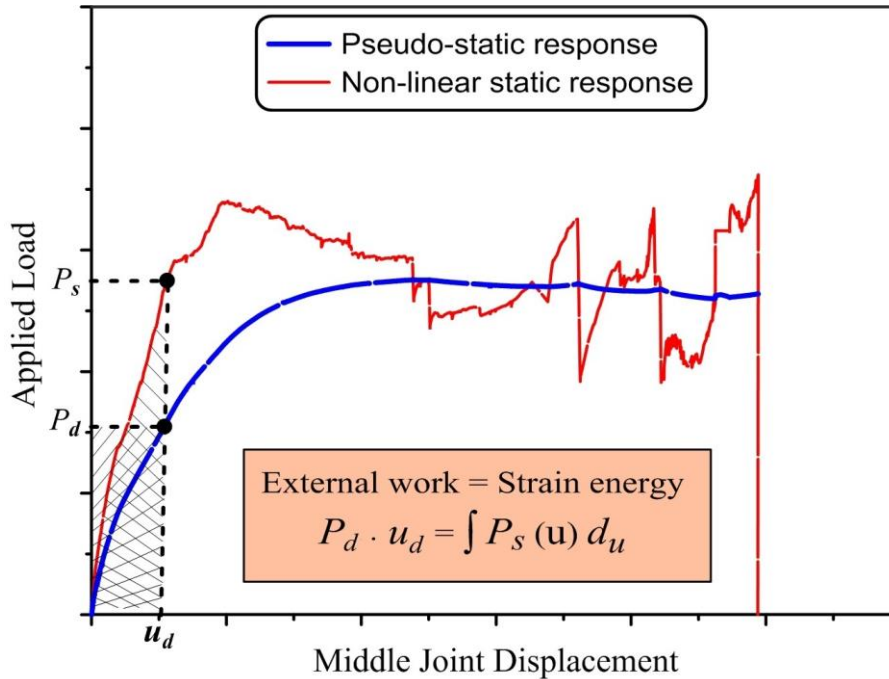
Figure 2-35 Calculating pseudo-static response

### 2.3.3 Bao et al. (2008)

In 2008, (Bao et al., 2008) conducted a numerical simulation of two prototype buildings to study the potential for progressive collapse of RC framed structures under CRS. A macro-model based approach was used in this study. In this model, a simplified beam-column joint is used to represent critical sections by using a series of non-linear spring elements to reflect the non-linear behaviour associated with the redistribution of loads under CRS to predict the large deformation associated with progressive collapse, as shown in Figure 2-36. A detailed finite element model was used to validate the proposed macro-model. Two sub-assemblages both seismically and non-seismically designed were considered in the study, gravity loads were applied to two-dimensional models of the frames and then one or more first storey columns were removed.

The open source platform Open-Sees (2007) was used to create and demonstrate the utility of the proposed macro-model, while for the detailed finite element model the commercial software DIANA (2006) was used.
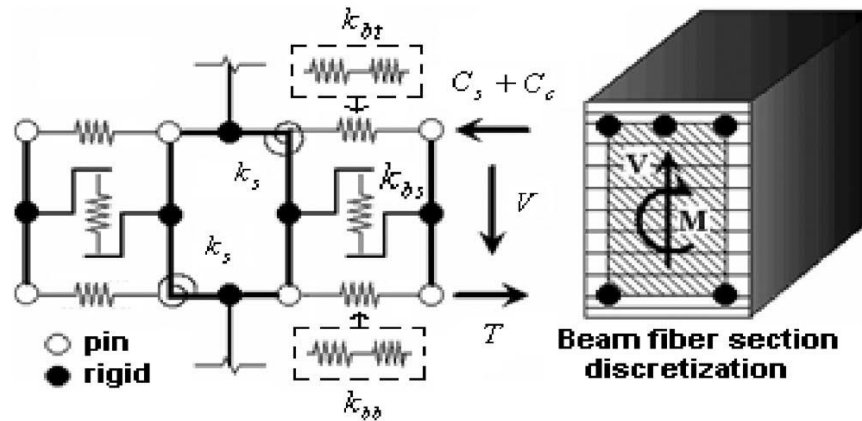
Figure 2-36 Spring Assembly (Bao et al. 2008)

It was concluded that the inelastic models more accurately characterise the non-linear behaviour to capture the large deformation occurring under CRS. In addition, they concluded that the macro-model is a viable alternative to the detailed finite element models, which can reduce the time consumed through building a model. Finally, they concluded that the frame designed for seismic loads was less vulnerable to progressive collapse than the frame designed without considering seismic loads.

## 2.3.4 Salem et al. (2011)

Finite element method is accepted as a reliable structural analysis approach, but the separation, falling and collision with other elements simulation would be relatively difficult. Another approach which was used by (Salem et al., 2011) is called Applied Element Method (AEM). This method is capable of applying dynamic analysis, to simulate and capture the falling and separation of different elements of structures. This method can be considered as an efficient method using the discrete cracking concept (Salem et al., 2011).

In the AEM method, the various elements of structures are virtually divided and then their surfaces are connected together using a set of normal and shear springs as shown in Figure 2-37. The contact points are distributed on the face of the elements and two adjacent elements are separated when one of these springs are ruptured. Extreme Loading for Structures (ELS) was used to simulate progressive collapse failure under CRS.

It was concluded that the AEM is an efficient, accurate and simple tool for progressive collapse analysis compared with FEM, and can be used as an analytical tool to suggest economical designs that are safe against progressive collapse of RC structure.
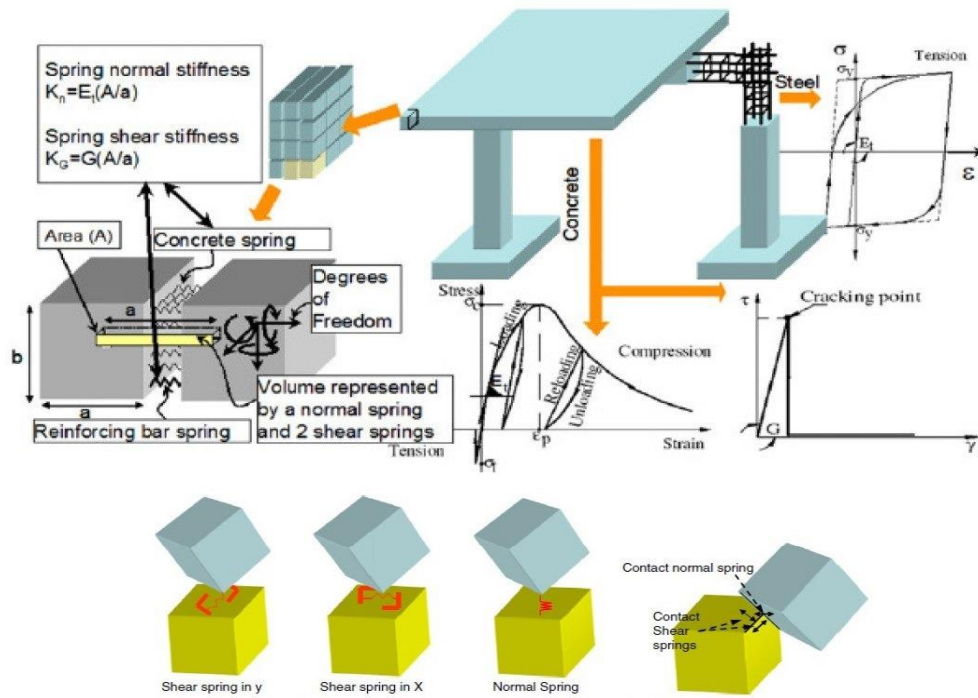
Figure 2-37 AEM modelling concept with shear and normal springs (Salem et al. 2011)

## 2.3.5 Kim and Yu (2012)

(Kim and Yu, 2012) conducted a study to investigate the potential of progressive collapse for RC frames subjected to a sudden column loss. Three RC frames were designed as a model structure for analysis with and without considering seismic load in accordance with ACI 318-02. They used fibre-based elements to represent the critical sections in the specimens.

The models were developed and analysed using the Open-Sees (2007) software, nonlinear static and dynamic analysis was performed. Dimensions and detailing of steel reinforcement are shown in Figure 2-38.

They concluded that the specimens designed without considering seismic load are more vulnerable to progressive collapse. Also, they concluded that the ratio of longitudinal reinforcement has a great effect on the development of catenary action. In addition, the increase in transverse reinforcement led to an increase in concrete confinement, this results as an increase in ductility, which causes an earlier development of catenary action.
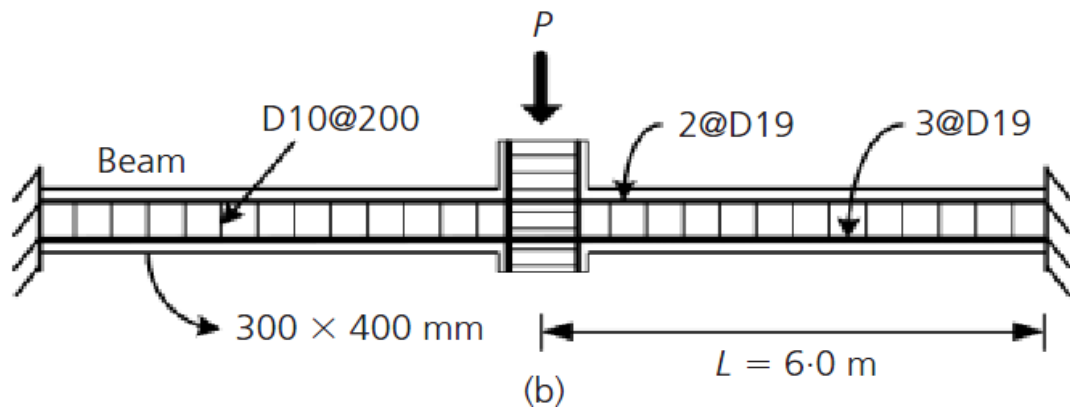
Figure 2-38: Beam–column sub-assemblage analysis Model (Kim and Yu 2012)

## 2.3.6 Yu and Tan (2013)

Yu and Tan carried out a finite element analysis and proposed a component-base model to simulate the structural response of two specimens after they were tested experimentally, then they compared the results with those obtained from the experimental study.

The joint model consisted of a series of nonlinear springs to characterise bond-slip behaviour under large tensioning. Figure 2-39 shows the joint model details. Beams and columns were modelled using fibre elements, which were able to simulate flexural and axial actions in structural members.
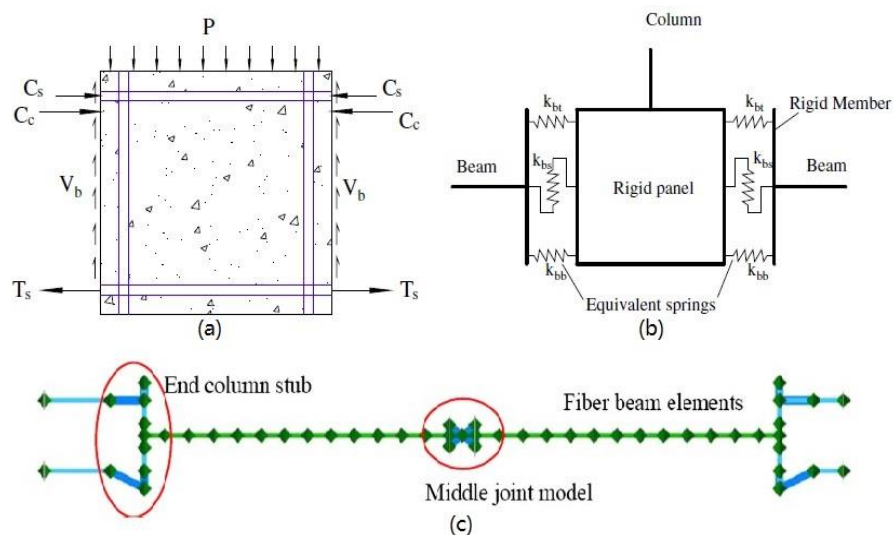


Figure 2-39 (a) Actual middle joint, (b) Joint model, (c) Specimen model (Yu and Tan 2013)

They noticed during the tests that, although no appreciable shear behaviour developed at the joint panel, significant bond-slip behaviour and bar fracture occurred near the middle joint. Therefore, simulation of the joint was realistic and compared well with the rigid joint behaviour, as shown in Figure 2-40.

49
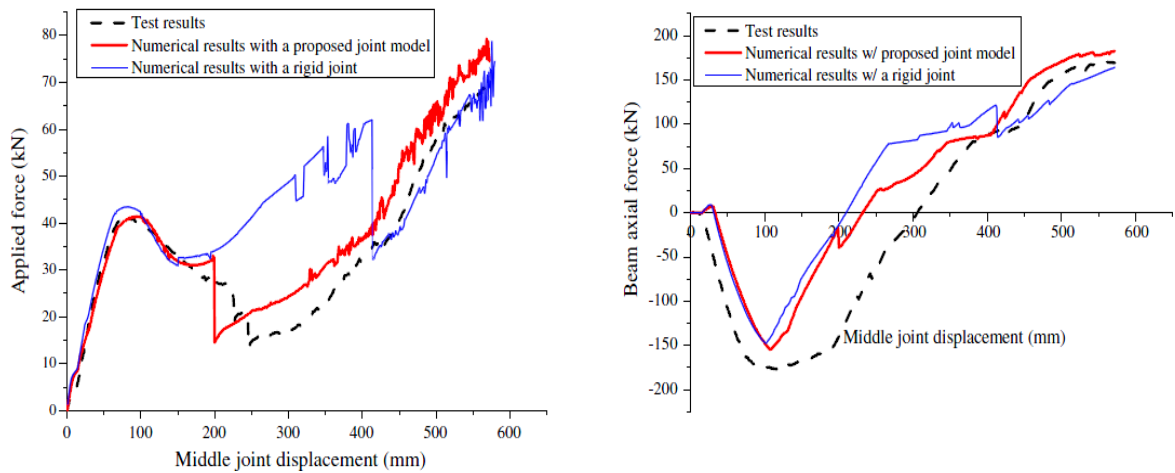
Figure 2-40 Comparison of Experimental and Numerical Results (Yu and Tan 2013).

From the failure modes of the specimen, it was concluded that it is imperative to model the joint behaviour separately. In the context of using a macro-model based FE analysis, compared with a rigid joint model, the proposed component-based joint model was capable of capturing the structural responses for different structural mechanisms.

## 2.3.7 Li et al. (2016)

(Li et al., 2016) conducted a nonlinear static pushdown analysis to evaluate the progressive collapse-resisting capacity curves of typical RC frames under different deformations. Unlike the previous studies in which only a few typical columns, such as a column on the bottom storey, are removed, in this study, they examined the column removal scenarios for various typical locations from different stories.

A fiber beam element model named THUFIBER was used to build the numerical model of the frames. THUFIBER takes into account the complex interaction mechanisms of the internal forces in the beam sections and has a robust material models covering both unloading and reloading paths.

The main finding was that the seismic designs significantly improve the progressive collapse resistance under the beam mechanism, especially for lower stories. However, such an improvement is less significant for the catenary mechanism and little improvement was found for the top regions of the frame structures.

## 2.4 APPROACHES TO MITIGATE PROGRESSIVE COLLAPSE

In this section, the approaches to mitigate progressive collapse will be presented and reviewed. Few researchers have proposed specific schemes to mitigate progressive collapse by increasing the integrity, continuity and ductility of structural members.

### 2.4.1 (Crawford, 2002)

(Crawford, 2002) suggested to increase column strength by wrapping the column with carbon fibre reinforcement polymer (CFRP). This will prevent the column failure resulting from blast and as a result mitigating the structure against progressive collapse as shown in Figure 2-41. Also, he suggested to increase progressive collapse resistance by tying the members using steel cables to provide an additional path to redistribute the load under CRS as shown in Figure 2-42.

It was recommended that much research is still needed with respect to retrofitting buildings to prevent progressive collapse. Predicting the ability of damaged structural systems to redistribute the load from damaged column was also is needed.



Figure 2-41 Composite wrap for reinforced concrete column (Crawford, 2002)
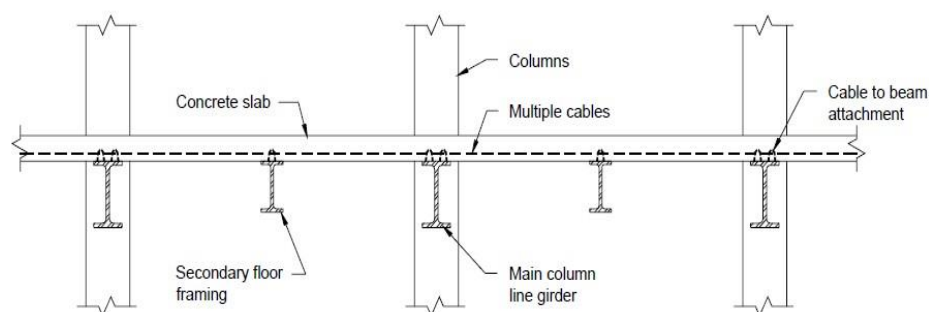


Figure 2-42 Cabling retrofit concept (Crawford, 2002)

## 2.4.2 (Astaneh-Asl, 2003)

(Astaneh-Asl, 2003) suggested to use steel cables embedded in the concrete beams and floors in order to provide the members with tensile forces and carry the loads by catenary means in the event of progressive collapse. Figure 2-43 shows the schematic of the proposed scheme to mitigate progressive collapse.
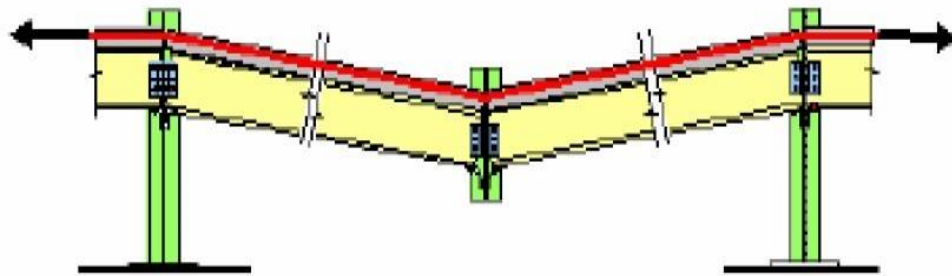


Figure 2-43 Mitigation scheme using steel cables (Astaneh-Asl 2003)

Based on the test results of full-scale specimen, it was concluded that using steel cables in the floor slabs of steel structures progressive collapse of steel structures could be easily and economically prevented. Also, existing buildings can be retrofitted to prevent their progressive collapse under CRS. The retrofit system consisting of cables placed on the side of steel beams could efficiently prevent progressive collapse of the floors when a column is removed.

## 2.4.3 (Orton, 2007)

In 2007, Orton tested eight half-scaled beams to study the effect of applying CFRP to replace the lack of continuity in RC beams without continuous reinforcement to develop catenary action under the column removal condition. The dimensions of the specimen were 12 in. by 6 in. cross section (300 mm by 150 mm), and 30 ft. length (9000 mm). The 30 ft. length consisted of two 12 ft. spans and an additional 3 ft. span on each end to provide restraint during testing.

The detailing and design of the beams were in accordance with ACI 318-1971 in which, negative and positive moment reinforcement were not continuous, accept one beam which was designed according to ACI 318-2005 in which continuous reinforcement was provided in order to compare the results with the results of CFRP retrofitting. Figure 2-44 shows detailing and dimension of the specimens.

CFRP was used to provide continuity through the positive and negative moment reinforcement for different beams, one of the specimens remains without retrofitting, and the specimens were tested in an inverted position in a force-controlled manner.
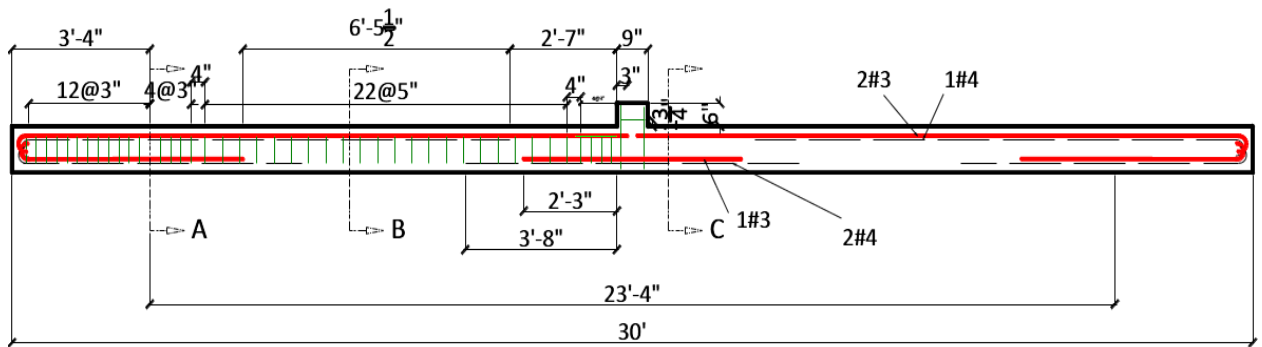
Figure 2-44: Specimen's Detail for Orton's tests (Orton 2007)

The test results indicated that the specimen NR-2, which was a beam without continuous reinforcement and with no retrofitting, experienced a compressive arch phase until the beam deflection reached about 17 in.(430mm) at midspan, which is about 5% of the length of the beam. This phase was followed by the catenary action phase, allowing the beam to carry a load twice the load observed before the beginning of catenary action, but still less than 10kip which is recommended by GSA to prevent progressive collapse.

Test results of specimen CR-1, which was a beam with continuous reinforcement indicated that the beam was not able to carry the recommended load by GSA due to limited ductility in the beam. This limited ductility caused the fracture of continuous reinforcement in the positive moment region, followed by the fracture of negative moment reinforcement. Orton noticed that the beam CR-1 behaved like beam NR-2, which had no continuous reinforcement after the fracture of continuous bars.

Orton concluded that the CFRP, which was used to improve the continuity in the positive moment region, was able to enhance the strength of the beam before catenary action developed. However, the specimens PM-1 and PM-2, which were retrofitted in the positive moment region, were not able to reach the recommended load by GSA, due to the retrofitting causing a concentrated hinge at the end of CFRP sheet, thus leading to fracture of CFRP sheet, and eventually the beam behaved like an un-retrofitted beam.

Orton also concluded that the specimens NM-1 and NM-2, which were retrofitted by CFRP in the negative moment region, were able to carry the load recommended by GSA. In both specimens, there was sufficient ductility to form a hinge at the supports which led to developing catenary action, thereby allowed the beam to carry more vertical loads.

In general, the findings of Orton's tests were similar to the results reported by Regan (1975), including the significance of ductility to develop catenary action, and catenary action would not develop until the beam deflection reach the beam depth (or slightly greater). A comparison of the vertical load versus displacement for the tests is shown in Figure 2-45.
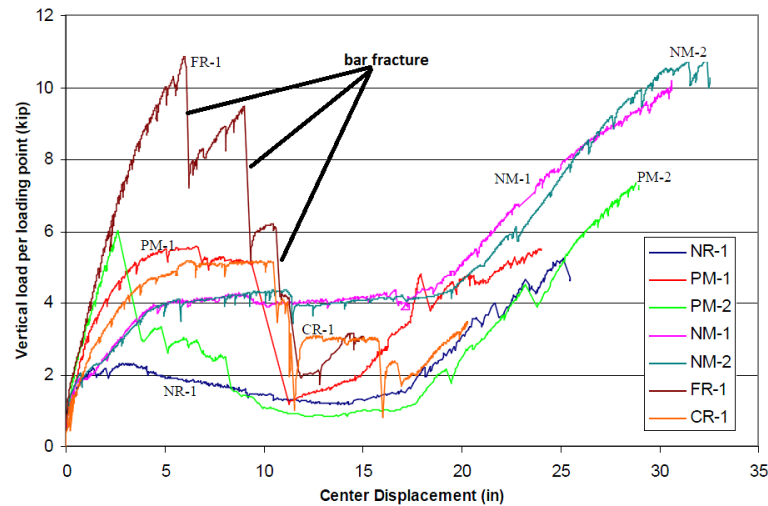


Figure 2-45 Vertical load versus displacement for all tests (Orton 2007)

## 2.4.4 (Mohamed, 2009)

(Mohamed, 2009) conducted three-dimensional analysis to investigate the effect of column loss of corner floor panels on the ability of RC structures to resist progressive collapse. Also, it was proposed using steel bracing in the corner panels to mitigate progressive collapse under corner column removal.

An eight storey RC building strengthened by steel bracings was utilized in the analysis. Different configurations of steel bracing were used including tension and compression diagonal bracings at corner panels of the building as shown in Figure 2-46.

Based on the analysis results, it was concluded that the bracing system was able to increase the building capacity against progressive collapse. The increase is related to the improvement in the building redundancy accomplished by using steel bracing system.
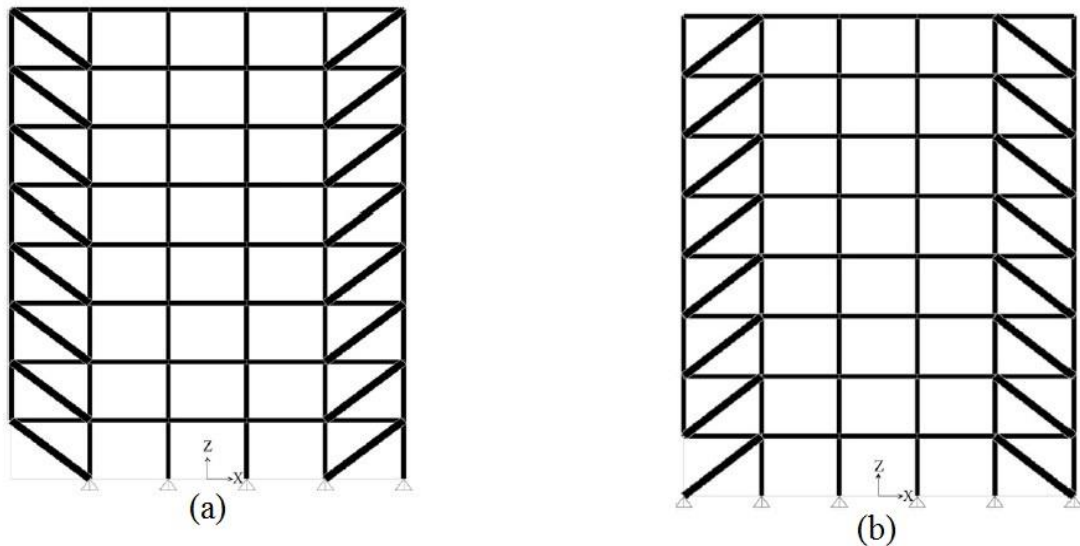
Figure 2-46: Bracing system, (a) Compression, (b) Tension (Mohamed, 2009)

It was recommended to conduct experimental tests to validate the obtained numerical analysis results. In addition, different configuration of steel bracing need to be investigated in order to optimize the best configuration in preventing progressive collapse in RC structures.

## 2.4.5 (Kim and Shin, 2011)

(Kim and Shin, 2011) suggested to use pre-stressed tendons as a mitigation scheme to prevent progressive collapse in RC structures. A finite element model of a six storey structure with three-by-four bays retrofitted with external pre-stressed tendons was analysed using the Opeen-Sees software. Two types of arrangement of high strength tendons were used as shown in Figure 2-47.
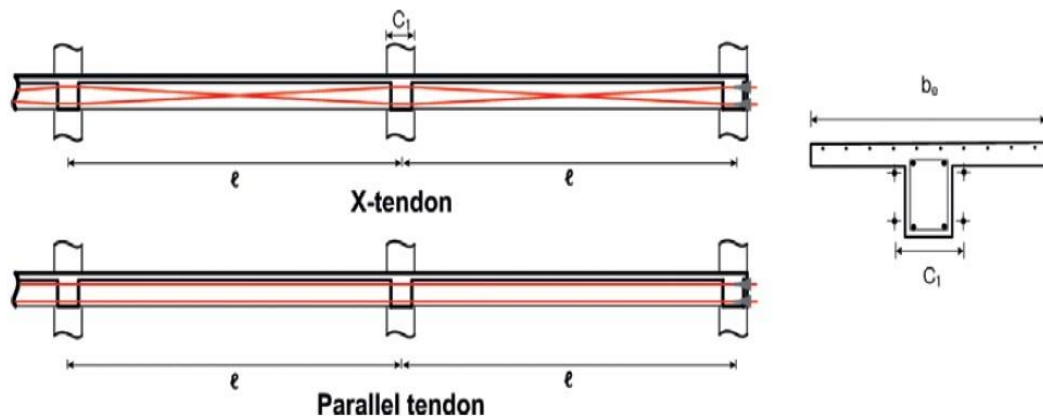


Figure 2-47 Arrangement of tendons along the beams

Nonlinear static and dynamic analysis were carried out to investigate the effect of tendons on the progressive collapse performance. From the test results, Figure 2-48, Kim and Shin concluded that the analysis model structure before retrofit was vulnerable to progressive collapse caused by sudden loss of a first-story column.

The RC model reinforced by external pre-stressing tendons showed stable behaviour against progressive collapse. They concluded that the retrofit of existing buildings using pre-stressing tendons could be effective for enhancing progressive collapse resisting capacity as well as seismic performance.
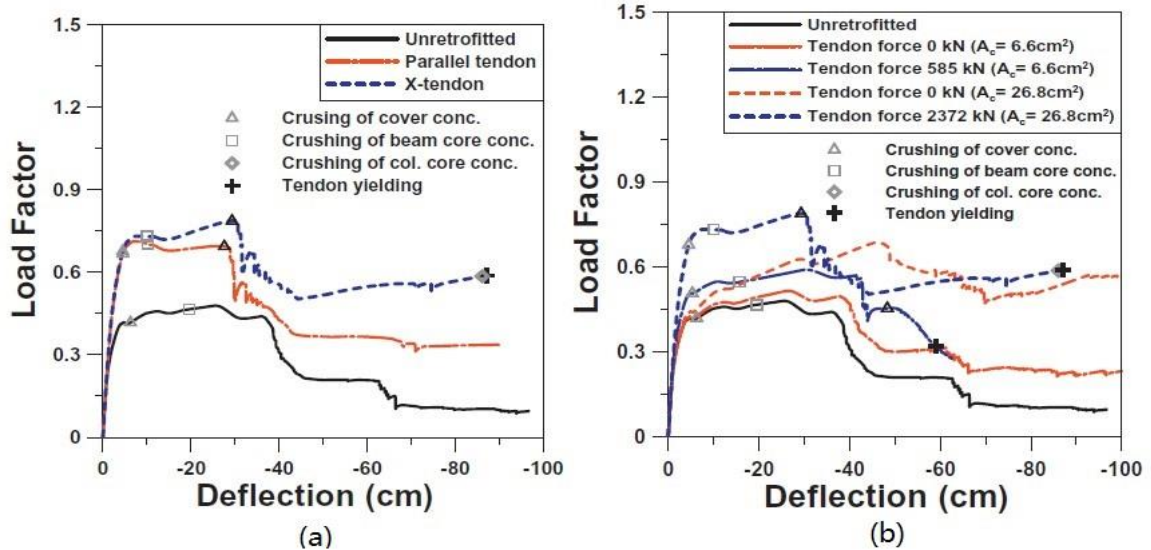


Figure 2-48: (a) Tendon arrangement, (b) Initial tension (x-tendon) (Kim and Shin (2011)

## 2.4.6 (Hadi and Alrudaini, 2012)

(Hadi and Alrudaini, 2012) proposed a new scheme for strengthening new and existing buildings in order to resist progressive collapse. The main idea of the scheme is to use vertical cables parallel to the building's columns. The cables to be connected at the beam ends and hanged from a steel braced frame seated on the top of the building as shown in Figure 2-49.

The proposed scheme was then validated through finite element analysis using ANSYS 11.0. The results showed that the proposed scheme was able to redistribute the load to the cables and mitigating progressive collapse in the building.

It was recommended by (Hadi and Alrudaini, 2012) conducting an experimental investigations on prototype of RC buildings retrofitted with the proposed scheme to compare the results with that obtained from the numerical study.
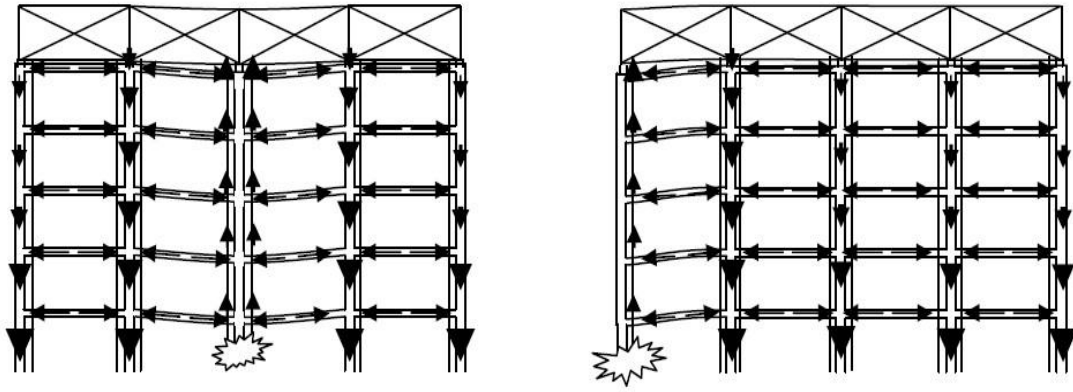
Figure 2-49 Building configuration with the cable mitigation (Hadi and Alrudaini, 2012)

## 2.4.7 (Yu and Tan 2014)

(Yu and Tan, 2014) suggested to use special techniques to improve structural resistance of RC structures against progressive collapse. The techniques included partially de-bonding bottom reinforcing bars in the beam-column region, placing an additional steel bars at the mid-height of beam section, and setting partial hinges at one beam depth away from the adjacent joint interfaces.

The de-bonding technique was used in an attempt to reduce the strain concentration in the steel reinforcement, while partial hinges were used to improve the rotation capacity of RC beam-column joint connection.

Based on experimental test results, it was concluded that using de-bonding technique is not recommended for structural design against progressive collapse as there was a decrease in the progressive collapse capacity by about 10% compared with the fully bonded steel reinforcement. Partial hinges were able to enhance progressive collapse capacity at catenary action stage by about 37% compared with the capacity of specimen without partial hinges.

It was recommended and suggested if more reinforcing bars are placed at beam sections, the locations of partial hinges and the additional steel bars can be optimized. More tests are needed on specimens with partial hinges to optimize the location of partial hinges.

## 2.4.8 (Kim and Choi, 2015)

(Kim and Choi, 2015) suggested to add a strand to the longitudinal reinforcement and a side steel plate at the beam-column connection in order to increase progressive collapse capacity. They tested five specimens, one specimen designed as gravity load-resisting and the other as a seismic load-resisting frame.

The remaining three specimens were reinforced with (i) bonded strand (ii) un-bonded strand (iii) side steel plates with stud bolts. The load was applied using hydraulic actuator by gradually increasing the displacement at the middle joint. Figure 2-50 shows the details of the specimens.
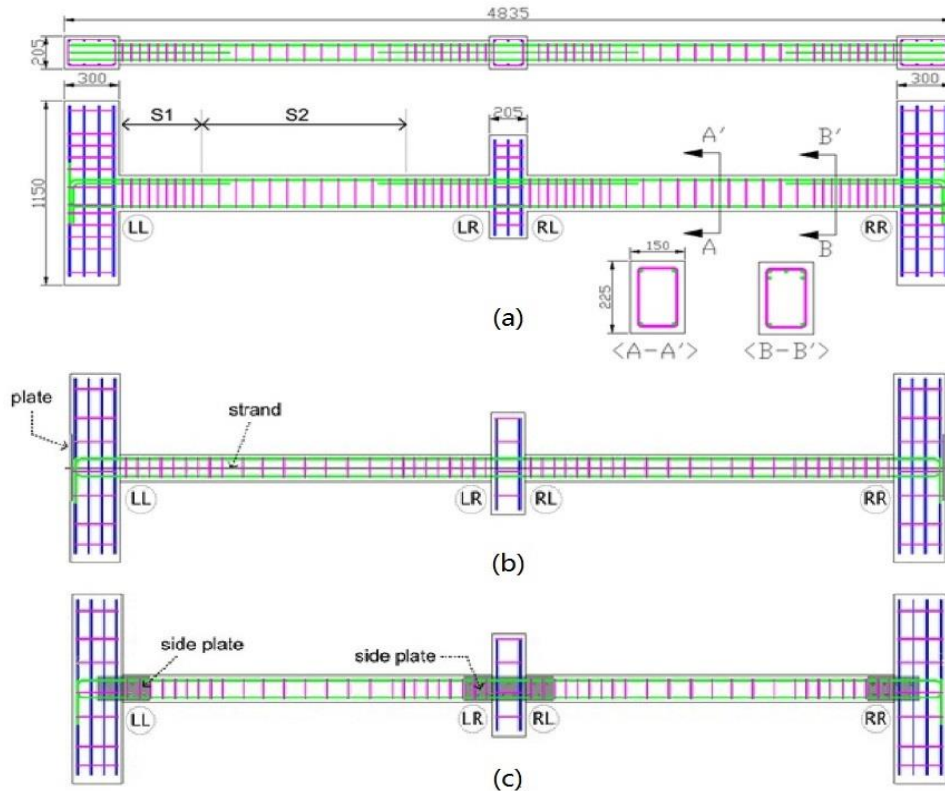


Figure 2-50: (a) un-retrofitted (b) with strand (c) with side steel plate (Kim and Choi, 2015)

Kim and Choi found that the specimen strengthened with un-bonded strand attained the highest strength. The test result for the specimen with side steel plates showed that the force–displacement curve increased without fracture of the steel bars.

Compared with the performance of the specimen strengthened with the strands, the specimen with side plates showed slightly smaller strength but more stable behaviour. Based on the test results, it can be concluded that the progressive collapse capacity of RC frames could be increased by using steel strand or steel side plates.

## 2.5 SUMMARY

Several research studies investigating progressive collapse have been carried out after the partial collapse of Ronan Point in 1968, the Murrah building in 1995 and the total progressive collapse of the World Trade Centre in 2001.

Until now, few experimental studies have been conducted to expand the understanding of structural behaviour of RC structures in the event of progressive collapse. (Yu and Tan 2013) pointed out that the study is at its beginning stage with very limited information of the effects of various parameters on the structural behaviour and progressive collapse capacity of RC structures.

These studies can be categorised into three main groups based on the scope and interest of the study as follows:

A) Presenting and evaluating analysis methods related to progressive collapse assessment, which is required by some guidelines.

B) Identifying and investigating progressive collapse performance of the buildings, mechanisms that can resist progressive collapse, such as compressive arch action and catenary action, and the parameters affecting these mechanisms, such as steel reinforcement ratio, steel placement, concrete strength and beam span-depth ratio.

C) Presenting new techniques or schemes to prevent or reduce the potential for progressive collapse, and study the effects of any parameter that may affect the performance or capability of the proposed scheme to resist progressive collapse.

Most of the previous studies were concerned about progressive collapse analysis and progressive collapse resisting mechanisms, and there is a lack of recommendation for new practical and economical schemes to mitigate progressive collapse. This lack was due to the need of a better understanding of the phenomenon itself, but this fact should not impede researchers from proposing new schemes to mitigate progressive collapse, and study the behaviour of the structure after implementing the new schemes. This will certainly lead to a better understanding of the progressive collapse phenomenon.

## 3. CHAPTER THREE   EXPERIMENTAL PROGRAM

### 3.1 GENERAL

Based on the alternate load path approach, a series of physical specimen tests have been carried out to investigate progressive collapse resistance mechanisms and their capacities for RC beam-column sub-assemblages under the middle CRS. In addition, the program aims to study the effect of the proposed steel reinforcing detail on progressive collapse resistance at the compressive arch action and catenary action stages.

The alternate load path method is one of the direct methods used to assess the ability of a structure to withstand abnormal loads without total collapse by removing one of the structural bearing members and evaluating the structural capacity of the remaining structure to prevent the initial damage from propagating to the total structure.

Currently, there is a limited amount of data and experimental tests concerning alternative resistance mechanisms of RC structures against progressive collapse. The lack of information regarding progressive collapse resistance mechanisms is the main obstacle for the design of buildings for progressive collapse to be included in the current guidelines and codes of practice. The understanding of these mechanisms may lead to better analysis techniques for new buildings or more efficient retrofit procedures for existing buildings that will allow them to be economically designed to prevent progressive collapse.

Figure 3-1 shows the effect of column removal on a typical building. As seen in Figure 3-1, the bending moment significantly increases (approximately 4 times) due to doubling the span. Furthermore, the moment over the missing column reverses direction, positive where the beam was designed for negative moment. All these changes are not considered in the conventional design of RC structures.

To overcome these changes and resist total collapse, a structure must be able to accommodate new and sudden load distribution through flexure, compressive arch action and catenary action and redistribute the loads into the remaining structure. As mentioned in the previous chapter, the catenary action depends on many factors such as steel reinforcement detailing. A new reinforcing scheme to increase resistance capacity against progressive collapse is introduced in this study.

Before column loss
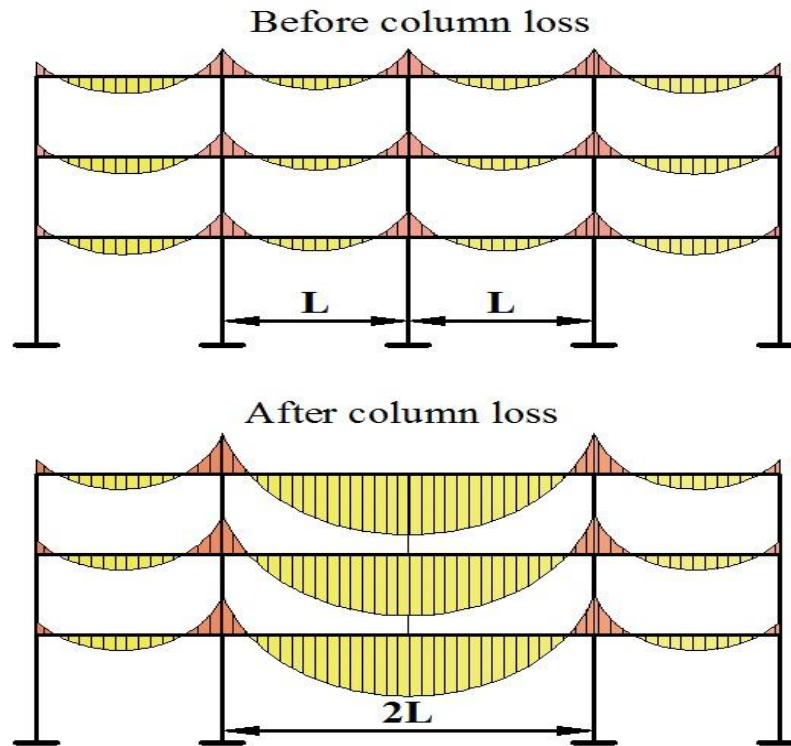
After column loss

Figure 3-1 Moment distribution for typical structure before and after column removal

## 3.2 EXPERIMENTAL WORK

The experimental work comprised of specimen design, specimen construction and finally specimen testing. Eight half-scale specimens were constructed and tested in the Structures Laboratory at the University of Salford. In order to simulate middle CRS, the specimens were tested under quasi-static loading until total failure to predict the structural nonlinear behaviour of RC structures under middle CRS. The non-linear static results were then converted into dynamic resistance through energy equilibrium.

The main objectives of the experimental program are to provide reliable data regarding the structural capacity of different mechanisms to resist progressive collapse, and to investigate the effect of the proposed scheme on the progressive collapse capacity of RC structures. Data obtained from the experimental study extends the understanding of structural resisting mechanisms (compressive arch action and catenary action) and the development of these mechanisms during the loading history. In addition, this data can be used to validate the proposed analytical model and the macro-model for the RC beam-column joint under CRS.

### 3.2.1 DESIGN OF SPECIMENS

Due to the limitations of size within the structures laboratory, the specimens were designed to be one-half-scale comprising of two bay beams, middle beam-column joint and two column stubs at the ends of each specimen. The specimen is assumed to be extracted from the middle of a multi-storey, multi-bay frame building. Figure 3-2 shows part of a structure with the shaded area being directly affected by a removed column which represents the test specimen.

A prototype frame building was designed and detailed according to ACI 318-05 for non-seismic regions. The specimens were then scaled down to one-half of the prototype frame. Figure 3-3 shows the dimensions and detailing of a typical specimen.
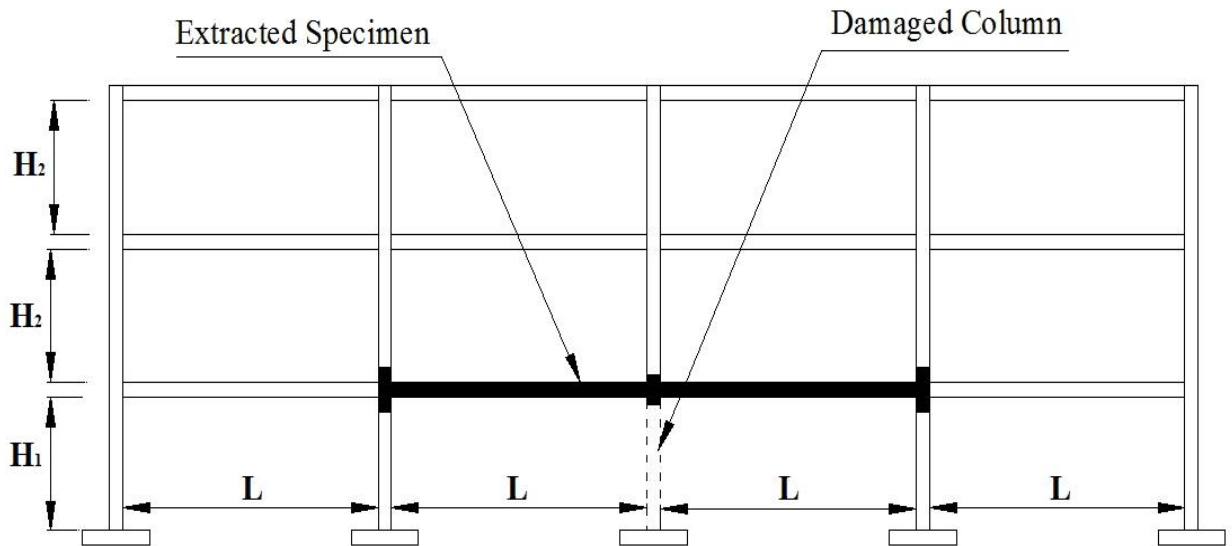


Figure 3-2 Test specimen in building front view

### 3.2.2 PROPOSED SCHEME

Catenary action is considered as the last line of defence in a structure to mitigate progressive collapse in the event of column loss. The catenary action mechanism requires that the concrete beam has a significant continuity, ductility and enough tensile strength in the beam-column joint connection, which depends on the detailing of steel reinforcement. In order to provide a beam and joint with the additional continuity, the scheme proposes to add two additional longitudinal bars at different levels of the beam section as shown in Figure 3-4.
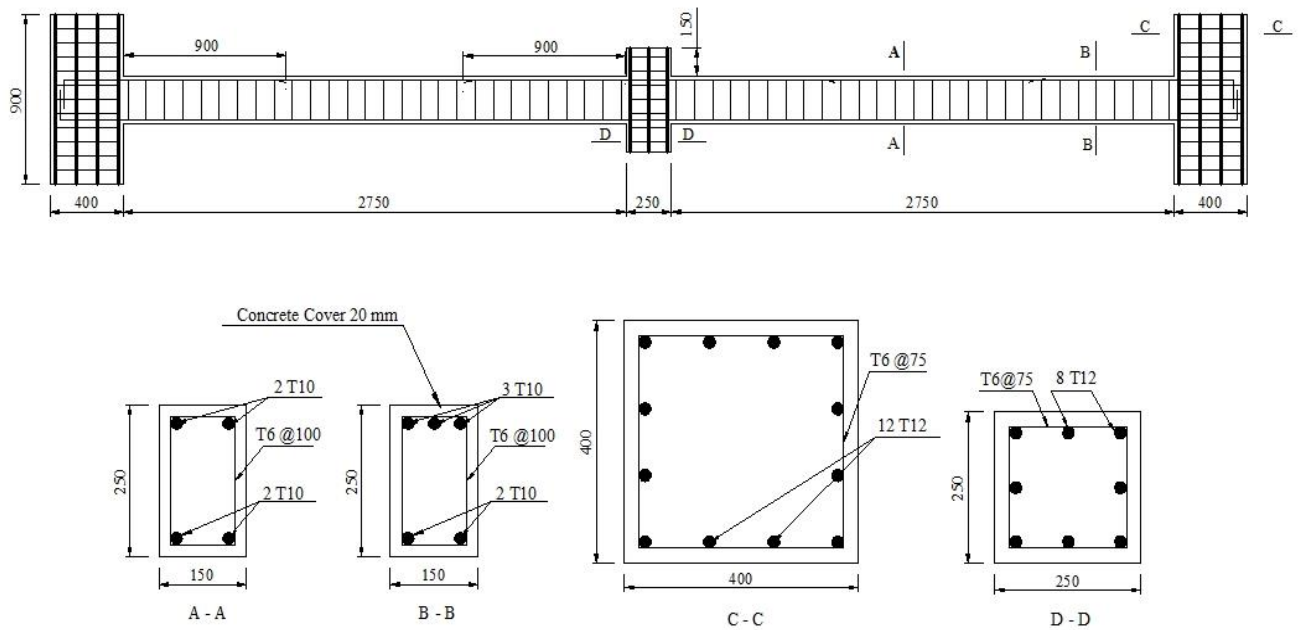
Figure 3-3 Conventional specimen dimensions and reinforcement details
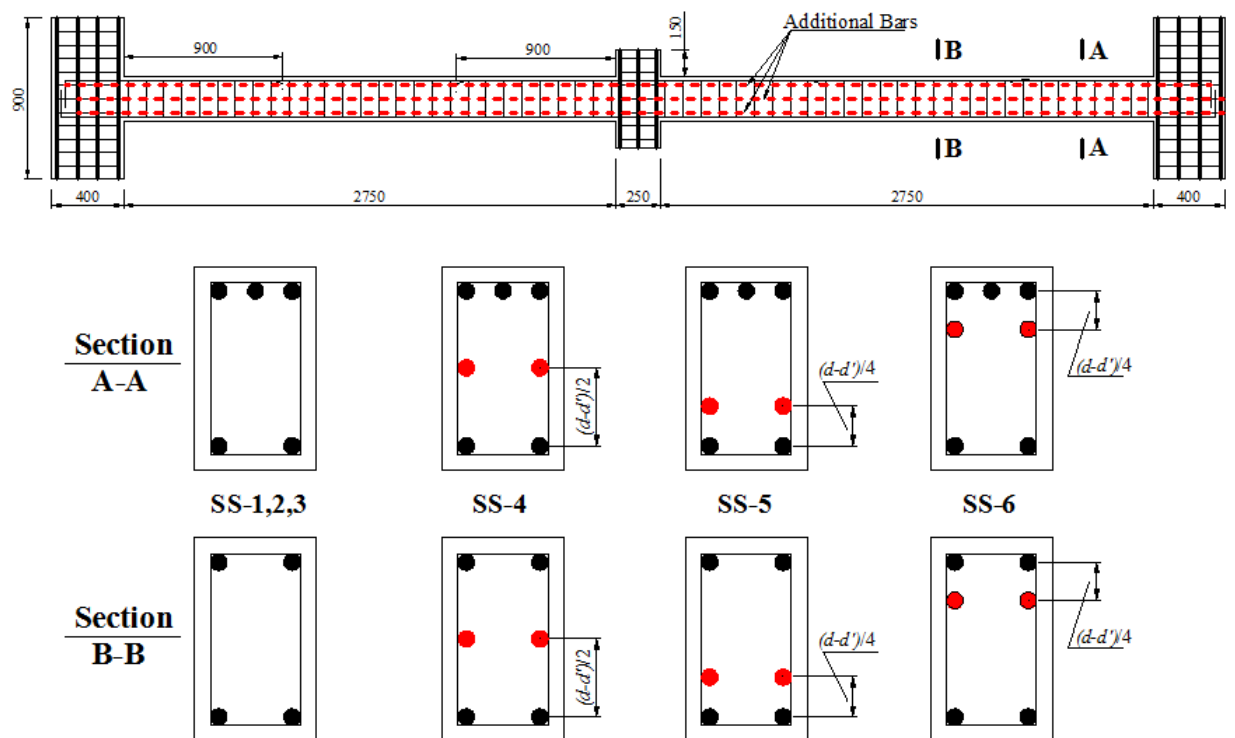


Figure 3-4 Proposed middle layer reinforcement

In order to increase rotation capacity, the scheme proposes to provide partial hinges at one beam depth and twice the beam depth away from the adjacent joint interfaces as shown in Figure 3-5.
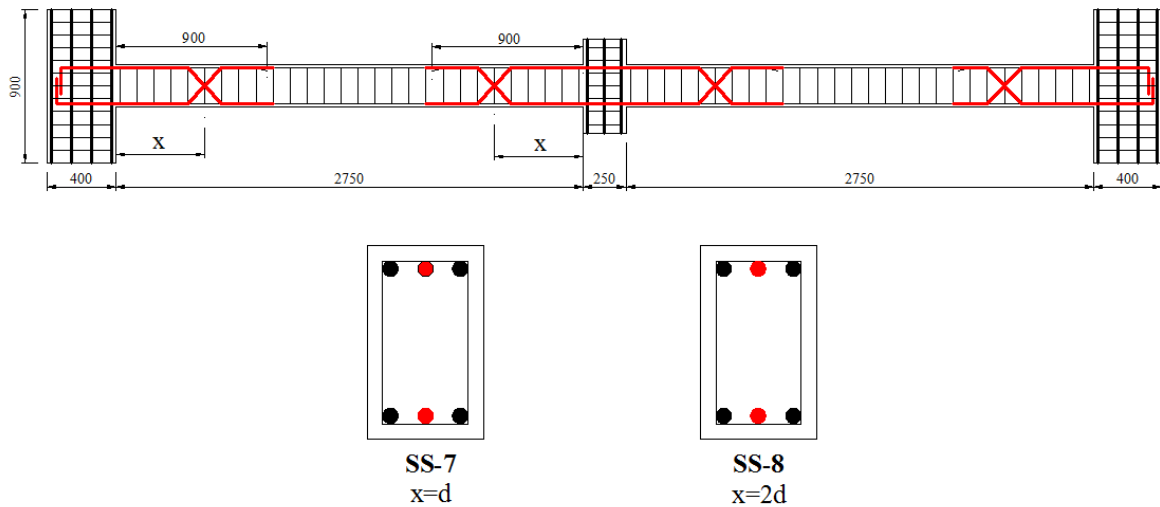


Figure 3-5 Partial Hinges Setup, x=d (SS-7), x=2d (SS-8)

The presence of partial hinges will ensure that plastic hinges form at these proposed locations and reduce the effective rotated beam length. Therefore, under a given axial tension and MJD, the structural resistance contributed by the vertical projection of axial tension will be increased. Figure 3-6 shows the effect of partial hinges on beam rotation.
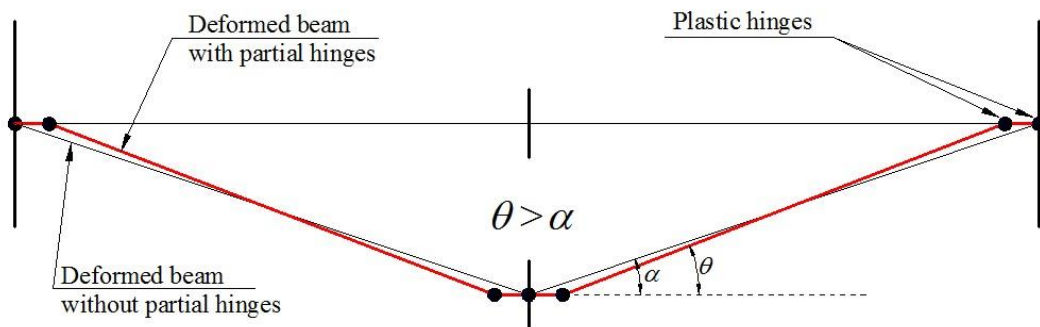


Figure 3-6 Effect of partial hinges on beam rotation capacity
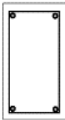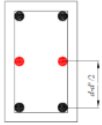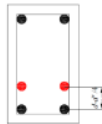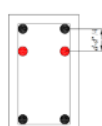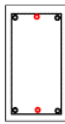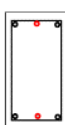
The experimental program comprised the testing of eight specimens divided into two main groups. The first group consisted of three specimens designed according to the conventional design without any additional reinforcement. The second group consisted of five specimens designed according to the conventional design and the additional reinforcement as proposed for the new scheme to prevent progressive collapse.

The structural behaviour and test results of the three specimens from the first group are used as reference data to compare with the test results of the second group and study the effect of additional steel reinforcement.

For all specimens, the ratio of top steel reinforcement at the middle joint and at the beam ends was 0.72% using 3T10 steel bars, and the ratio of bottom steel reinforcement at the middle joint and at the beam ends was 0.48% using 2T10 steel bars. The 'T' symbol refers to deformed reinforcement bars. Table 3-1 shows the specimen's designation and details.

In order to shed light on the development of internal stresses and forces at different structural mechanism phases, strain gauges were installed on the longitudinal steel reinforcement and attached at critical sections, such as faces of joints and at the additional steel reinforcement. Figure 3-7 shows the layout of strain gauges and their locations in the sub-assemblage specimens.

Table 3-1 Specimen's Designation and details

| Specimen | Modified detailing | Amount of steel added | Beam section |
|---|---|---|---|
| SS-1 SS-2 SS-3 | None | None | |
| SS-4 | Middle Layer Bars | 2T10 | |
| SS-5 | Middle Layer Bars | 2T10 | |
| SS-6 | Middle Layer Bars | 2T10 | |
| SS-7 | Partial Hinge | 1T10 | |
| SS-8 | Partial Hinge | 1T10 | |
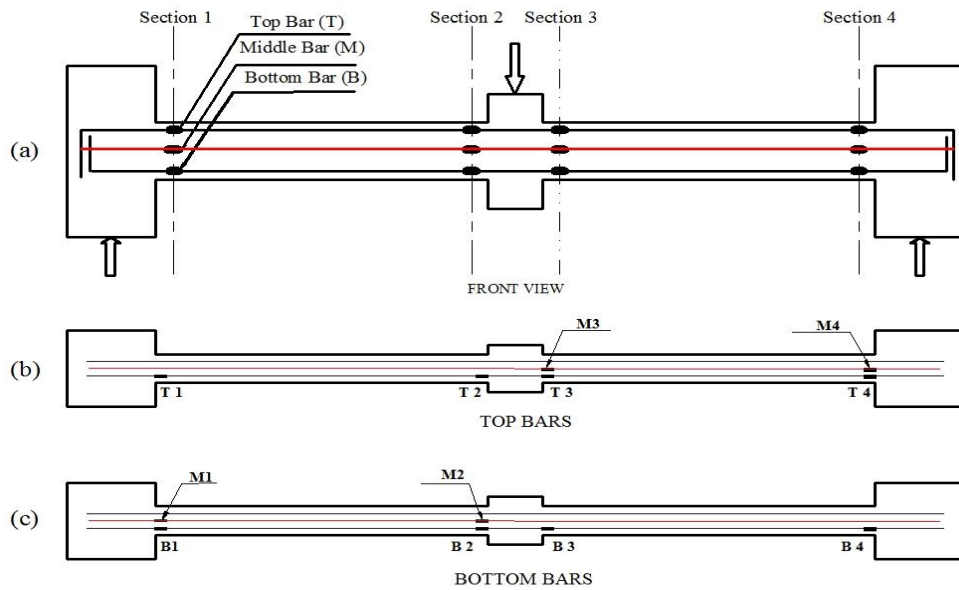
Figure 3-7 Strain gauge locations

Specimens with additional reinforcement have the same strain gauge locations with additional strain gauges attached to the added steel bars at the same critical section locations. Development of stresses and forces in the additional steel bars provides insight as to how these bars affect the structural resistance mechanisms at both compressive and catenary action stages.

## 3.2.3 TEST SETUP

Figure 3-8 shows a schematic plot for the loading test rig. To simulate the axial horizontal restraint for the beams, the ends of the specimens were connected to a steel frame by two load cells at each end, and these load cells were used to measure the horizontal forces that develop through the specimen during the test. In the vertical direction, a hinge roller support is used to restraint each end of the specimen. The reason for using a hinge roller support is to eliminate the effect of the vertical reaction on the horizontal reaction in order to ensure that the vertical and horizontal reactions were independent of each other.

The load cells used to measure the reactions in the horizontal direction had the ability to measure compressive and tensile forces with a carrying capacity of 250 kN each. The load was applied at the top of the middle joint using a hydraulic actuator with displacement control until total failure of the specimens occurred. The actuator with a built-in load cell was attached to a steel frame fixed into the strong floor of the structural laboratory. A steel plate and roller were used to support the bottom of each of the end column stubs. Because the specimens were quite slender, a lateral steel frame restraint was installed near the centre of the specimens to prevent out-of-plane movement as shown in Figure 3-9.
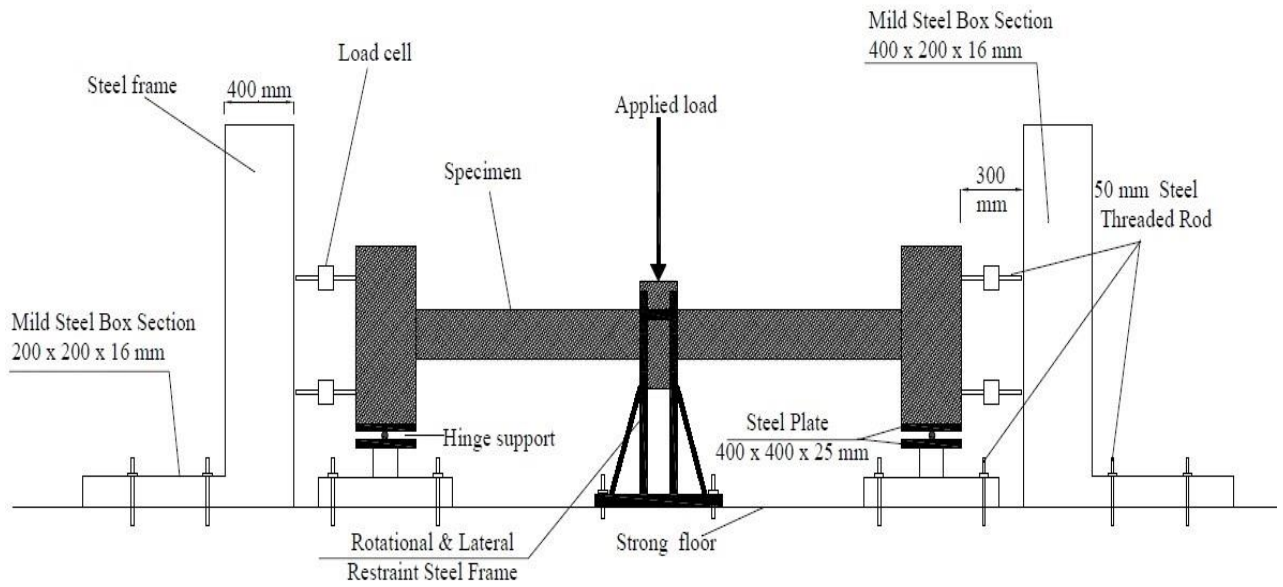
Figure 3-8 Schematic of the test Rig
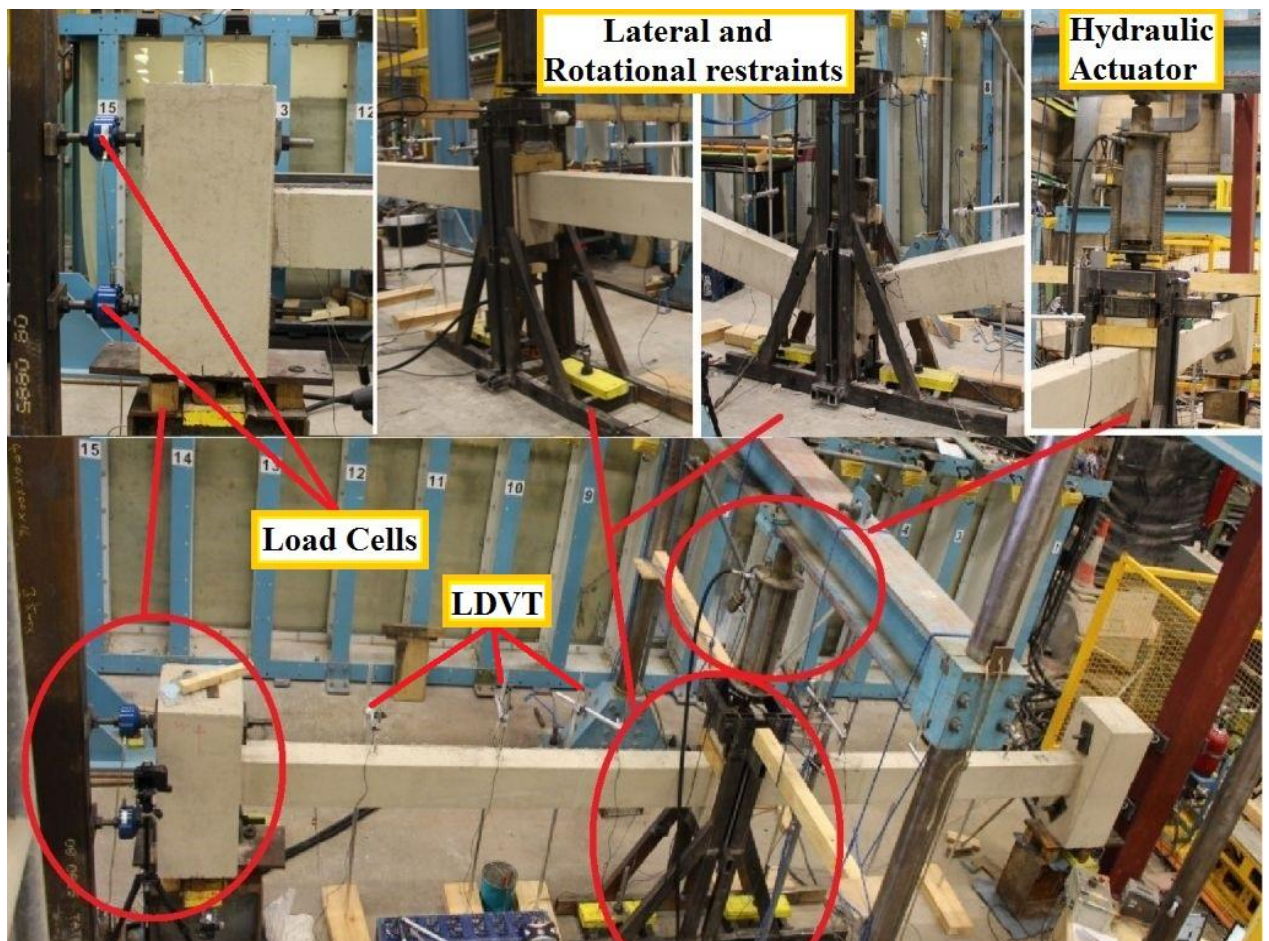


Figure 3-9 Test Rig Restraints

## 3.2.4 INSTRUMENTATION

The RC sub-assemblage specimens were mounted with measuring instruments both internally and externally. The applied load imposed by the actuator was measured by using an in-built load cell which is connected in series with the hydraulic actuator jack. Seven external linear differential variable transformers (LDVT) were mounted along the specimen to measure vertical displacement at the locations shown in Figure 3-10.

Four load cells were attached to the column stubs at the ends of the specimen to measure axial forces developed during the tests. These load cells have the ability to measure tensile and compressive forces. Strain gauges were installed internally onto the longitudinal steel bar at specific locations to measure the development of stresses and forces while applying the loads. Strain gauges were used to measure strains in both directions (the strains readings were then converted into stresses and forces).
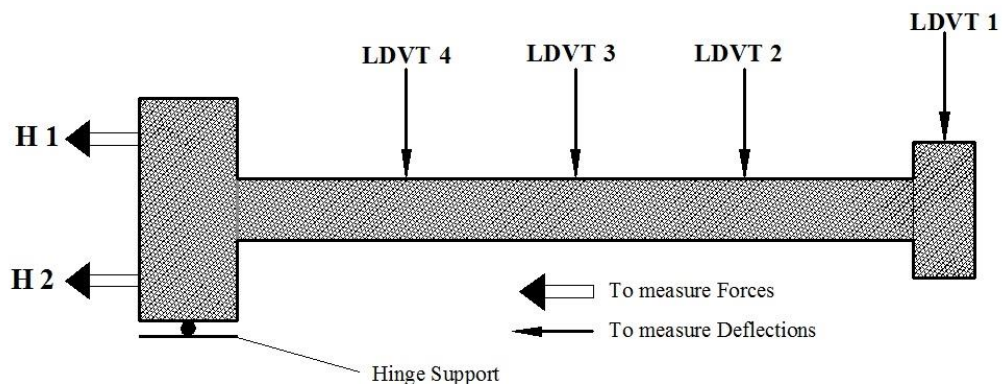


Figure 3-10 Arrangement of instrumentation

It should be mentioned; every measurement is subject to some uncertainty. Measurement uncertainties can come from the measuring instrument, from the item being measured, from the environment, from the operator, and from other sources. The use of good calibration, careful calculation, good record keeping, and checking can reduce measurement uncertainties. Measurement uncertainties can cause a difference between experimental and theoretical results within the acceptable limits.

All of the instrumentation was calibrated on United Kingdom Accreditation Service (UKAS) certified machinery which ensured that uncertainty of measurement was known and minimised during testing.

## 3.2.5 TEST PROCEDURE

As mentioned earlier, the load was applied using a hydraulic actuator jack with a monotonic loading regime until total failure of the specimens. During the test, all reaction forces at each side indicated H1 and H2, (as shown in Figure 3-10), were measured using load cells, and the applied load was measured using the in-built load cell of the actuator.

The displacement at the middle joint and along the length of the beam were measured using LDVT's as shown in Figure 3-10. Therefore, the beam deflection at each load step could be determined, and axial forces developed through the beam were able to be calculated for each deflection value corresponding to each load step. In addition, strain gauges, which were attached to the steel reinforcement, measured the strain in the steel bar at each load step. These strains were converted into stresses and then into forces, which will indicate the development of each resisting mechanisms such as compressive arch action and catenary action.

The test data and results were collected and recorded simultaneously at a sampling rate of 1.0 HZ using an MTS data acquisition system. Relationships of MJD, axial forces, and bar strains are plotted for each magnitude of applied load for all specimens.

Due to limitation in the length of stroke of the hydraulic actuator, which was limited to 200 mm only, a hanging steel frame was used to fix the sample at this stage of deflection, then resetting the actuator to continue applying the load for another 200 mm and so on to complete the test.
The effect of this procedure can be seen on the relationships of applied load versus middle joint deflection as a small decrease in load at some points. This has no effect on the final results and overall structural behaviour of the specimens.

In order to check the stability and the ability of the test rig frame to carry out the tests, one specimen was initially used to debug the system. One issue observed during this test was the rotation of the middle joint due to bar fracture on one side, which may not reflect the actual case in a RC structural frame as the upper middle column would restraint the middle joint from rotating. This issue was solved by restraining rotation of the middle joint using a steel frame with vertical steel rollers to minimise the effects of friction affecting the vertical movement. This stabilising frame was fixed to the strong floor in the laboratory as shown in Figure 3-8.

## 3.3 CONSTRUCTION STAGE

At the beginning, material quantities for specimens were calculated. A bar schedule was produced for the rebar, and the strain gauges were acquired. The stages of construction includes mould construction, steel cage assembling, strain gauge installation and concrete casting.

## 3.3.1 MOULD CONSTRUCTION

The moulds for casting the concrete specimens were fabricated from rectangular plywood with 25 mm thickness. The mould was made from five main removable parts, two beam cases and three column stub cases. The clear dimensions of the beam cases were (2750 x 250 x 150 mm). The total length of the mould was (6550 mm). The moulds are clearly shown in Figure 3-11.



Figure 3-11 Wooden moulds used for concrete casting

## 3.3.2 STEEL CAGES

High yield steel bars of 6, 10 and 12 mm diameter were acquired for the reinforcement cages for the specimens. T10 steel bars were used in the longitudinal direction, while T12 steel bars were used to reinforce the column stubs. T6 steel bars were used as tie reinforcements. High tensile steel wires were used to tie steel bars together. At the beginning, steel cages for column stubs were assembled for all specimens, and then beam steel cages were assembled and connected to column steel cages later. Figure 3-12 shows photographs of the steel cages.

Figure 3-12 Steel Cages with Wooden Moulds

### 3.3.3 STRAIN GAUGE INSTALLATION

High-sensitivity strain gauges based on a single wire were used for attachment to the longitudinal steel reinforcement. In this study, a universal general purpose strain gauge with a resistance of $120\pm0.5$ Ohms and a strain range of $\pm5\%$ was used, which means, these strain gauges had the ability to measure tensile and compressive forces (strains). A total of 18 strain gauges were installed at critical locations for each specimen.

High strength adhesive material was used to attach and install strain gauges to the steel bars and each strain gauge was coated and protected from the surrounding concrete by using rubber and special protecting paint. Figure 3-13 shows pictures of the installation process.
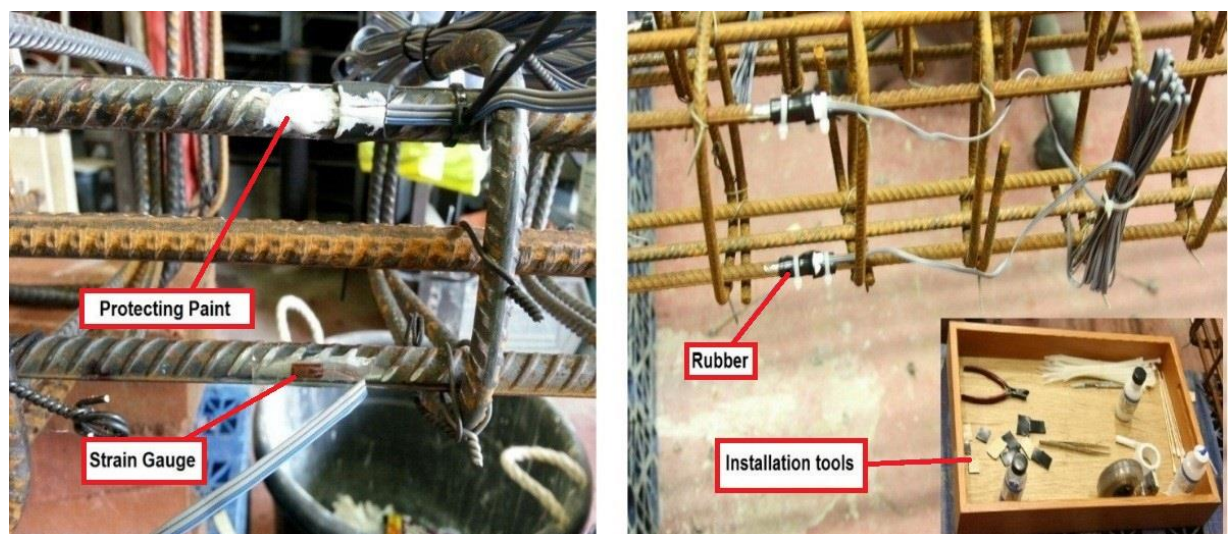

Figure 3-13 Strain Gauge Installation

### 3.3.4 CONCRETE CASTING

Ready mix concrete was used for casting the samples with a 28-day compressive strength target of 28 MPa and a maximum aggregate size of 10 mm. Specimens were cast in four batches, two samples in each batch. The moulds were cleaned and oiled before pouring the concrete and special care was taken when compacting the poured concrete so as not to damage the attached strain gauges. After the top layer had been compacted, it was tamped and levelled with the top of the mould by using steel trowels. After finishing, the specimens were covered by nylon to prevent evaporation of water from the fresh concrete. Figure 3-14 shows the specimens after the casting procedure.



Figure 3-14 Concrete Specimens

### 3.4 MATERIAL TESTS

Several samples of reinforcing steel bars were chosen to be tested during the stage of assembling the steel cages. Two strain gauges were attached to each sample at the outer surface of steel in order to measure strain when applying the load. Steel bar samples were used for tensile tests to obtain the yield strength, modulus of elasticity, ultimate tensile strength and fracture strain of steel bars. Figure 3-15 shows the steel samples with their test.
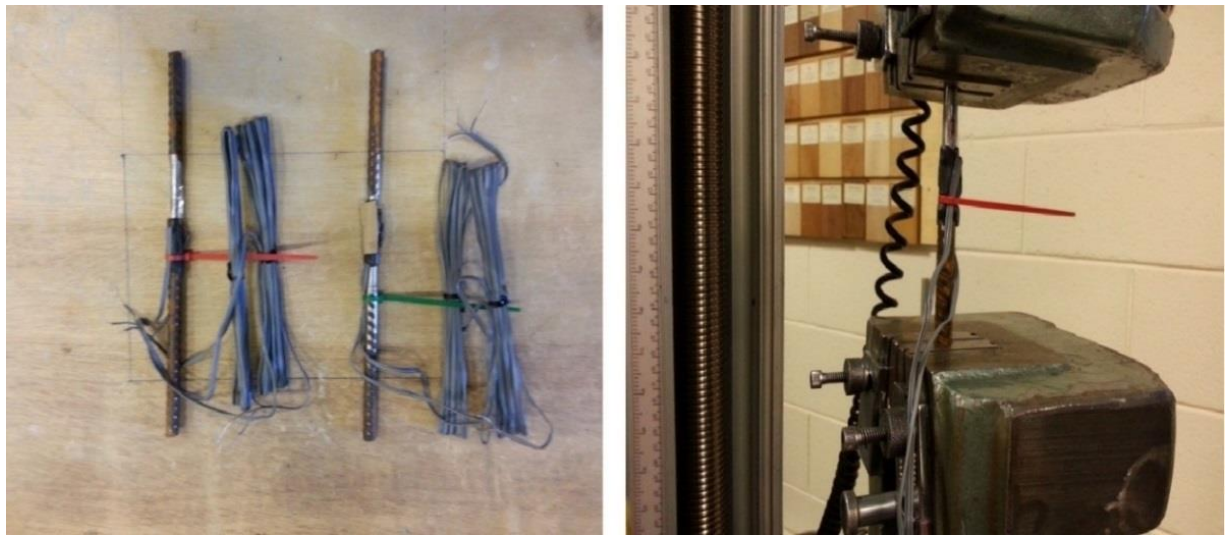
Figure 3-15 Steel Bars Tests

Concrete sampling was carried out during the casting of the specimens. For each batch, one cylinders with 300 mm height and 150 mm diameter, three cubes with $100 \times 100 \times 100$ mm and one prism with $400 \times 100 \times 100$ mm were cast. Cylinder test were used to obtain the modulus of elasticity, cubes for compressive strength and prism for modulus of rupture. Figure 3-16 shows these tests.



Figure 3-16 Concrete Cylinder Tests

## 3.5 SUMMARY

In this chapter, the preparation for the experimental program of testing eight-half scale RC sub-assemblages under CRS has been described. The following provides a summary of the experimental preparation in this chapter:

1- Description of the specimen design, specimen's dimension and steel detailing are presented.

2- Proposed new steel detailing to increase RC beam capacity against progressive collapse is presented and described.

3- Internal and external instrumentation for measurement is described. Strain gauges were considered as the internal devices, while LDVT's as external devices.

4- Description of the test rig is presented. The steel frame was designed to conduct the test under CRS at Salford University structural lab.

5- The test procedure is described. The test was conducted by applying the load using a hydraulic actuator.

6- The construction details of the eight half-scale specimens are presented. Four stages of construction were conducted, mould fabrication, steel cages assembling, strain gauge installation and concrete casting.

7- Material tests are described. Sampling and testing of concrete and steel reinforcement bars were conducted to obtain material properties.

## 4.  CHAPTER FOUR    EXPERIMENTAL RESULTS

## 4.1 GENERAL

Although studying the structural behaviour of RC structures numerically is always an option; the assumptions and the approaches made through the modelling and the potential issues due to the limitations of finite element software used need to be checked and verified against available experimental data. For the progressive collapse of RC structures, there is very limited data available to be used to study the behaviour of the structures for verification of the analytical models.

In order to understand the progressive collapse resistance mechanisms of RC structures at the global level, it is necessary to understand the structural behaviour of RC members under CRS at the local level. For this reason, eight sub-assemblages were constructed and tested in this study. In this chapter, experimental results are presented and comprehensively discussed. The relationship between applied load, axial forces and MJD are illustrated and compared for various specimen's steel detailing.

## 4.2 MATERIAL PROPERTIES

Due to limited space in the laboratory and the large size of the specimens, the construction of the specimens was divided into four batches, two samples were cast in each batch. For each batch, three concrete cubes of dimension $(100 \times 100 \times 100)$ mm were sampled during the process of casting to obtain concrete compressive strength. One cylinder of dimensions 300 mm height and 150 mm diameter was sampled and tested to obtain the modulus of elasticity and one beam test of dimension $(400 \times 100 \times 100)$ mm to obtain the modulus of rupture.

The compressive strength test of concrete was carried out in accordance with (BS1881-116, 1983), the modulus of elasticity testing was carried out in accordance with (BS1881-121, 1983), and the modulus of rupture test was carried out in accordance with (BS1881-118, 1983). According to the specimen design, the targeted concrete compressive strength at 28 days was 28 MPa. Each set of cubes was tested at the day (or day before) of specimen test and the average value of cubes for each patch was taken as listed in Table 4-1.

For the steel reinforcing bars, three samples of longitudinal bars were tested in tension in accordance with (ASTM-A370, 2005). The average actual stress-strain curve was simplified to a bilinear curve in order to use it for both numerical and theoretical analysis.  Stresses and their

corresponding strains were recorded and plotted as shown in Figure 4-1.  Steel reinforcement properties are listed in Table 4-2.

Table 4-1 Concrete Mechanical Properties

| Specimens | Compressive Strength MPa | Modulus of Elasticity MPa | Modulus of Rupture MPa |
|---|---|---|---|
| SS-1 SS-2 | 28.5 | 24400 | 3.1 |
| SS-3 SS-4 | 26.8 | 23100 | 2.9 |
| SS-5 SS-6 | 27.5 | 24200 | 3.0 |
| SS-7 SS-8 | 28.0 | 24400 | 3.1 |
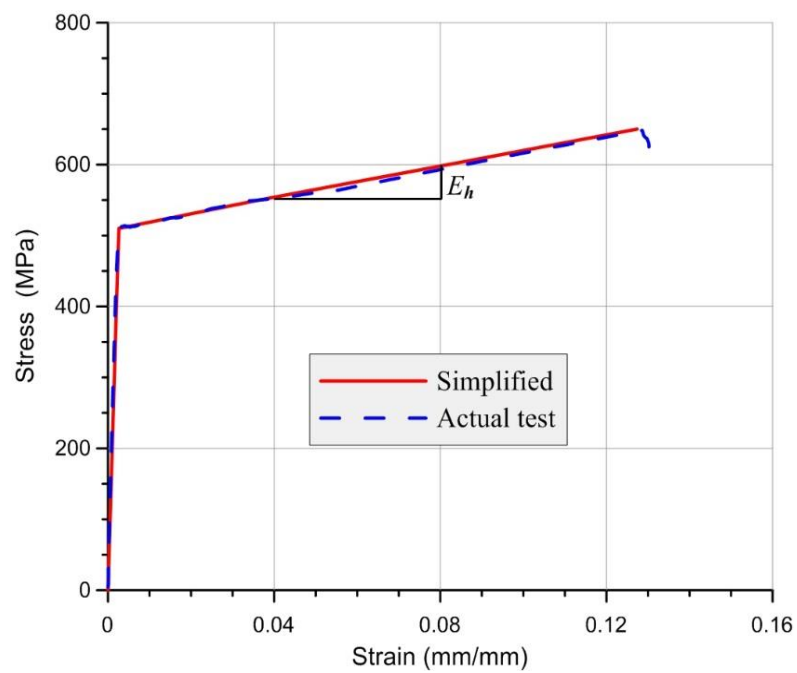


Figure 4-1 Stress-Strain Relationship of Steel Reinforcement Bars

Table 4-2 Steel Properties

| Steel Type | Yield Strength MPa $f_y$ | Yield Strain $\varepsilon_y$ | Elastic Modulus MPa $E_s$ | Ultimate Strength MPa $f_u$ | Ultimate Strain $\varepsilon_u$ | Hardening Modulus MPa $E_h$ |
|---|---|---|---|---|---|---|
| T10 | 510 | 0.0026 | 196150 | 650 | 0.13 | 1099 |

## 4.3 TEST RESULTS

In this section, experimental test results will be presented and illustrated at both the global level and local level. Test results at the global level include the relationship between applied load and MJD, axial forces vs. MJD, failure mode and crack pattern. Test results at the local level include the relationship of bar forces at critical sections vs. MJD. Moreover, test results will be categorised according to the resistance mechanism for three stages, flexural, compressive arch action and catenary action.

Test results will be presented in two main sections, i.e. global and local levels. Test results of specimens with modified steel detailing will be compared with the conventionally designed specimens. The effect of this new detailing on structural behaviour and resistance capacity against progressive collapse at both compressive arch action and catenary action will be also investigated.

In general, for a building, global refers to the whole of the building system structure in question, while local refers to each structural member individually. In this instance, global refers to the whole structural behaviour of the specimen, while local refers to the internal forces that develop at particular locations in the specimen during the test.

## 4.3.1 TEST RESULTS FOR GLOBAL BEHAVIOUR

Structural behaviour of any member can be represented by the relationship of load-deflection history and axial force-deflection history. In this section, structural behaviour of each specimen will be presented and examined.

## 4.3.1.1 TEST RESULTS OF SPECIMENS SS-1, SS-2, SS-3

Specimens SS-1, SS-2 and SS-3 were designed and detailed without adding additional steel reinforcing bars. Therefore, these specimens were used as a benchmark to compare with specimens that have additional steel reinforcing bars.

As mentioned in chapter three, seven external linear differential variable transformers were mounted along the specimen's length to measure vertical displacement for each step of the load. Figure 4-2 shows the displacement curves for specimen SS-1, SS-2 and SS-3 at different critical load steps.

(a)



(b)



(c)
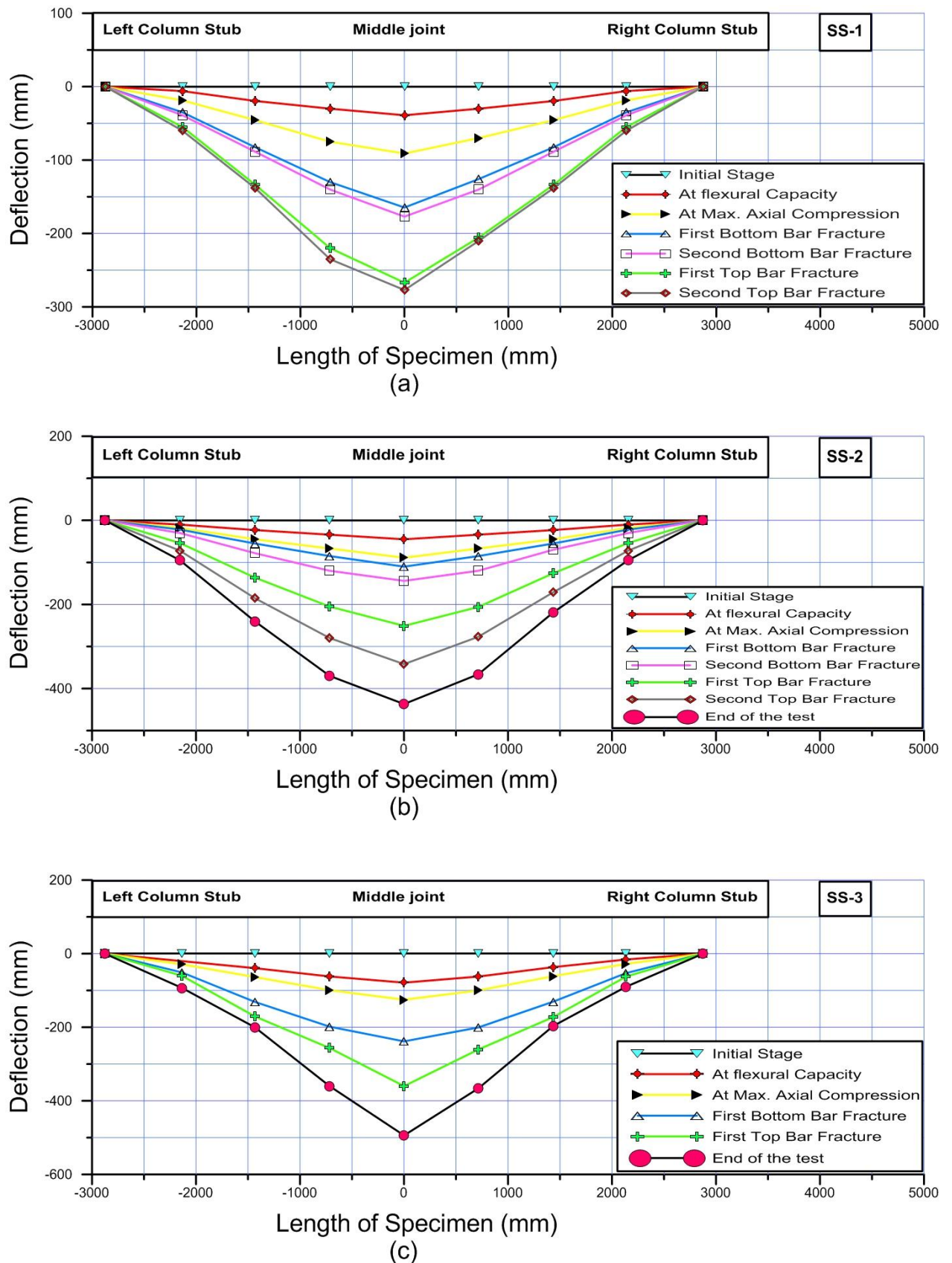
Figure 4-2 Beam Deformation for (a) SS-1, (b) SS-2, (c) SS-3

It should be mentioned that during the test of specimen SS-1, the middle joint was not restrained against rotation in the plane of the beam, which resulted in bar fracture on one side with the joint rotating towards this side. This can be seen from the deflection curves of the specimen, which are symmetric for both sides except near the middle joint at large deflections.

It should be mentioned that due to safety issues, the test of specimen SS-1 was stopped at a deflection of 282 mm. In the proceeding tests, the aim was to ensure total failure of the specimens in order to investigate the structural behaviour of the specimen at catenary action with full resisting capacity.

It can be observed from the deflection curves that there is a large gap in displacement between the stage of bottom bar fracture and top bar fracture. This can be related to the formation of plastic hinges at the middle joint, which caused a large deflection at that stage.

Figures 4-3 and 4-4 show the relationships of applied load vs. MJD and axial force vs. MJD for specimen SS-1, SS-2 and SS-3. Table 4-3 lists forces and their corresponding middle joint displacements at critical stages of the load-deflection history.

It is clear from Figures 4-3 and 4-4 that the specimen SS-1 did not reach the advanced stage of catenary action phase due to large in-plane rotation of the middle joint, which caused bar fracture on one side as mentioned earlier. Therefore, the discussion will concentrate on specimen SS-2 and SS-3.

The general trend of the load-displacement history can be divided into three stages, flexural action, compressive arch action and catenary action as shown in Figure 4-3. The overall trends of the load-displacement relationship for specimen SS-2 and SS-3 were quite similar despite that they have different concrete strengths, which results in different flexural capacity as can be seen from Figure 4-3.

The peak load capacities were 34.9 and 34.0 kN for SS-2 and SS-3 respectively. After the peak loads were reached, plastic hinges developed and bar fracture occurred. The abrupt drops in the applied load shown in Figure 4-3 were due to subsequent fracture of steel reinforcing bars at the bottom and top of the beam section.

Figure 4-3 Applied Load vs. Middle Joint Displacement Relationship of SS-1, SS-2, SS-3
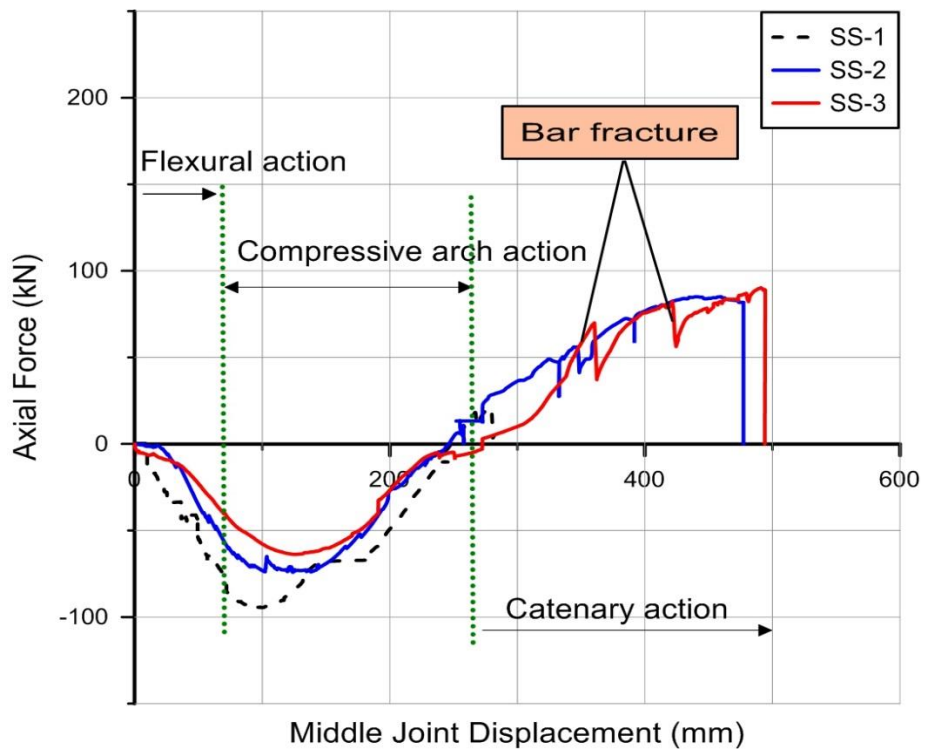


Figure 4-4 Axial Force vs. Middle Joint Displacement Relationship of SS-1, SS-2, SS-3

As shown in Figure 4-4 there is no separation point between flexural action and compressive arch action due to the fact that the compressive arch action developed at the beginning of the loading in axially restrained members.

On the other hand, it is clear from Figure 4-4 that the transition point from compressive arch action to catenary action occurred only when axial loads changed from a compressive force to a tensile force. For SS-2 and SS-3, the catenary action commenced at middle joint displacements of 246 mm and 272.5 mm respectively.

Table 4-3 Forces with their MJD's at Critical Stages

| Specimen | Calculated flexural capacity | | Max. load at CAA | | Max. Axial compression Force | | Max. Axial Tension Force | | Max. Load at Catenary Action | |
|---|---|---|---|---|---|---|---|---|---|---|
| | $P_f$ (kN) | MJD (mm) | $P_{com}$ (kN) | MJD (mm) | $N_{com}$ (kN) | MJD (mm) | $N_{ten}$ (kN) | MJD (mm) | $P_{cat}$ (kN) | MJD (mm) |
| SS-1 | 29.8 | 41.0 | 38.5 | 91.1 | 94.5 | 99.5 | 20.7 | 279.7 | 12.1 | 280.0 |
| SS-2 | 29.8 | 40.4 | 34.9 | 89.3 | 74.1 | 123.9 | 85.1 | 459.7 | 33.2 | 477.3 |
| SS-3 | 28.0 | 57.9 | 34.0 | 101.0 | 63.8 | 125.6 | 89.2 | 494.0 | 36.2 | 494.0 |

It is clear from Table 4-3 that the experimental flexural capacities were larger than the calculated flexural capacities. This is because the development of axial compressive force through the beam occurred in the early stages of loading where flexural action is assumed to dominate. At this stage, axial compression is not considered in the calculation of flexural capacity for the beam section.

After the compressive arch action attained its maximum capacity, which depends on many factors such as concrete strength, catenary action commenced after the middle joint vertical displacement surpassed the beam depth. The stage at which catenary action started to develop was after the fracture of bottom bar reinforcements at the middle joint, which means that the catenary action then utilised the top bars in the middle joint.

As the MJD increased further, the top reinforcement at the beam ends fractured, which is clearly shown in Figure 4-3. At this stage, catenary action depends on the bottom reinforcement at the beam ends only.

As can be seen in Table 4-3, the maximum tensile forces at catenary action for SS-2 and SS-3 were quite similar, which means that the tensile forces depend only on the steel reinforcement. On the other hand, the large deformation for SS-3 may be related to the concrete strength and the crushing of concrete at the bottom fibre at the beam ends.

The overall crack pattern and failure mode for SS-2 and SS-3 were quite similar. At the flexural action stage, the cracks were concentrated at the beam-column joint interfaces, which are mainly caused by bending moments at these sections.

Cracks developed during flexural action with the presence of compressive arch action beginning from the extreme tension face of the concrete, running vertically through the beam section and terminating at the location of the neutral axis. As the applied load increased, the neutral axis moved towards the compression face until the concrete crushed at the extreme surface in the compression zone.

Different from flexural action, at the catenary action stage, cracks started to develop throughout the beam length and passed completely through the depth of the beam section. With an increase in applied load, cracks widened and bar fracture occurred at the beam-column joint interfaces.

It is worth mentioning, at catenary action, the cracks were uniformly distributed along the beam length and a large slip between steel bars and concrete was observed at the beam-column joint interfaces. Figure 4-5 shows a photograph of specimen SS-3 before applying the load.
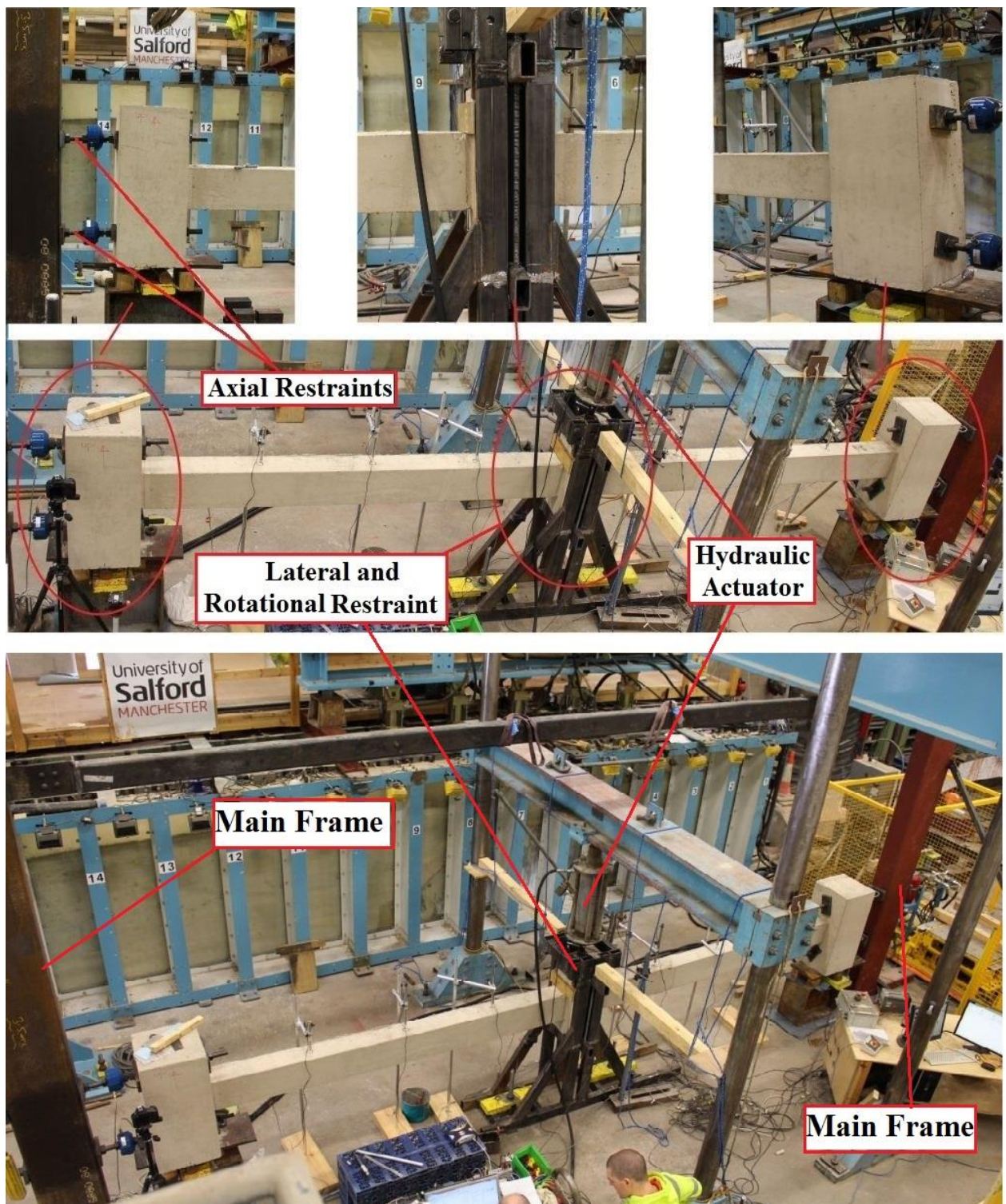
Figure 4-5 Photograph for Specimen SS-3

Figure 4-6 shows the crack pattern of specimen SS-3 at flexural action. It shows clearly the developed flexural cracks at the beam-column joint interfaces. Figure 4-7 shows the crack pattern of specimen SS-3 at catenary action, which displays a uniform distribution of the cracks along the beam length.
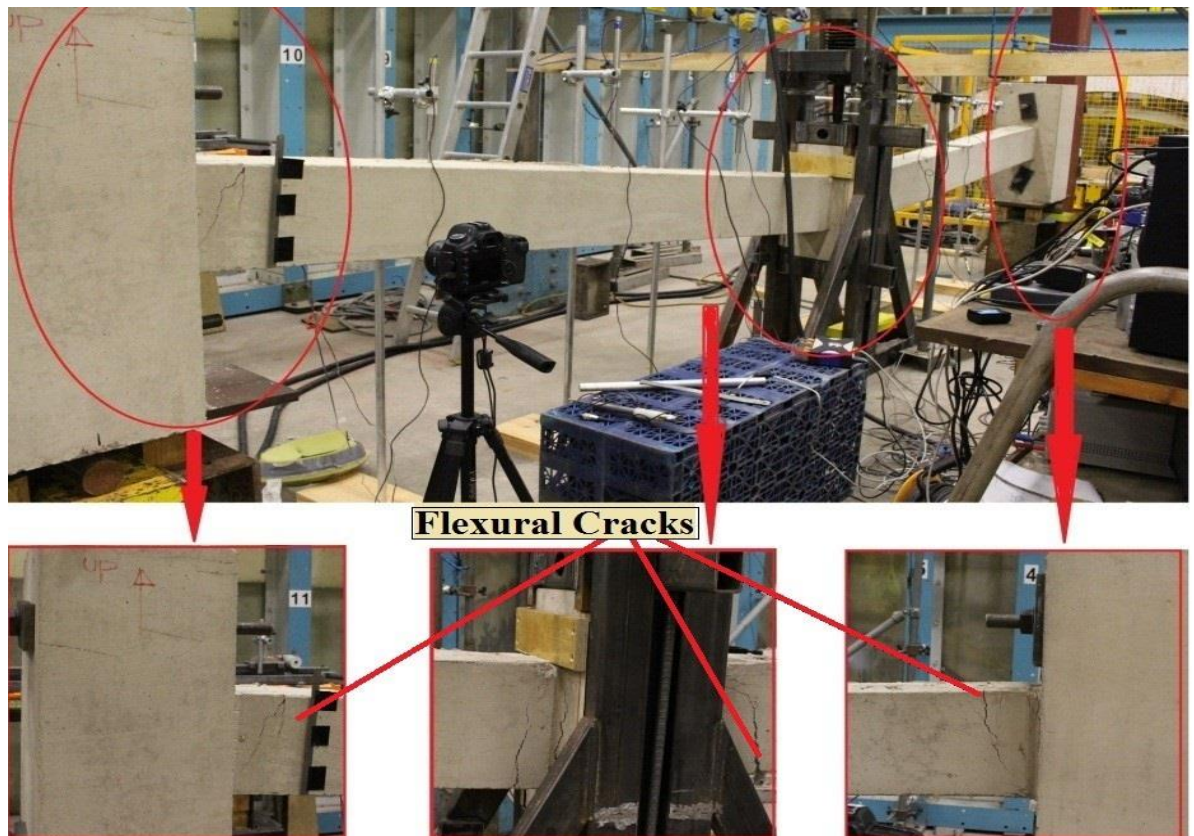
Figure 4-6 Crack Pattern of Specimen SS-3 at Flexural Action
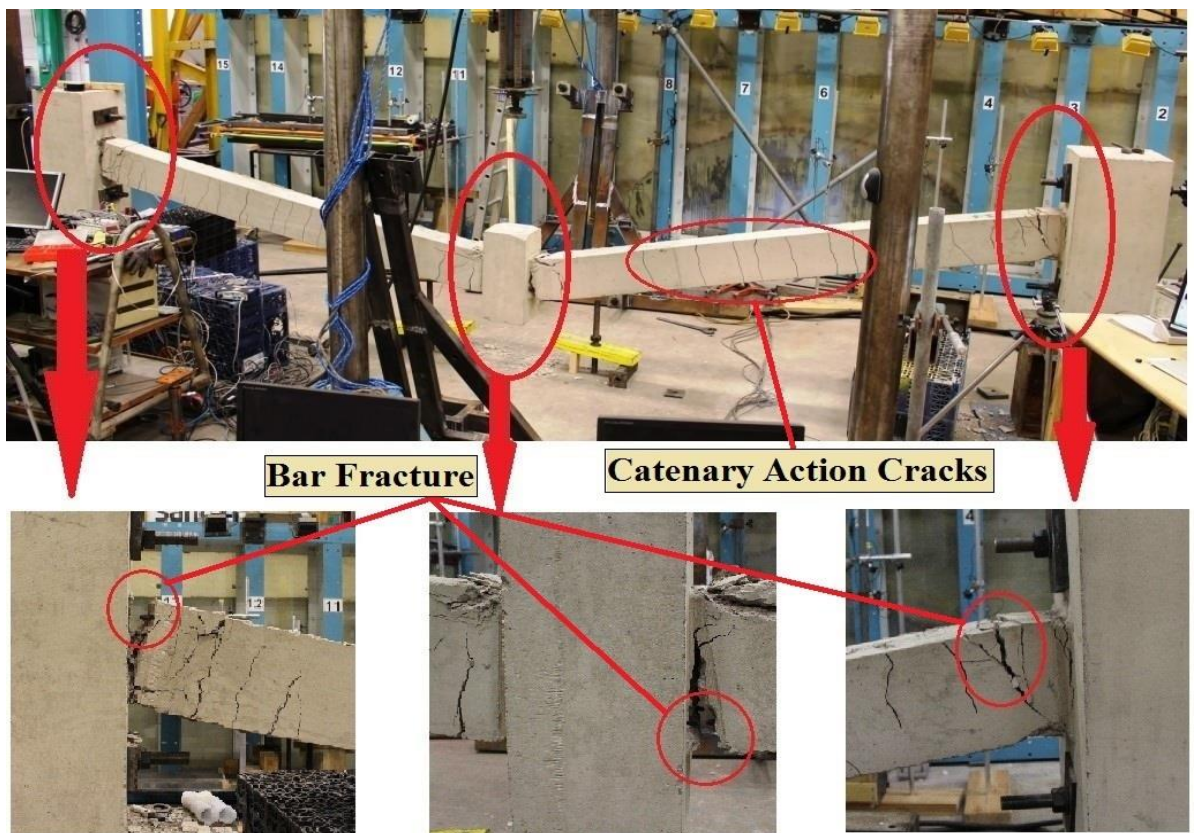


Figure 4-7 Crack pattern of specimen SS-3 at Catenary action

In order to obtain progressive collapse capacity for each specimen, the non-linear static structural behaviour 'i.e. quasi-static response' is converted into non-linear dynamic behaviour. The proposed approach by Izzuddin et al. 2008 was used to obtain progressive collapse capacity. This approach is based on energy equilibrium, which states that for the structure to be stable, the work done by applied gravity loads should be equal to the energy absorbed by the structure. In other words, the structure should have enough strain energy supply to absorb any energy demand caused by sudden loss of vertical support.

The converted non-linear dynamic behaviour is called the pseudo-static structural behaviour. Figures 4-8 and 4-9 show the pseudo-static structural behaviour of specimen SS-2 and SS-3.
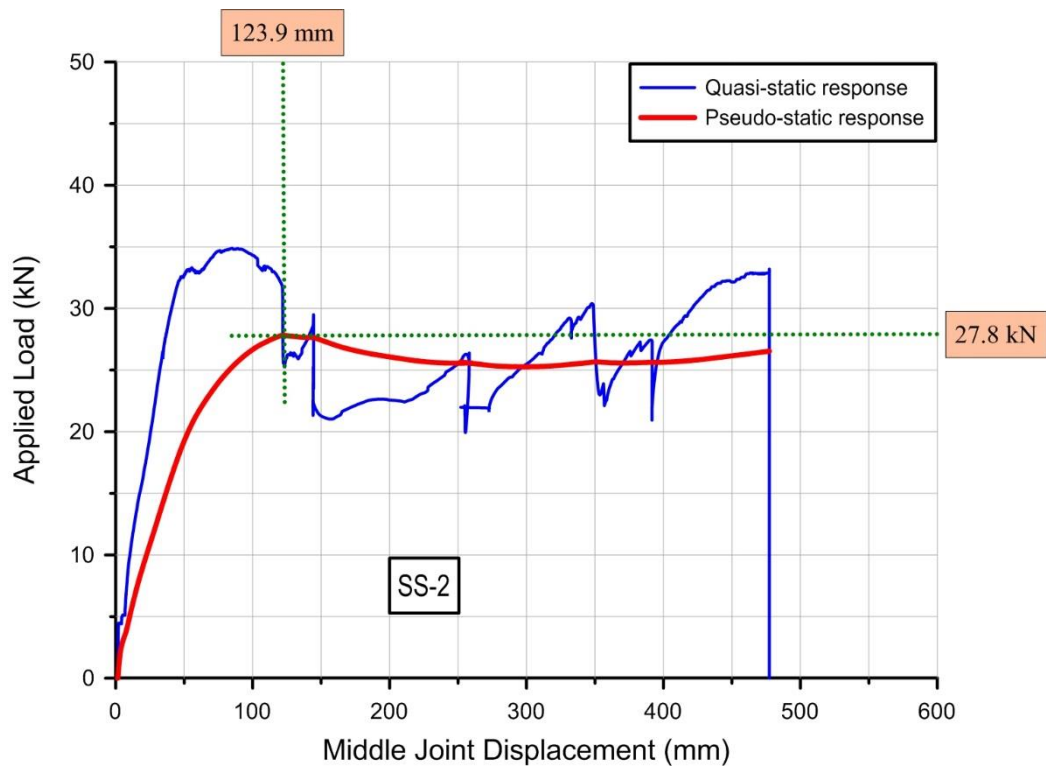


Figure 4-8 Non-linear Pseudo-Static Response of Specimen SS-2

From Figure 4-8, the progressive collapse capacity for specimen SS-2 is 27.8 kN with a corresponding middle joint displacement of 123.9 mm. Total collapse would occur if the load increased beyond the load of 27.8 kN and the deflection cannot then be predicted. The middle joint displacement corresponding to the maximum progressive collapse capacity occurs within the deflection range of compressive arch action. This means that the specimen was not able to increase its progressive collapse capacity into the catenary action stage and benefit from this structural action.
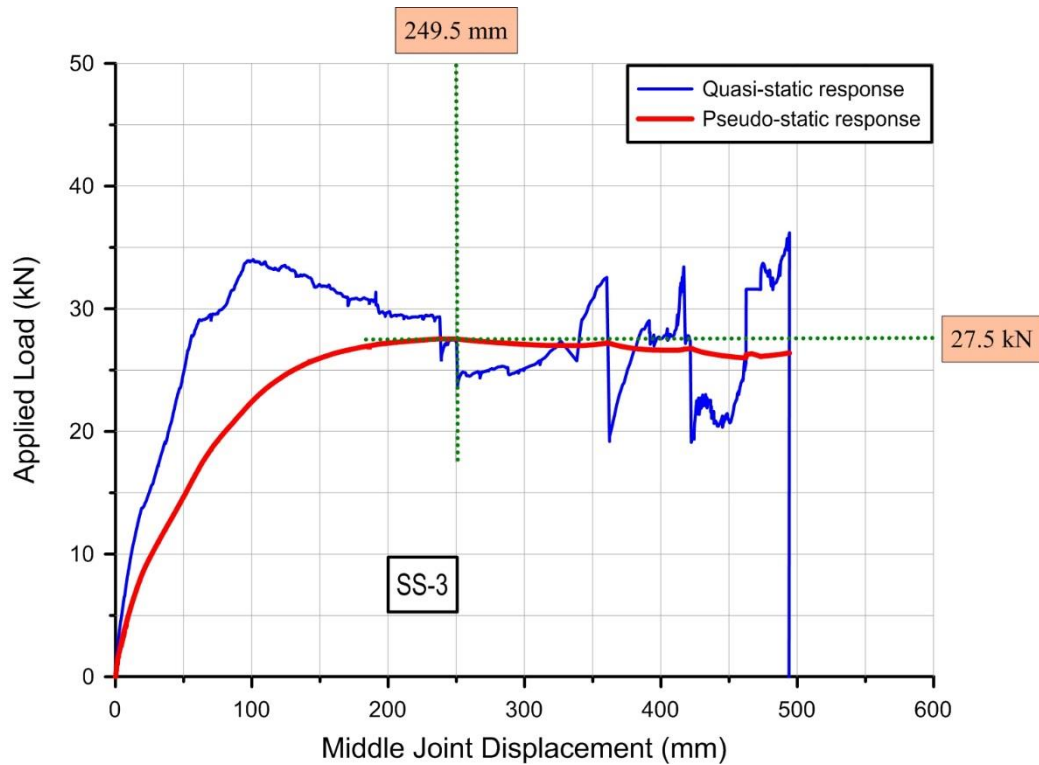
Figure 4-9 Non-linear Pseudo-Static Response of Specimen SS-3

From Figure 4-9, the progressive collapse capacity for specimen SS-3 is 27.5 kN with a corresponding middle joint displacement of 249.5 mm. The same conclusions for specimen SS-2 can be drawn as for specimen SS-3. Figure 4-10 shows the comparison between specimen SS-2 and SS-3. The overall pseudo-static response for SS-2 and SS-3 were quite similar, the main difference was the MJD at which maximum progressive collapse capacity was attained. The MJD for SS-3 was much larger than the MJD for specimen SS-2. This can be related to the difference in concrete compressive strength, which is larger for SS-2 than for SS-3. Concrete members with larger concrete compressive strength may fail in a brittle mode while concrete members with smaller concrete compressive strength may have inherent ductility.

It is clear from Figures 4-8 and 4-9, that the first peak pseudo-static resistance coincided with the first fracture of reinforcing bars in each specimen, indicating that bar fracture weakens progressive collapse resistance. The overall trends of pseudo-static responses were similar to those of quasi-static responses, but it is remarkable that the large catenary action capacities obtained from quasi-static tests were significantly reduced under dynamic situations.
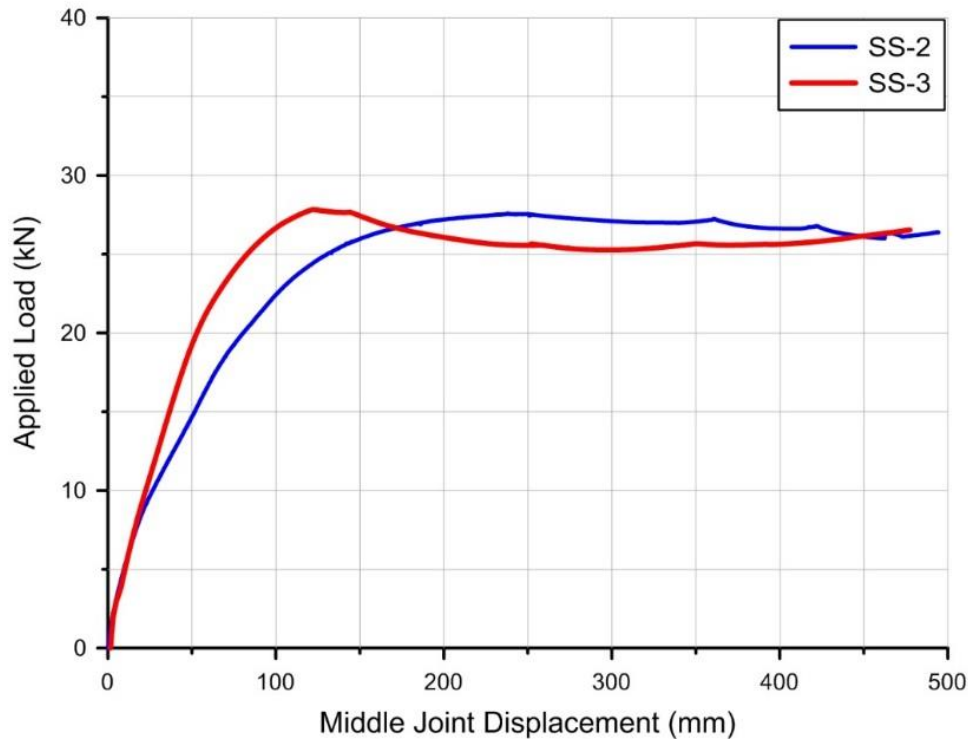
Figure 4-10 Comparison of Pseudo-Static Response for SS-2 and SS-3

## 4.3.1.2 TEST RESULTS OF SPECIMEN SS-4

Specimen SS-4 was designed and detailed according to conventional design. In addition, two steel bars were added at the centre of the beam section to increase the progressive collapse resistance as shown in Figure 3-4. Figure 4-11 shows deflection curves along the length of the beam at different stages of loading.

It can be seen from Figure 4-11 that the beam deflected symmetrically at both sides of the specimen, also it can be seen that there is a large difference in displacement between when the first top bar fractured and the end of the test. This indicates that after the fracture of the top bars at the beam ends, the middle bar layer then acted as the tensile reinforcement and enhanced the total progressive collapse resistance and increased the final middle joint displacement. The middle joint travelled downward about 231 mm after the first top bar fracture until the total failure of the specimen.
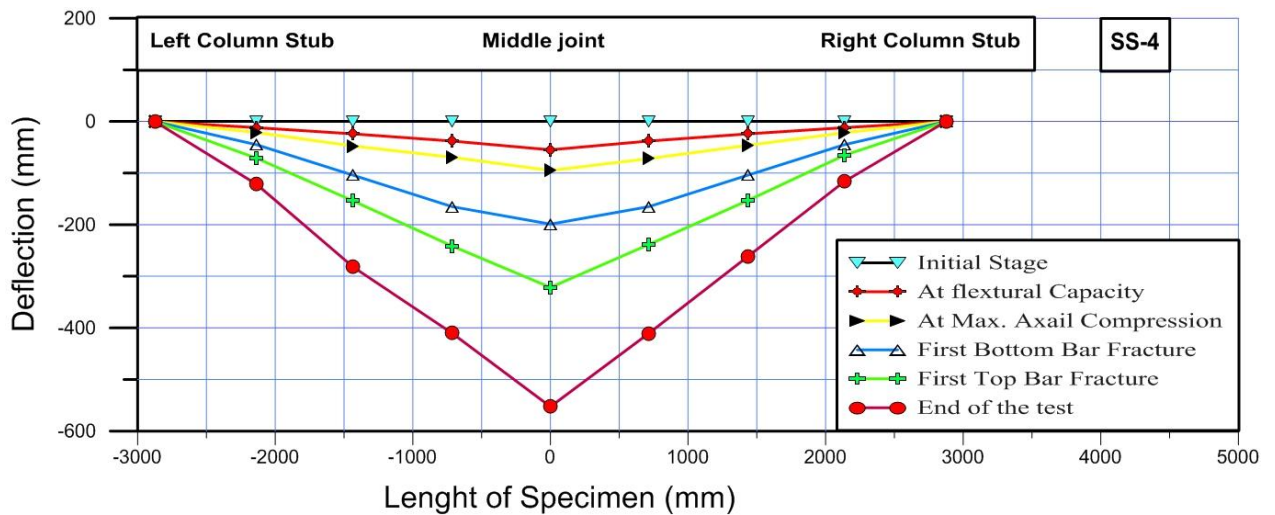
Figure 4-11 Beam Deformation for Specimen SS-4

From Figure 4-12, which shows the applied load-deflection relationship, it is clear that the load capacity at catenary action was larger than the theoretical flexural load by about 96%. The general trend of the structural behaviour of specimen SS-4 was similar to specimen SS-2 and SS-3. Catenary action started to develop at a deflection of 283 mm, which is about 1.13 times the beam height, and 0.1 of the beam span length. First bottom bar fracture occurred at a large deflection of 200 mm, which reflects the effect of the additional middle layer of bars by increasing the tension strength of the beam section.

Figure 4-13 shows the relationship between the axial forces developed throughout the beam and the middle joint deflection. At the beginning of the test, the specimen experienced axial compressive forces followed by tension forces and the transition point from compression to tension indicates the onset of catenary action, which occurred at a deflection of 283 mm. It is clear that the tensile forces developed were much larger than the compressive forces. This was due to the presence of the additional steel bars.

From Table 4-4, the increase of the applied load due to the enhancement of compressive arch action upon the flexural capacity was 16.3%, while the increase of the applied load due to the enhancement of catenary action upon the compressive arch action was 68.9%.
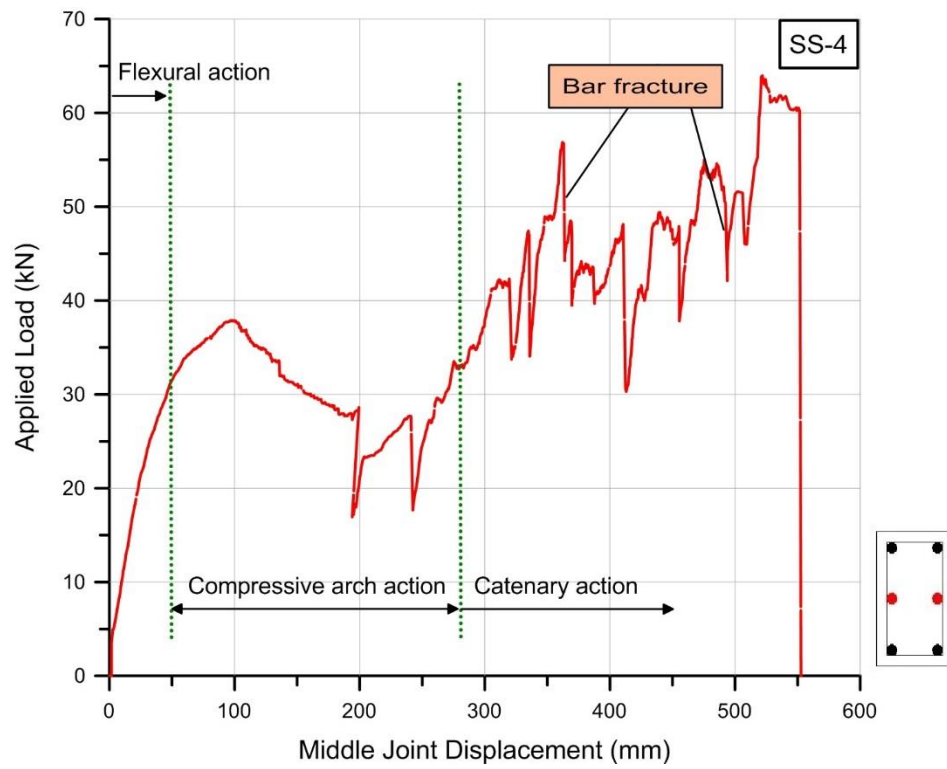
Figure 4-12 Applied Load vs. Middle joint Displacement Relationship of Specimen SS-4
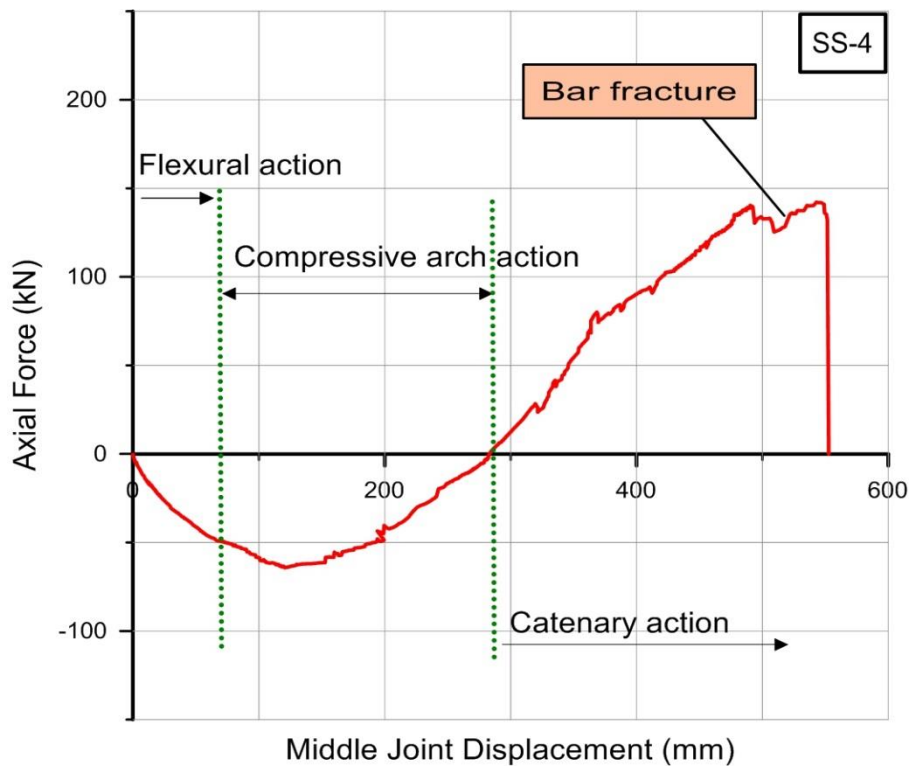


Figure 4-13 Axial Force vs. Middle Joint Displacement Relationship of Specimen SS-4

The increase in the applied load from CAA to catenary action corresponds to the increase in the deflection of about 424.9 mm. The MJD corresponding to the maximum applied load was 521.7 mm, which is smaller than the MJD corresponding to the maximum tensile axial force at catenary action, which was 542.9 mm. This can be explained by the occurrence of strain hardening for steel reinforcement at catenary action.

Table 4-4 Forces with their MJD's at critical stages for SS-4

| Specimen | Calculated flexural capacity with MJD | | Max. load at CAA | | Max. Axial compression Force | | Max. Axial Tension Force | | Max. Load at Catenary Action | |
|---|---|---|---|---|---|---|---|---|---|---|
| | $P_f$ (kN) | MJD (mm) | $P_{com}$ (kN) | MJD (mm) | $N_{com}$ (kN) | MJD (mm) | $N_{ten}$ (kN) | MJD (mm) | $P_{cat}$ (kN) | MJD (mm) |
| SS-4 | 32.6 | 55.1 | 37.9 | 96.8 | 64.3 | 120.6 | 142.2 | 542.9 | 64.0 | 521.7 |

Figure 4-14 and 4-15 show crack development at different stages of loading. At the beginning of the test, flexural cracks were developed. Flexural cracks were concentrated at the interfaces of the beam-column joints. Flexural cracks started to develop from the extreme tension fibre of concrete, penetrate through the beam section and stopped at the location of neutral axis.

With the increase of loading, plastic hinges were developed at nearly a distance equals to the beam depth from the face of the column. The formation of plastic hinges occurred at point "C" as indicated in Figures 4-14 and 4-15. Large cracks at the location of bar fracture were accompanied by slippage between steel bars and the concrete. Point "D" represents the transition point from CAA to catenary action. Similar to specimen SS-2 and SS-3, at catenary action, uniform vertical cracks began to develop along the length of the beam. At the end of the test, the specimen failed by the fracture of all remaining steel bars at the left side of the specimen.

Figure 4-16 shows the Pseudo-Static behaviour for specimen SS-4. At a deflection of 163.8 mm, the specimen attained its first peak capacity of 29.7 kN, which is located within the CAA stage. Catenary action was able to increase the progressive collapse resistance to 37.4 kN, which is larger than the first peak by about 26%.
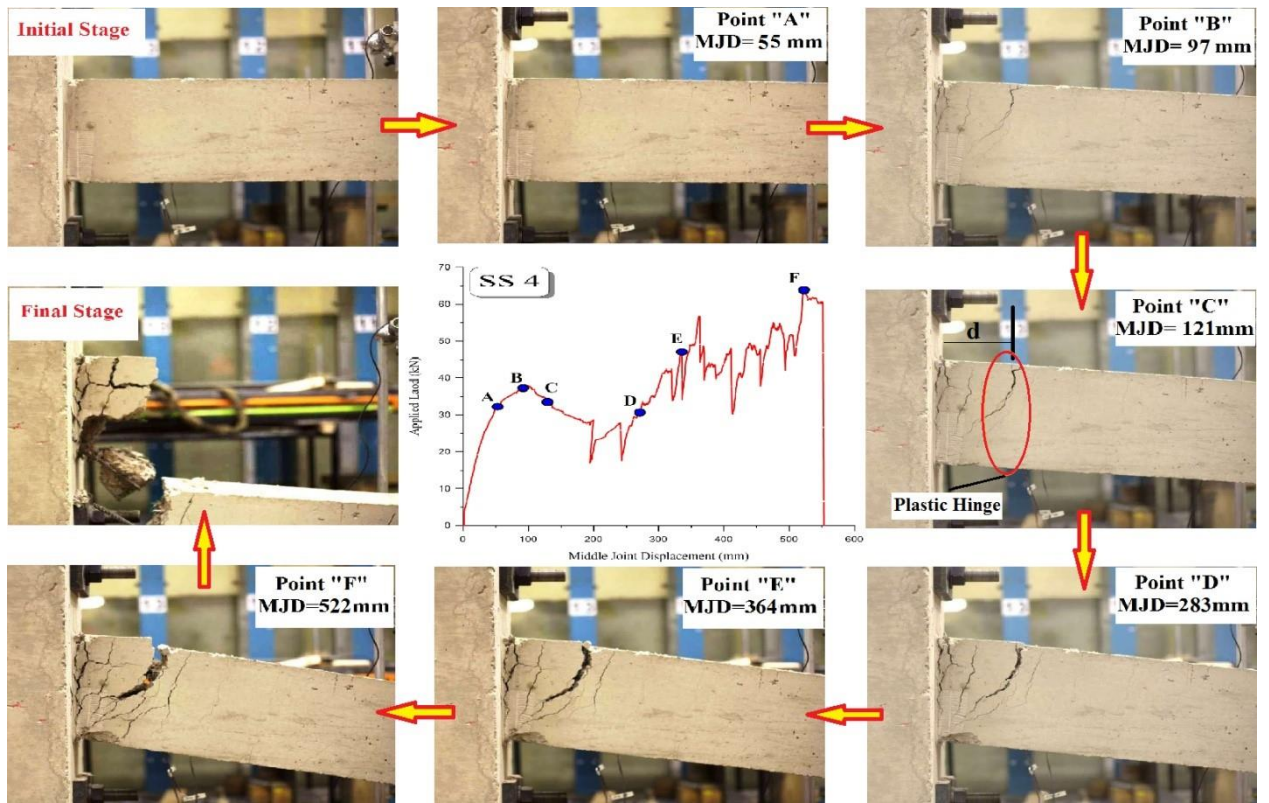
Figure 4-14 Crack Development at the Right Beam End for Specimen SS-4
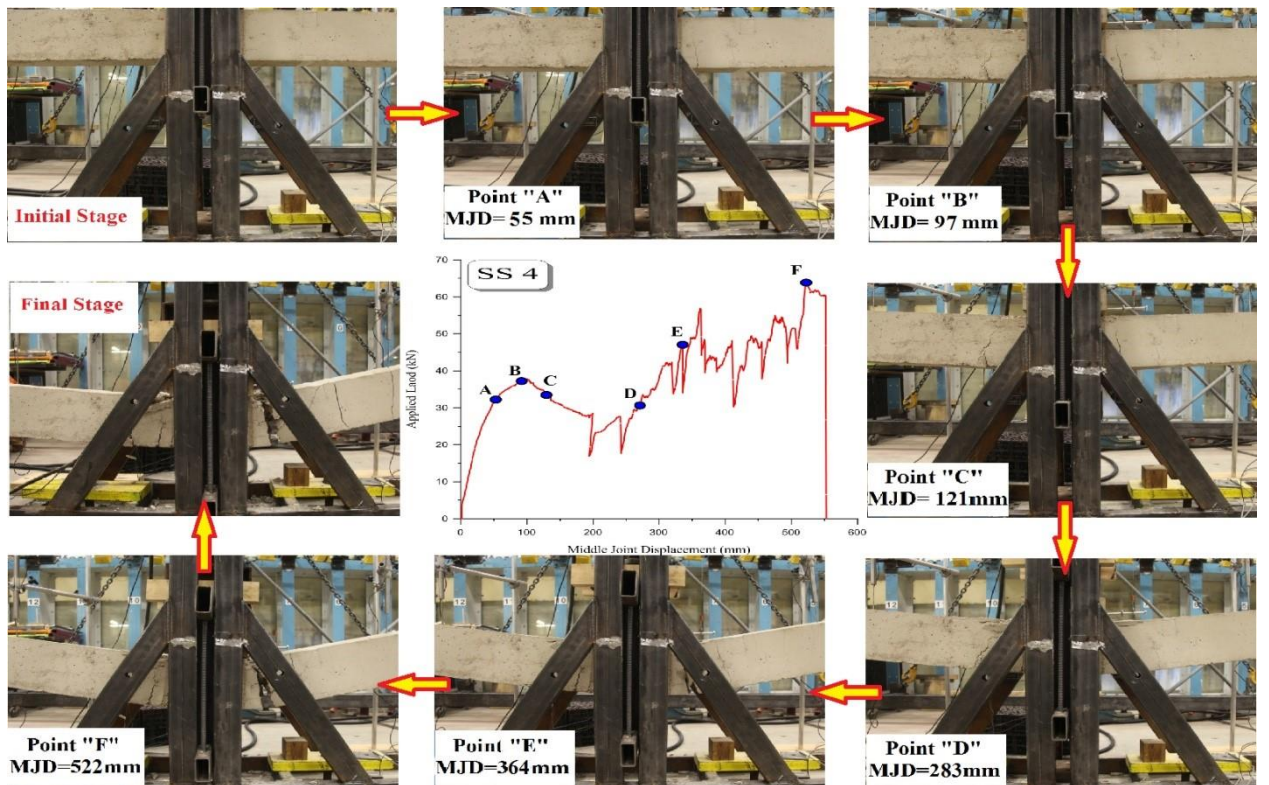


Figure 4-15 Crack Development at the Middle Joint for Specimen SS-4
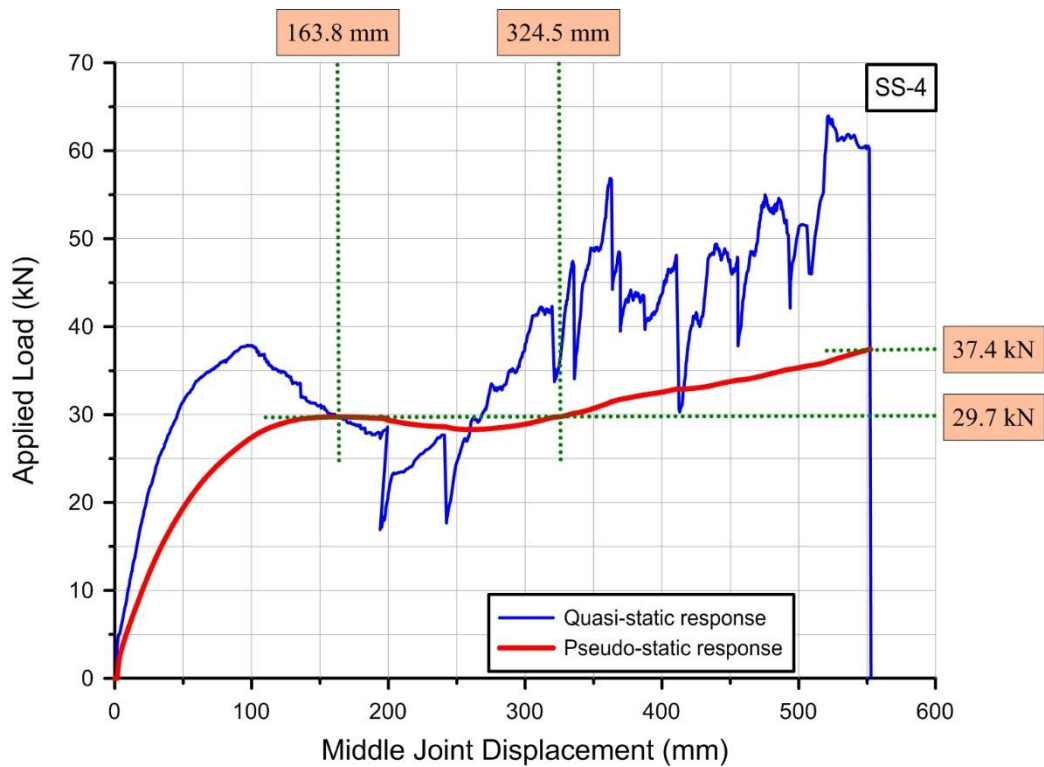
Figure 4-16 Non-linear Pseudo-Static Response for the Specimen SS-4

It should be mentioned, if the applied load is increased beyond 29.7 kN, the specimen would collapse unless it can provide enough strain energy capacity at the catenary action stage to resist the external loads. The green dotted horizontal line in Figure 4-16 indicates the stage after the first peak load 29.7 kN. Also, it indicates that the load 29.7 kN will cause a deflection of 324.5 mm at the stage of catenary action.

## 4.3.1.3 TEST RESULTS OF SPECIMEN SS-5

Specimen SS-5 was designed and detailed according to conventional design. In addition, two steel bars were included at a vertical distance of $(d - d')/4$ from the centre of the bottom reinforcement as shown in Figure 3-4. Figure 4-17 shows the deflection curves along the length of the beam at different stages of loading. It can be seen from Figure 4-17 that the beam deflected symmetrically and there is a large deflection increase between the stage of maximum axial compression and the fracture of the first top bar. Different from other specimens, there is no sign of bottom bar fracture during flexural and compressive arch action.
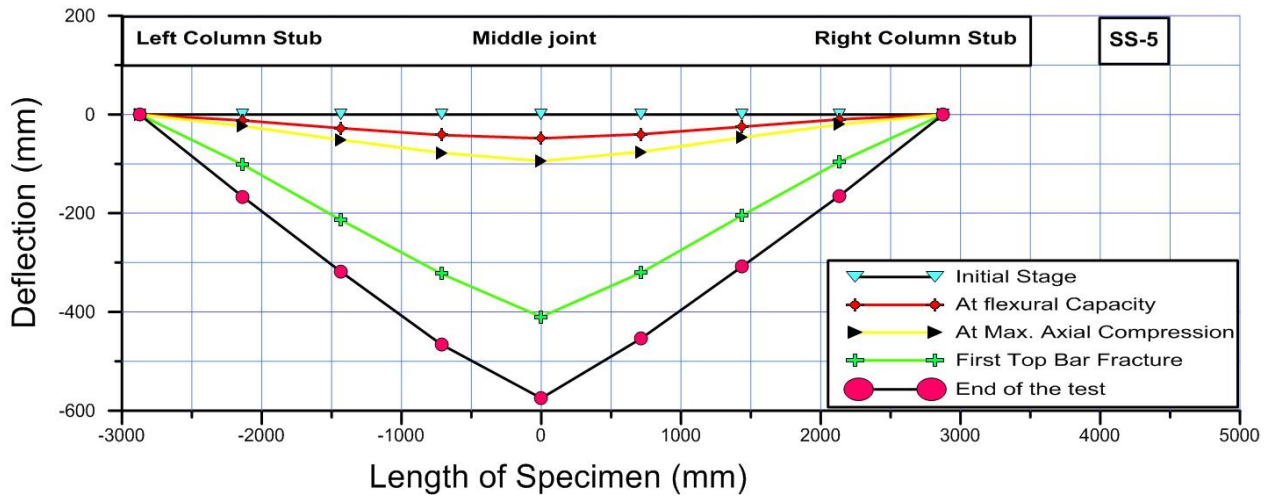
Figure 4-17 Beam Deformation for Specimen SS-5

The additional steel reinforcing bars enhanced the force carrying capacity in the tension zone in the beam section, which results in fracture of the top bars first at a relatively large middle joint displacement. Flexural capacity was attained at a relatively small deflection. Large rotation at the beam ends occurred as can be seen from Figure 4-17.

Figures 4-18 and 4-19 show the relationships of applied load vs. middle joint displacement and axial force vs. middle joint displacement for specimen SS-5.
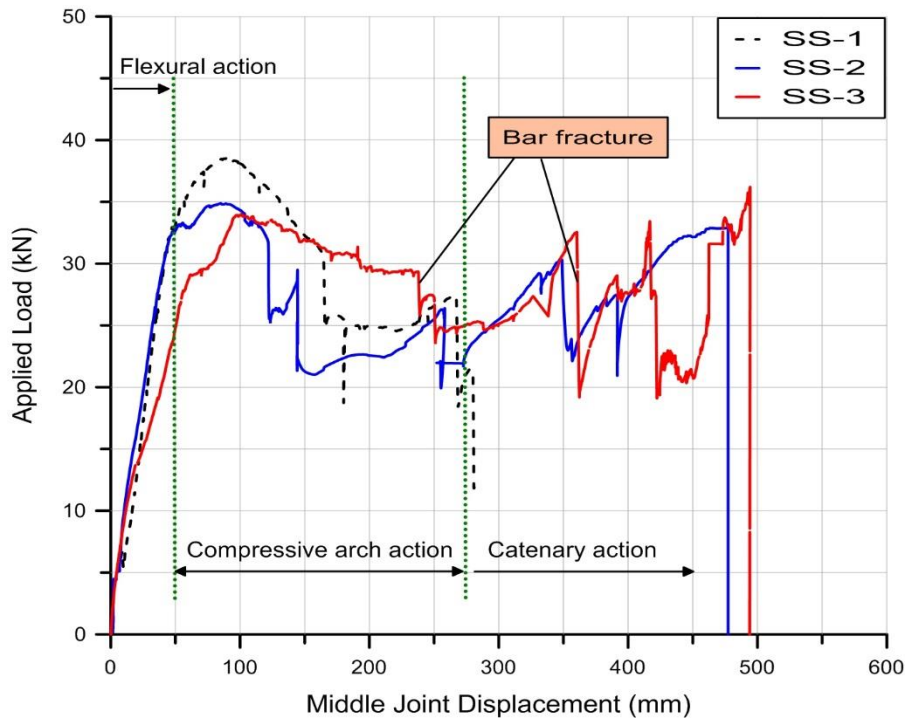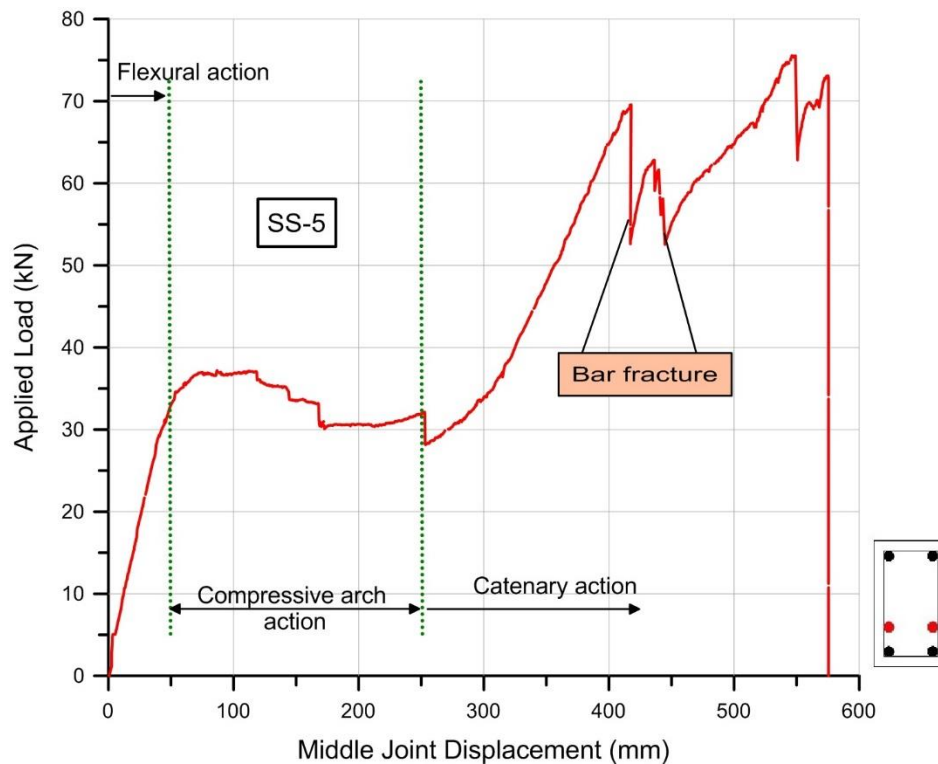


Figure 4-18 Applied Load vs. Middle Joint Displacement Relationship of Specimen SS-5
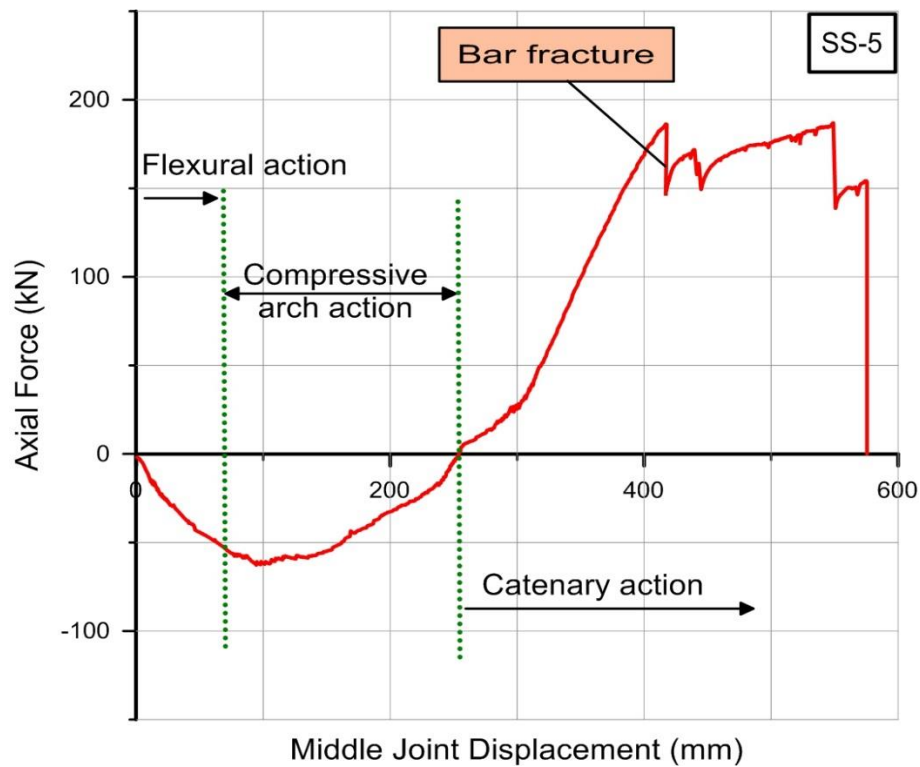
Figure 4-19 Axial Force vs. Middle Joint Displacement Relationship of Specimen SS-5

The general trend of the non-linear relationship between the applied load and the middle joint displacement was similar to the benchmark specimens except that there was no bar fracture during compressive arch action. The applied load-MJD history can be divided into three resisting mechanism stages and the catenary action stages began to mobilise at 254.3 mm of deflection, which is nearly equal to the beam height.

The first peak of applied load occurred at the compressive arch action stage at 37.2 kN with a deflection of 86.8 mm. This peak was followed by a softening in the curve due to concrete crushing. The peak of axial compressive force occurred at 94.6 mm slightly larger than the deflection of the peak of the applied load. The enhancement of compressive arch action to the flexural action was 15.5%, which is nearly the same for specimen SS-4. This clearly indicates that the effect of the additional bar at these locations has the same effect on flexural capacity at the compressive arch action.

At catenary action, the maximum applied load carried by the specimen was 75.6 kN at a deflection of 549 mm. The maximum axial tension force carried by the specimen was 186.9 kN occurring at a deflection of 549.0 mm. The increase in the applied load at catenary action was 103%, which is larger than those for specimen SS-4. Table 4-5 summarises the forces and their corresponding middle joint displacements at critical stages of the load-deflection history.

Table 4-5 Forces with their MJD's at critical stages for specimen SS-5

| Specimen | Calculated flexural capacity with MJD | | Max. load at CAA | | Max. Axial compression Force | | Max. Axial Tension Force | | Max. Load at Catenary Action | |
|---|---|---|---|---|---|---|---|---|---|---|
| | $P_f$ (kN) | MJD (mm) | $P_{com}$ (kN) | MJD (mm) | $N_{com}$ (kN) | MJD (mm) | $N_{ten}$ (kN) | MJD (mm) | $P_{cat}$ (kN) | MJD (mm) |
| SS-5 | 32.2 | 48.2 | 37.2 | 86.8 | 62.7 | 94.6 | 186.9 | 549.0 | 75.6 | 549.0 |

After the peak of applied load at catenary action, the tensile force decreased with the increase of the middle joint displacement due to the sequence of fracture of the top bars and the yield of the longitudinal bottom and middle steel bars. No further load carrying capacity was attained and the specimen failure occurred at a deflection of 575.5 mm.

Figure 4-20 and 4-21 shows crack development at different stages of loading. Similar to the specimen SS-4, flexural cracks were developed at the beginning of the test followed by uniformly penetrating cracks along the length of the beam at the catenary action stage. Flexural cracks were concentrated at the interfaces of beam-column joints. Flexural cracks started to develop from the extreme tension fibre of concrete, penetrated through the beam section and stopped at the location of neutral axis.

Different from specimen SS-4, at early stages, wide cracks were concentrated at the beam ends as can be seen in Figure 4-20. Point "B" in Figure 4-20 represents the point of maximum axial compressive force developed throughout the beam in which the indication of concrete crushing was clear. After that point, concrete spalling occurred indicated by the point "C".

The failure of the specimen occurred after the point "F" at a deflection of 575.5 mm, indicated by a rapid increase in the deflection associated with a decrease in the applied load.
.
Figure 4-22 shows the converted non-linear static behaviour to the pseudo-static behaviour for specimen SS-5. The progressive collapse resistance at compressive arch action was 30.5 kN and the corresponding deflection was 172.7 mm. Catenary action was able to increase the progressive collapse resistance to 44.1 kN at a deflection of 575.5 mm.
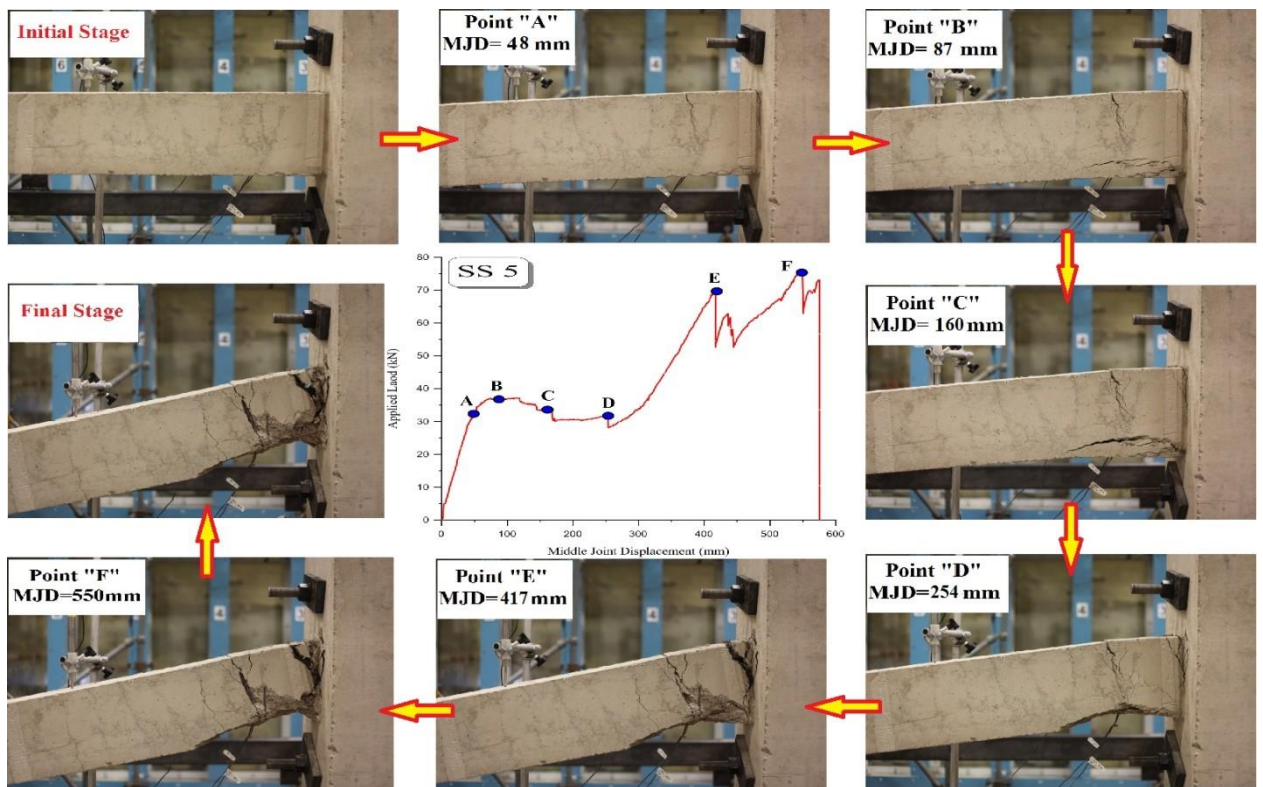
Figure 4-20 Crack Development at the Left Beam End for Specimen SS-5
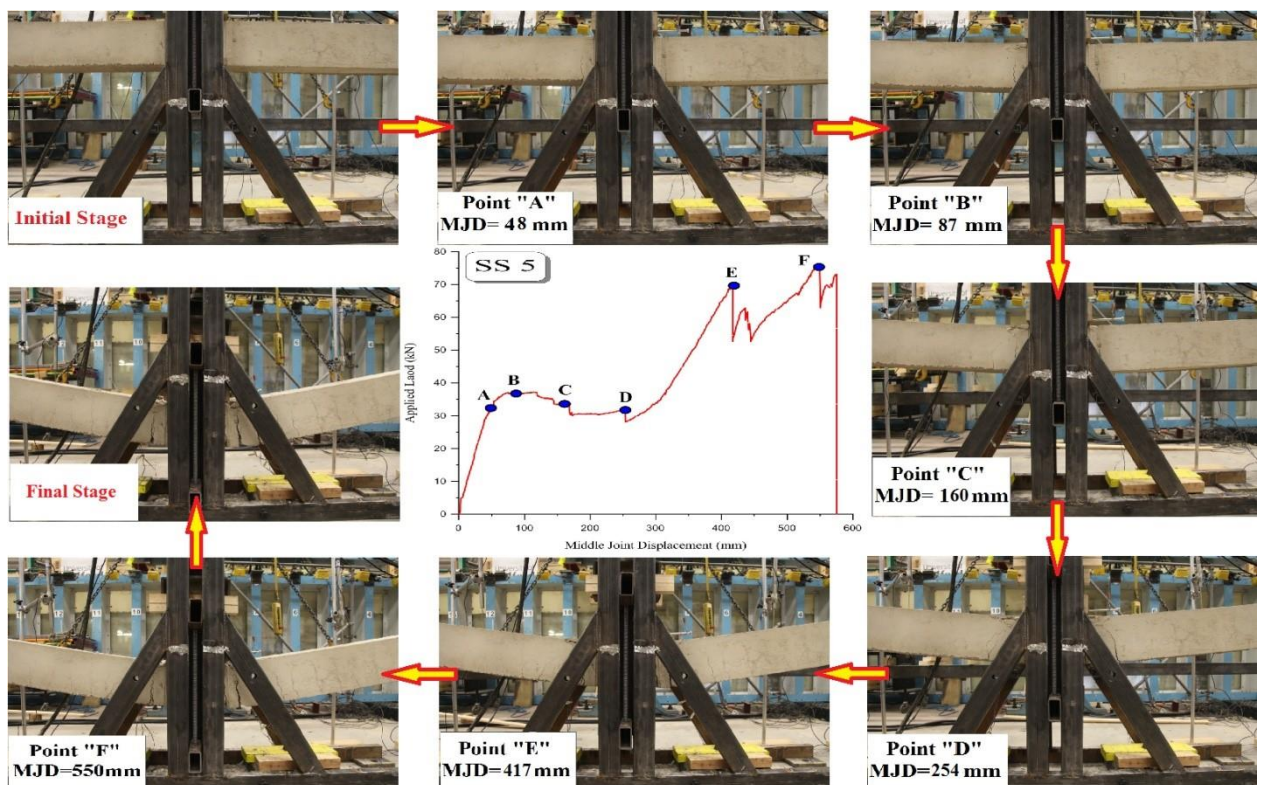


Figure 4-21 Crack Development at the Middle Joint for Specimen SS-5
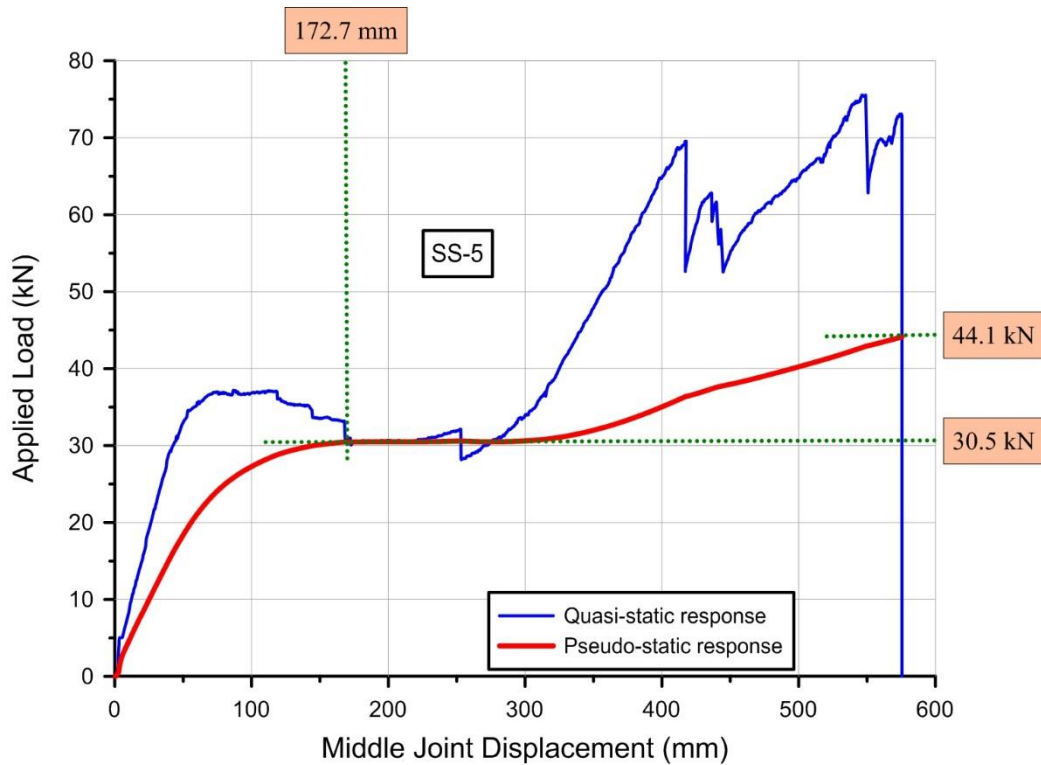
Figure 4-22 Non-linear Pseudo-Static Response for the Specimen SS-5

The enhancement of catenary action to the progressive collapse resisting capacity was 44.6% and the specimen did not fail until a deflection of 575.5 mm. It is clear that the effect of the additional bars was not limited to the catenary action stage, but also influenced the compressive arch action.

It is clear from Figures 4-18,4-19 and 4-22, that the structural behaviour of specimen SS-5 was more stable, and there is no reduction in the progressive collapse capacity after first peak of the non-linear pseudo-static response as can be seen in Figure 4-22.

Due to the presence of additional bars, the bottom bars did not fracture at the early stages of loading. This provided the beam specimen with enough strain energy to absorb the shock of the applied load, which is reflected in the curve by no reduction in the capacity after the first peak during compressive arch action. In addition, the extra bars provided the specimen with enough ductility after the first peak and the middle joint travelled about 400 mm from the first peak until the total failure of the specimen.

## 4.3.1.4 TEST RESULTS OF SPECIMEN SS-6

Specimen SS-6 was designed and detailed according to the conventional design. In addition, two steel bars were included at a vertical distance of $(d - d')/4$ mm from the centre of the top reinforcement as shown in Figure 3-4. Figure 4-23 shows deflection curves along the length of the beam at different stages of loading.

It can be seen from Figure 4-23 that the beam deflected symmetrically and there is a large displacement difference between the fracture of bottom bars and the fracture of the top bars. This was due to the contribution of strength provided by the additional steel bars in the top quarter of the section. The rotation capacity of the beam at the ends was limited before the fracture of the top steel bars. After the fracture of the top bars, the rotation of beam at the ends increased significantly.
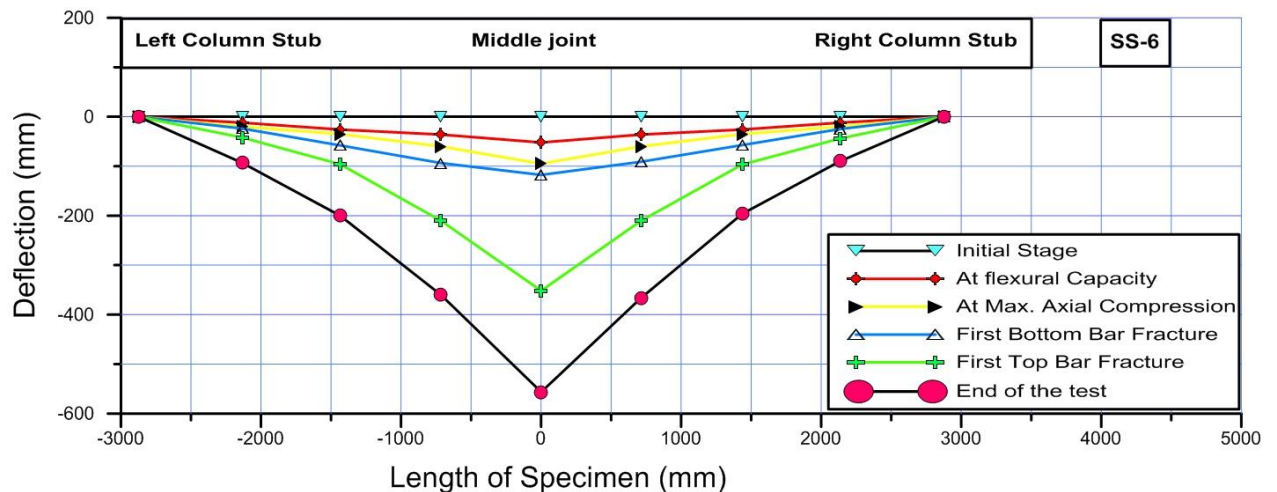


Figure 4-23 Beam Deformation for Specimen SS-6

Figures 4-24 and 4-25 show the relationships of applied load vs. MJD and axial force vs. MJD for specimen SS-6. Table 4-6 summarises forces and their corresponding MJD at critical stages of the load-deflection history.

The general trend of the non-linear behaviour of specimen SS-6 was similar to those for specimen SS-2 and SS-3, and the load-deflection history can be also divided into three stages as stated for SS-2 and SS-3.
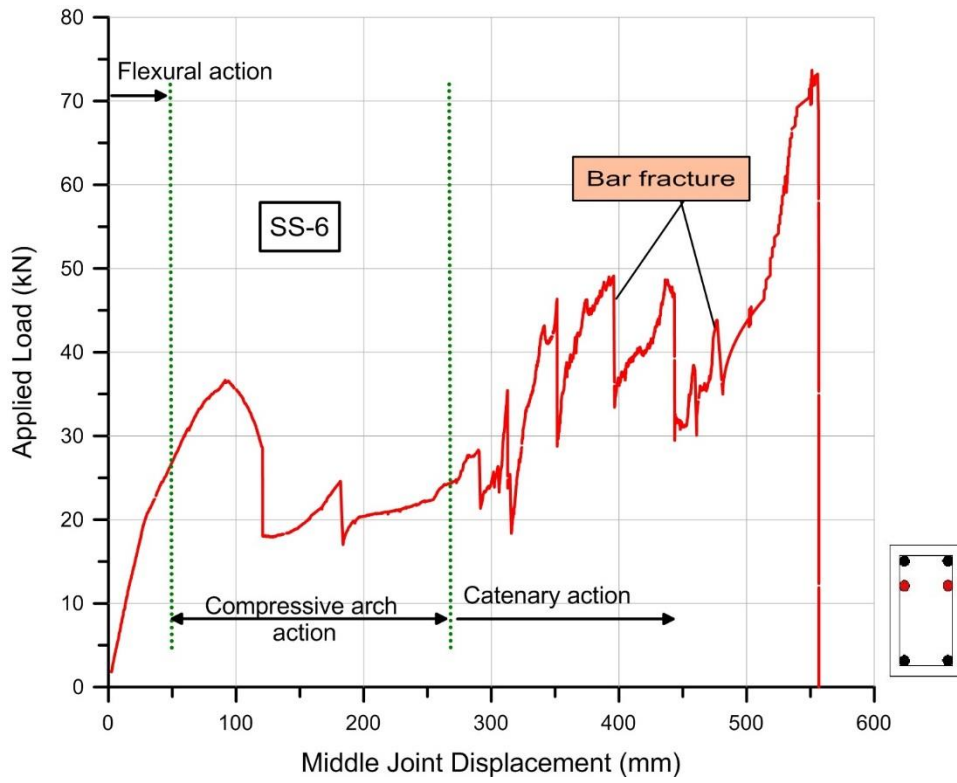
Figure 4-24 Applied Load vs. Middle Joint Displacement Relationship of Specimen SS-6
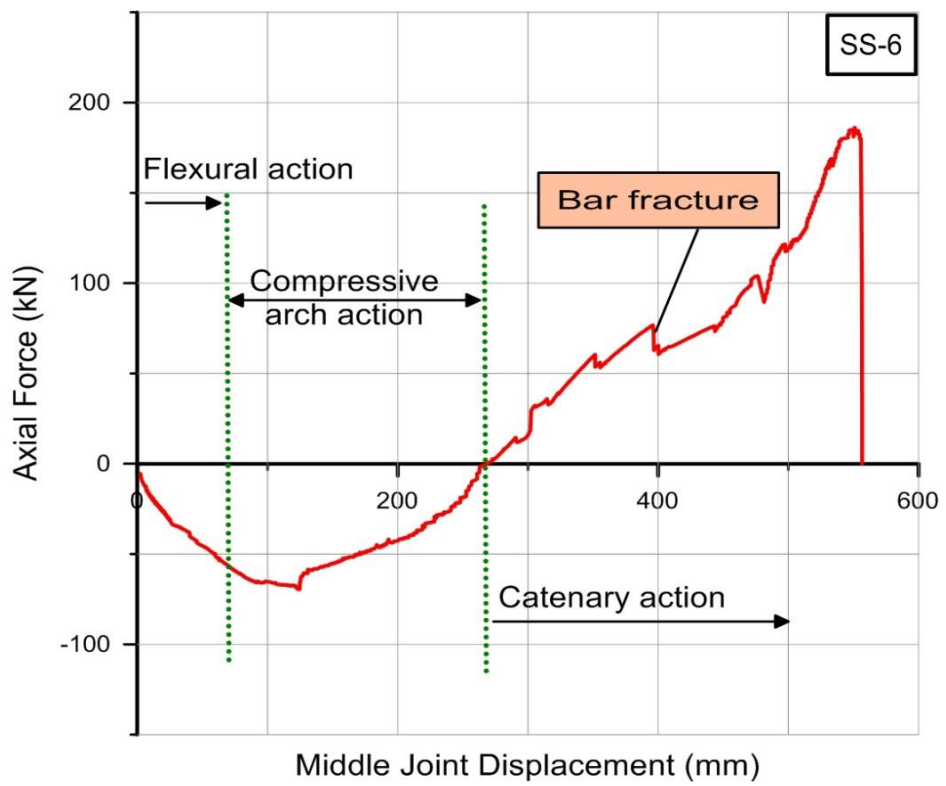


Figure 4-25 Axial Force vs. Middle Joint Displacement Relationship of Specimen SS-6

As expected the additional layer of steel bars at the top or bottom quarter of the beam section did not increase the flexural capacity because it is located near the neutral axis of the section after the stage where the cracking moment is exceeded. Different from normal loading, under middle column removal scenario, the effect of additional steel bars can significantly increase the capacity of RC structures by providing RC members with more tensile capacity at catenary action.

As can be seen from Figure 4-25, catenary action started to develop at a middle joint displacement of 268.2 mm, which is nearly the same for specimen SS-3 and it is roughly equal to the beam section height. The enhancement of compressive arch action to the flexural action was 21.5%. The maximum axial compressive force developed during compressive arch action was 69.6 kN, which is nearly the same for specimen SS-3. This is because the axial compression depends mainly on concrete strength. It was also noticed that the maximum axial compressive force occurred at a deflection of about half the beam height for both SS-3 and SS-6.

The additional two steel bars were able to increase the structural resistance significantly at catenary action. At a middle joint displacement of 91.4 mm, the applied load was 36.7 kN, while it was twice this amount at catenary action. This means that the additional bars can increase the carrying load capacity by about 100% of the capacity at the compressive arch action. Fracture of additional steel bars occurred during catenary action at the middle joint interfaces, and the abrupt drops in the applied load shown in Figure 4-24 were due to subsequent fracture of steel reinforcing bars at bottom and top of the beam section. Gradual decrease in the applied load was due to concrete crushing and yielding of the steel bars.

Table 4-6 Forces with their MJD's at critical stages for SS-6

| Specimen | Calculated flexural capacity with MJD | | Max. load at CAA | | Max. Axial compression Force | | Max. Axial Tension Force | | Max. Load at Catenary Action | |
|---|---|---|---|---|---|---|---|---|---|---|
| | $P_f$ (kN) | MJD (mm) | $P_{com}$ (kN) | MJD (mm) | $N_{com}$ (kN) | MJD (mm) | $N_{ten}$ (kN) | MJD (mm) | $P_{cat}$ (kN) | MJD (mm) |
| SS-6 | 30.2 | 60.1 | 36.7 | 91.4 | 69.6 | 124.5 | 185.0 | 549.7 | 73.7 | 551.2 |

Figures 4-26 and 4-27 show the crack development at different stages of loading. Wide cracks and bar fracture occurred at the middle joint interfaces during the test with large slippage. Concrete crushing and cover spalling occurred at the ends of the beam before concrete crushing at the middle joint interfaces. This indicates that the enhancement and the effect of the additional steel bars reduced the stress concentration on the concrete at early stages of loading.

Local failure was concentrated at the middle joint interfaces where wide cracks started to develop at a MJD of 350 mm.

Uniformly distributed and penetrating cracks along the length of the beam indicated the commencement of the catenary action stage, as shown in Figure 4-28.

Figure 4-29 shows the conversion of non-linear static behaviour to the Pseudo-Static behaviour for specimen SS-6. The progressive collapse resistance at compressive arch action was 25.9 kN and the corresponding deflection was 120.7 mm. Catenary action was able to increase the progressive collapse resistance to 32.3 kN at a deflection of 554.0 mm.

It should be mentioned, if the applied load was increased beyond the 25.9 kN point, the specimen would collapse unless it can provide enough strain energy at the catenary action stage to resist the external loads. The green dotted horizontal line in Figure 4-29 indicates the stage after first peak load. Also, it indicates that the load of 25.9 kN will cause a deflection of 380.3 kN at the stage of catenary action. The enhancement of catenary action to the progressive collapse resistance upon the compressive arch action was 24.7%.
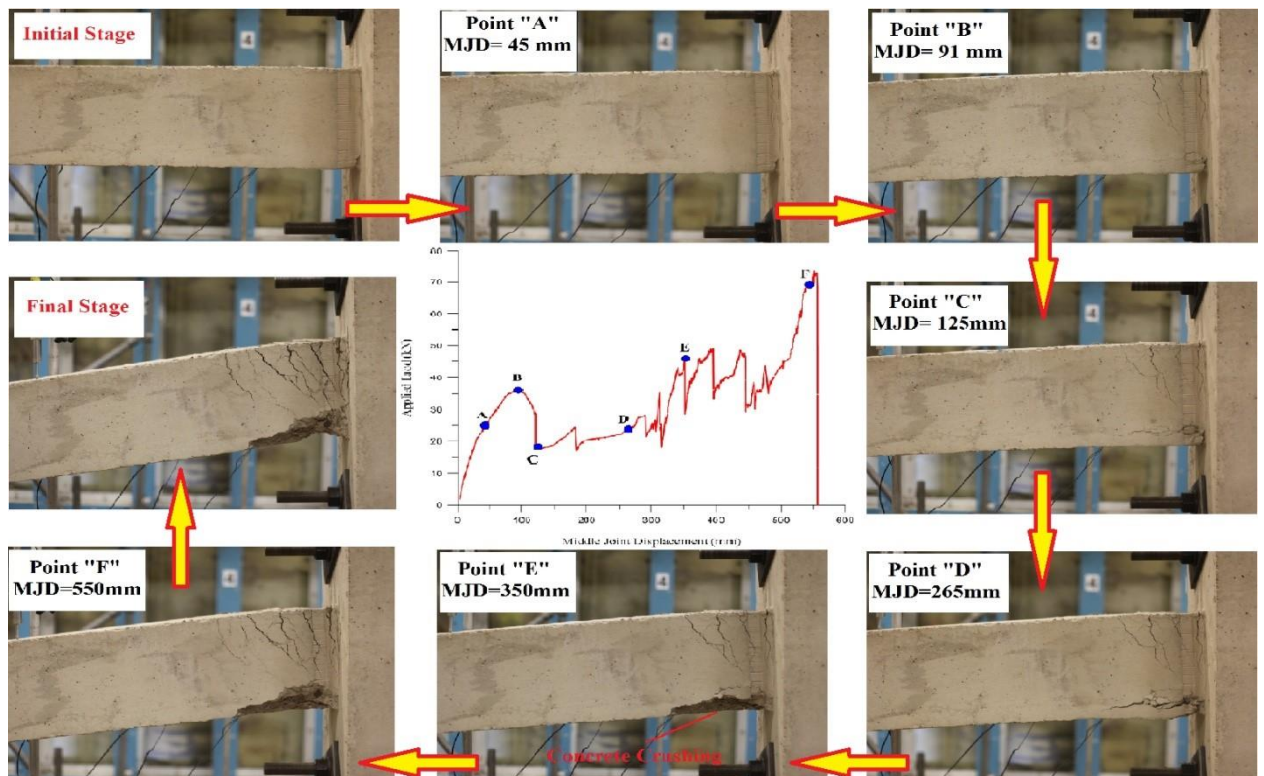


Figure 4-26 Crack Development at Different Stages for Left Beam End of Specimen SS-6
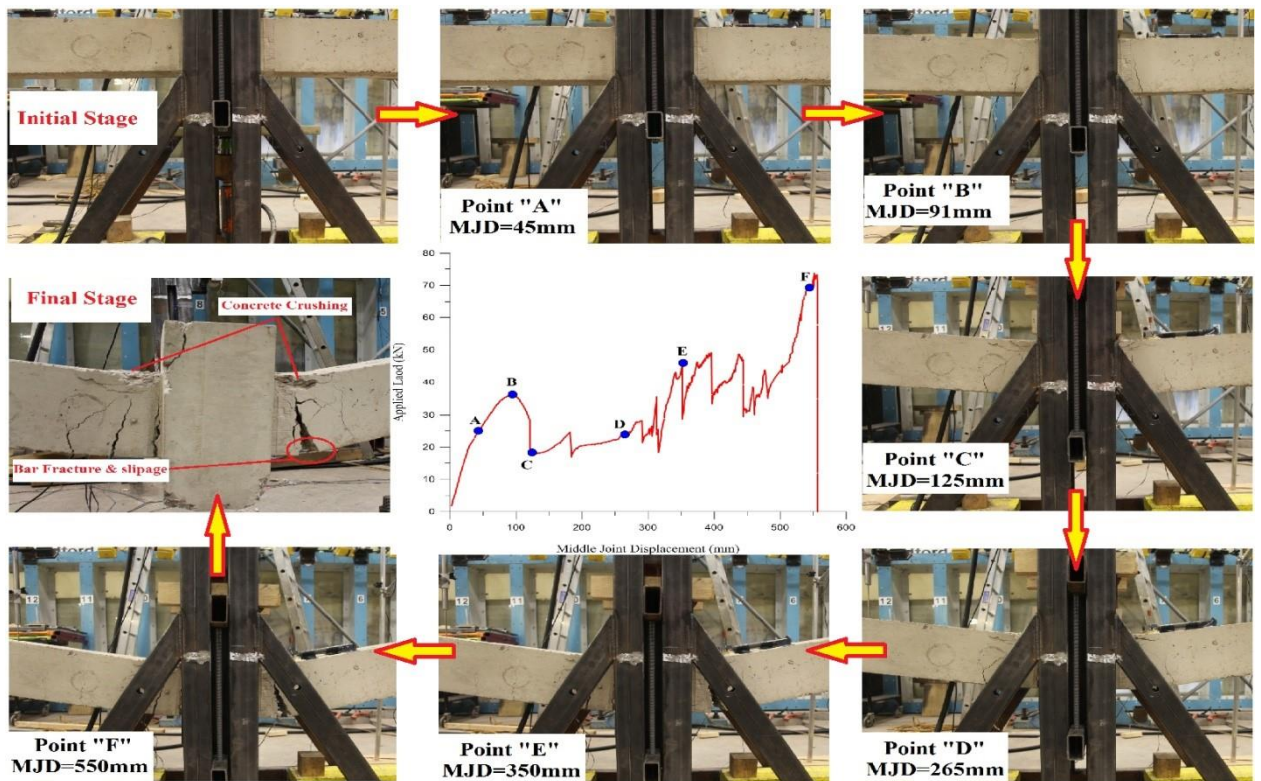
Figure 4-27 Crack Development at Different Stages for the Middle Joint of Specimen SS-6
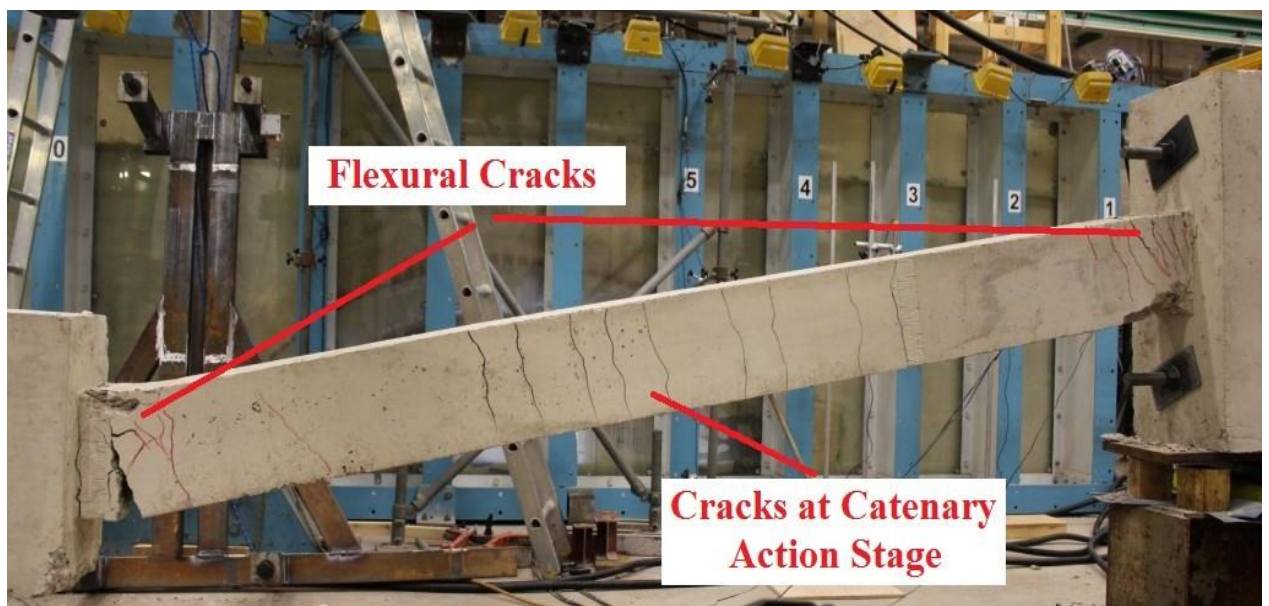


Figure 4-28 Crack Patterns at Flexural and Catenary Stages for Specimen SS-6
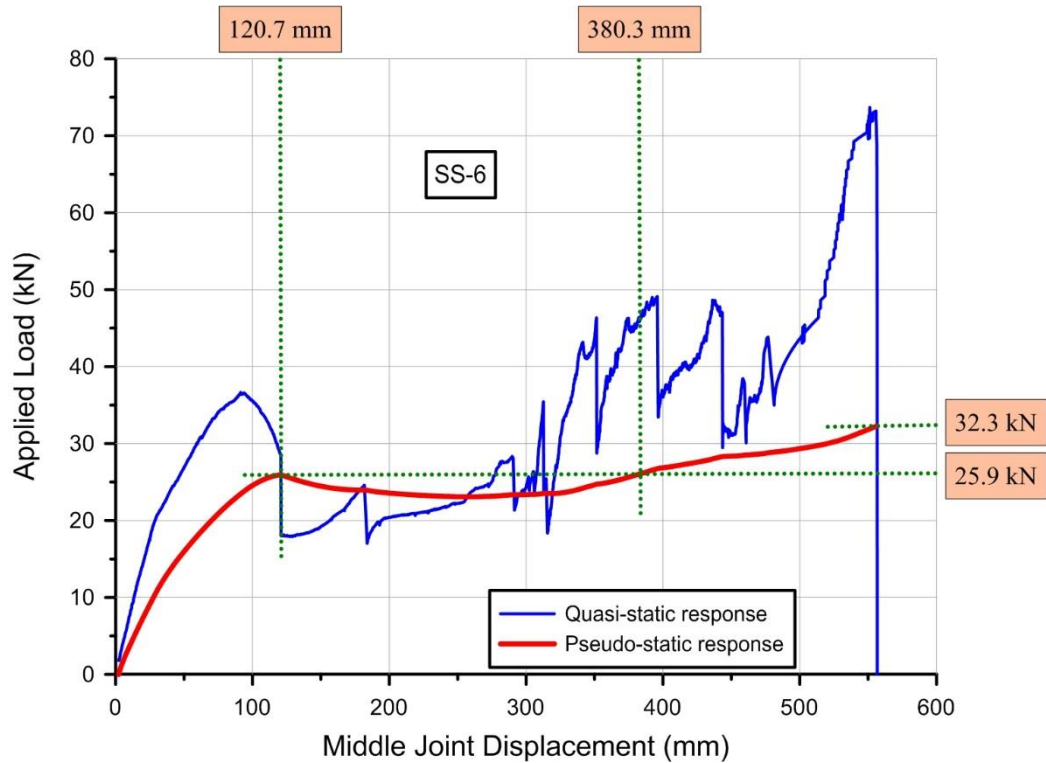
Figure 4-29 Non-linear Pseudo-Static Response for the Specimen SS-6

## 4.3.1.5 TEST RESULTS OF SPECIMEN SS-7

Specimen SS-7 was designed and detailed according to the conventional design. In addition, a partial hinge was provided to the beam section at a distance equal to the beam depth away from the beam-column interface. The intention of providing the partial hinges was to increase the rotational capacity of the RC beams and trigger catenary action stage at a smaller middle joint displacement. In the partial hinge regions, an additional T10 bottom bar was added and bent up at a distance of 125 mm away from the beam column joint interface and one of the top layer T10 bar was bent down at the same distance. The two bent bars levelled off at the bottom and top reinforcement layers, respectively. Finally, the pin of the partial hinges was formed at a distance of 220 mm from the beam-column joint interface, as shown in Figure 3-5.

Figure 4-30 shows the deflection curves along the length of the beam at different stages of loading. It can be seen from Figure 4-30 that the beam deflected symmetrically at both sides and the final deflection was 622 mm, which is larger than the other specimens. Also, it can be seen that the deflection uniformly increased from the initial stage until the maximum axial compressive force developed, and from first bottom bar fracture until the end of the test.

The rotation capacity was increased due to the presence of partial hinges, and this was indicated by the large final deflection. Figures 4-31 and 4-32 show the relationships of the applied load vs. MJD and axial force vs. MJD for specimen SS-7.

Table 4-7 summarises forces and their corresponding middle joint displacements at critical stages of the load-deflection history. The general trend of the non-linear behaviour of specimen SS-7 was similar to those for specimen SS-2 and SS-3, and the load-deflection history can also be divided into three stages as stated for SS-2 and SS-3.
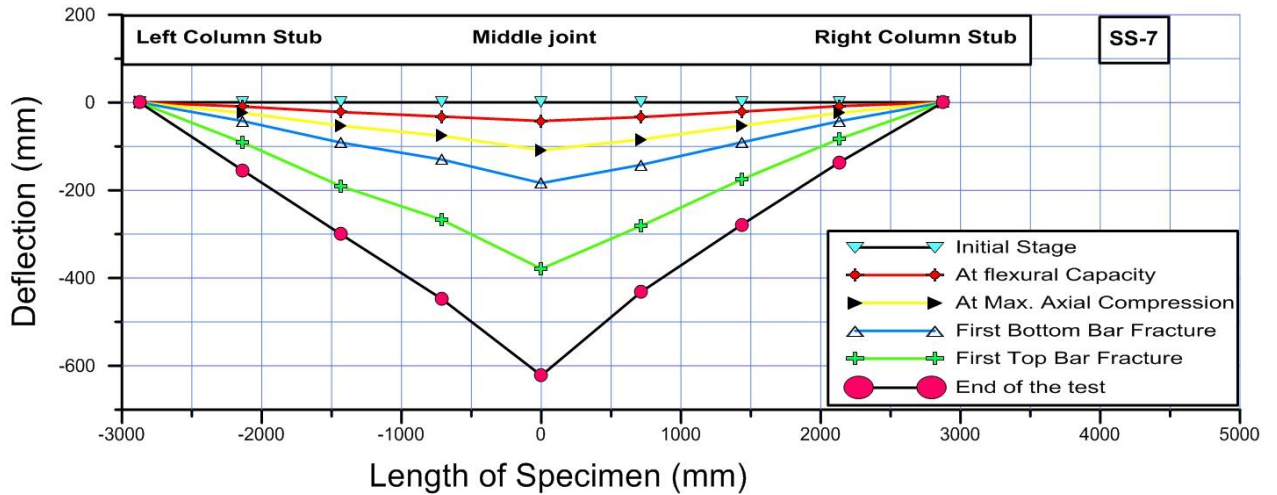


Figure 4-30  Beam Deformation for Specimen SS-7
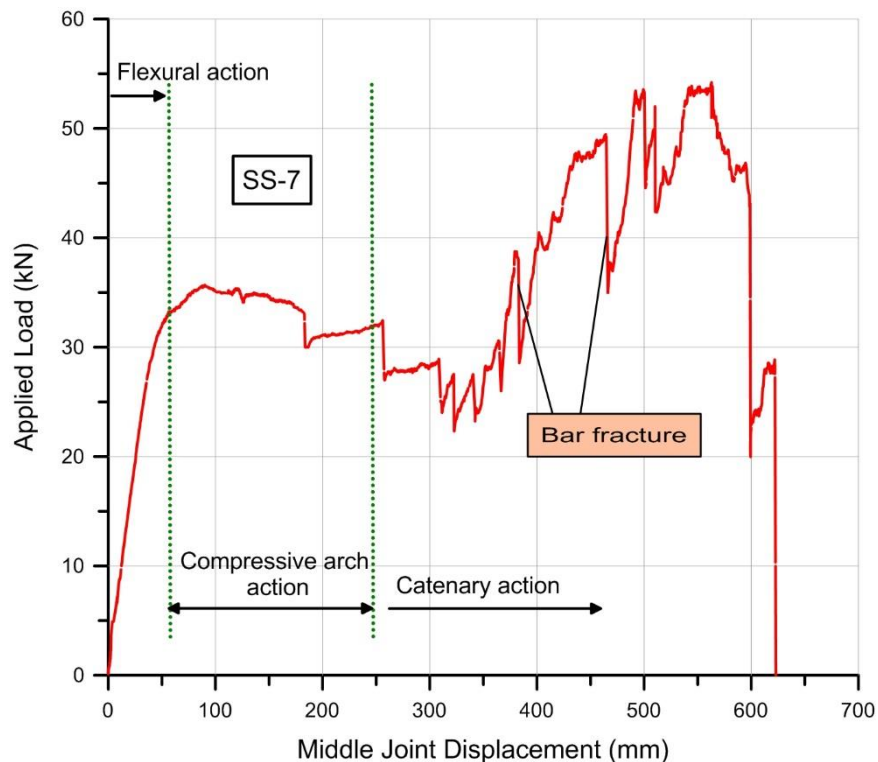


Figure 4-31 Applied Load vs. Middle Joint Displacement Relationship of Specimen SS-7

With the presence of partial hinges, the flexural capacity was attained at a relatively small deflection. The theoretical flexural capacity was calculated according to section analysis, and was equal to 29.8 kN, which was achieved at a displacement of 42.1 mm. The maximum applied load at compressive arch action was 35.6 kN corresponding to a displacement of 87.7 mm. The enhancement of compressive arch action to the applied load was 19.5%. The catenary action stage started to develop at a deflection of 245 mm.

The difference between the deflections at theoretical flexural capacity and the onset of catenary action was 202.9 mm, which was relatively smaller compared to other specimens. The maximum applied load at catenary action was 53.7 kN which is larger than the applied load at compressive arch action by about 50.8%. From experimental observations, most of the steel bars forming the partial hinges remained intact until the advanced stages of deflection were reached. This indicates that the stress concentration was much larger in the longitudinal steel bars than the steel bars of the partial hinges. From Figure 4-32, the maximum axial compressive force was 57.4 kN attained at 108.8 mm of deflection, and the maximum tensile force was 98.4 kN attained at 562.4 mm of deflection.
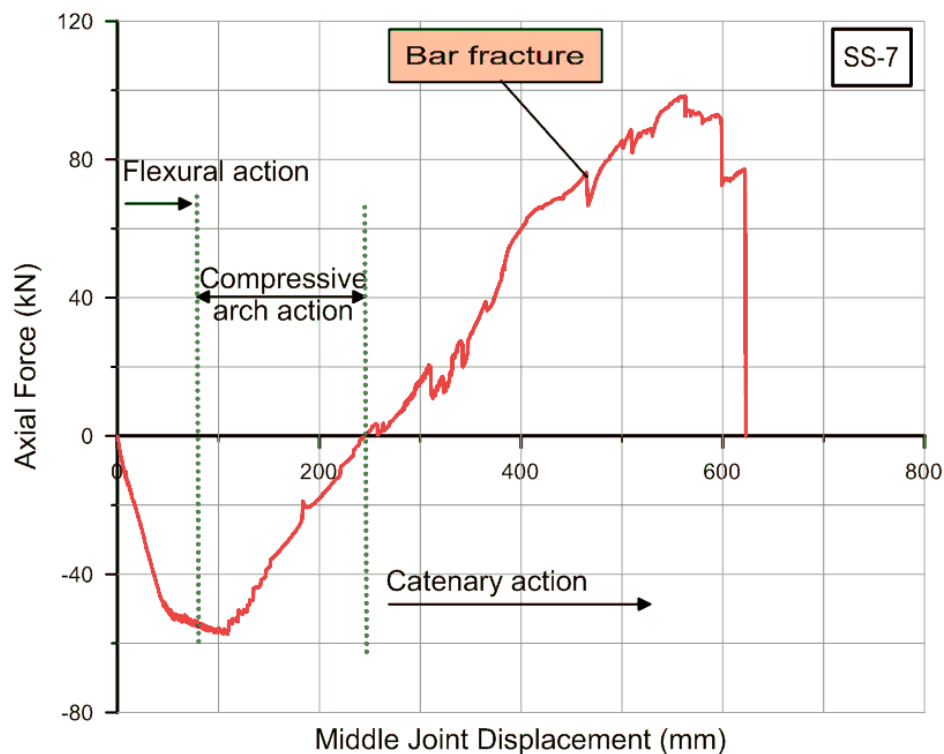


Figure 4-32 Axial Force vs. Middle Joint Displacement Relationship of Specimen SS-7

Table 4-7 Forces with their MJD's at critical stages for SS-7

| Specimen | Calculated flexural capacity with MJD | | Max. load at CAA | | Max. Axial compression Force | | Max. Axial Tension Force | | Max. Load at Catenary Action | |
|---|---|---|---|---|---|---|---|---|---|---|
| | $P_f$ (kN) | MJD (mm) | $P_{com}$ (kN) | MJD (mm) | $N_{com}$ (kN) | MJD (mm) | $N_{ten}$ (kN) | MJD (mm) | $P_{cat}$ (kN) | MJD (mm) |
| SS-7 | 29.8 | 42.1 | 35.6 | 87.7 | 57.4 | 108.8 | 98.4 | 562.4 | 53.7 | 558.0 |

Figure 4-33 shows the conversion of non-linear static behaviour to the Pseudo-Static behaviour for specimen SS-7. The first peak of progressive collapse resistance was 30.5 kN and the corresponding deflection was 256.1 mm. The second peak of the applied load was 35.5 kN with a corresponding MJD of 600 mm. Different from the other specimens, the first peak of the applied load was within the catenary action, while it was within compressive arch action for the other specimens. It can be concluded that the presence of partial hinges could move the first peak from compressive arch action to catenary action, due to the provision of more rotation capacity.
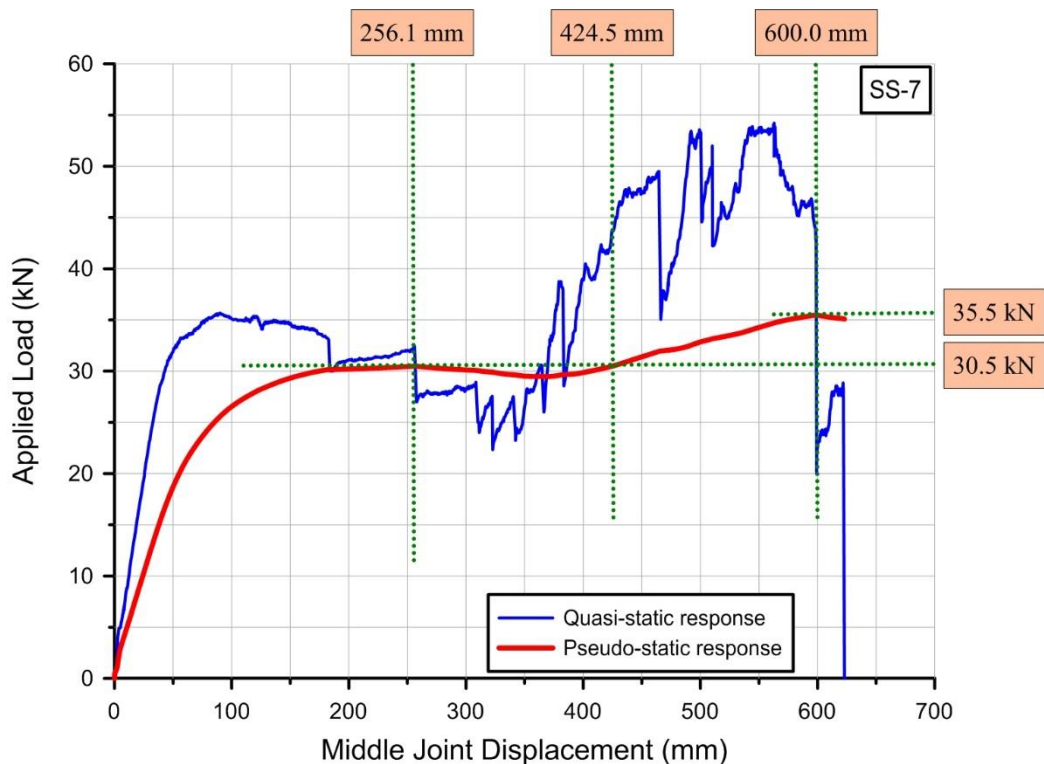


Figure 4-33 Non-Linear Pseudo-Static Response for the Specimen SS-7

Figure 4-34 and 4-35 show crack development at different stages of loading. There is no difference in crack pattern and failure mode compared to other specimens. Large cracking, concrete crushing and spalling, and bar fracture were primarily concentrated at the beam-column connections. Points A, B and C were at flexural and compressive arch action, point D was the transition point from CAA to catenary action, and points E and F were at catenary action.

It was noticed that the cracks widened after point D near the location of partial hinges at the middle joint. In addition, the large axial tension caused the cracks to penetrate the beam section after point D.
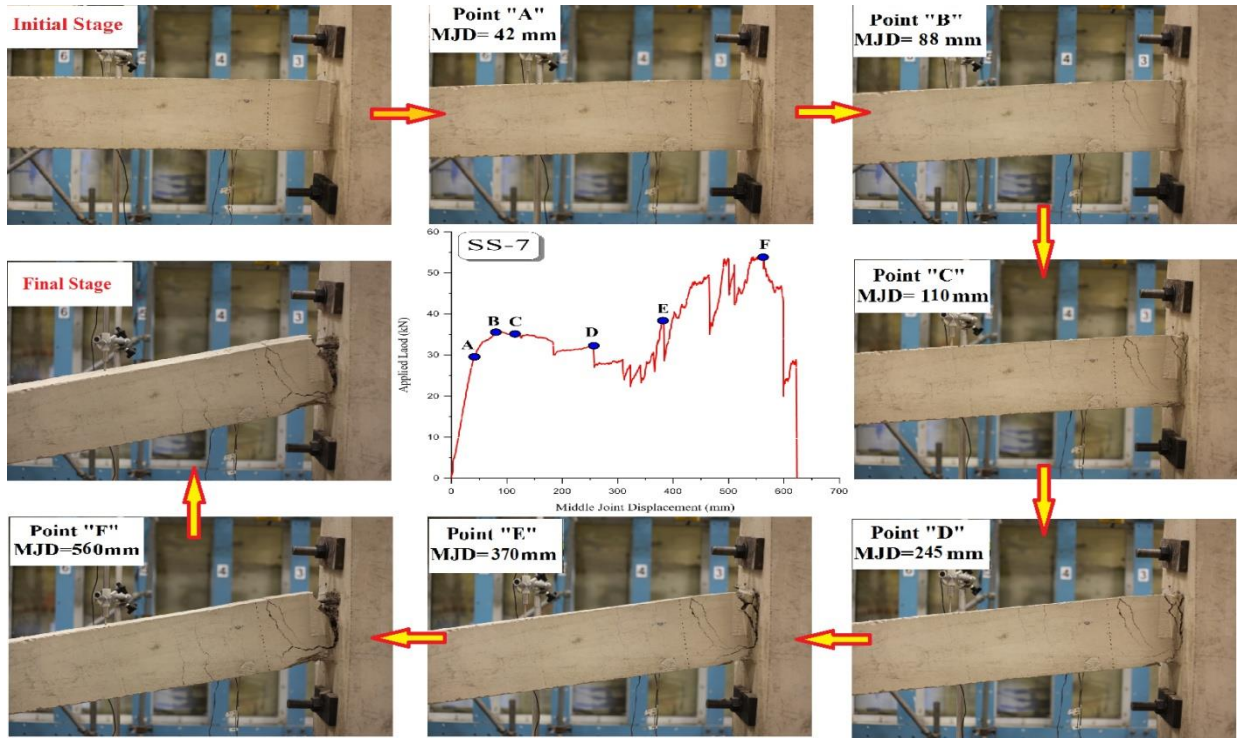


Figure 4-34 Crack Development at Different Stages for Left Beam end of SS-7
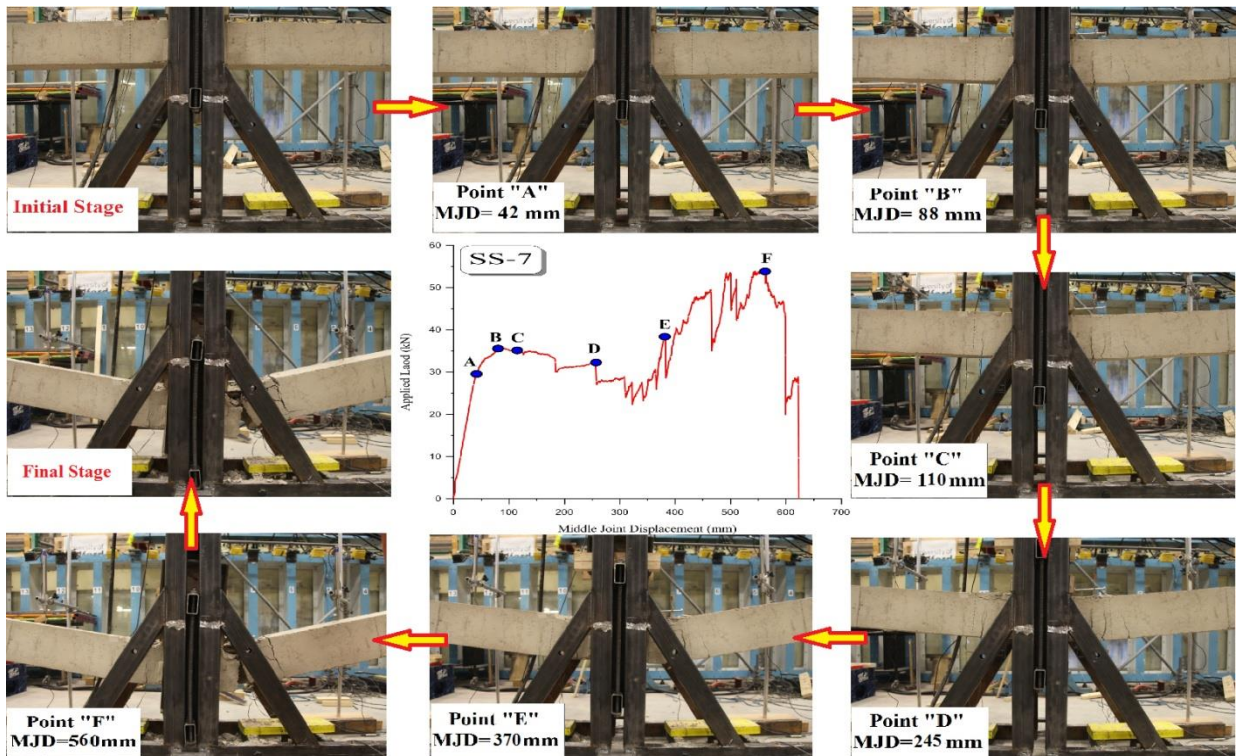


Figure 4-35 Crack Development at Different Stages for the Middle Joint of SS-7

## 4.3.1.6 TEST RESULTS OF SPECIMEN SS-8

Specimen SS-8 was designed and detailed according to the conventional design. In addition, a partial hinge was provided to the beam section at a distance equal to twice that of the beam depth away from the beam-column interface. The intention of providing the partial hinges was to increase the rotational capacity of the RC beams and trigger the catenary action stage at a smaller middle joint displacement.

In the partial hinge regions, an additional T10 bottom bar was added and bent up at a distance of 345 mm away from the beam column joint interface and one of the top layer T10 bars was bent down at the same distance. The two bent bars levelled off at the bottom and top reinforcement layers, respectively. Finally, the pin of the partial hinges was formed at a distance 440.0 mm from the beam-column joint interface, as shown in Figure 3-5.

Figure 4-36 shows deflection curves along the length of the beam at different stages of loading. It can be seen from Figure 4-36 that the beam deflected symmetrically and the final deflection was 664 mm, which is larger than the other specimens. Also, it can be seen that the deflection increased uniformly from the initial stage until the maximum axial compressive force developed.

The middle joint travelled vertically about 313 mm from the first top bar fracture until the end of the test which is approximately twice the distance from the first bottom bar fracture to the first top bar fracture. This can be explained by the presence of partial hinges, in which the steel bars forming these partial hinges enhanced the ductility of the beam after the fracture of the top bars.
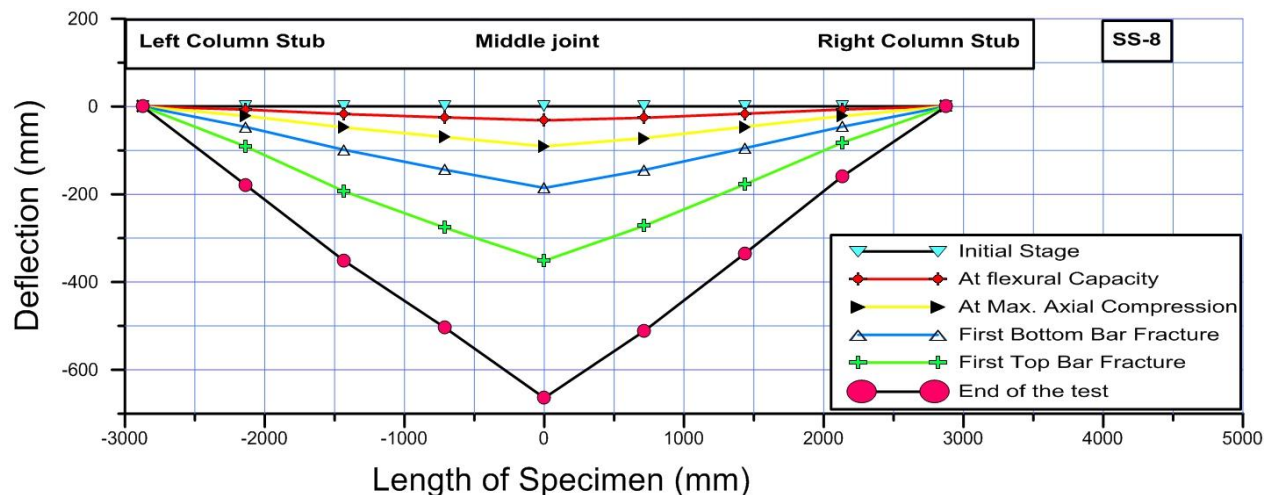


Figure 4-36 Beam Deformation for Specimen SS-8

Figures 4-37 and 4-38 show the relationships of applied load vs. MJD and axial force vs. MJD for specimen SS-8. Table 4-8 summarises forces and their corresponding middle joint displacements at critical stages of the load-deflection history.

The general trend of the non-linear behaviour of specimen SS-8 was similar to those for specimen SS-2 and SS-3, and the load-deflection history can also be divided into three stages as stated for SS-2 and SS-3. Flexural capacity was attained at a deflection equal to 31.7 mm, which is the smallest deflection compared to other specimens. At a relatively small deflection of 86.7 mm, the maximum applied load of 35.8 kN was attained at CAA.

After first and second bar fracture, catenary action started to develop at a deflection equal to 250.5 mm. At the catenary action stage, the applied load increased to 54.9 kN, which is larger than the applied load at CAA by about 53%. At a deflection of 550 mm, top bars forming the partial hinges at the ends of the specimen fractured simultaneously, which caused a large reduction in the applied load. At that point, the specimen was deemed to have failed, but it could still carry a reduced load until a total collapse at a deflection of 664 mm occurred.
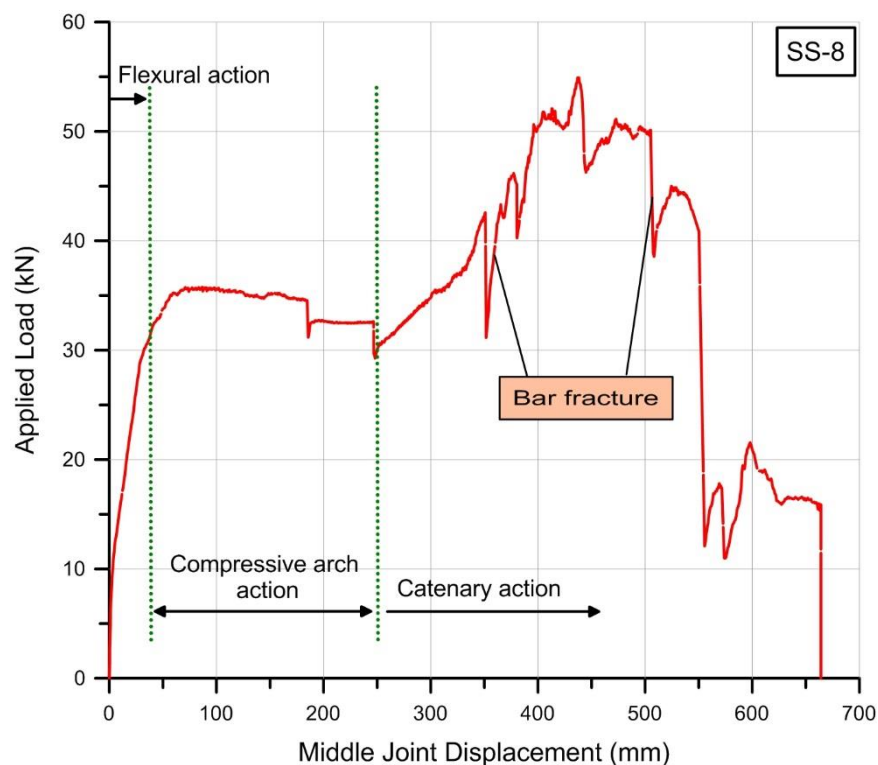


Figure 4-37 Applied Load vs. Middle Joint Displacement Relationship of Specimen SS-8
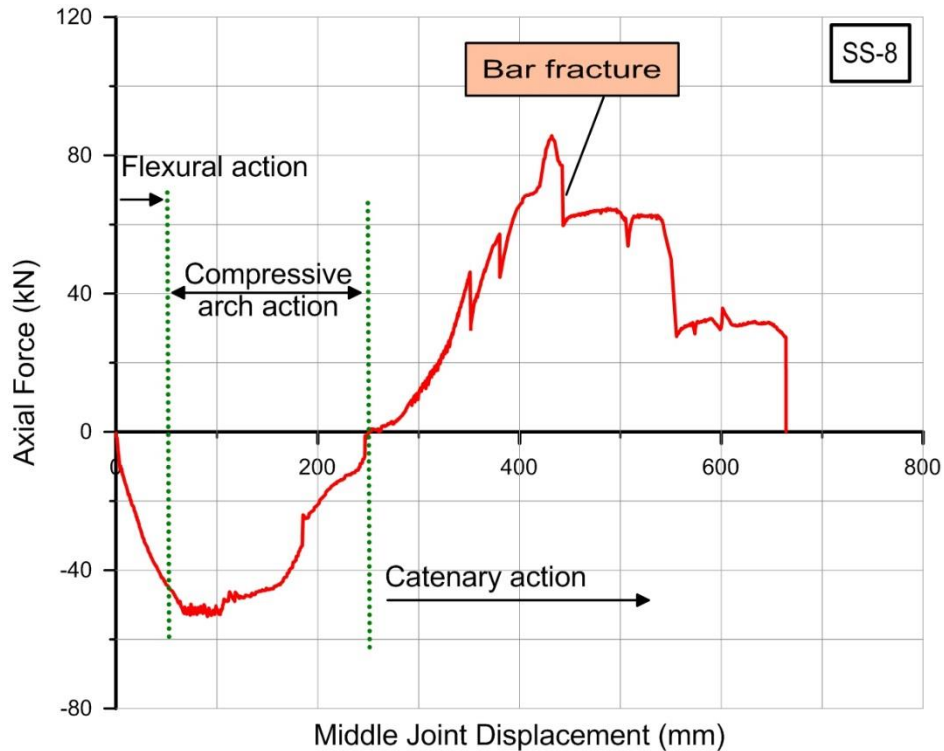
Figure 4-38 Axial Force vs. Middle Joint Displacement Relationship of Specimen SS-8

The maximum axial compressive force was 53.4 kN attained at 90.6 mm of deflection, and the maximum tensile force was 85.7 kN attained at 431.8 mm of deflection. Compared to specimen SS-7, the axial compressive force developed was smaller and the deflection at which the axial tension was attained was also smaller.

Table 4-8 Forces with their MJD's at critical stages for SS-8

| Specimen | Calculated flexural capacity with MJD | | Max. load at CAA $P_{com}$ | | Max. Axial compression Force | | Max. Axial Tension Force | | Max. Load at Catenary Action | |
|---|---|---|---|---|---|---|---|---|---|---|
| | $P_f$ (kN) | MJD (mm) | $P_{com}$ (kN) | MJD (mm) | $N_{com}$ (kN) | MJD (mm) | $N_{ten}$ (kN) | MJD (mm) | $P_{cat}$ (kN) | MJD (mm) |
| SS-8 | 29.8 | 31.7 | 35.8 | 86.7 | 53.4 | 90.6 | 85.7 | 431.8 | 54.9 | 437.1 |

Figure 4-39 shows the converted non-linear static behaviour to the Pseudo-Static behaviour for specimen SS-8. The first peak of progressive collapse resistance was 32.3 kN and the corresponding deflection was 252.2 mm. The second peak of progressive collapse capacity was 38.1 kN with a corresponding deflection 550.2 mm. Similar to specimen SS-7, the first peak was within the catenary action stage, while it was within the compressive arch action stage for the other specimens. Progressive collapse capacity for specimen SS-8 was larger than the capacity for specimen SS-7 by about 7%.
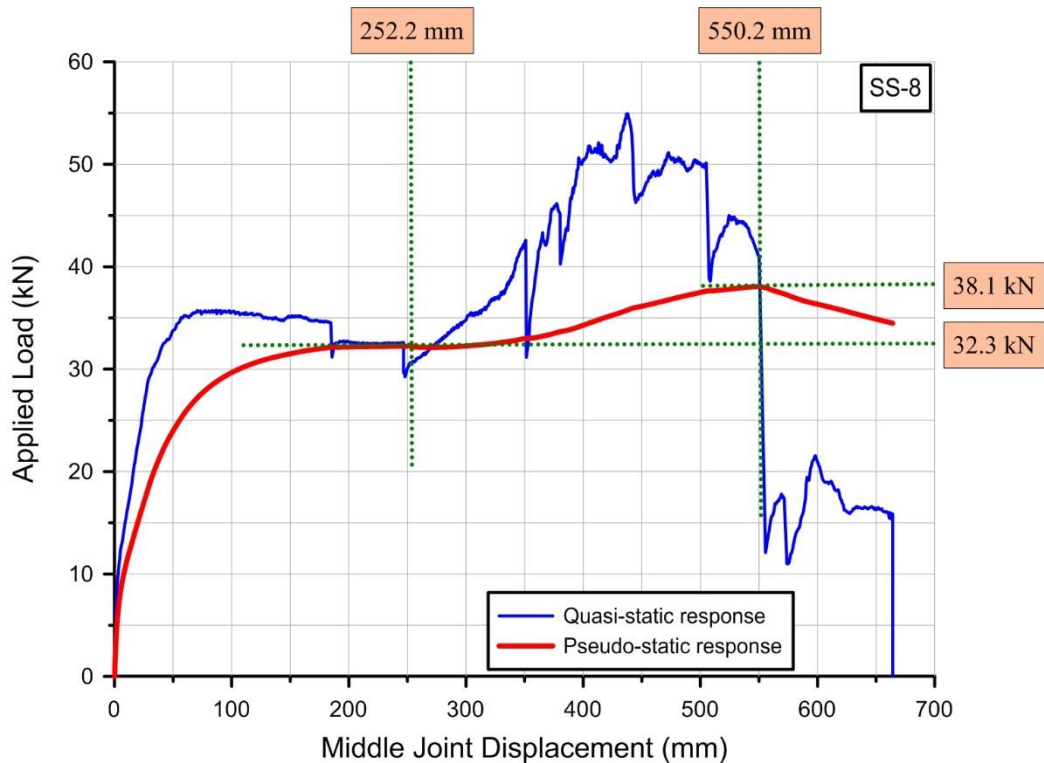


Figure 4-39 Non-linear Pseudo-static response for the specimen SS-8

Figure 4-40 and 4-41 show crack development at different stages of loading. There is no difference in crack pattern and failure mode compared to other specimens. Severe crack and concrete spalling occurred at the left side of the specimen after point "D". Points A, B and C occur at flexural and compressive arch action, point "D" was the transition point from CAA to catenary action, and points E and F were at catenary action. In addition, the large axial tension caused a crack penetrating the section of the beam, which is shown in the points E and F.
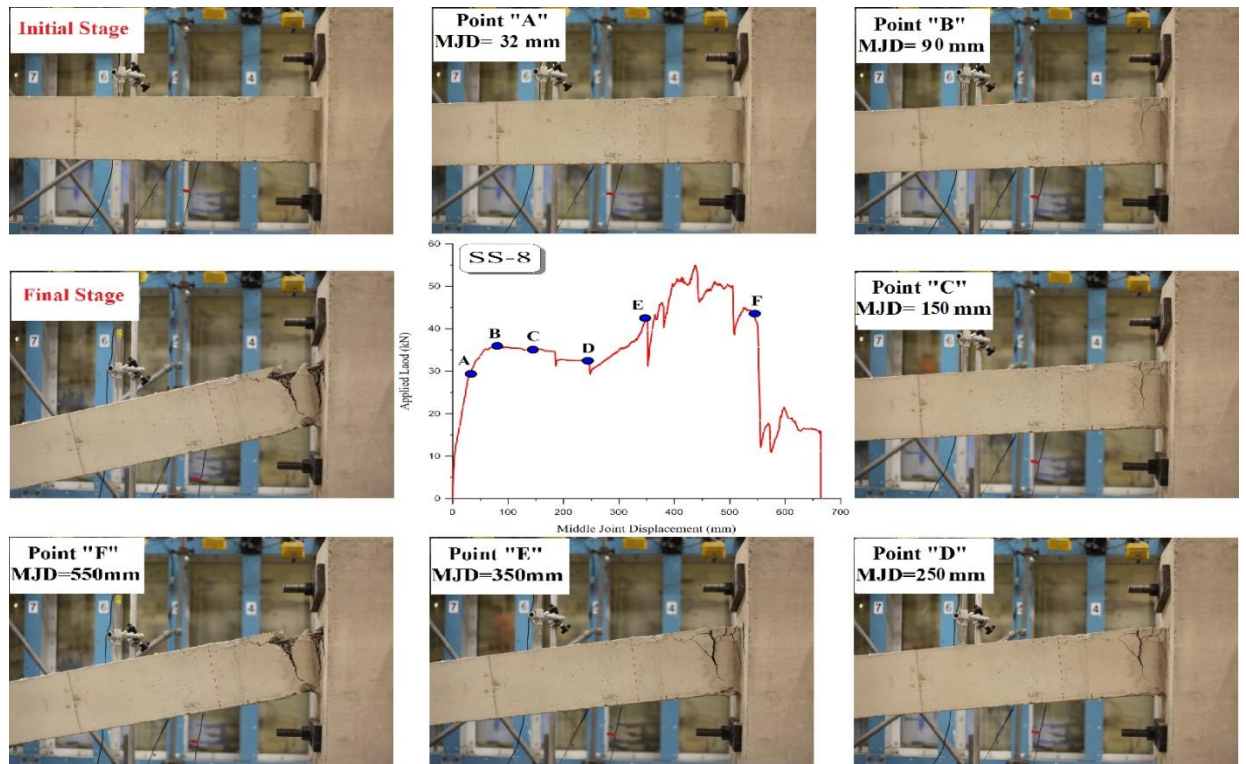
Figure 4-40 Crack Development at different stages for right beam end of specimen SS-8
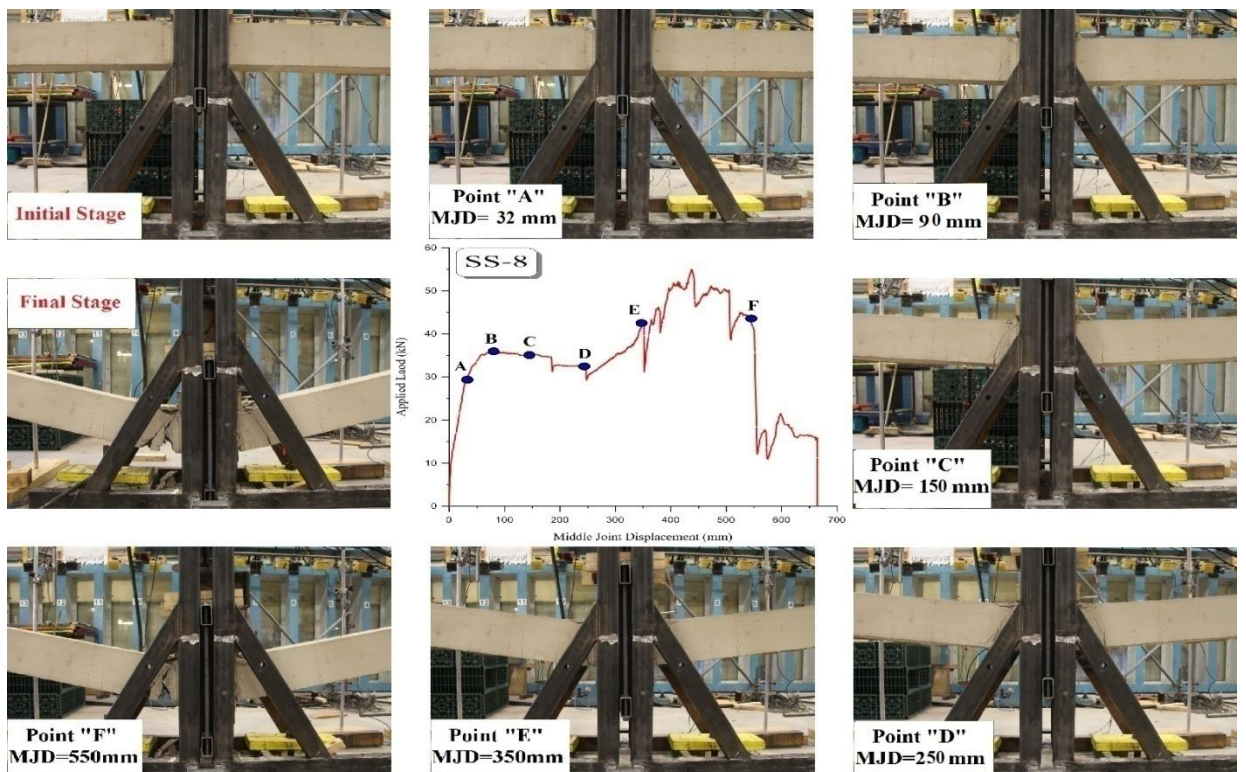


Figure 4-41 Crack Development at Different Stages for the Middle Joint of Specimen SS-8

## 4.3.2 TEST RESULTS AT LOCAL LEVEL

In order to investigate the development of internal forces within the beam sections, several strain gauges were attached to the steel reinforcing bars at critical locations. Bar strain measurements, which can be converted to bar forces, can shed light on the contributions of reinforcing bars to the mobilization of different mechanisms. Figure 4-42 shows the layout of strain gauges along the beam length.
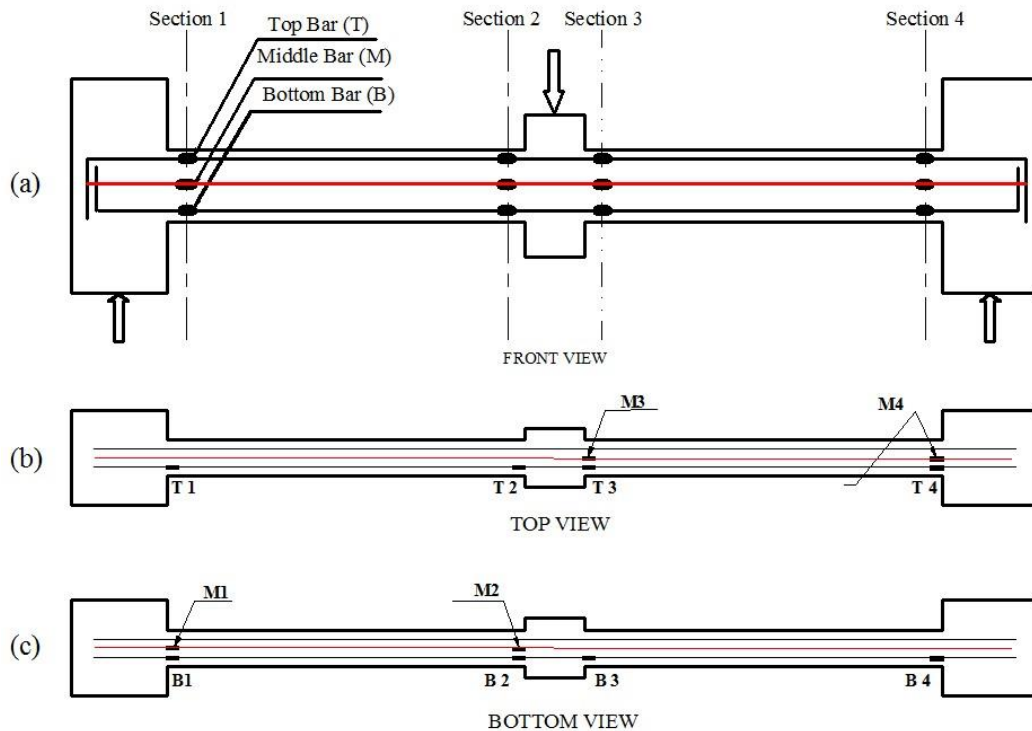


Figure 4-42 Front View of Strain Gauges Layout

Development of stresses and forces at the additional steel bars provides insight as to how these bars affect the structural resistance mechanisms at both compressive arch and catenary action stages. Strain readings were converted into bar forces by multiplying the strains by the steel modulus of elasticity and the area of the bar. The converted bar forces were plotted against the middle joint displacement for each specimen. In this section, the relationship between bar forces and middle joint displacement will be introduced and discussed for each specimen.

It was noticed during the tests, that the strain readings of most steel bars did not return to zero after the fracture of these bars. This was due to the residual strains in the steel bars and the fracture did not occur at the location of strain gauges.

Some strain gauges were damaged during the test and the recorded readings were (-$10^6$ μm). A value of zero strain was used instead of damaged strain reading when calculating bar forces, in which may not represent the actual strain in the steel bar.

It should be mentioned that the bar forces calculated are relative to the initial conditions rather than absolute values due to the presence of initial strains in the steel bars.

## 4.3.2.1 STEEL BAR FORCES IN SPECIMEN SS-2

In order to investigate the force development in the steel reinforcing bars during the different resisting mechanisms, the bar force distributions plotted against MJD. Figure 4-43 shows the relationship between bar forces and MJD for each section of specimen SS-2.
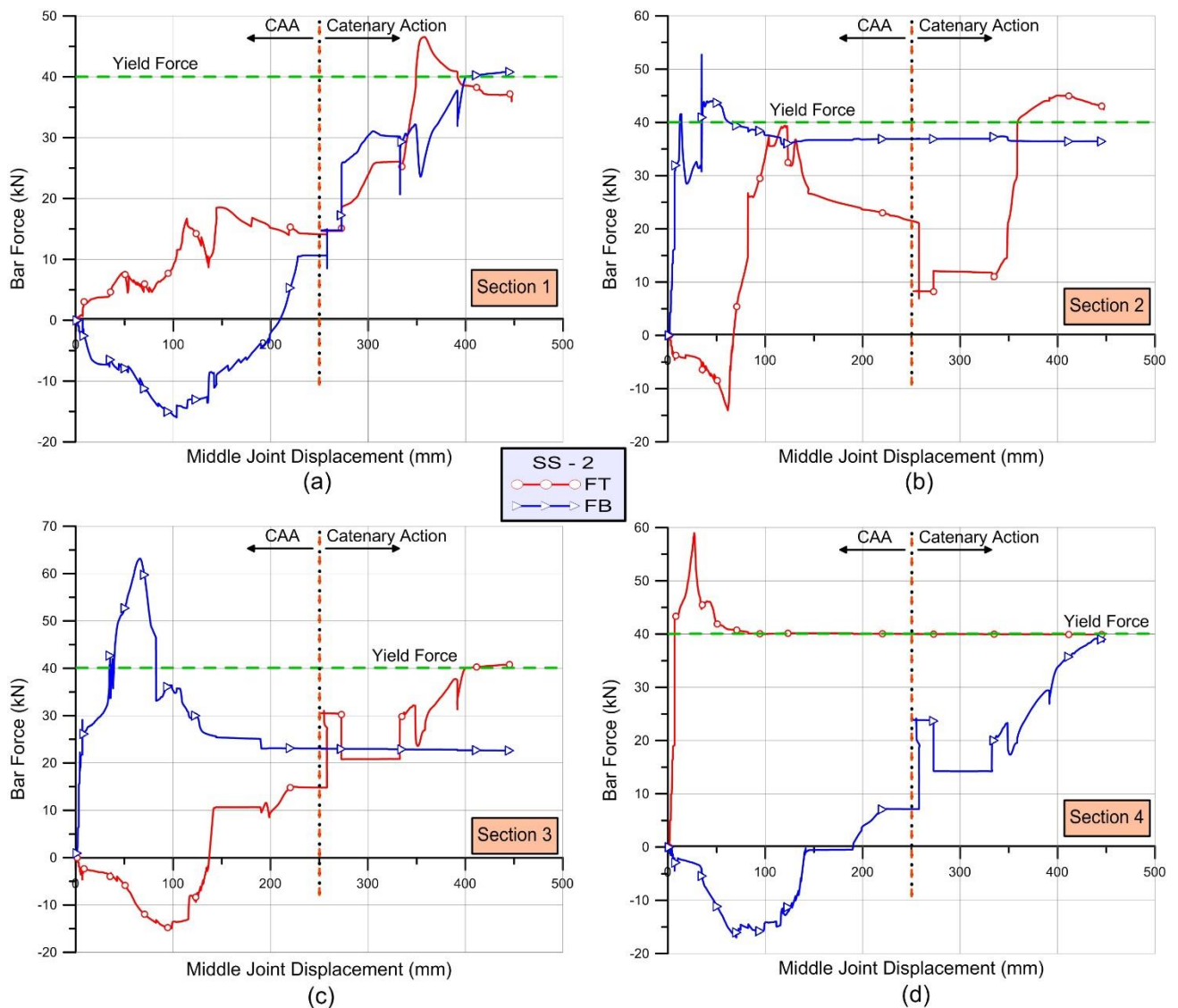


Figure 4-43 Bar Forces vs. MJD for Specimen SS-2

The designations FT and FB refer to the forces in the top and bottom bars at the various beam sections. It can be seen from Figure 4-43(a-d), the tensile forces during catenary action were carried only by bottom bars at the beam ends, and only by top bars at the middle joint interfaces.

It is also clear from Figure 4-43 that the tensile forces developed during catenary action were carried only by steel bars, while the contribution of concrete to the compressive forces at CAA was about 50%. Figure 4-44 shows bar forces for each section at specific deflections.
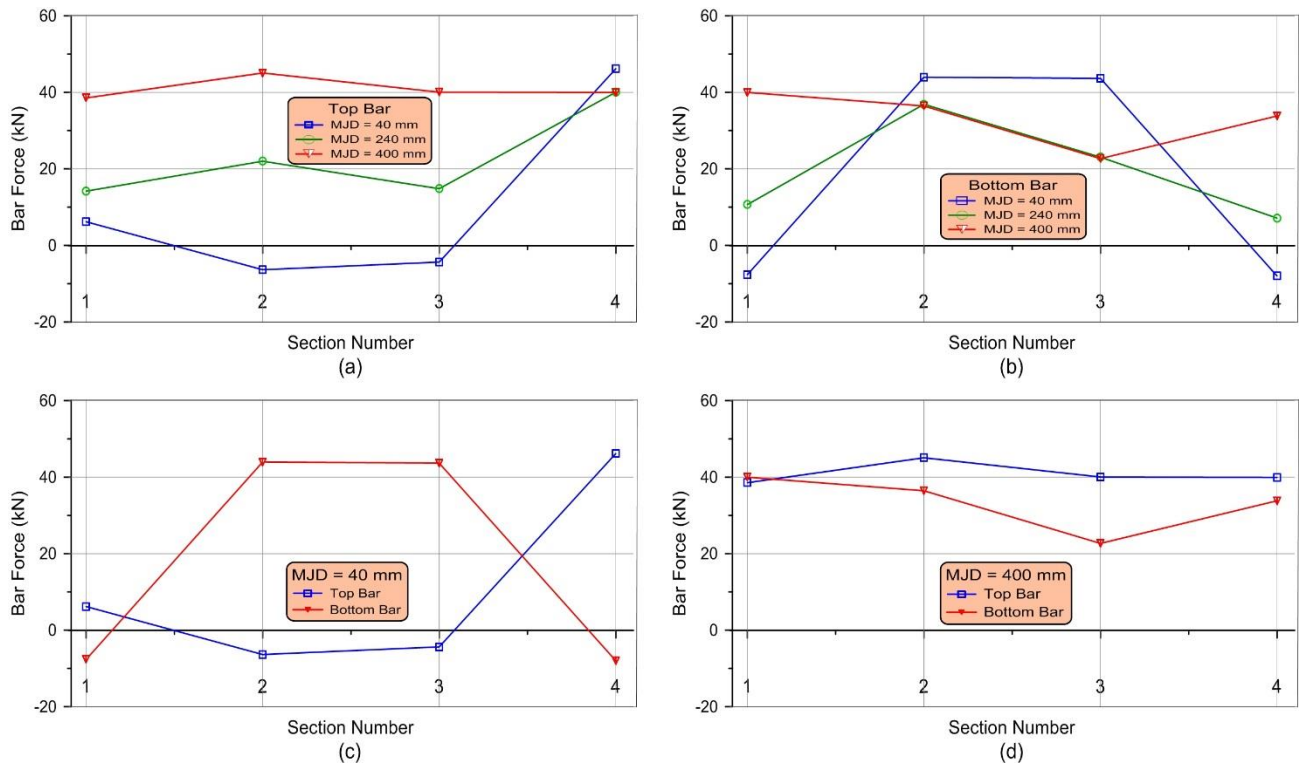


Figure 4-44 Bar Forces at Different Resisting Mechanisms for Specimen SS-2

Each deflection value in Figure 4-44 represents a point at each stage of the resisting mechanisms. At a MJD of 40 mm within the CAA, top and bottom bars contributed to the compressive forces by nearly the same amount at all sections, despite the difference in the steel ratio at the top and bottom of the section, as shown in Figure 4-44(c). This can be related to the confinement provided by the concrete to the steel bars at compression zones and the difference in compression zone depths between the middle joint and beam ends.

At the early stages of loading, the bottom bars yielded at sections 2 and 3, followed by fracture at both sections as shown in Figure 4-44(b). This means, that the bottom bars are more vulnerable at early stages in the event of progressive collapse. Due to imperfections in the specimen's construction, some steel bars may behave un-symmetrically as shown in Figure 4-44(a).

At the mid stages of loading, it can be seen that the top bar is still carrying the loads at three locations, while at the advanced stages of loading, top and bottom bars were fractured at two sections at least. It is clear that the need for additional bars at certain locations was crucial in order to reduce the probability of failure at critical sections, Figure 4-44(a), (b).

## 4.3.2.2 STEEL BAR FORCES IN SPECIMEN SS-3

Figure 4-45 shows the relationship between bar forces and MJD for specimen SS-3. The general trend of bar force – MJD relationship for SS-2 and SS-3 were quite similar. The changing in bar forces from compressive to tensile at sections 1 and 3 occurred at a deflection more than the deflection measured at the onset of catenary action for the specimen. It can be seen that the top bar force transition occurred simultaneously with the fracture of the bottom bar.
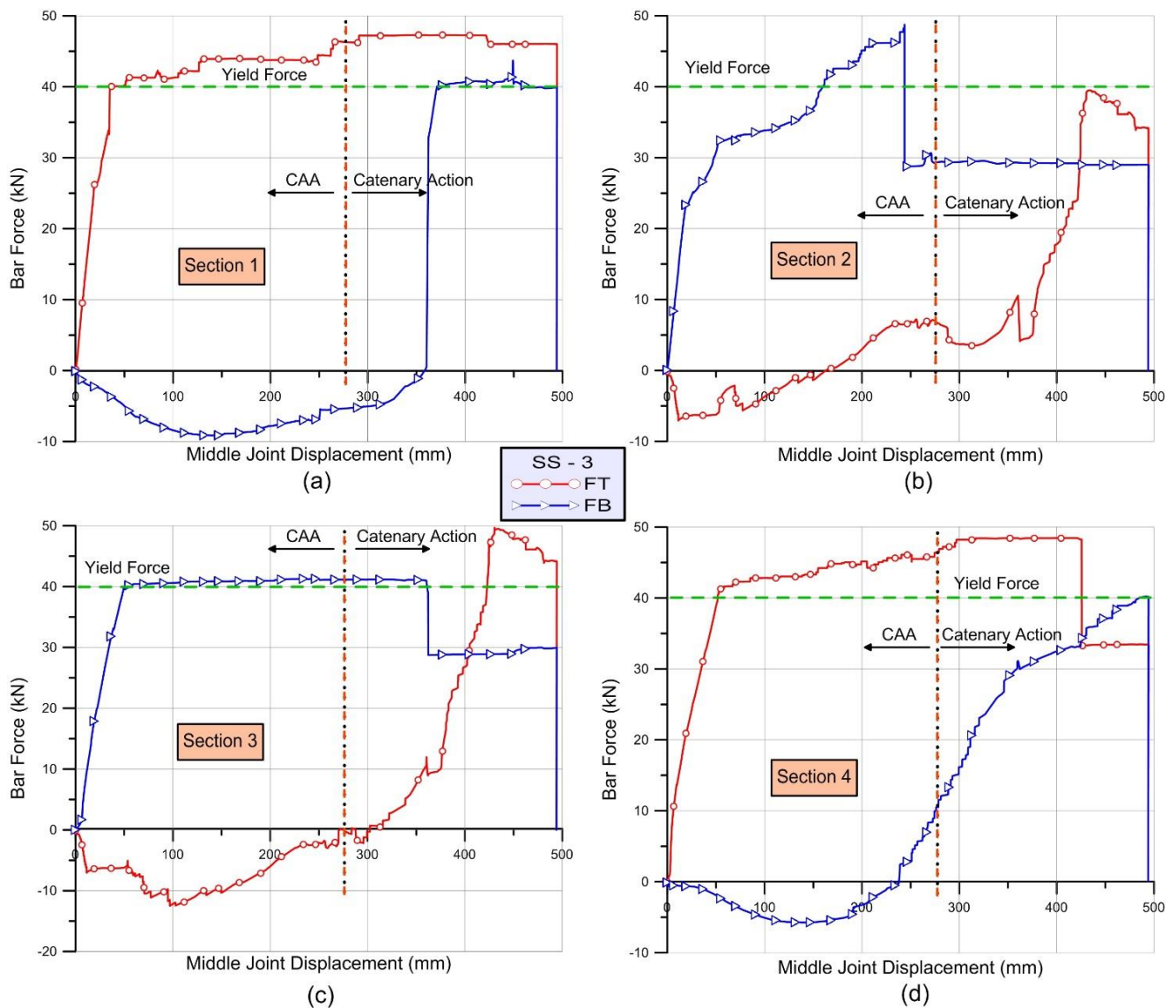


Figure 4-45 Bar Forces vs. MJD for Specimen SS-3

The same conclusions can be made from Figure 4-45 as have been made for specimen SS-2.

 Figure 4-46 shows bar forces for each section at specific deflections. These deflection values were chosen to represent each of the resisting mechanism stages.

It should be mentioned, that after the fracture of some bars, residual strains remain, which is reflected as residual bar forces in the force-displacement relationship. As shown in Figure 4-46(b), at 400 mm of deflection the bar at sections 2 and 3 was fractured and the values of the curve should be equal to zero.
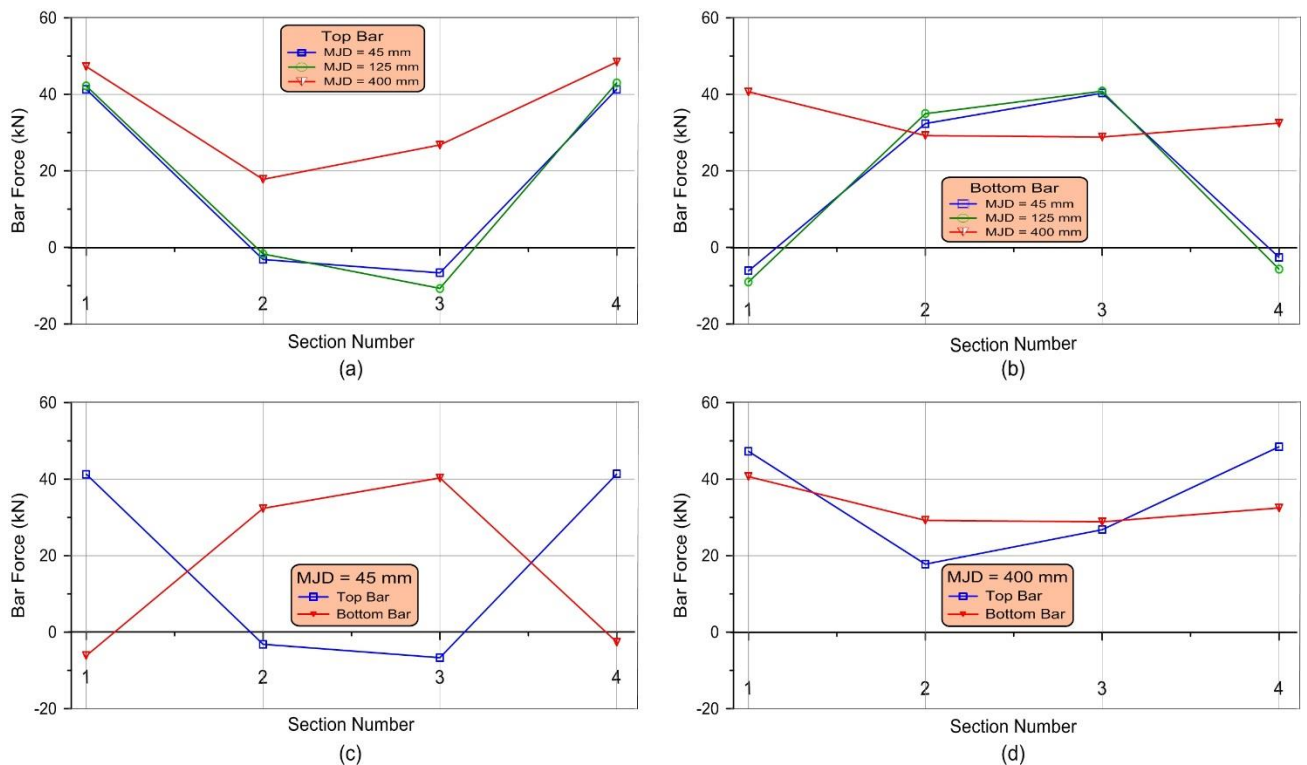


Figure 4-46 Bar forces for Different Resisting Mechanisms for Specimen SS-3

It can be seen that both bars contribute to the tensile forces developed at the catenary action stage. The change in the top and bottom bar forces during compressive arch action was smaller than the change in forces during catenary action, as can be seen from Figures 4-46(a) and 4-46(b).

At 45 mm deflection, the top and bottom bars were nearly symmetrical by contributing in their contribution to the axial forces throughout the beam, as can be seen from Figure 4-46(c). At 400 mm of deflection, it can be seen that the top and bottom bars were in tension, which indicates the action at catenary stage.

## 4.3.2.3 STEEL BAR FORCES IN SPECIMEN SS-4

As mentioned earlier, the middle layer of steel bars was added to the specimen SS-4. Two T10 steel bars were added at the centre of the beam section. Strain gauges were attached to the middle steel bars at the same sections for top and bottom bars, as shown in Figure 4-42. Therefore, another curve has been added to the Figures with a label 'FM', which refers to the force in the middle bar.

Figure 4-47 shows the relationship between bar forces and MJD for specimen SS-4. The general trend of the curves was similar to the specimen SS-2 and SS-3. Unfortunately, the strain gauge of the middle bars at section 2 was corrupted, as can be seen from Figure 4-47(b).
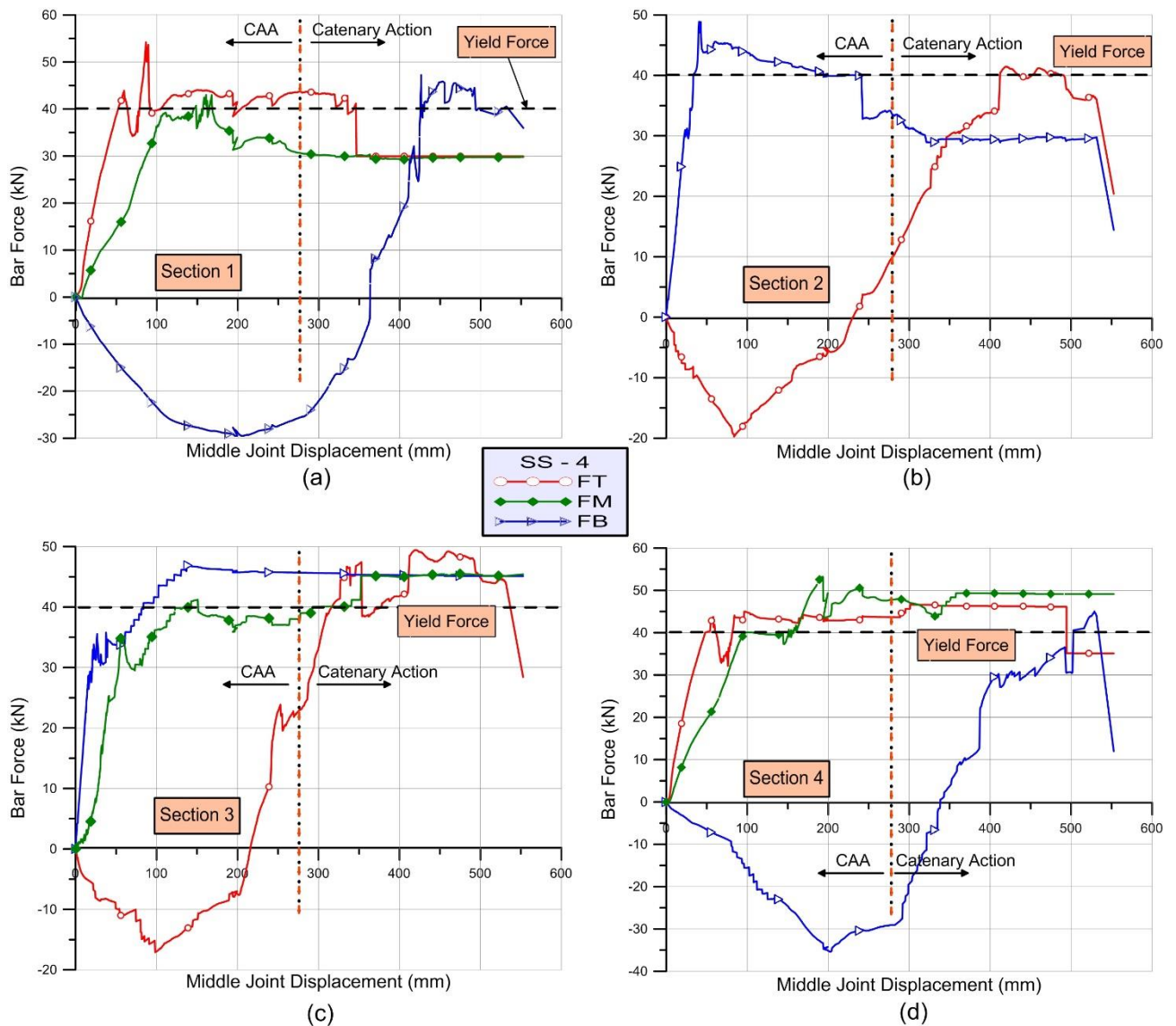


Figure 4-47 Bar Forces vs. MJD for Specimen SS-4

For all sections, the middle bar layer was mobilised at the tension zone of the section and carried tensile forces as can be seen from Figure 4-47. At the onset of catenary action, the middle steel bars provided the specimen with a tying force an average of more than 75.0 kN. The fracture of the middle steel bars occurred after the onset of catenary action.

Compared to the specimen SS-2 and SS-3, the compressive forces developed in the steel bars were larger, specifically at sections 1 and 4. Figure 4-48 shows the bar forces for each section at specific deflections. These deflection values were chosen to represent each of the stages of the resisting mechanisms.
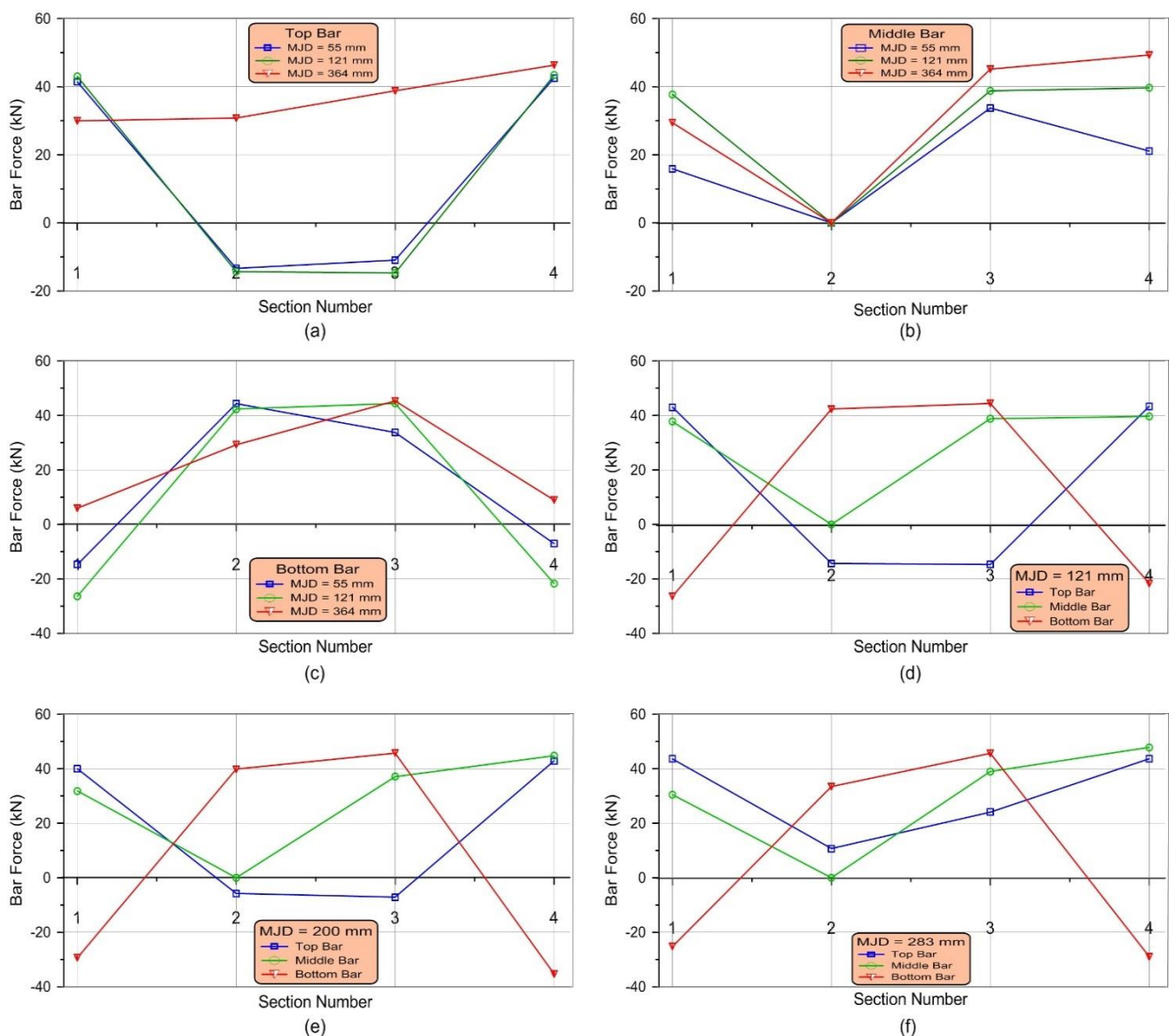


Figure 4-48 Bar Forces at Different Resisting Mechanisms for Specimen SS-4

At 200 mm of MJD, Figure 4-48(e), a maximum compressive force was developed in the bottom bars at the ends of the specimen, and this was about 60% larger than that at the middle joint interfaces developed in the top bars. This can be explained by the enhancement of the middle layer to the tension zones with three steel bars at the top of the section at the ends of the beam. It is clear that the middle layer contributes to the tensile forces at catenary action as can be seen in Figure 4-48(f).

### 4.3.2.4 STEEL BAR FORCES IN SPECIMEN SS-5

For specimen SS-5, two steel bars were added at a distance of $(d - d')/4$ from the centre of bottom reinforcement. Figure 4-49 shows the relationship between bar forces and MJD for SS-5.
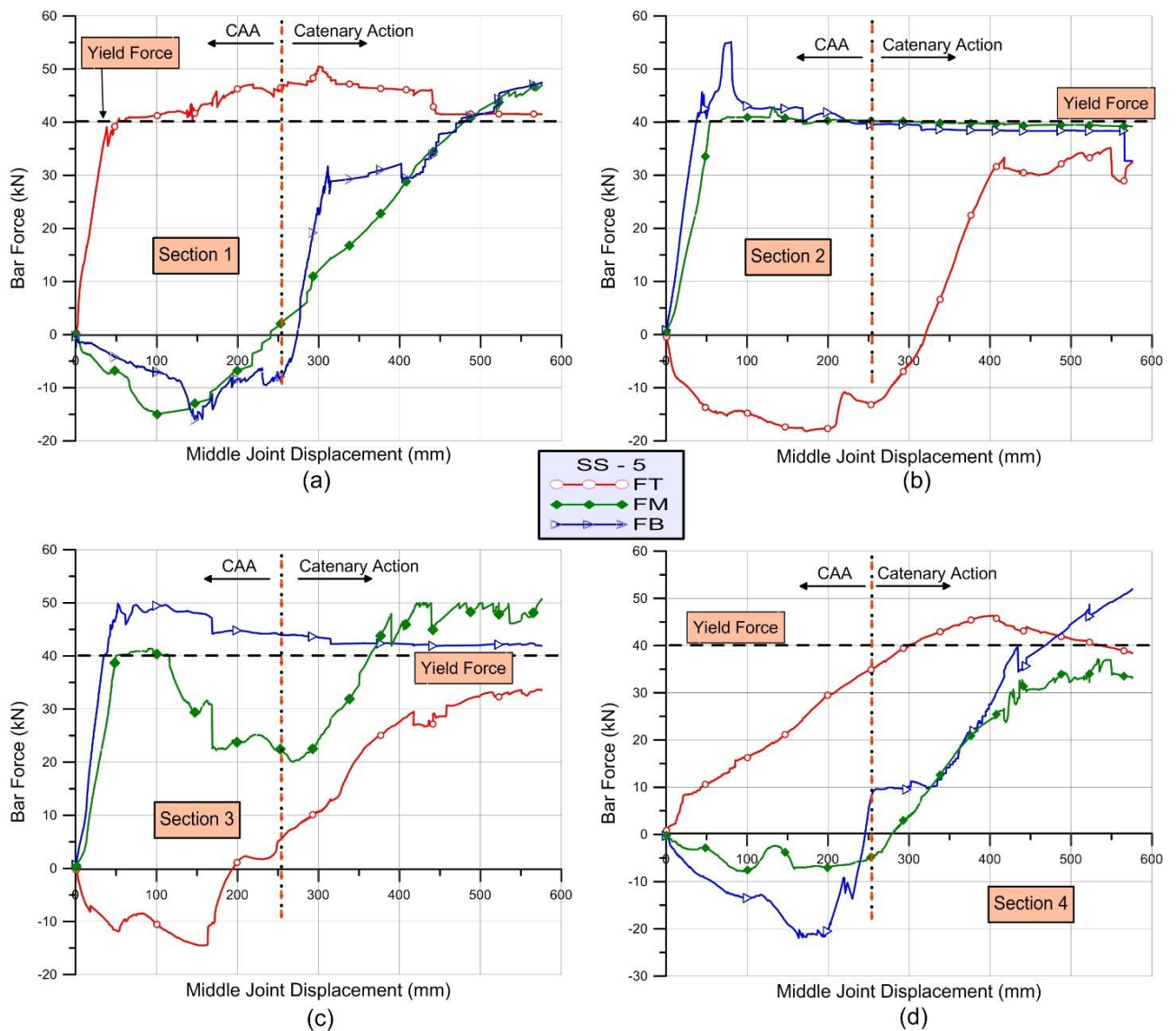


Figure 4-49 Bar Forces vs. MJD for Specimen SS-5

It can be seen from Figure 4-49 that the middle layer of bars enhanced the tensile capacity of the beam by more than 80.0 kN at catenary action, which is about 50% of the total force provided by the top and bottom steel bars. Due to the location of the added bars, they behaved similarly to the bottom bars, i.e. carried compressive forces at sections 1 and 4, while at sections 2 and 3 they carried tensile forces. Figure 4-50 shows bar forces for each section at specific deflections.
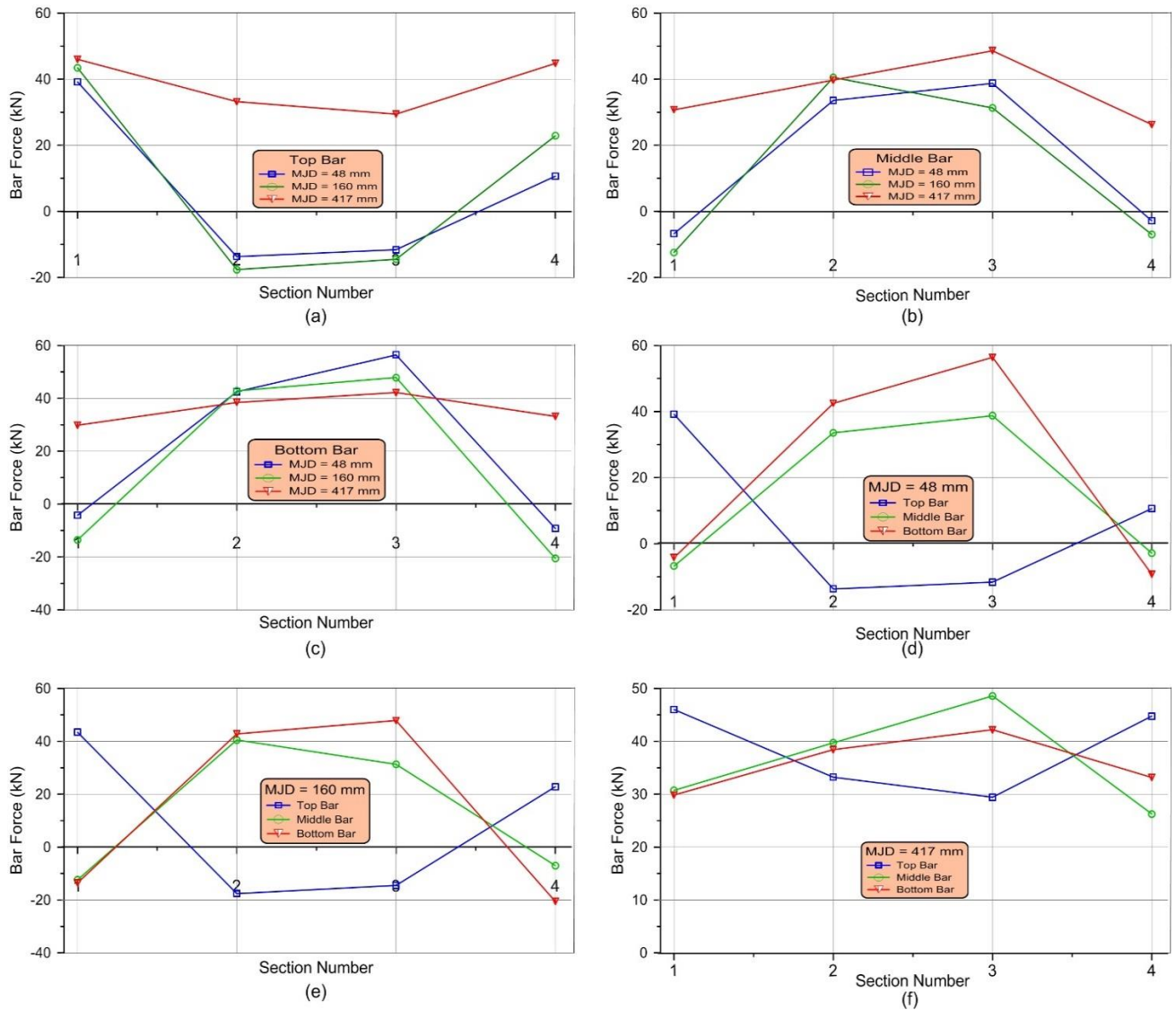


Figure 4-50 Bar Forces for Different Resisting Mechanisms for Specimen SS-5

Figure 4-50(b) and (c) show that at early stages, the middle and bottom bars carried tensile forces at the middle joint, and compressive forces at the beam ends. Figure 4-50(d), (e) and (f) show that the change in bar forces during the transition from CAA to catenary action was much larger than the change during the transition from flexural to CAA. At the advanced stage of loading, all bars at all sections carried a tensile force as can be seen in Figure 4-50(f).

## 4.3.2.5 STEEL BAR FORCES IN SPECIMEN SS-6

Figure 4-51 shows the relationship between bar forces and MJD for SS-6. Different from specimen SS-5, the two steel bars were added at a distance of $(d - d')/4$ from the centre of the top reinforcement for specimen SS-6. The middle steel bars enhanced the tension zone at sections 1 and 4. The contribution of the middle layer to the maximum tensile force at catenary action stage was about 80.0 kN. The contribution of the middle layer to the axial compressive forces at sections 2 and 3 was very limited as can be seen from Figure 4-51(b) and (c). Figure 4-52 shows the bar forces for each section at specific deflections.
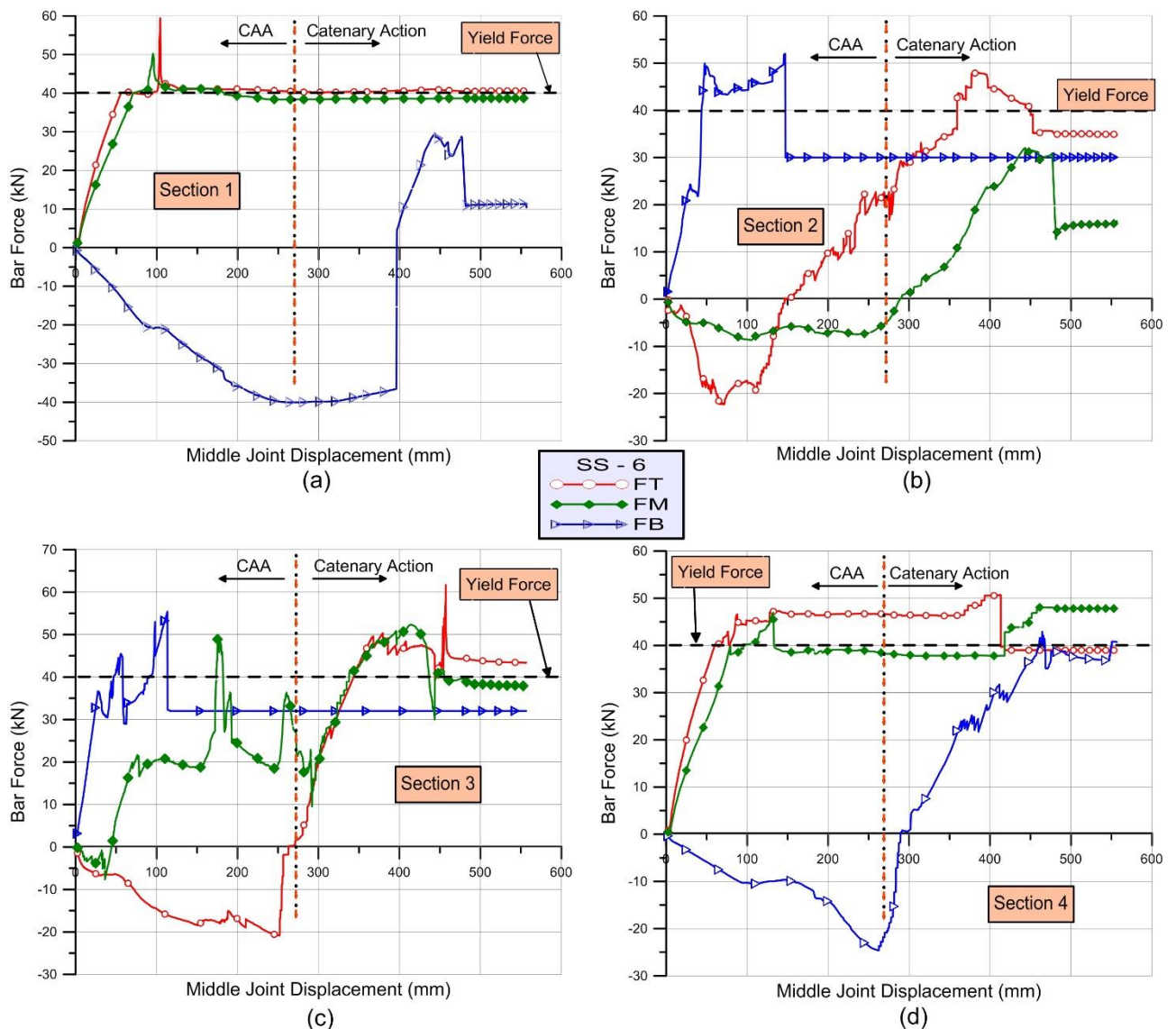


Figure 4-51 Bar Forces vs. MJD for Specimen SS-6
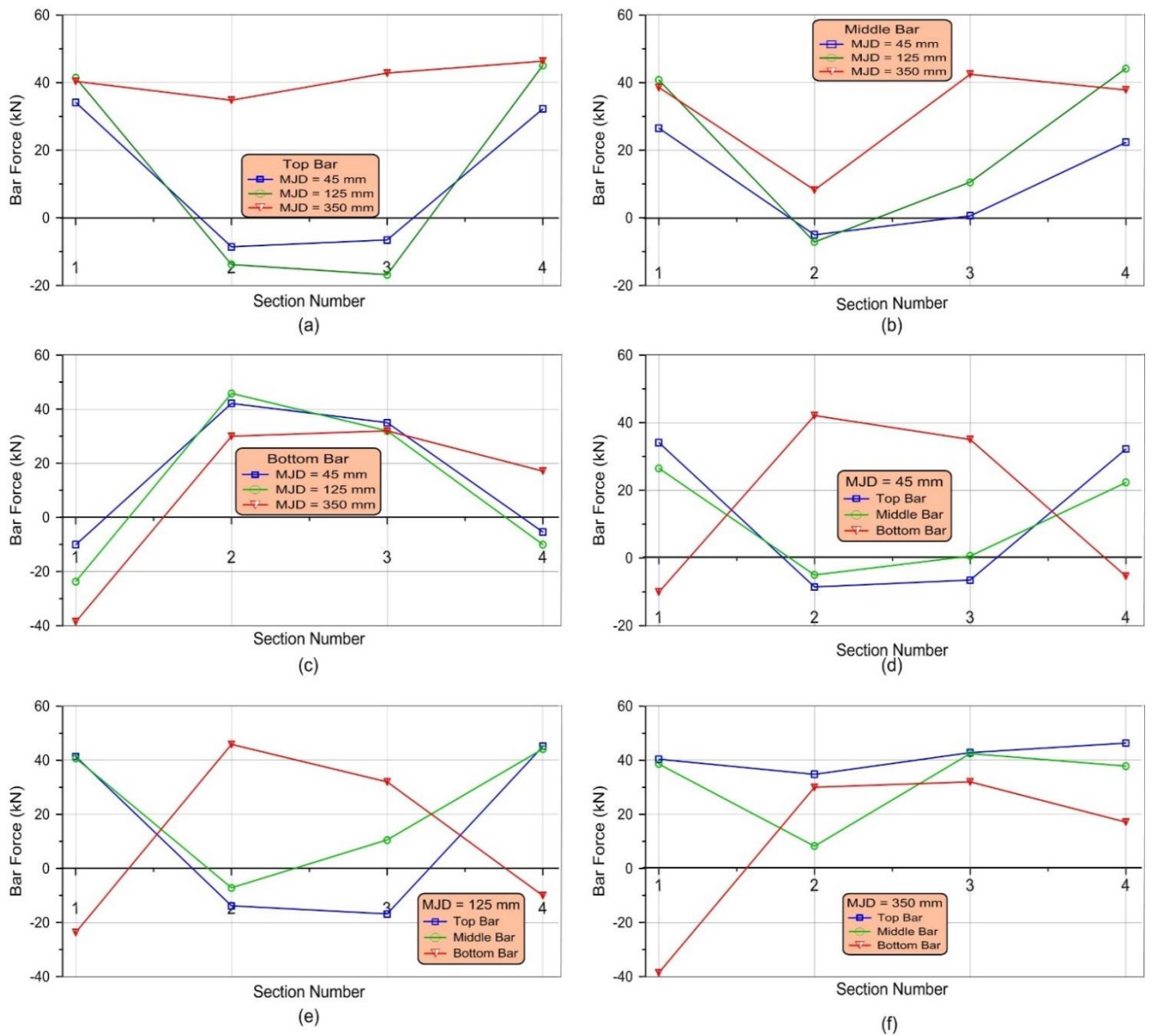
Figure 4-52 Bar Forces at Different Resisting Mechanisms for Specimen SS-6

Figure 4-52(a) shows that the forces developed in the top bars did not vary significantly during compressive arch action, but the variation was larger once it reached the maximum axial compressive force at 125.0 mm of deflection.

It is clear from Figure 4-52(d) and 4-52(f) that the middle bars behaved in the same way as the top bars at both CAA and catenary action, but the developed forces were less. Figure 4-52(e) and 4-52(f) show the state of forces at the transition from CAA to catenary action.

## 4.3.2.6 STEEL BAR FORCES IN SPECIMEN SS-7

Different from specimen SS-2 and SS-3, partial hinges were provided to the beam section at a distance equal to the beam depth away from the beam-column interfaces for specimen SS-7. An additional T10 bottom bar was added and bent up at a 125 mm away from the beam column joint interface and one of the top bar layer T10 was bent down at a same distance.

The strain gauges were attached to the added bottom bars at the left side of the specimen, and they were attached to the top bent bars at the right side of the specimen. Figure 4-53 shows the layout of the strain gauges for the specimen SS-7.
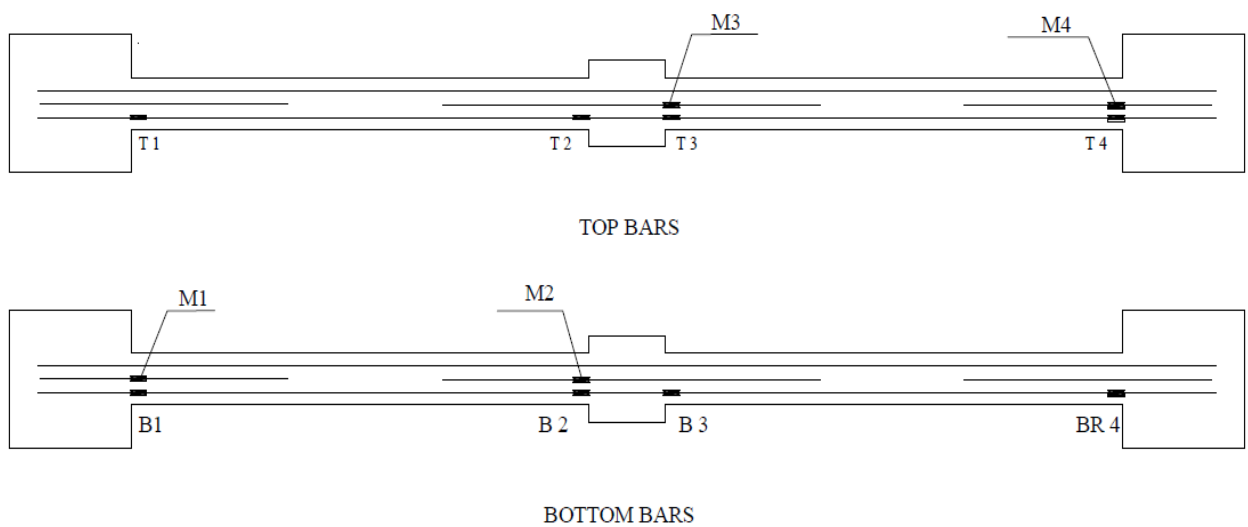


Figure 4-53 Strain Gauge Layout for Specimen SS-7

More redundant strain gauges were attached in specific locations in order to compensate for the strain gauges that may have become damaged during the test. Figure 4-54 shows the relationship between bar forces and MJD for SS-7.

The presence of partial hinges enhanced the bottom bars at an early stage of loading as can be seen from Figure 4-54(a). The enhancement of partial hinges to axial tensile capacity was limited because of the top bars already present from the original design.
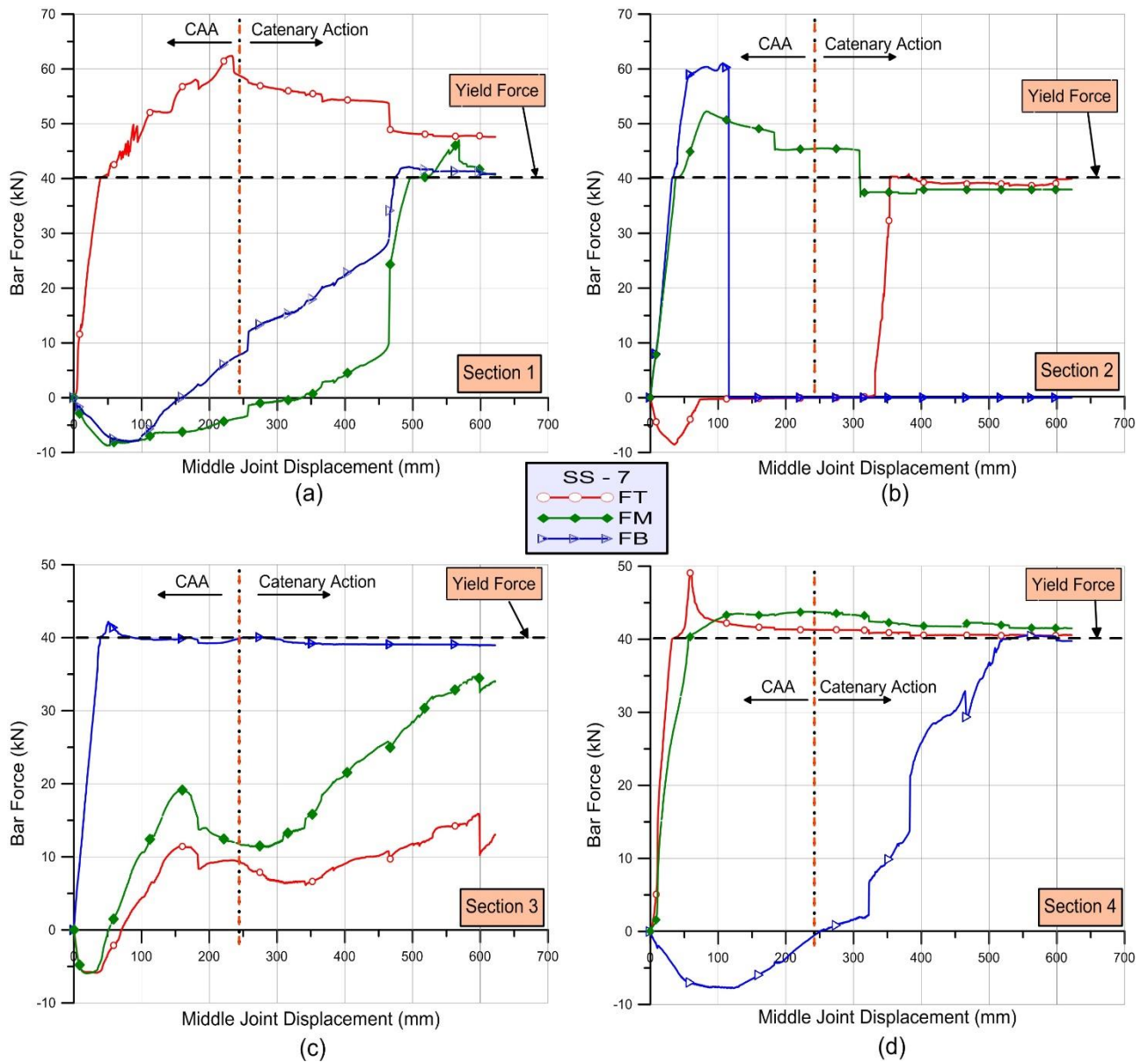
Figure 4-54 Bar Forces vs. MJD for Specimen SS-7

It is clear from Figure 4-54, that the presence of partial hinges affected the axial compressive forces developed in the steel bar reinforcement. Figure 4-54(c), (d) show the similarity in forces developed in the top bars with the bar forming the partial hinge.

For the middle joint, at the sections 2 and 3, forces in the top bars changed from compression to tension at a small deflection. At section 4 the bottom bar forces changed from compression to tension at a deflection nearly equal to the deflection at catenary action onset, Figure 4-54(a), (d)

Figure 4-55 shows bar forces for each section at specific deflections. The bottom bar at section 2 shows a zero bar force at a deflection of 350 mm, this has been caused by strain gauge damage. The variation of forces for the bars forming the partial hinges was small during the loading as can be seen from Figure 4-55(b). All bars were carrying tensile forces at a deflection of 350.0 mm as shown in Figure 4-55(f).
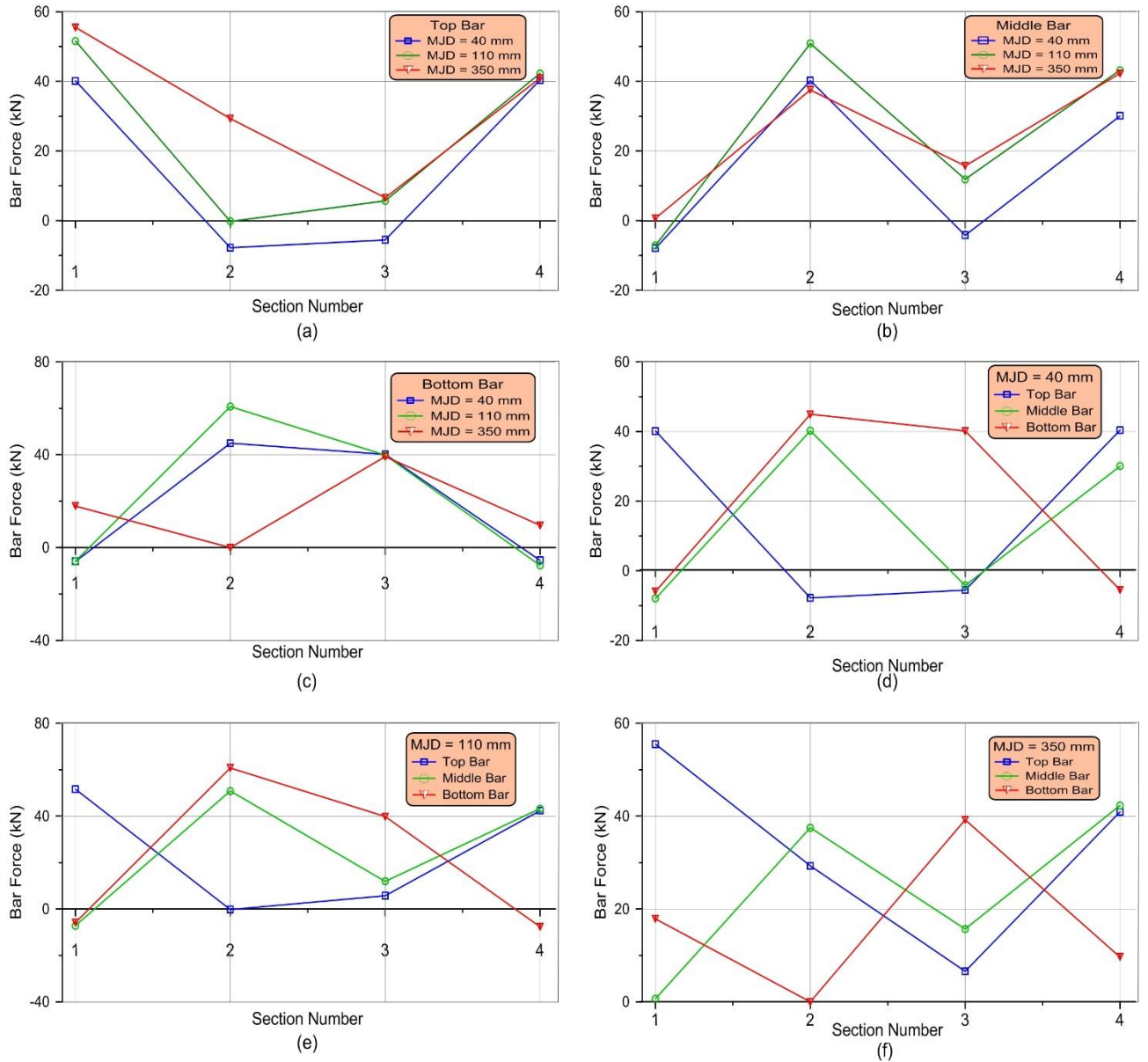


Figure 4-55 Bar Forces at Different Resisting Mechanisms for Specimen SS-7

## 4.3.2.7 STEEL BAR FORCES IN SPECIMEN SS-8

Similar to specimen SS-7, a partial hinge was provided to the beam section but at a distance equal to twice that of the beam depth away from the beam-column interface. Different from specimen SS-7, all strain gauges were attached to the top bars forming the partial hinges. The presence of partial hinges enhanced the total applied load at the catenary action stage despite the axial load developed throughout the beam being the same for specimen SS-2 and SS-3. Figure 4-56 shows the relationship between bar forces and MJD for SS-8.
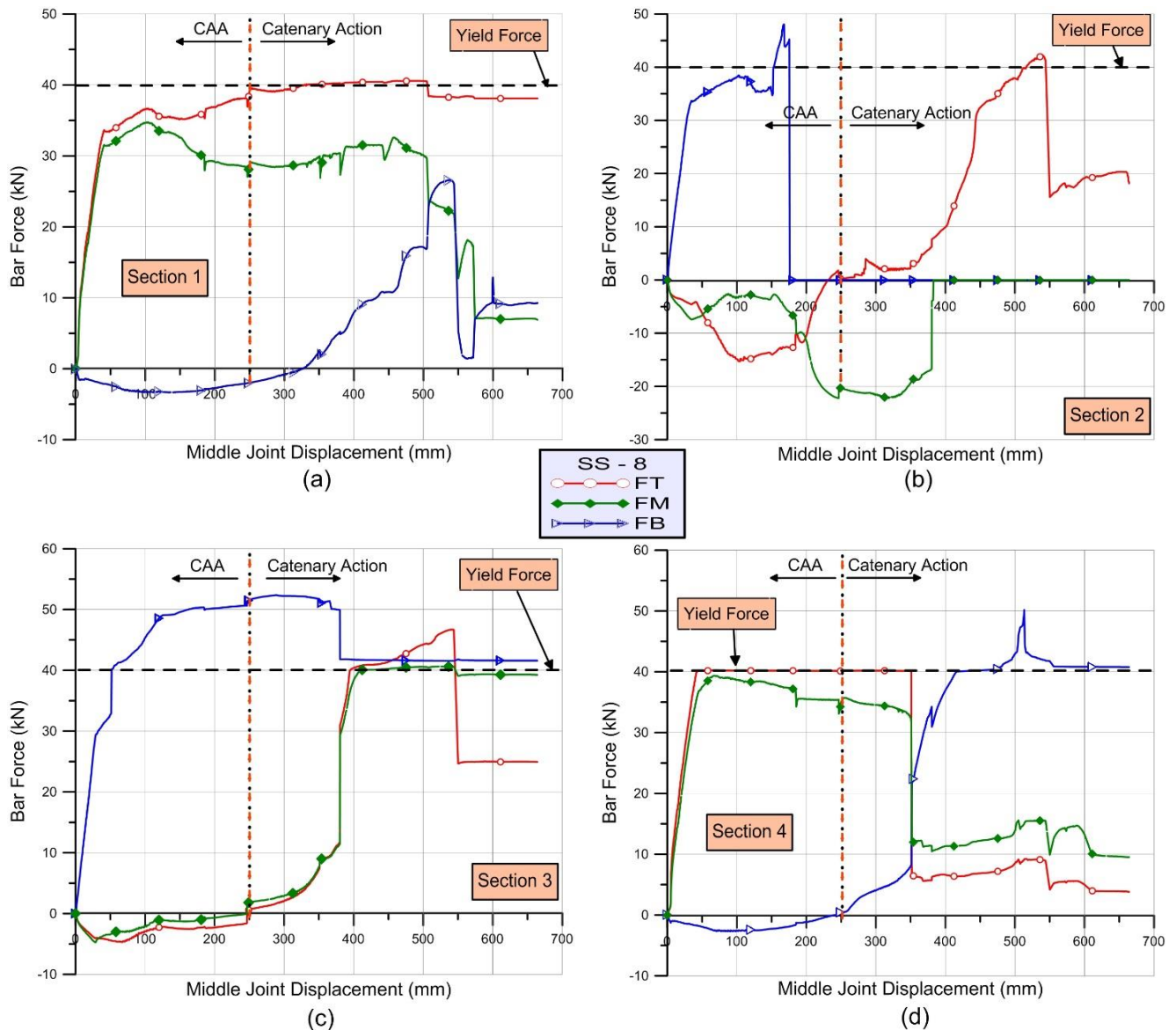


Figure 4-56  Bar Forces vs. MJD for Specimen SS-8

The force distribution for the bars forming the partial hinges was similar to the top bars and they followed the same path as shown from Figure 4-56. The compressive forces carried by the top and bottom bars were very small except at section 2, which was larger by about 50%. For most of the bars, the transition from compression to tension occurred at nearly at 250 mm deflection, which was the same deflection for the onset of catenary action. Figure 4-57 shows bar forces for each bar at specific deflections. The force distribution in bars was similar to specimen SS-7.
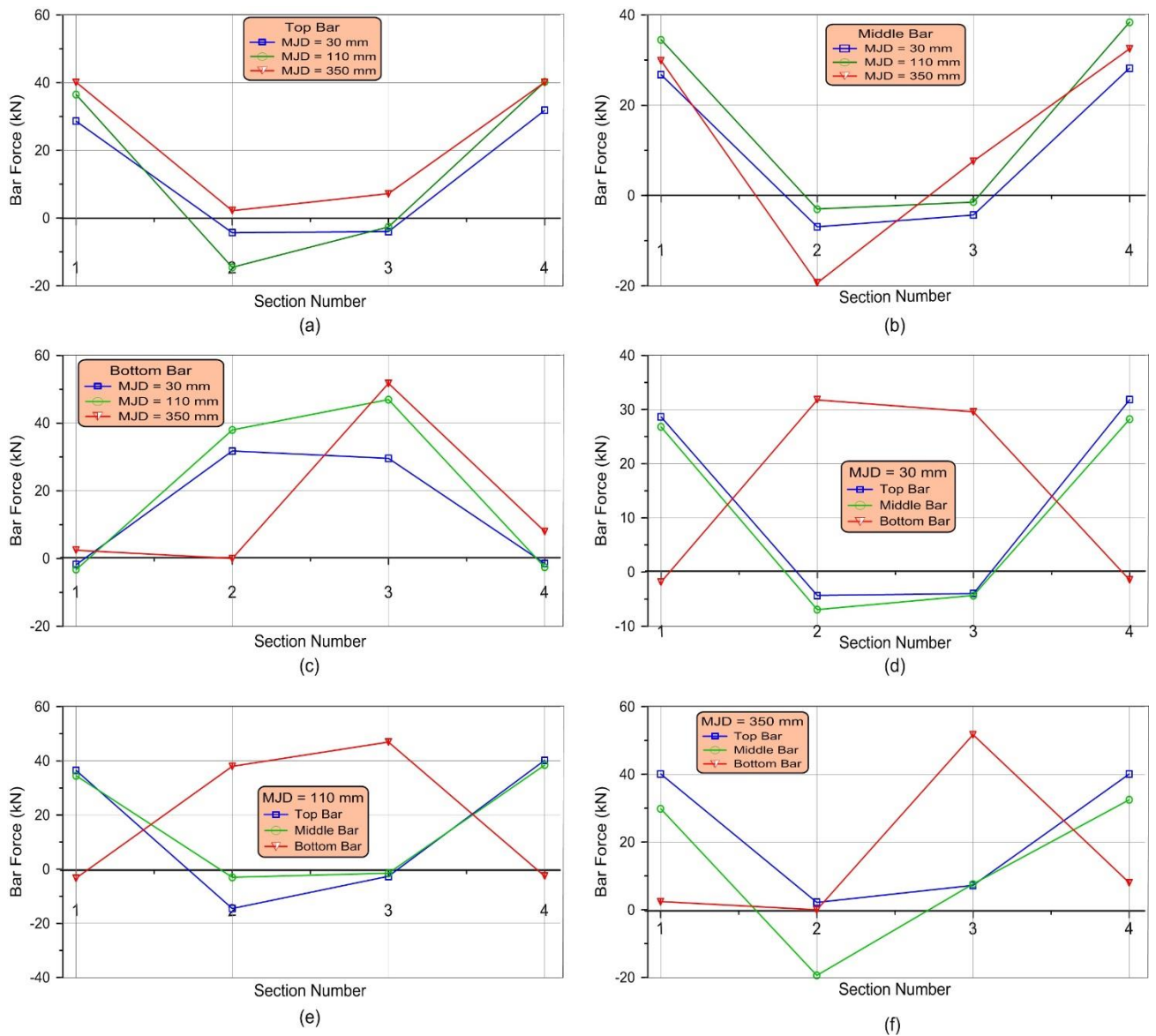


Figure 4-57 Bar Forces at Different Resisting Mechanisms for Specimen SS-8

## 4.4 EFFECT OF THE PROPOSED SCHEME

Figure 4-58 shows the effect of the additional middle steel bars on the structural behaviour of the RC specimens. Within compressive arch action, the applied load for all specimens was larger than specimen SS-3 by at least 8% for SS-6, and the peak applied load for specimen SS-4 was the largest.

At the catenary action stage, the applied load for all specimens was larger than specimen SS-3 by at least 77% and the peak applied load for specimen SS-5 was the largest. This indicates that the effect of the middle layer on catenary action was greater than its effect on CAA. In other words, the additional middle layer is beneficial for an increase in tying capacity of RC structures rather than flexural capacity.

The optimum tying capacity can be obtained in the event of progressive collapse, by placing the middle layer at a distance $(d - d')/4$ vertically above the centre of the bottom bars. The final MJD for all specimens was larger than that for specimen SS-3 and the largest MJD was for specimen SS-5. This means that the additional steel bars can increase the rotational capacity for RC specimens and the optimum result can be obtained by placing the middle layer at a distance $(d - d')/4$ from the centre of bottom bars.
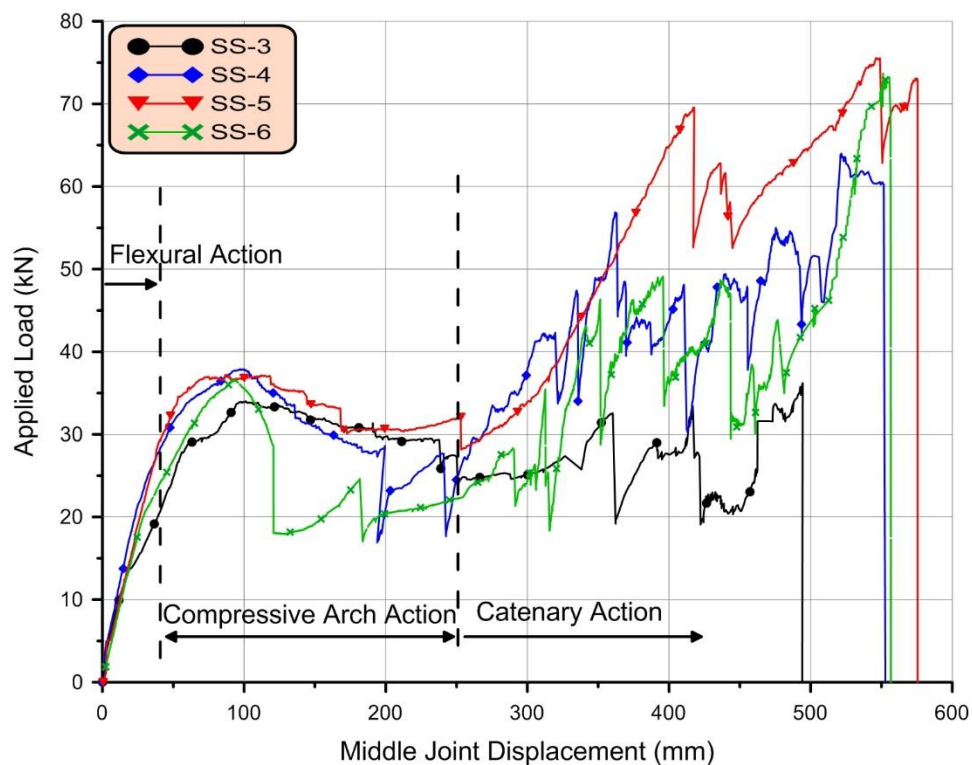


Figure 4-58 Structural Behaviour for Specimens with Additional Steel Bars.

Figure 4-59 shows the comparison of the distribution of axial forces for specimens with additional steel bars. Within CAA, the axial forces developed were close to each other for all specimens.

Transition points from CAA to catenary action ranged from 254.3 mm to 283 mm of deflection for SS-5 and SS-4 respectively. Due to the presence of additional longitudinal steel bars, the axial tensile forces increased significantly. The tensile force for specimen SS-5 was the largest, being more than twice the tensile force for specimen SS-3.
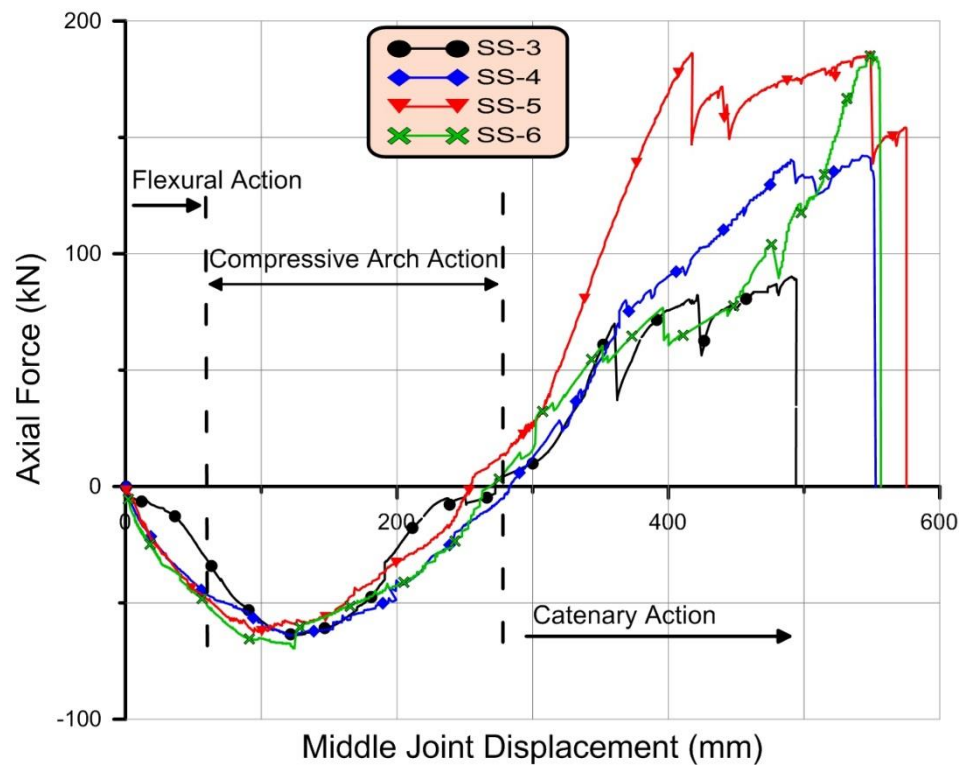


Figure 4-59 Axial force distribution for all specimens with additional bars

Figure 4-60 shows the effect of providing partial hinges on the structural behaviour of RC specimens. The general trend of structural behaviour for specimen SS-7 and SS-8 was similar to that for specimen SS-3.

The presence of partial hinges was able to increase the applied load during CAA by 5% for both specimens. At catenary action, the increase in the applied load was 48% and 52% for specimen SS-7 and SS-8 respectively.

Compared to the contribution of the middle layer, the contribution of partial hinges was smaller. The final middle joint displacement for specimens with partial hinges was much larger than for

the specimen without partial hinges. This also indicates that the rotational capacity can be increased by setting partial hinges into the RC beams.

In the event of progressive collapse, the column removal and the redistribution of the gravity loads will occur suddenly in a very short space of time. Due to this sudden occurrence, early warning cannot be achieved by large displacement. Therefore, it can be concluded that both specimens have similar structural performance.
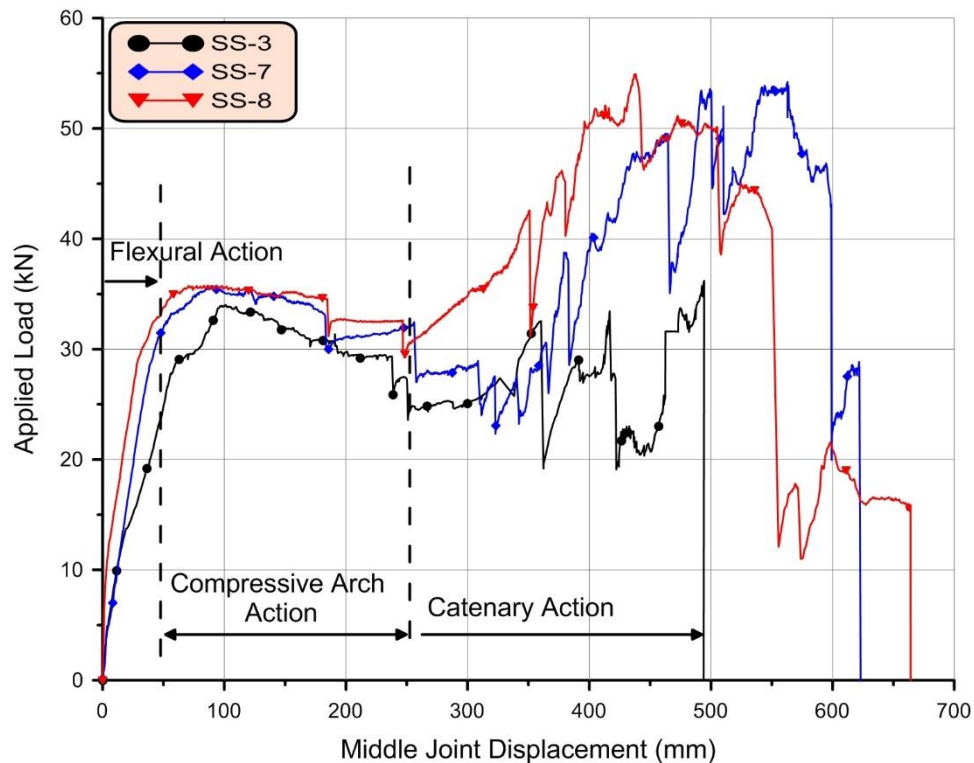


Figure 4-60 Structural Behaviour for Specimens with Partial Hinges

Figure 4-61 demonstrates the effect of partial hinges on the axial forces developed during the tests. The axial compressive forces for specimen SS-7 and SS-8 were smaller than those for SS-3 by about 10% and 16% respectively.

At catenary action, the tensile forces developed were nearly similar to those for SS-3. Transition points from CAA to catenary action for specimen SS-7 and SS-8 were 245.0 mm and 250.5 mm of deflection, respectively, which were less than the transition point for all specimens. This means that the presence of partial hinges can enhance the onset of catenary action.
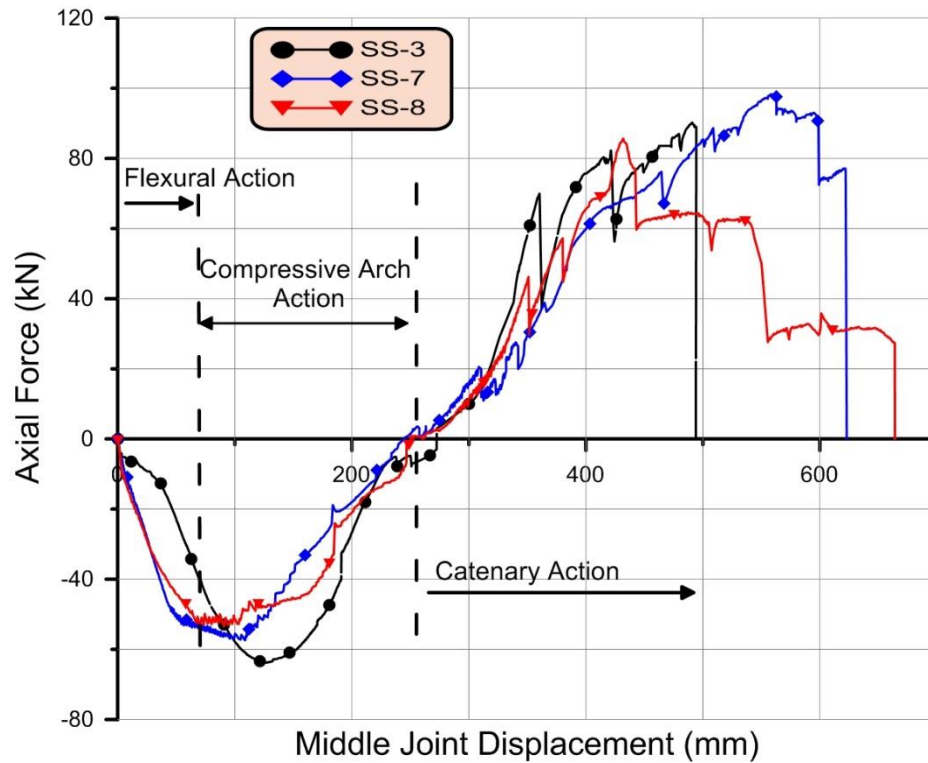
Figure 4-61 Axial force distribution for specimen SS-3, SS-7 and SS-8

Tables 4-9 and 4-10 summarise the critical values of applied loads and axial forces for all specimens.

Table 4-9 Applied Loads Compared to Specimen SS-3

| Specimen | Applied Load (kN) | | | $\dfrac{P_{com}}{P_{com(SS-3)}}$ | $\dfrac{P_{cat}}{P_{cat(SS-3)}}$ |
|----------|-------|-----------|-----------|------|------|
|          | $P_f$ | $P_{com}$ | $P_{cat}$ |      |      |
| SS-3     | 28.0  | 34.0      | 36.2      | 1    | 1    |
| SS-4     | 32.6  | 37.9      | 64.0      | 1.12 | 1.77 |
| SS-5     | 32.2  | 37.2      | 75.6      | 1.10 | 2.09 |
| SS-6     | 30.2  | 36.7      | 73.7      | 1.08 | 2.04 |
| SS-7     | 29.8  | 35.6      | 53.7      | 1.05 | 1.48 |
| SS-8     | 29.8  | 35.8      | 54.9      | 1.05 | 1.52 |

Table 4-10 Axial Forces compared to Specimen SS-3

| Specimen | Max. Axial Forces(kN) | | $\dfrac{N_{com}}{N_{com\,(SS-3)}}$ | $\dfrac{N_{ten}}{N_{ten(SS-3)}}$ |
| :---: | :---: | :---: | :---: | :---: |
| | $N_{com}$ | $N_{ten}$ | | |
| SS-3 | 63.8 | 89.2 | 1 | 1 |
| SS-4 | 64.3 | 142.2 | 1.01 | 1.59 |
| SS-5 | 62.7 | 186.9 | 0.98 | 2.10 |
| SS-6 | 69.6 | 185.0 | 1.09 | 2.07 |
| SS-7 | 57.4 | 98.4 | 0.90 | 1.1 |
| SS-8 | 53.4 | 85.7 | 0.84 | 0.96 |

Where

$P_f$, $P_{com}$, $P_{cat}$ , are the applied load at flexural, CAA and catenary action stages.

$N_{com}$, $N_{ten}$, are the axial forces at CAA and catenary action.

Figure 4-62 shows the pseudo-static relationship between the applied load and the MJD for all specimens.
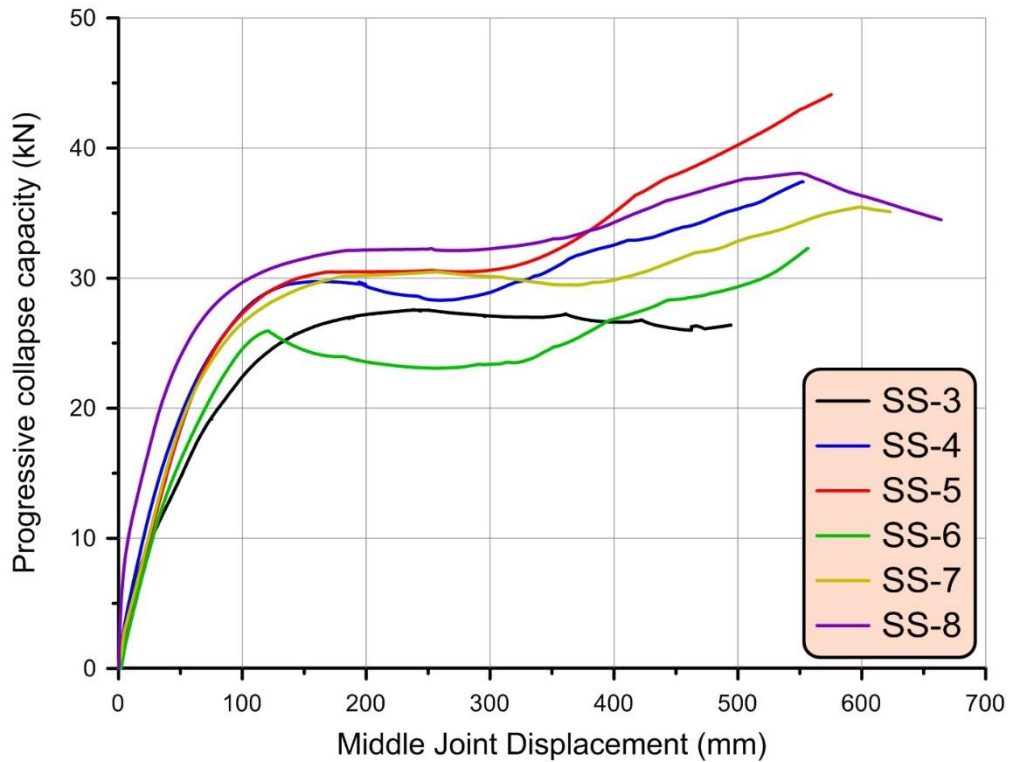


Figure 4-62 Pseudo-Static Relationship for All Specimens

The overall trends of the specimens were similar, but with different peak load values. Different from specimen SS-3, catenary action was able to increase the progressive collapse capacity. The largest enhancement was 45% of the first peak at CAA for specimen SS-5. The first peak load for specimen SS-8 was the largest at about 32.3 kN. The largest peak load at catenary action was 44.1 kN for specimen SS-5.

It should be mentioned that the first peak of progressive capacity for specimens with partial hinges lay within the catenary action stage. This means, the presence of partial hinges may reduce the effect of sudden bar fracture on the progressive collapse resistance at CAA.

Table 4-11 lists the peak loads with their corresponding deflections and the ratio of enhancement of catenary action stage. The lowest first peak was 25.9 kN for specimen SS-6 with lowest MJD of 120.7 mm. This indicates, the adding of steel bars near the top reinforcement will be dangerous in the event of progressive collapse unless the specimen can provide more resistance at the catenary action stage. Setting partial hinges at a distance equal to the beam depth is not preferable due to the lowest enhancement at catenary action stage.

Table 4-12 lists the peak loads with comparison ratios with the specimen SS-3. It is clear that the modified detailing for specimen SS-5 was the most preferable in the event of progressive collapse due to large enhancement of catenary action.

Table 4-11 Peak Loads with Their Corresponding Deflections for All Specimens

| Specimen | First Peak Load | | Max. Load At Catenary action | | $\dfrac{P_{cat} - P_{st}}{P_{st}}$ x 100% |
|---|---|---|---|---|---|
|  | $P_{st}$ (kN) | MJD (mm) | $P_{cat}$ (kN) | MJD (mm) |  |
| SS-3 | 27.5 | 249.5 | 26.4 | 494.0 | - |
| SS-4 | 29.7 | 163.8 | 37.4 | 553.0 | 26 |
| SS-5 | 30.5 | 172.7 | 44.1 | 576.0 | 45 |
| SS-6 | 25.9 | 120.7 | 32.3 | 557.0 | 25 |
| SS-7 | 30.5 | 256.1 | 35.5 | 599.0 | 16 |
| SS-8 | 32.3 | 252.2 | 38.1 | 550.0 | 18 |

Table 4-12 Peak Loads with Comparison Ratios with SS-3

| Specimen | $P_{st}$ (kN) | $P_{cat}$ (kN) | $\dfrac{P_{st}}{P_{st(SS-3)}}$ | $\dfrac{P_{cat}}{P_{cat(ss-3)}}$ |
|----------|----------|----------|----------|----------|
| SS-3 | 27.5 | 26.4 | 1 | 1 |
| SS-4 | 29.7 | 37.4 | 1.08 | 1.42 |
| SS-5 | 30.5 | 44.1 | 1.11 | 1.67 |
| SS-6 | 25.9 | 32.3 | 0.94 | 1.22 |
| SS-7 | 30.5 | 35.5 | 1.11 | 1.34 |
| SS-8 | 32.3 | 38.1 | 1.17 | 1.44 |

## 4-5 SUMMARY

In this chapter, the test results of eight RC sub-assemblages were presented and compared. The test results were categorised into two main groups, test results at global level and local level. The test results comprise of, applied load-MJD relationship, axial force-MJD relationship, bar forces-MJD relationship and crack pattern.

The following provides a summary of the chapter:

1- At the beginning, material test results were presented.

2- Test results at the global level in terms of the deflection along the length of the beam, applied load-MJD, axial force-MJD and crack pattern for each specimen were presented.

3- Non-linear static test results were converted into non-linear pseudo-static using the approach proposed by Izzuddin (2008).

4- Test results at the local level in terms of bar force-MJD were presented and compared with the specimens designed according to the conventional approaches.

5- A comparison between the test results of the specimens conventionally designed and specimens detailed with the proposed scheme were made.

The main conclusion from this chapter can be summarised as follows:

1- In the event of column loss, the RC structure undergoes three stages of resisting mechanisms, flexural, CAA and catenary action stages.

2- Due to lateral restraints, the capacity was increased by about 15.5% - 21.5% of the flexural capacity at CAA. During CAA, the displacement of middle joint at which the specimens attained peak capacity was about $0.35h$.

3- Test results showed that the proposed scheme was efficient to increase progressive collapse capacity. Adding two additional steel reinforcement bars could increase the capacity by about 22% - 67% depend on the location of the added steel layer.

## 5. CHAPTER FIVE    NUMERICAL ANALYSIS

## 5.1 GENERAL

In the event of progressive collapse, large deflections, plastic hinge formation, concrete crushing, steel bar slippage, steel bar pull-out and bar fracture may occur. Therefore, both geometrical and material nonlinearities must be included and considered in the analysis of RC structures subjected to abnormal loads which may lead to progressive collapse.

During the experimental tests on RC beam-column sub-assemblages, bottom bars at the middle joint and top bars at the beam end were fractured. In addition, severe and wide cracks occurred at the interfaces of the middle joint and at the beam ends. Severe and wide cracks indicate bar slip occurrence at these locations. Slippage and fracture of steel bars near joint interfaces caused a discontinuity in the component of the sub-assemblage (beams and column stubs), allowing the beams to rotate easily which led to the development of catenary action through the beams and increasing progressive collapse resistance capacity.

It should be noted that modelling geometric and material nonlinearities using the finite element method almost always requires repeating updates of the tangent stiffness matrix and solutions of the corresponding system of equations, which is the most time-consuming step in the iterative numerical scheme.

Therefore, it is not efficient to use a detailed finite element model to simulate the behaviour of RC structures under CRS including geometrical and material nonlinearities and all possible failure modes. This is because of the high computational cost for nonlinear analysis of a large structure such as a multi-storey RC building, which is always exorbitant since a large number of finite elements are needed to model the structure to obtain reasonably accurate predictions of the structural response (Hartmann et al., 2008).

However, in many practical problems involving nonlinear analysis of large-scale structures, the material nonlinearity phenomena are usually localised at certain critical structural members (Department of Defence (DoD) 2005) and may not dramatically spread throughout the whole structure. Thus, at each load increment, the computational effort spent on assembling the tangent stiffness matrix and updating the structural members properties could be avoided using a macro-model approach to simulate the behaviour of RC structures under CRS (Long, 2013).

## 5.2 MACRO-MODEL APPROACH

In order to gain a better understanding of the beam-column joint behaviour with effective and efficient computational cost, a macro-model approach was used to simulate RC structures under seismic loading and progressive collapse (Fleury et al., 2000); Lowes and Altoontash 2003;(Mitra, 2007); (Bao et al. 2008).

The main concept of the Macro-Model approach is to decompose multiple complicated behaviours of RC beam-column joint into several simple components such as flexural, axial, bond-slip, interface shear and shear panel behaviour. Each component can be characterised by an equivalent set of nonlinear springs, which can be defined by a relationship between force and displacement of each component.

The application of the Macro-model approach requires the following steps (Jaspart, 2000):
    1) Identification of active components for a joint.
    2) Evaluation of the mechanical characteristics of individual basic components.
    3) Assembly of the components to represent the mechanical characteristics of the whole joint.

In this sense, the accuracy of component-based joint models depends highly on the force-displacement relationships adopted for the equivalent springs and the number of components included in the analysis. Therefore, the key point of this type of modelling is to extract the characteristics of these equivalent springs and to calibrate them based on test results (Yu, Jun. 2013).

## 5.2.1 COMPONENTS OF THE MACRO-MODEL FOR RC JOINTS

For a 2D RC beam-column joint, various component-based approaches have been proposed to predict the joint deformation behaviour (Alath and Kunnath, 1995);(Youssef and Ghobarah, 2001); (Lowes and Altoontash 2003); (Bao et al. 2008).

Figure 5-1 shows the typical configuration of the joint model adapted by Lowes and Altoontash 2003, which comprises of eight bar force-slip spring components to simulate axial loads carried by the section of the structural member. Additionally, these springs represent the stiffness and strength loss due to the potential anchorage failure of beam and column longitudinal reinforcement embedded into the joint, and the coupled action of the compressive and tensile forces at each section represents the flexural strength of the RC beam.

138

In addition, four interface shear components were incorporated to simulate the loss of shear transfer capacity due to shear failure at the beam joint and the column joint interfaces.
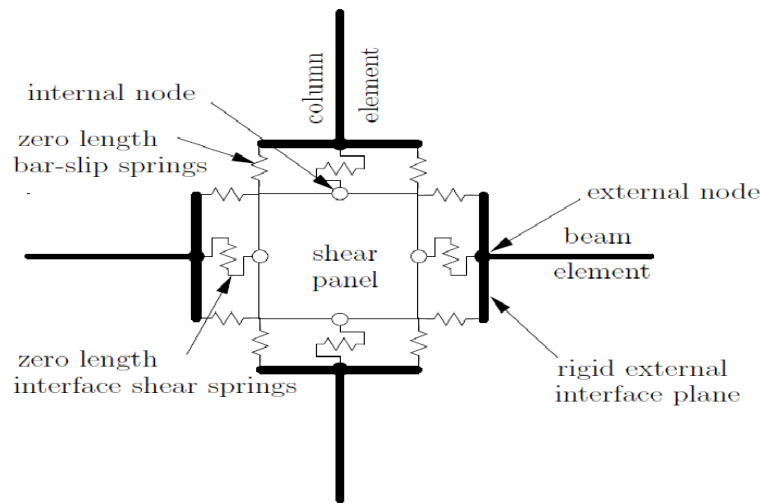


Figure 5-1 Lowes-Altoontash's Joint Model (2003)

The dimensions of the bar force-slip component springs were zero, which means that the internal and external planes shown in Figure 5-1 were coincident at the same physical position in the FE model. In order to carry out a finite element analysis using the Macro-Model approach, properties of each nonlinear spring must be calibrated by including the force – deformation envelope with bar force-slip and bar fracture to accurately predict the compressive and catenary action of RC structures.

According to the concept of designing columns stronger than beams, the joint model proposed by Lowes and Altoontash can be modified or reduced by assuming a rigid connection between column and beam. Therefore, the bar force-slip springs of the column-joint can be deleted from the model. Based on the experimental tests, it is clear that there is no failure in the shear panel. Therefore, it is assumed to act as a rigid panel.  The new proposed model shown in Figure 5-2 comprises of three types of elements:
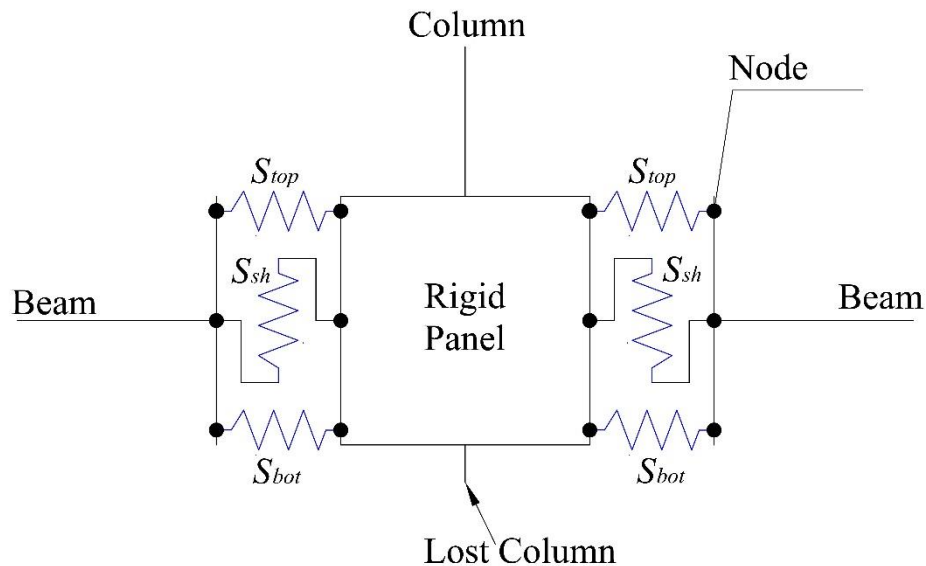
Figure 5-2 Proposed Model (Middle joint)

1- Bar force-slip springs ($S_{bot}$ and $S_{top}$): Four springs in the interior joint and two for the exterior joints. These springs are able to simulate beam axial compressive and or tensile forces that develop through the beam under column removal or any applied load. In addition, the coupled action of these springs will simulate the bending moment capacity of the beam section at the critical sections. Compression springs should include the contribution from both concrete and steel reinforcement, while the tensile contribution of concrete for the tension springs can be ignored because all specimens failed due to bar fracture.

2- Shear springs ($S_{sh}$): Shear spring $S_{sh}$ simulates shear forces developed at joint interfaces of beam-joint panel. Shear forces can be transferred from beam to joint panel through shear strength of flexural compression zone and aggregate interlock at small cracks or by dowel action provided by steel reinforcing bars at large cracking and catenary action stage. (Lowes et al., 2003b) suggested that the shear spring can be taken as an elastic linear spring with a large stiffness due to the fact that conventional frame members have sufficient shear capacity to prevent shear failure.

3- Rigid members: These members are able to simulate the assumed rigid behaviour of the beams at non-critical locations, and can be represented by linear elements with large stiffness as the failure of the RC beam-column structures is concentrated at joint connection interfaces. This was clear from the experimental tests.

From the experimental tests, it was evident that the bar force-slip spring is the most important and critical element in the Macro-model approach. This can affect the structural behaviour of RC sub-assemblages, and maximum capacity achieved by these sub-assemblages under compressive arch action and catenary action.

Therefore, it is crucial to obtain the property envelopes and calibrate the values of force-deformation of these springs to obtain an accurate representation of the structural behaviour of the RC beam-column sub-assemblages.

It should be noted that the term *slip* describes the relative movement between the main bar reinforcement and the confining concrete in the longitudinal direction, while slip in the transverse direction is assumed to be zero, due to sufficient confinement from the surrounding concrete and steel stirrups.

It is also worth mentioning, (Alsiwat and Saatcioglu, 1992) pointed out that the pull-out failure does not occur in the beam-column joints with transverse steel reinforcement, which also was clear from the experimental results.

## 5.2.2 STEEL-CONCRETE BOND STRENGTH

Bond capacity or bond strength between the steel and surrounding concrete can be related to three main structural mechanisms. The first mechanism is the adhesion between concrete and steel reinforcement, and the second mechanism is the mechanical interlock between the deformed steel bar and surrounding concrete which commences after internal concrete cracks start to form. Shear failure of concrete keys will terminate this resource of bond strength and what remains is the third mechanism which is the friction between concrete and steel reinforcement (Goto, 1971).

Figure 5-3 shows the three resistance mechanisms between concrete and steel reinforcement. According to experimental research regarding the relationship of bond stress – slip between concrete and steel reinforcement, bond resistance mechanisms can be simulated by the relationship shown in the graph of Figure 5-4 (Long 2013).
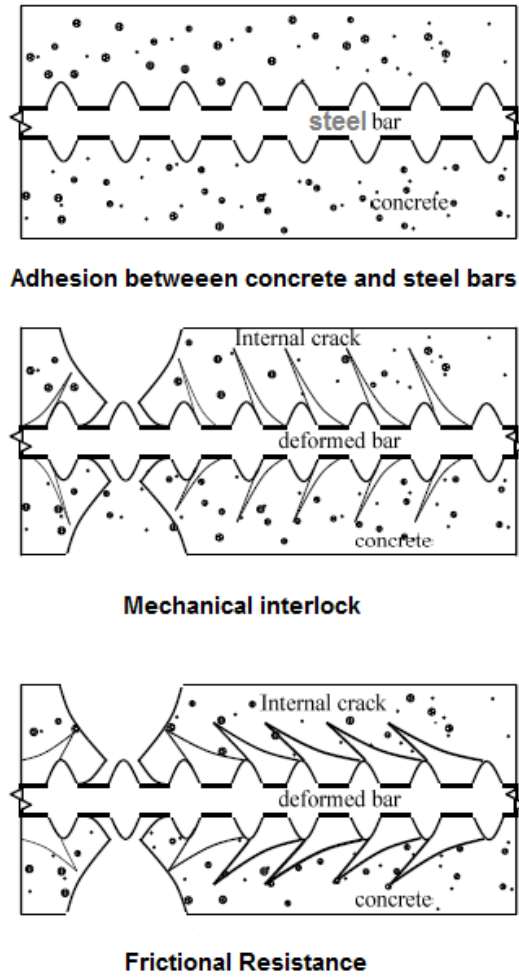
Figure 5-3: Resisting Mechanisms Goto (1971)
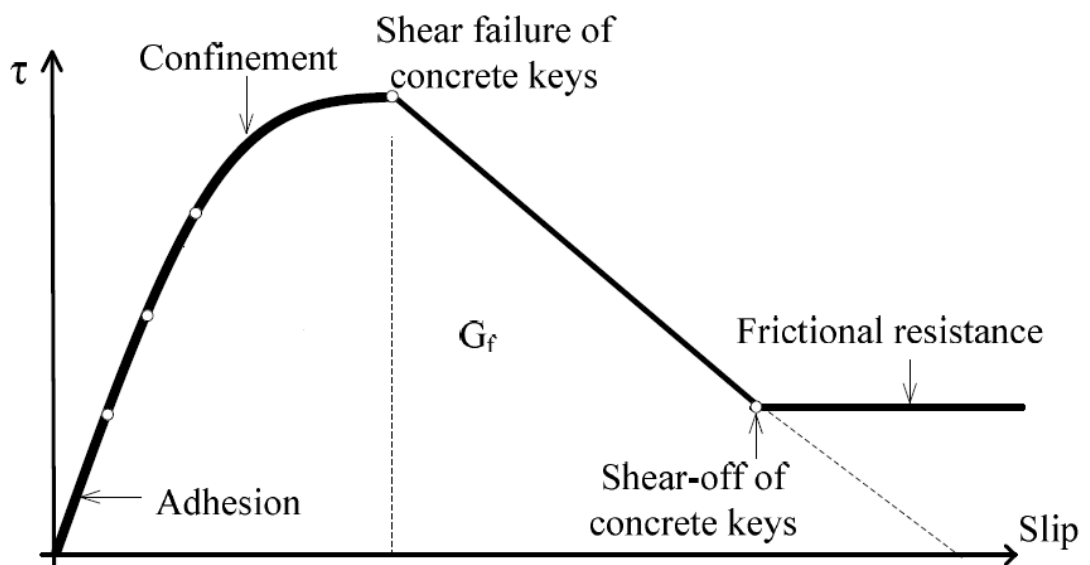


Figure 5-4: Relationship between Bond Stress and Slip (Long 2013)

As shown in Figure 5-4, (Haskett et al., 2008) pointed out that the area under the bond-slip graph is the interfacial fracture energy $G_f$, which controls the pull-out strength and de-bonding resistance. (CEB-FIP, 2000) suggests that there is a plateau over which the maximum bond resistance remains constant as shown in Figure 5-5 with values for each parameter shown in the graph, which is listed in Table 5-1.
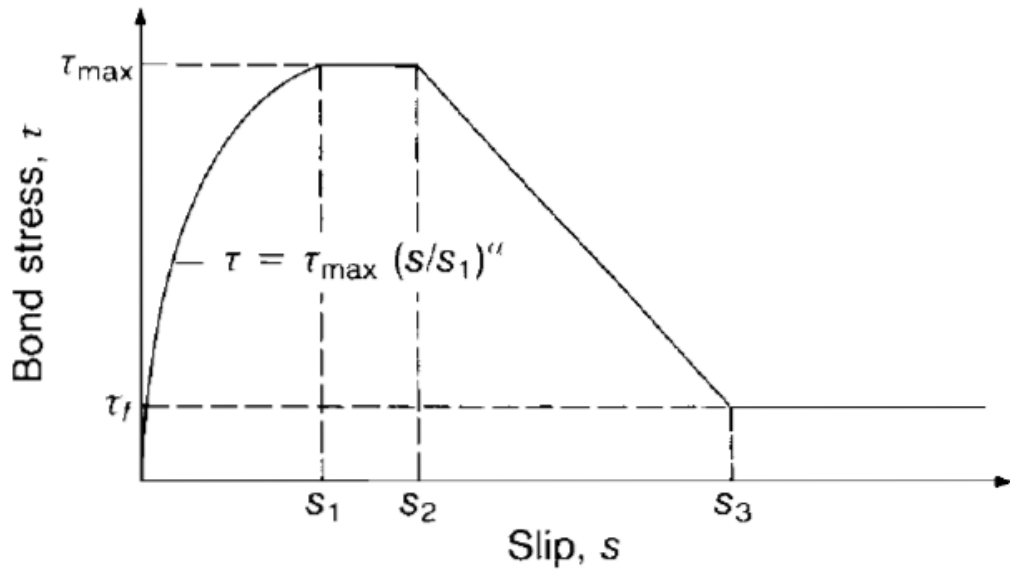


Figure 5-5 Analytical Bond Stress-Slip Relationship (CEB Model Code 2000)

Table 5-1 Parameters for defining the mean bond stress –slip relationship (CEB 2000)

| NO | Unconfined Concrete | | Confined Concrete | |
|---|---|---|---|---|
| | Good Bond Conditions | All Other Bond Conditions | Good Bond Conditions | All Other Bond Conditions |
| S1 | 0.6 mm | 0.6 mm | 1.0 mm | 1.0 mm |
| S2 | 0.6 mm | 0.6 mm | 2.0 mm | 2.0 mm |
| S3 | 1.0 mm | 3.0 mm | Clear rib spacing | Clear rib spacing |
| $\alpha$ | 0.4 | 0.4 | 0.4 | 0.4 |
| $\tau_{max}$ | $2.0\sqrt{f_c}$ | $1.0\sqrt{f_c}$ | $2.5\sqrt{f_c}$ | $1.25\sqrt{f_c}$ |
| $\tau_f$ | $0.15\tau_{max}$ | $0.15\tau_{max}$ | $0.40\tau_{max}$ | $0.40\tau_{max}$ |

The bond-slip relationship is modified by many researchers to simplify slip calculation. The modification assumes a uniform distribution of bond stress at both elastic ($\tau_E$) and inelastic ($\tau_Y$) parts of the model with the same equivalent interfacial fracture energy $G_f$ as shown in Figure 5-6.
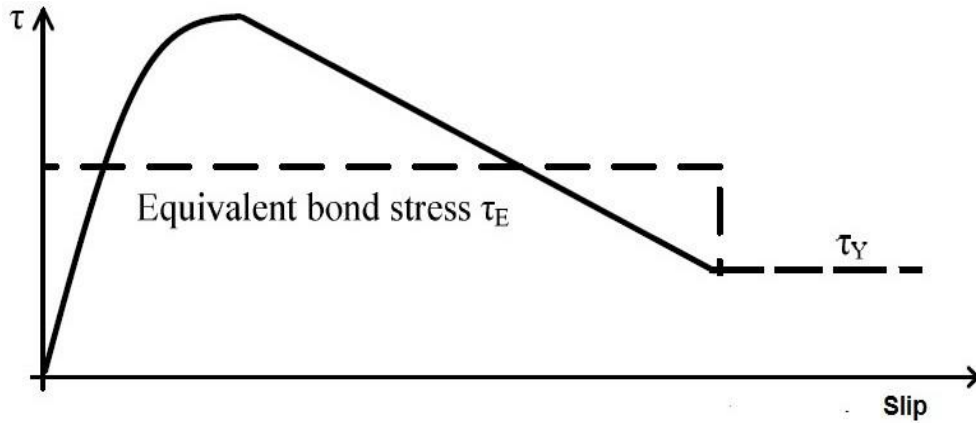


Figure 5-6 Equivalent Bond Stress in Bond Stress-Slip Relationship

Based on many experimental tests, a representation of a constant uniform bond strength for both the elastic and inelastic stages has been evaluated by many researchers. Table 5-2 lists the empirical values for bond stress for elastic ($\tau_E$) and inelastic ($\tau_Y$) values, and also for tension and compression, which have been adopted by many researchers.

Table 5-2 Empirical Values for bond strength

| Researcher | Average Bond Strength (MPa) | | | |
|---|---|---|---|---|
| | Tension | | Compression | |
| | Elastic $\tau_E$ | Inelastic $\tau_Y$ | Elastic $\tau_E$ | Inelastic $\tau_Y$ |
| (Sezen and Setzler, 2008) | $1.0\sqrt{f_c}$ | $0.5\sqrt{f_c}$ | | |
| Lowes and Altoontash (2003) | $1.8\sqrt{f_c}$ | $0.4\sqrt{f_c}$ | $2.2\sqrt{f_c}$ | $3.6\sqrt{f_c}$ |
| (Sozen and Moehle, 1990) | $0.83\sqrt{f_c}$ | $0.5\sqrt{f_c}$ | | |
| (Eligehausen et al., 1982) | $2.0\sqrt{f_c}$ | $0.5\sqrt{f_c}$ | $3.1\sqrt{f_c}$ | $3.1\sqrt{f_c}$ |

It is clear from table 5-2 that the elastic bond stress ($\tau_E$) is larger than inelastic bond stress ($\tau_Y$) in tension, while in compression, the elastic bond stress ($\tau_E$) is less than inelastic bond stress ($\tau_Y$). This is due to the effect of Poisson ratio, in which the diameter of steel bars increases under compression, leading to increase in bond stress. Lowes and Altoontash (2003) pointed out that the bond stress-slip behaviour of RC beam column joints under compressive force is governed by surrounding concrete, neglecting the effect of bond stress. Therefore, it is not useful to include bond stress resistance in the bond-slip behaviour under compression, and Lowes and Altoontash (2003) suggested calibration of the bond-slip behaviour according to design regulations and section analysis.

The bond stress-slip relationship can be directly converted into a bar force-slip relationship by multiplying bond stress with the bar cross sectional area. Another way to obtain the bar force–slip relationship is by using experimental results and models of bar force-slip tests under certain bond conditions such as the model proposed by (Zhao and Sritharan, 2007) for bars with adequate embedment length. However, available test data is very limited.

In this section a derivation of bar force-slip relationship is presented with a number of assumptions, focusing specifically on tensile bar force-slip relationship, whilst compressive bar force-slip behaviour is calibrated according to the section analysis and design regulations as suggested by Lowes and Altoontash (2003).

It should be noted that there are two possible bond failure mechanisms between concrete and steel bars:

1- Splitting failure: this failure may occur when the surrounding concrete has insufficient thickness and strength.

2- Pull-out failure: this failure may occur when the length of embedded steel reinforcement is insufficient.

If bond failure is avoided, material strength of bars can be fully utilised and the reinforcing bars will fail by fracture (Yu, Jun 2013). During experimental tests, no splitting or pull-out failure occurred, which indicates that there was sufficient confinement from surrounding concrete to the steel bars and sufficient embedment length of the bars passing the middle joints or anchored into the end column stubs. Therefore, in this chapter, there is no consideration for splitting and pull-out failure taken into account in developing the bar force-slip relationship.

## 5.2.3 BOND STRESS-SLIP RELATIONSHIP UNDER AXIAL TENSION

In order to simplify the development of the bond-slip model, several simplifying assumptions were taken into account. Firstly, a uniform bond stress along the anchored length of steel bars for both the elastic and plastic zones is assumed. Secondly, slip is the relative movement between steel bars and concrete due to the extension of steel bar computed based on the steel bar strain distribution along the anchored length. Thirdly, a bilinear stress-strain relationship for steel reinforcement and the steel strain is given by the Eq. (5-1).

$$\varepsilon_s = \begin{cases} f_s/E_s & \text{when } f_s \leq f_y \\ \\ f_y/E_s + (f_s - f_y)/E_h & \text{when } f_s > f_y \end{cases} \tag{5-1}$$

Where $\varepsilon_s$ is the steel strain at the point of investigation, $f_s$ is the bar stress at the point of investigation, $E_s$ is the steel modulus of elasticity, $f_y$ is the steel stress at yield, and $E_h$ is the steel hardening modulus. Figure 5-7 shows the assumed bond stress distribution along the steel bars and corresponding distributed steel bar stress along its length.
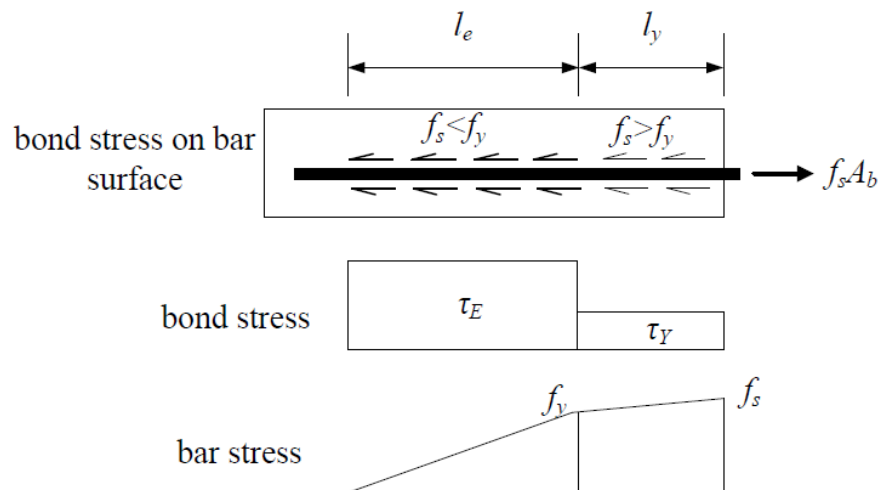


Figure 5-7 Bond stress and bar stress based on the first assumption

Using equilibrium equations, stress distributions in Figure 5-7 and the constitutive model for the steel bars in equation 5-1, the bar force- slip envelope can be determined under any applied load. Due to the difference of boundary conditions for both interior and exterior joints, each joint model will be developed individually.

## 5.2.3.1 EXTERIOR JOINTS

In practice, anchorage of reinforcing bars, such as hooks and bend up bars, at exterior joints are usually employed, and this reproduced in the sub-assemblage tested in the experimental study. Based on the experimental results, additional assumptions were taken into account. It is assumed that there is a sufficient embedment length for the steel bars, which means that the steel bar has a zero slip at the point of zero bar stress. Figure 5-8 shows bar and bond stress distribution at the exterior joint. There are two possible cases, elastic and elastic-inelastic cases.
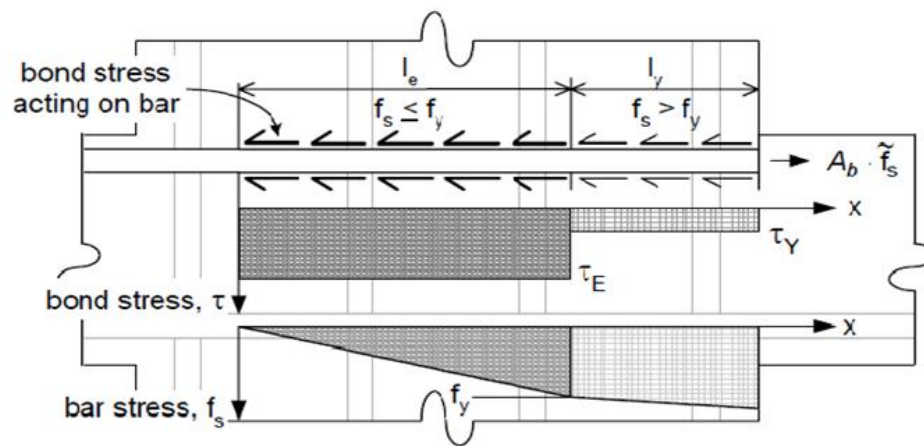


Figure 5-8 Bond and bar stress at exterior joint (Lowes-Altoontash 2003)

### A) ELASTIC CASE:

Based on equilibrium and considering an infinitesimal length of the steel bar ($dx$), the bond force should be equal to the bar force, that is,

$$df_s . A_b = \tau_E \pi\, d_b\; dx \tag{5-2}$$

Where

$A_b$ is the area of steel bar, $d_b$ is the bar diameter.

To obtain the required elastic length, force equilibrium along the elastic length should be applied, so then the equation will be:

$$l_e \tau_E \pi\, d_b = f_s A_b$$

$$l_e = \frac{f_s . d_b}{4\, \tau_E} \tag{5-3}$$

Where, $l_e$ is the required elastic length so that the bar stress is completely transferred to the confining concrete, and also denoted as the stress propagation length ($l_{fs}$) (Long, Xu.2013). It is clear from equation 5-3 that the required elastic length increases when the applied stress $f_s$ increases, and decreases when $f_c$ increases. It should be mentioned that the stress propagation length is equal to $l_{fs} = l_e + l_y$, and $l_y$ equals zero in this case. Slip can be obtained by integrating both sides of equation (5-2), that is:

$$slip = \int_0^{le} \frac{\tau_E \pi \, d_b \, x dx}{E_s A_b}$$

$$slip = \frac{\tau_E \pi \, d_b l_e^2}{2E_s A_b} + C \tag{5-4}$$

By substituting Eq. (5-3) into Eq. (5-4), bar slip can be expressed in terms of the bar stress $f_s$

$$slip = \frac{d_b f_s^2}{8E_s \tau_E} + C \tag{5-5}$$

The magnitude of C depends on the boundary condition, and for the assumption of zero slip at zero stress, the value of C will be zero.

**B) ELASTIC-INELASTIC CASE:**

If the applied force induces stresses $f_s$ at the beam-column joint interfaces more than the yield strength of steel, a uniform elastic-inelastic bond stress will be developed a long the stress propagation length. This case is more complicated since it includes two levels of bond stress ($\tau_E$ and $\tau_y$) with their related required bond lengths ( $l_e$ and $l_y$). Bar force slip can be obtained from force equilibrium along the total length of the bar as shown below:

$$l_e \tau_E \pi \, d_b \; = \; f_y A_b \qquad \text{for the elastic zone}$$

$$l_e = \frac{f_y d_b}{4 \tau_E} \tag{5-6}$$

$$l_y \tau_y \pi \, d_b = \left( f_s - f_y \right) A_b \qquad \text{for the inelastic zone}$$

$$l_y = \frac{(f_s - f_y) d_b}{4 \, \tau_y} \tag{5-7}$$

Slip can be obtained by calculating the total extension over the elastic and inelastic length. From Figure 5-9, which shows the distribution of bar strains over the total length, bar extension (slip) can be obtained from the area as follows:
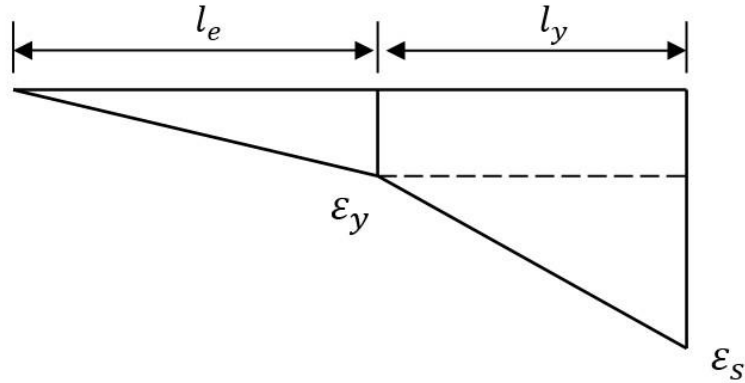


Figure 5-9 Strain Distribution over elastic and inelastic zone

$$slip = \frac{\varepsilon_y l_e}{2} + \frac{l_y}{2}(\varepsilon_y + \varepsilon_s) \tag{5-8}$$

By substituting eqs. (5-1), (5-6) and (5-7) into Eq. (5-8), and simplifying the resulting equation, the bar stress slip relationship will be given by Eq. (5-9):

$$slip = \frac{d_b f_y^{\,2}}{8 E_s \tau_E} + \frac{(f_s - f_y) f_y d_b}{4 \tau_y E_s} + \frac{(f_s - f_y)^2 d_b}{8 \tau_y E_h} \tag{5-9}$$

Based on material properties from experimental tests for SS-1 and SS-2, the bar stress – slip relationships are plotted for different bond stress values as suggested by previous researchers as shown in Figure 5-10.

It should be noted that the experimental data of bond strength indicates that the bond strength decreases significantly once the slip limit is exceeded, and it is suggested that the slip limit is 3mm (0.1 in) Eligehausen el al (1982). Figure 5-10 shows bar stress-slip for different bond strengths as listed in Table (5-3).

Table 5-3 Empirical Values for bond strength for $f_c = 28.5$ MPa

| Researcher | Average Bond Strength (MPa) | | | |
| --- | --- | --- | --- | --- |
| | Tension | | Compression | |
| | Elastic $\tau_E$ | Inelastic $\tau_y$ | Elastic $\tau_E$ | Inelastic $\tau_y$ |
| Sezen and Setzler (2008) | 5.34 | 2.67 | | |
| Lowes and Altoontash (2003) | 9.61 | 2.14 | 11.75 | 19.22 |
| Sozen and Moehle (1990) | 4.43 | 2.67 | | |
| Eligehausen el al (1982) | 10.68 | 2.67 | 16.55 | 16.55 |
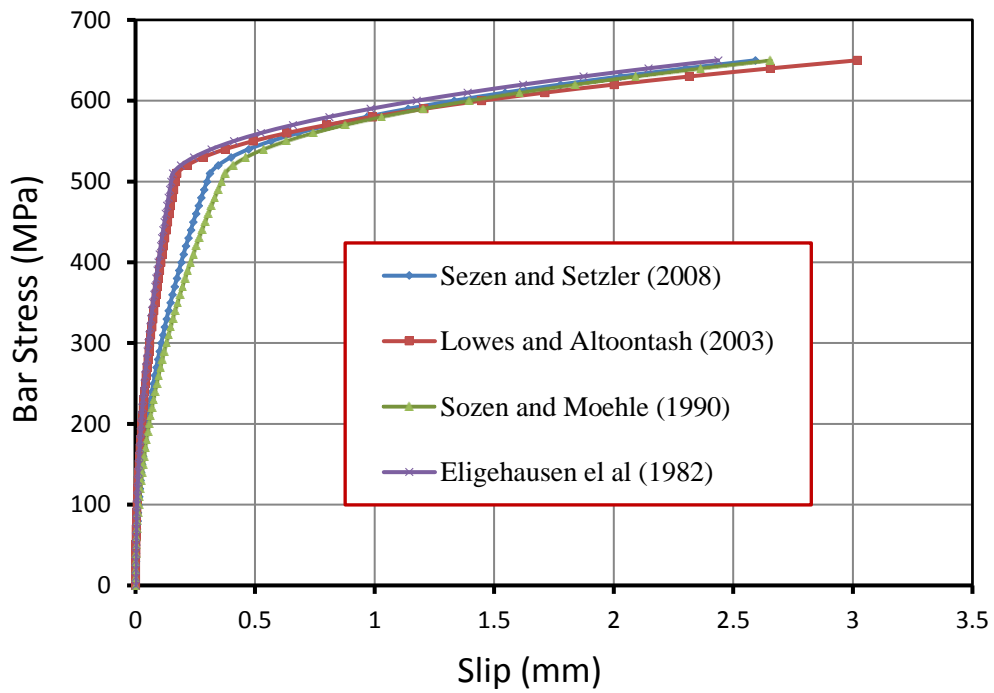


Figure 5-10: Bar stress – slip envelopes for different bond strengths

## 5.2.3.2 INTERIOR JOINTS

Interior joints are usually provided with continuous steel reinforcement, which is recommended by many guidelines and codes of practice. Under column removal and high deflection at the catenary stage, the embedment length of steel bars within the joint may become insufficient, and the stress at the centre of the joint is not always zero, while the slip at that point will be zero due to symmetry as shown in Figure 5-11.

Therefore, the assumption of zero slip at the point of zero stress will not be valid at interior joints subjected to column removal or progressive collapse. Thus, the effect of insufficient embedment length for bond stress should be taken into account when deriving the bar stress slip relationship along the stress propagation length.

As a result, the sub-assemblage can only fail due to bar fracture at the middle joint, which is similar to the assumption adopted for exterior joint.
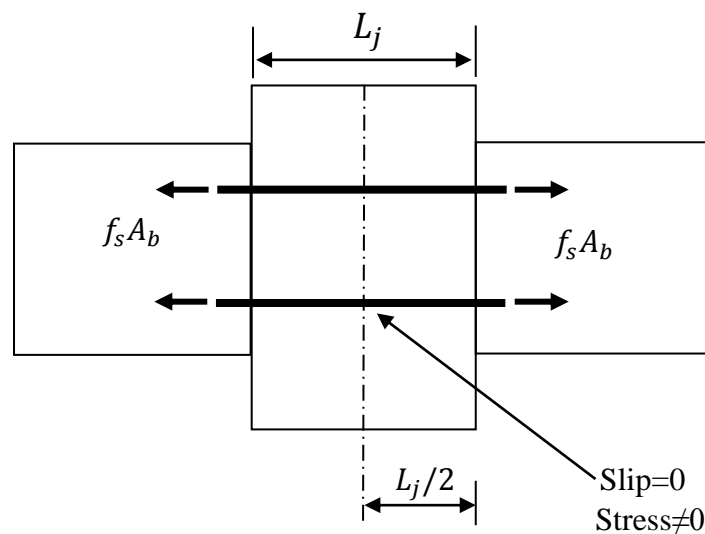


Figure 5-11 Interior Joint with Embedment Length

The distribution of bond and bar stresses with their associated required bar lengths for the interior joint under increasing load can take five possible cases. In order to simplify the classification of the possible cases, another assumption was made in that the load transfer at interior joint interfaces under column removal scenario is symmetric. Therefore, the anchorage length of the steel bars within interior joint will be half of the joint width as shown in Figure 5-11.

**A) Elastic case with zero bar stress at the joint centre**

Figure 5-12 shows the bond and bar stress distribution with their development lengths. At this case, the applied load produces a bar stress less than steel yield strength $f_s \leq f_y$, and there is an adequate anchorage bar length to resist the bar stress.
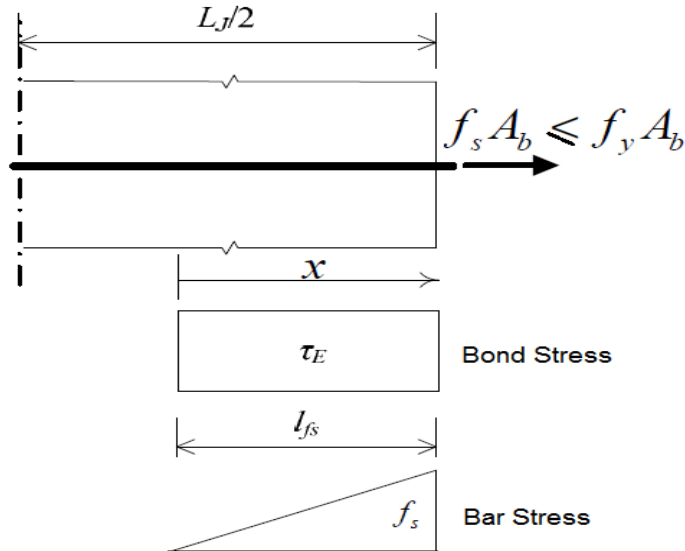


Figure 5-12 Bond and Bar stress distributions and their propagation length. Case A

This case is similar to the elastic case of exterior joints and the propagation length $(l_{fs}) \leq L_j/2$, where:

$$l_{fs} = \frac{f_s \, d_b}{4\tau_E}$$

Which is same as equation (5-3), and the slip can be obtained from equation (5-5)

$$slip = \frac{d_b f_s^{\,2}}{8E_s \tau_E}$$

**B) Elastic case with non-zero bar stress at the joint centre**

As the applied load increases, with insufficient joint width $(L_j/2 < l_{fs})$, the developed stresses at the steel reinforcement penetrate through the joint towards its centre. At that point a bar stress $(f_0)$ will be developed at the joint centre. With high steel yield strength, $(f_s)$ remains less than $(f_y)$ $f_s \leq f_y$. Figure 5-13 shows the bond and bar stresses with their associated anchored bar lengths.
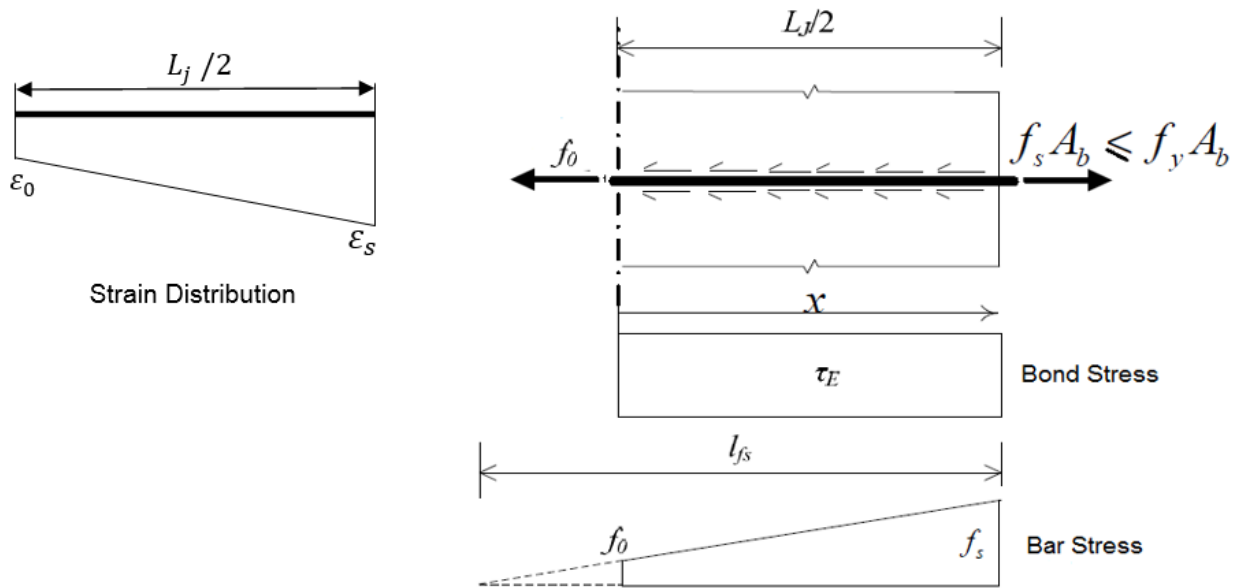
Figure 5-13 Bond and Bar stress distributions and their propagation length. (Case B)

Based on force equilibrium, $f_0$ can be obtained from equation (5-10):

$$f_0 = f_s - \frac{2\,\tau_E L_j}{d_b} \tag{5-10}$$

From the strain distribution diagram, slip can be obtained by calculating the area of the diagram as follows:

$$slip = \frac{L_j}{4}(\varepsilon_0 + \varepsilon_s)$$

$$= \frac{L_j}{4E_s}(f_0 + f_s)$$

$$slip = \frac{f_s L_j}{2E_s} - \frac{\tau_E L_j{}^2}{2E_s d_b} \tag{5-11}$$

## C) Elastic-Inelastic Case with zero bar stress at the joint centre

This case is similar to the elastic-inelastic case for an exterior joint, and it occurs when the applied load develops stresses in the steel bars more than the steel yield strength, $f_s > f_y$, and the required bar length is less than ($L_j/2$). Figure 5-14 shows the bond and bar stress distributions with their associated lengths.
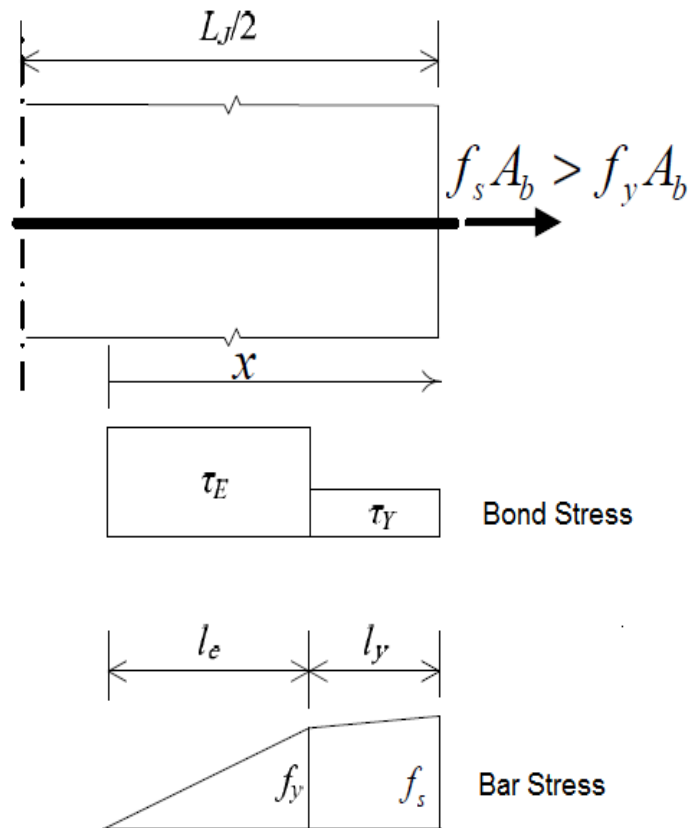
Figure 5-14 Bond and Bar stress distributions and their propagation length. Case C

Slip can be obtained from the same equation (5-9) for an exterior joint:

$$slip = \frac{d_b f_y{}^2}{8E_s \tau_E} + \frac{(f_s - f_y)f_y d_b}{4\tau_y E_s} + \frac{(f_s - f_y)^2 d_b}{8\tau_y E_h}$$

**D) Elastic-Inelastic Case, non-zero bar stress at the joint centre**
When the applied loads are increased until the developed bar stresses penetrate through joint width, a bar stress ($f_0$) at the centre of joint is mobilized. At a certain stage, the required inelastic development length ($l_y$) is less than ($L_j/2$) $l_y < L_j/2$, with the applied stress exceeding the yield steel strength $f_s > f_y$. Hence, the distribution of bond stresses, bar stresses and bar strain will be as shown in Figure 5-15.
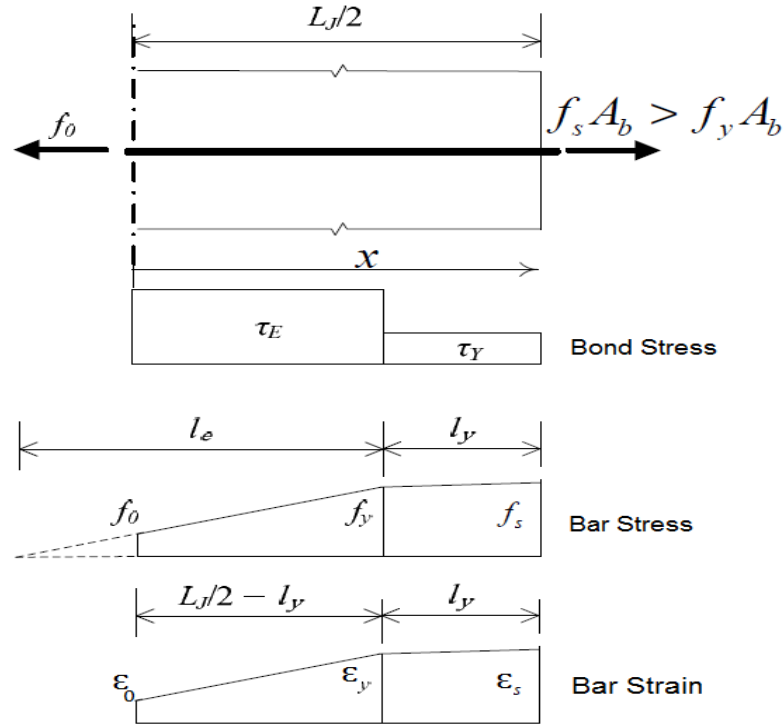
Figure 5-15 Bond and Bar stress distributions and their propagation length. Case D

Based on force equilibrium, $(f_0)$ can be obtained from equation (5-12)

$$f_0 = f_y - \frac{4\,\tau_E}{d_b}\left(\frac{L_j}{2} - l_y\right)$$
(5-12)

From the area of the bar strain diagram, the slip can be obtained as follows:

$$slip = \frac{1}{2}[\,(\varepsilon_0 + \varepsilon_y)\left(\frac{L_j}{2} - l_y\right) + (\varepsilon_y + \varepsilon_s)l_y]$$
(5-13)

By substituting equations (5-1) and (5-12) into equation (5-13), slip can be obtained in terms of $f_s$

$$slip = \frac{f_y L_j}{2E_s} + \frac{f_s - f_y}{2E_h}l_y - \frac{\tau_E}{2b_d E_s}(L_j - 2L_y)^2$$
(5-14)

Where

$$l_y = \frac{(f_s - f_y)d_b}{4\,\tau_y} \qquad equation\ (5-7)$$

**E) Inelastic Case, non-zero bar stress at the joint centre**

When the applied load is increased further until the developed bar stresses penetrate through joint width, a bar stress ($f_0$) at the centre of the joint is mobilized. At a certain stage, the required inelastic development length ($l_y$) will be more than ($L_j/2$), $l_y > L_j/2$, with the applied stress exceeding the yield steel strength and ($f_0$) exceeds ($f_y$), which means that the whole steel embedment within the joint region has yielded $f_s > f_y$. The distribution of bond stresses, bar stresses and bar strain will be as shown in Figure 5-16.
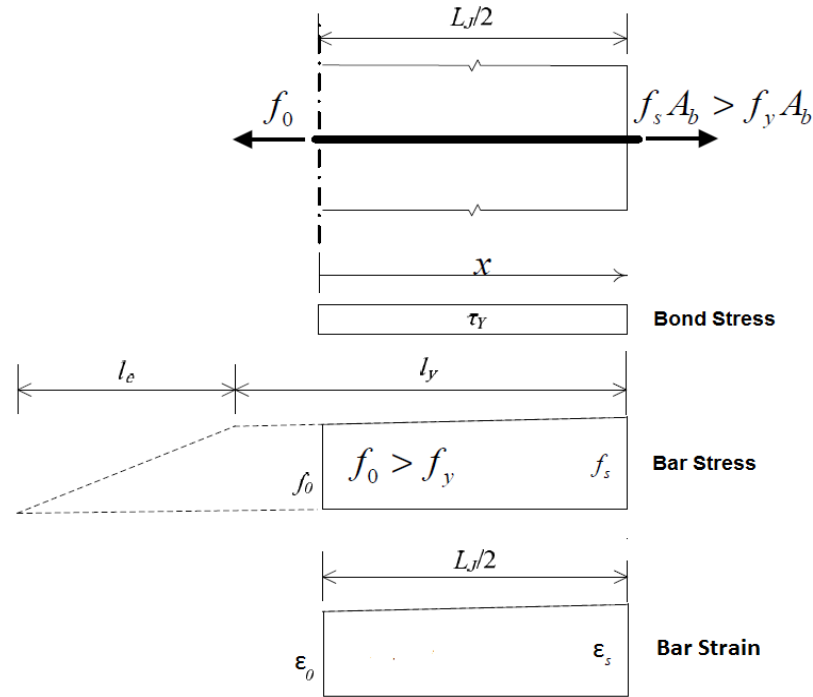


Figure 5-16  Bond and Bar stress distributions and their propagation length. Case E

Based on force equilibrium, ($f_0$) can be obtained from equation (5-15)

$$f_0 = f_s - \frac{2\,\tau_y L_j}{d_b} \qquad (5\text{-}15)$$

From the area of the bar strain diagram, the slip can be obtained as follows:

$$slip = \frac{L_j}{4}(\varepsilon_0 + \varepsilon_s) \qquad (5\text{-}16)$$

*For $f_o$ , $f_s > f_y$*

$$\varepsilon_0 = \frac{f_y}{E_s} + \frac{f_o - f_y}{E_h} \quad , \quad \varepsilon_s = \frac{f_y}{E_s} + \frac{f_s - f_y}{E_h}$$

By substituting the above equations and equation (5-15) into equation (5-16) slip can be obtained in terms of $f_s$ from equation (5-17):

$$slip = \frac{L_j}{2}\left(\frac{f_y}{E_s} + \frac{f_s - f_y}{E_h} - \frac{\tau_y L_j}{d_b E_h}\right) \tag{5-17}$$

It is clear from the above five cases that the slip of the steel bars depends on the steel stress state ($f_s$), material properties of steel and concrete and the steel bar embedment length. However, Yu, Jun. (2013) pointed out that for a specific material and geometric properties, it is not necessary for a steel bar in the joint to pass through each stage in a consecutive way.

Table 5-4 summarises the equations for different bar slip conditions, bar stresses, and boundary conditions in the interior joints under axial tension loading.

## 5.2.4 BAR STRESS-SLIP FOR COMPRESSION ZONE:

It is clear that the concrete contribution to the compression zone can not be neglected, and the compressive force includes both the steel compressive force and the concrete compressive force. Lowes and Altoontash (2003) suggested that the relationship of bar stress-slip for compression should be calibrated according to the section analysis and design regulations.

It should be noted that the spring compressive force depends on the compression zone for the beam section. The location of the neutral axis will affect the compression zone during the loading phase. Therefore, to simplify the analysis for bar stress-slip for the compression zone, Yu, Jun. (2013) suggested the use of a constant neutral axis depth.

Figure 5-17 shows the internal forces in a beam section with the distribution of stress and strain along the section. Based on the assumption above, concrete and steel compression forces can be obtained from the equations below:

$$C_c = 0.85 f'_c \, b\beta \, c \tag{5-18}$$

$$C'_s = f'_s A'_s = 0.003 \frac{c - d'}{c} E_s A'_s \tag{5-19}$$

Where $C_c$ is the compression force carried by concrete, $C'_s$ is the compression force carried by steel reinforcements, $A'_s$ is the area of reinforcing steel carrying compression and $E_s$ is the modulus of elasticity for steel.

For simplicity, the total compression force is assumed to act at the centre of concrete compression zone. Based on this assumption, the total force can be obtained as follows:

$$C = C_c + C_s' = f_s' A_s' \left(1 + \frac{0.85 f_c' b d}{E_s A_s'} \frac{2(1-j)}{0.003\beta \left(1 - \frac{\beta d'}{2d(1-j)}\right)}\right) \qquad (5\text{-}20)$$

Where $jd$, is the lever arm. Typically, in reinforced concrete section design, ($j$) is assumed as a constant value of 0.75 for columns and 0.85 for beams. Lowes and Altoontash (2003).
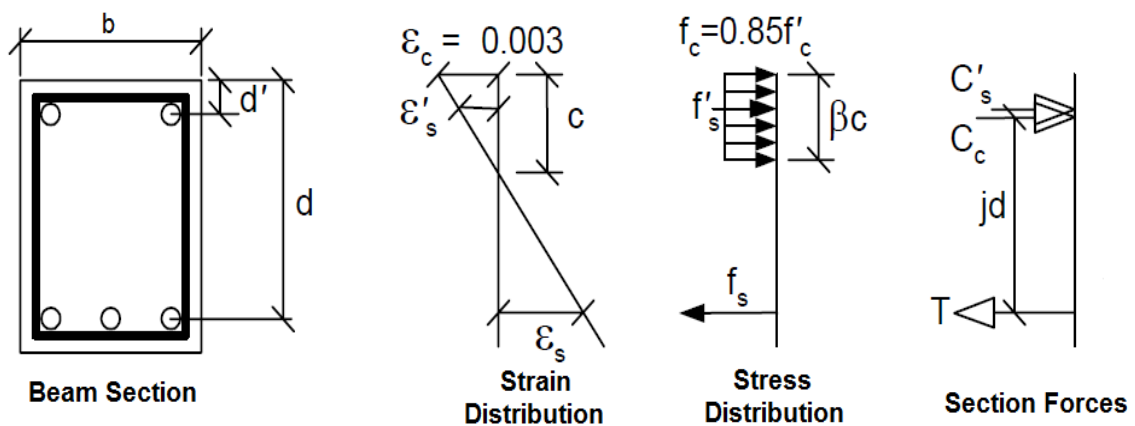


Figure 5-17 Stress, strain and force distribution of beam section

At the catenary action stage, a transition from compressive arch action to a tensile action will occur at the compression zone. Therefore, Yu, Jun. (2013) suggested to move the compressive force resultant C to the centre of steel reinforcement in compression, and he pointed out that this movement will lead to a certain error in calculating the ultimate moment of resistance due to a small change of the lever arm.

Similar to the tensile bar force-slip derivation, the compressive bar force-slip relationship is obtained. It is assumed that the stress-strain relationship for concrete will be perfectly elastic-plastic. However, (Yu, Jun. 2013) pointed out that the concrete in the compression zone is not able to follow the entire stress-strain curve of the steel reinforcement in the compression zone. Typical failure of sub-assemblages is in tension due to the transition of the compression zone into the tension zone when the catenary phase develops under the removal of the middle column.

Table 5-4: Summary of slip in the interior joint for all cases.

| Case No. | Bar Stress $f_s$ | $l_e$ | $l_y$ | $l_{fs}$ | Bar Stress $f_0$ | Slip |
|---|---|---|---|---|---|---|
| (a) | $f_s \leq f_y$ | $\dfrac{f_s\, d_b}{4\tau_E}$ | $0$ | $l_{fs} \leq \dfrac{L_j}{2}$ | $0$ | $\dfrac{d_b f_s^{\,2}}{8 E_s \tau_E}$ |
| (b) | $f_s \leq f_y$ | $\dfrac{L_j}{2}$ | $0$ | $l_{fs} > \dfrac{L_j}{2}$ | $f_s - \dfrac{2\,\tau_E L_j}{d_b}$ | $\dfrac{f_s\, L_j}{2 E_s} - \dfrac{\tau_E L_j^{\,2}}{2 E_s d_b}$ |
| (c) | $f_s > f_y$ | $\dfrac{f_y d_b}{4\tau_E}$ | $\dfrac{(f_s - f_y)d_b}{4\,\tau_y}$ | $l_{fs} \leq \dfrac{L_j}{2}$ | $0$ | $\dfrac{d_b f_y^{\,2}}{8 E_s \tau_E} + \dfrac{(f_s - f_y)f_y d_b}{4\tau_y E_s} + \dfrac{(f_s - f_y)^2 d_b}{8\tau_y E_h}$ |
| (d) | $f_s > f_y$ | $\dfrac{L_j}{2} - l_y$ | $\dfrac{(f_s - f_y)d_b}{4\,\tau_y}$ | $l_{fs} > \dfrac{L_j}{2}$ | $f_y - \dfrac{4\,\tau_E}{d_b}\left(\dfrac{L_j}{2} - l_y\right)$ | $\dfrac{f_y L_j}{2 E_s} + \dfrac{f_s - f_y}{2 E_h} l_y - \dfrac{\tau_E}{2 b_d E_s}(L_j - 2L_y)^2$ |
| (e) | $f_s > f_y$ | $0$ | $\dfrac{L_j}{2}$ | $l_{fs} > \dfrac{L_j}{2}$ | $f_s - \dfrac{2\,\tau_y L_j}{d_b}$ | $\dfrac{L_j}{2}\left(\dfrac{f_y}{E_s} + \dfrac{f_s - f_y}{E_h} - \dfrac{\tau_y L_j}{d_b E_h}\right)$ |

## 5.2.5 FORCE – DEFLECTION RELATIONSHIP FOR SHEAR SPRING

Design regulations for RC frame structures ensure an adequate shear capacity in order to prevent shear failure. In addition, shear failure is not the main mechanism for RC members subjected to column removal and progressive collapse. Therefore, Lowes and Altoontash (2003) suggested that the shear spring can be taken as an elastic linear spring with a large stiffness.

Based on the mechanics of materials, a force – deformation envelope can be derived and used for the shear spring properties. Based on the beam geometry and material properties, the force – deformation equation can be obtained as follows:

$$\tau = G\gamma \tag{5-21}$$

Where

$$\tau = \frac{V}{A} \quad , \quad \gamma = \frac{\delta}{L}, \quad G = \frac{E}{2(1+v)}$$

Substituting in equation (5-21)

$$V = \frac{A_c E_c}{2(1+v)} \frac{\delta}{L} \tag{5-22}$$

Where, $V$ is the shear force acting on the beam section, $A_c$ is the area of the beam section and it is equal to $(b{\times}d)$, $E_c$ is the concrete modulus of elasticity, $\delta$ is shear deformation, $v$ is Poisson's ratio of concrete, and $L$ is the shear span.

Equation (5-22) represents the concrete contribution for RC beams in shear strength neglecting the contribution of steel ties and longitudinal steel reinforcement. As mentioned earlier, the conventional design provides sufficient shear strength for RC members to prevent shear failure. Due to this fact, neglecting the steel contribution for shear strength will not affect the results at this stage of numerical analysis.

## 5.3 IMPLEMENTATION OF THE MACRO-MODEL

In order to study the structural behaviour of RC structures during progressive collapse, numerical simulation is required. In the event of progressive collapse, it is expected that both geometric and material nonlinearity will be necessary. In addition, the formation of plastic hinges will be expected to occur at the critical sections, which are near joint interfaces.

Therefore, the effect of both geometric and material nonlinearities should be taken into account when modelling RC structures.

A finite element model has been developed using the finite element program ANSYS 11.0, and static analysis has been carried out taking into account geometric and material nonlinearity to investigate the structural mechanisms following the removal of the middle column. The ANSYS software package allows a variety of structures or objects to be modelled, using finite element analysis techniques to demonstrate the behaviour of the model under specific loading conditions.

ANSYS is ideal for this project due to the fact that both 2D and 3D structures can be modelled and results such as deflection, bending moment and shear force can be obtained quickly via static analysis.

## 5.3.1 MODEL CONFIGURATION AND ELEMENT TYPES

The finite element modelling includes the modelling of the conventional specimens designed for static tests in the experimental program. The same dimensions, steel reinforcement and mechanical properties of both the concrete and steel from the experimental work will be used. Figure 5-18 shows the model layout with element types.

Beams and columns were modelled using the 2D beam element (BEAM3), which is available in ANSYS 11.0 element library. This element is a line element with two nodes at the ends with tension, compression and bending capabilities, and it acts only in the x-y plane of its 2D plane. This element also requires the cross-sectional area $A$ and the second moment of area $I$ to be defined. In addition, material properties including elastic modulus, Poison's ratio and mass density were defined.

In order to account for material non-linearity, a second element was used. The non-linear element (COMBIN39), which is available in ANSYS 11.0 element library, was used at critical sections to simulate sections that will undergo nonlinearity. (COMBIN39) is essentially a nonlinear spring and damper element, which only requires a force deflection relationship to be defined.
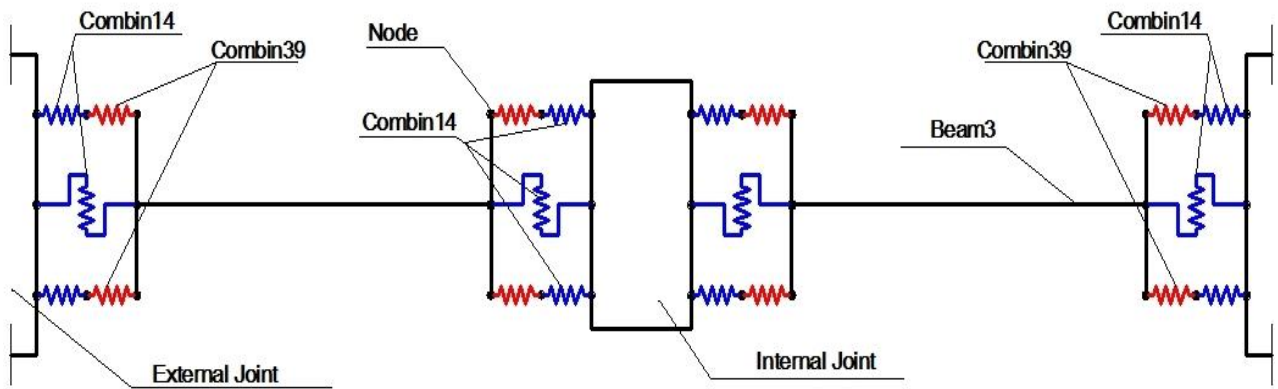
(a)
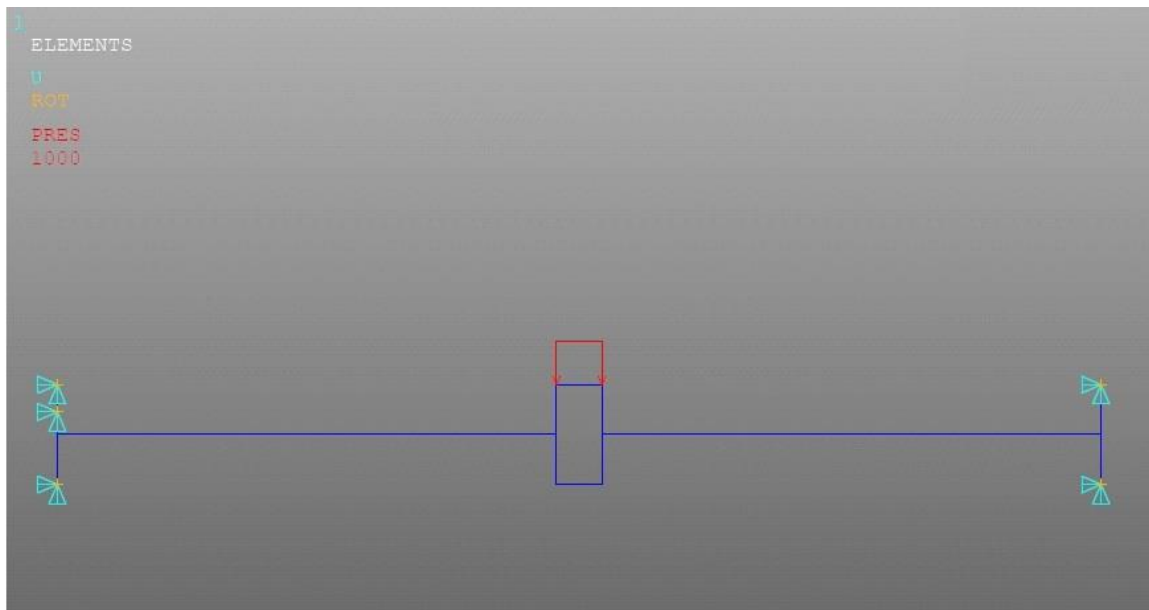


(b)

Figure 5-18 a) Schematic of Macro-model configuration b) ANSYS Macro-model

To capture bar fracture, a linear element (COMBIN14) was used. The element is defined by two nodes, a spring constant (k) and damping coefficients $(c_v)_1$ and $(c_v)_2$. The damping capability is not used for static or un-damped modal analysis. The longitudinal spring constant (k) should have units of Force / Length, the damping coefficient units are Force x Time/Length. Due to the elements capability of Birth and Death (a feature included in ANSYS), this element was used to capture bar fracture.

In addition, (COMBIN14) was used as a shear spring to simulate shear capacity of RC beam section. It should be noted that the elements (COMBIN39) and (COMBIN14) are zero length spring elements with no mass, and all nodes attached to these elements were at the same location as shown in Figure 5-18(b).

## 5.3.2 SPRING ELEMENTS PROPERTIES

The ANSYS software requires that each nonlinear spring should have a force-deformation which is input into the element properties, with no limit on the number of the data points. To simplify the analysis and reduce the time/cost, the nonlinear force-deformation relationship of the springs ($S_{top}$ and $S_{bot}$) were simplified into a tri-linear relationship. Figure 5-19 shows the critical points of the simplified force-deformation relationship.
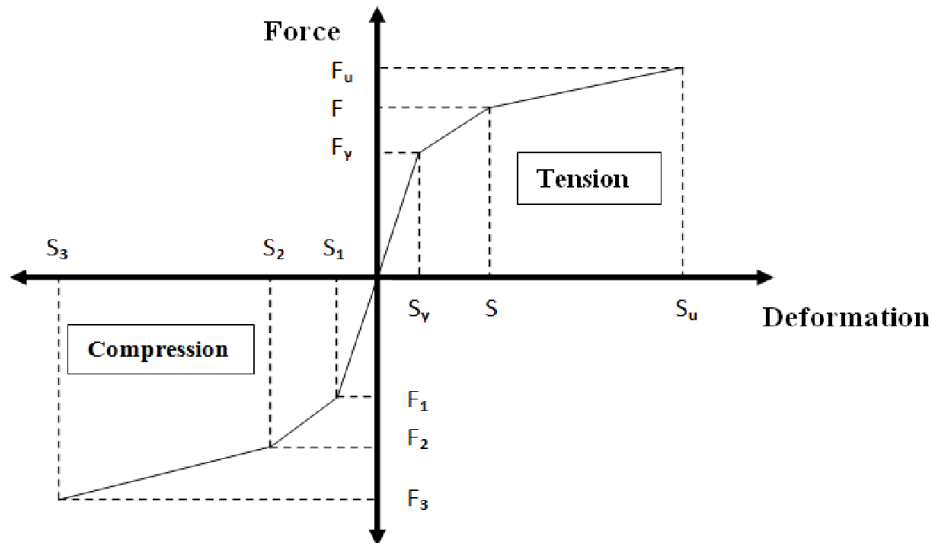


Figure 5-19 Bar force- deformation properties for the springs ($S_{top}$ and $S_{bot}$)

The values of critical points shown in Figure 5-19 depend on many factors such as the material properties of the steel reinforcement and concrete, and detailing of the steel bars and section properties. $F_y$ and $S_y$ represent steel bar yielding in the tension zone and corresponding slip of the steel bar. $F_u$ and $S_u$ represent the bar fracture and its corresponding bar slip. $F$ is chosen to be the average value between $F_y$ and $F_u$, and $S$ is the bar slip corresponding to the average value.

In the compression zone, $F_1, F_2$ and $F_3$ represent compression force at the point of concrete crushing, yielding of steel bars in compression and ultimate spring capacity with their corresponding values of bar slips $S_1, S_2$ and $S_3$ respectively.

It should be noted that under middle column removal, the bottom reinforcement of the middle joint interfaces undergo tension only, while the top reinforcement undergoes compression at flexural and compressive arch action then changes to tension when catenary action is mobilised.

At the ends of the beam, the top reinforcement undergoes tension for both compressive arch action and catenary action, while the bottom reinforcement undergoes compression at flexural and compressive arch action then changes to tension when catenary action is mobilised. Therefore, the springs ($S_{bot}$) at the middle joint interfaces and ($S_{top}$) at the end beam joint interfaces undergo tension only, hence only the tensile envelope of the bar stress-slip of these springs is required.

Based on bond strengths suggested by Sezen and Setzler (2008) for tension, and values suggested by Lowes and Altoontash (2003) for compression, the spring properties of ($S_{top}$) and ($S_{bot}$) for specimens (SS-1 and SS-2) were obtained and listed in the Table 5-4. The reason for choosing the bond strength proposed by (Sezen and Setzler 2008), was because these values were the latest available estimation for bond capacity. Also it provides smaller capacity in order to provide a conservative value when calculating the RC sub-assemblages progressive collapse capacity.

Properties for linear springs (COMBIN14), which were used to simulate the failure at critical sections, can be obtained by taking the largest value in the compression zone for interior or exterior joints. In addition, these springs will simulate the stiffness gap between the specimen and the axial restraint attached to the frame used for the test. From Table 5-4, the maximum stiffness value (k) for (COMBIN14) is ($6.1 \times 10^6\ N/mm$).

Based on equation 5-22, the shear spring (COMBIN14) properties can be obtained. Figure 5-20 shows the relationship between shear force and deformation for specimen SS-1 and SS-2. From Figure 5-20, (k) is obtained which is equal to ($1.33 \times 10^5\ N/mm$).

Table 5-5 Spring Properties for SS-1 and SS-2

| Middle Joint Interface | | | | | | | | |
| --- | --- | --- | --- | --- | --- | --- | --- | --- |
| $S_{bot}$ | | | $S_{top}$ | | | | | |
| | Tensile Branch | | Tensile Branch | | | Compressive Branch | | |
| | $F$ (kN) | $S$ (mm) | $F$ (kN) | $S$ (mm) | | | $F$ (kN) | $S$ (mm) |
| $F_y$ , $S_y$ | 80.14 | 0.24 | 120.21 | 0.24 | $F_1$ , $S_1$ | | 365.2 | 0.06 |
| $F$ , $S$ | 91.14 | 2.39 | 136.71 | 2.39 | $F_2$ , $S_2$ | | 527.6 | 0.14 |
| $F_u$ , $S_u$ | 102.14 | 8.65 | 153.21 | 8.65 | $F_3$ , $S_3$ | | 672.5 | 0.23 |
| End Joint Interfaces | | | | | | | | |
| $S_{top}$ | | | $S_{bot}$ | | | | | |
| | Tensile Branch | | Tensile Branch | | | Compressive Branch | | |
| | $F$ (kN) | $S$ (mm) | $F$ (kN) | $S$ (mm) | | | $F$ (kN) | $S$ (mm) |
| $F_y$ , $S_y$ | 120.21 | 0.31 | 80.14 | 0.31 | $F_1$ , $S_1$ | | 337.6 | 0.06 |
| $F$ , $S$ | 136.71 | 2.57 | 91.14 | 2.57 | $F_2$ , $S_2$ | | 487.7 | 0.14 |
| $F_u$ , $S_u$ | 153.21 | 9.00 | 102.14 | 9.00 | $F_3$ , $S_3$ | | 621.6 | 0.23 |
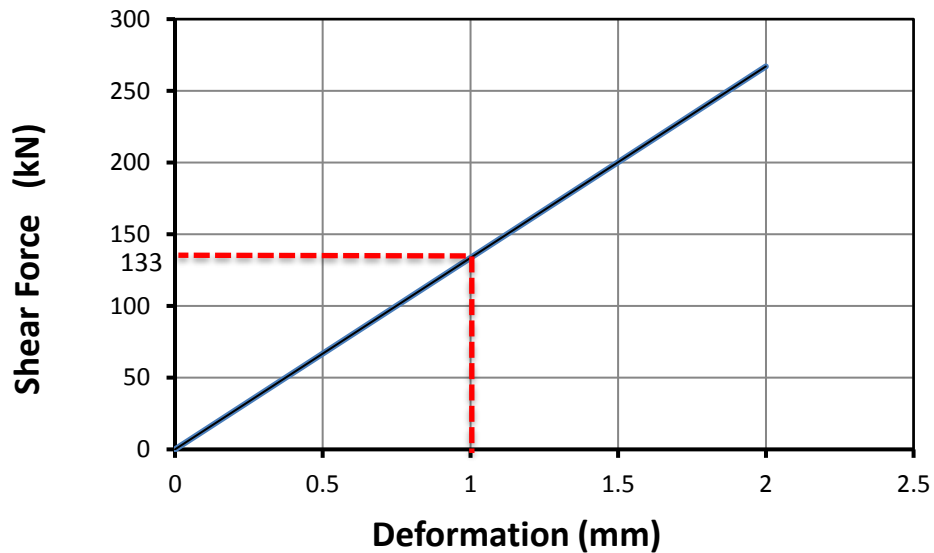


Figure 5-20 Shear Force-Deformation relationship for SS-1 and SS-2

## 5.4 NUMERICAL RESULTS

ANSYS version 11.0 was used to analyse and simulate the structural behaviour of specimen SS-1, SS-2 and SS-3 using the macro-model approach by representing critical sections with spring elements as shown in Figure 5-18(a).

The load was applied at the middle joint by a static controlled displacement with a constant incremental value of (1mm/step) until total failure of the specimens as shown in Figure 5-21. Material nonlinearity was already included in the spring properties, while geometry nonlinearity was activated by using large displacement option, which is one of the features available in ANSYS 11.0. The main reason for choosing controlled displacement to simulate the applied load is to capture the softening in the structural behaviour of the sub-assemblages.
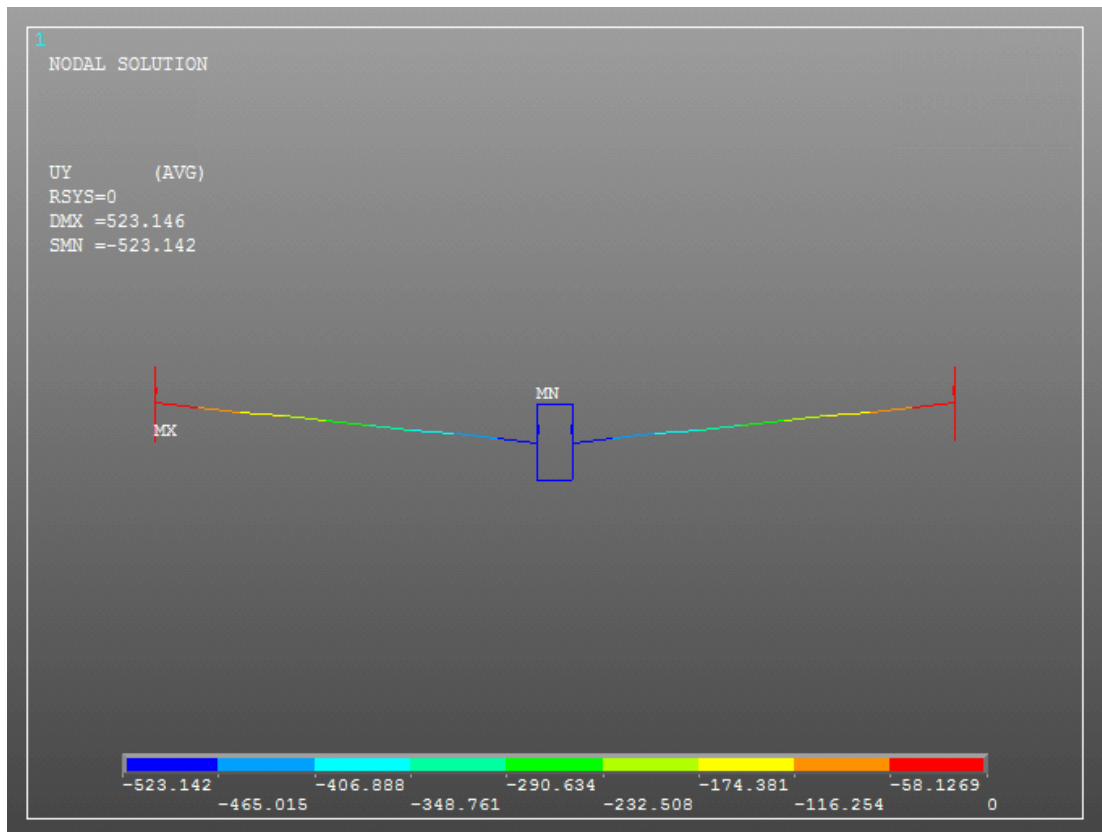


Figure 5-21 ANSYS Macro-Model before the Failure

The macro-model approach outlined in section 5-2 was validated by comparing the structural behaviour observed from the numerical analysis with that from the experimental tests. The aim was to find out the capability of the proposed model to capture the structural behaviour of RC structures under middle CRS and prediction of the structural resistance capacities at both compressive arch action and catenary action and their corresponding deformations.

All reactions and axial forces were recorded and plotted against vertical displacement of the middle joint. Figures 5-22 and 5-23 show the comparison between experimental and numerical results for specimen SS-1, SS-2 and SS-3.

Figure 5-22 represents the structural behaviour of RC sub-assemblages in terms of applied load and axial forces vs. MJD for SS-1 and SS-2, which showed a good agreement between numerical and experimental results in terms of applied load and their corresponding deflections at both compressive arch and catenary action.

It can be seen that the numerical results underestimate structural resistance at the flexural phase. The reason for this difference is that the slip of the steel bars in the elastic phase was overestimated when calculating the spring properties, while in the actual tests no slip occurred during the flexural phase. In addition, the friction between the restraints and the specimens could cause an increase in the experimental test results.

Unlike the experimental tests, the fracture of the steel reinforcing bars within the same layer either at the middle joint or at the beam ends occurred at the same time in numerical analysis, which was not the case in the experimental tests. This was due to the imperfection during the construction of specimens and non-homogeneous nature of the material used such as concrete in experimental tests, while ANSYS considers perfect construction and uniform material properties.

However, the macro-model approach including the bar stress-slip relationship can predict the overall structural behaviour of RC sub-assemblages during the compressive and catenary phases.
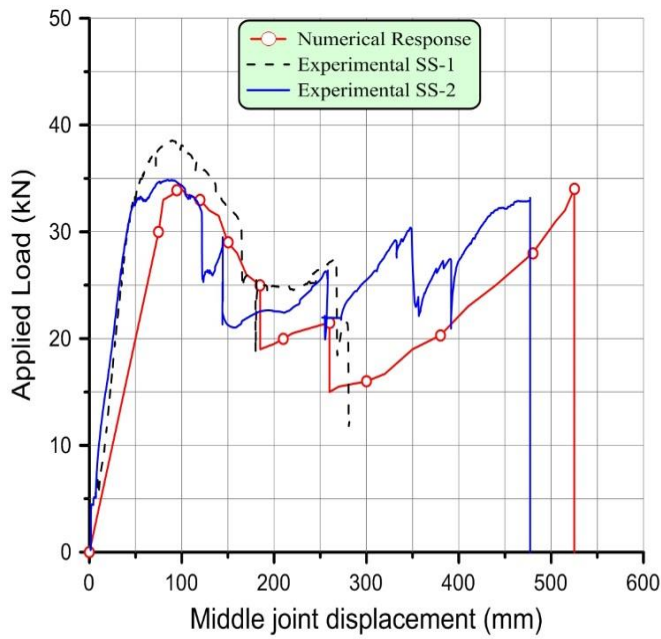
(a)Applied load vs. MJD
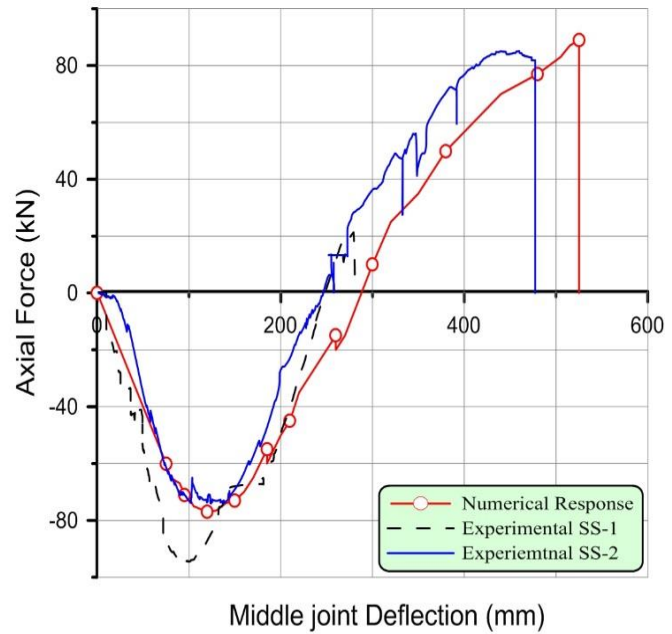
(b) Axial load vs. MJD

Figure 5-22 Structural Behaviour of specimen SS-1, SS-2
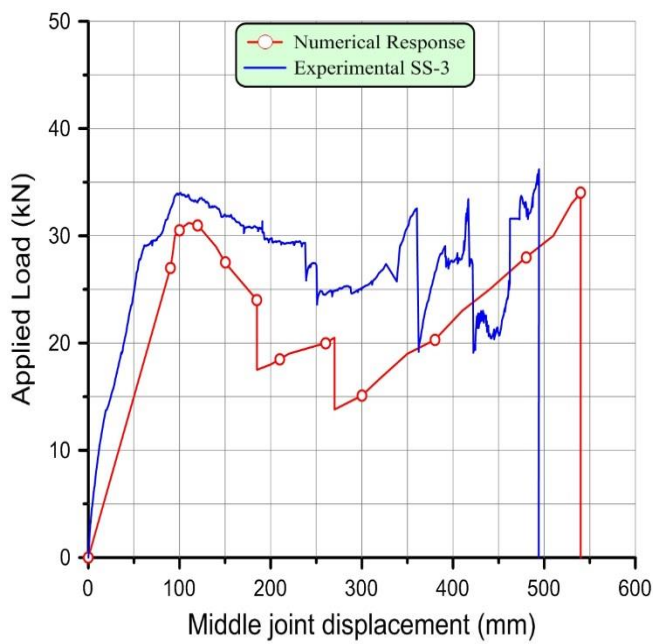


(a) Applied load vs. MJD
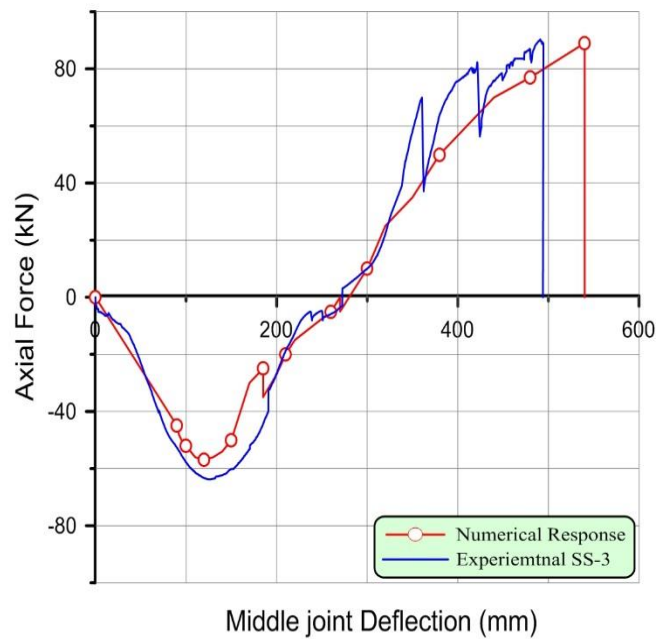
(b) Axial load vs. MJD

Figure 5-23 Structural Behaviour of specimen SS-3

## 5.5 SUMMARY

In this chapter, a numerical study was carried out to investigate the structural behaviour of RC beams under CRS. A macro-model was used to simulate the specimens and the ANSYS software was used to implement the analysis.

Bond-slip is the main feature that was included in this approach. The main conclusion of this study is that the macro-models consisting of beam and spring elements can accurately predict the response characteristics of RC beam-column sub-assemblages.

Numerical results underestimate the progressive collapse capacity compared with the experimental results. This can be explained by many factors such as the presence of friction due to restraints and the imperfection of the construction of the specimens, which is a consequence of the real nature of the material in reality.

## 6. CHAPTER SIX      ANALYTICAL APPROACH

## 6.1 GENERAL

Few experimental studies have been conducted to investigate the structural response of RC structures subjected to progressive collapse, which has been reviewed in chapter two. Due to the high cost of carrying out experimental studies on RC structures under CRS, many researchers have conducted numerical studies using available finite element software packages.

It should be mentioned that finite element models also usually require a considerable amount of time and experience to construct and debug in addition to solution time. But in contrast, practising engineers prefer theoretical approaches and models to predict the structural responses of RC structures under CRS.

This chapter is devoted to developing an analytical model to predict the structural response of RC structures at both CAA and CTA stages. A series of equations will be developed in order to predict the load-deflection relation of the RC beams under CRS. The equations will be based on the fundamental concepts of equilibrium, compatibility, and material properties.

This chapter comprises of four sections. In the first section, previous analytical studies will be reviewed. In the second section, the detailed development of the model will be presented. In the third section, the model will be validated against the available experimental data. In the last section, a parametric study will be conducted to investigate the effect of various parameters on the progressive collapse capacity of RC structures.

## 6.2 PREVIOUS STUDIES

Based on the experimental test results, it has been found that the beams experienced two stages after flexural action, namely CAA and CTA stages. Research studies have shown that CAA and CTA can significantly increase the load-carrying capacity of restrained RC beams under CRS. However, the development of these actions in RC beams has not been fully explored and understood. Therefore, further analytical investigations should be carried out to thoroughly explore the development of CAA and CTA.

A vast number of theoretical approaches related CAA and CTA were developed for slab using compressive and tensile membrane action (CMA and TMA). Although the concern of the current study is for RC beams, slab related theoretical models can be applied to RC beams with some

modifications. In this section, analytical models to predict the structural behaviour of RC beams and slabs under membrane action effect will be presented and reviewed.

In 1943, (Johansen, 1943) developed the yield line theory to evaluate the capacity of two-way RC slabs. The theory is based on the assumption that the failure mechanism occurs when the plastic hinges form in lines across the slab as shown in Figure 6-1. The theory takes no consideration of membrane forces when calculating bending moments. Hence, it may underestimate the ultimate capacity of slabs with adequate lateral restraint supports. After 1950, there were many attempts to incorporate membrane action in the evaluation of the structural capacity of RC slabs.

The earliest verification of the effect of CMA on the structural capacity of slabs was made by (Ockleston, 1958). Ockleston found that the experimental capacity of restrained slabs is three times more than the capacity predicted by yield line theory. Several analytical and experimental studies have been conducted to investigate the effect of membrane action on the capacity of RC beams and slabs. ((Christiansen, 1963); (Park and Gamble, 1980); (Eyre, 1990); (Rankin and Long, 1997); (Taylor et al., 2001)).
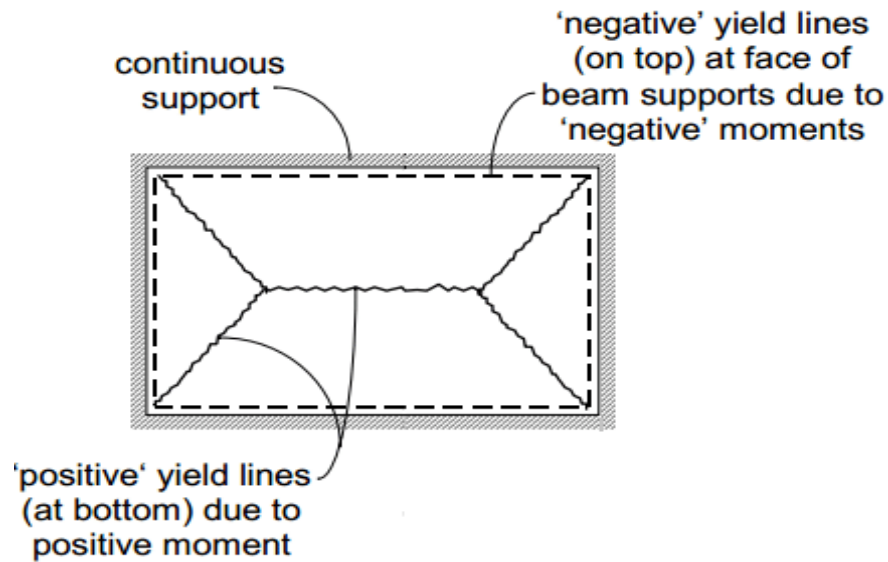


Figure 6-1: The mode of failure in plastic analysis of two-way slabs (Johansen, 1943).

Christiansen 1963 suggested a formula to determine the depth of concrete in compression available for arching. He assumed a uniform stress in the compression zone of the cross-section and elastic-plastic assumptions were made for a concrete beam that has fully developed plastic hinges at the supports and at mid-span (Figure 6-2). Based on the lateral elongation compatibility, the depth of concrete in compression available for arching is calculated as follows:

$$\alpha_1 = h - \Delta - \frac{T_1 + T_2 + 2C_c}{f_c} \tag{6 - 1}$$
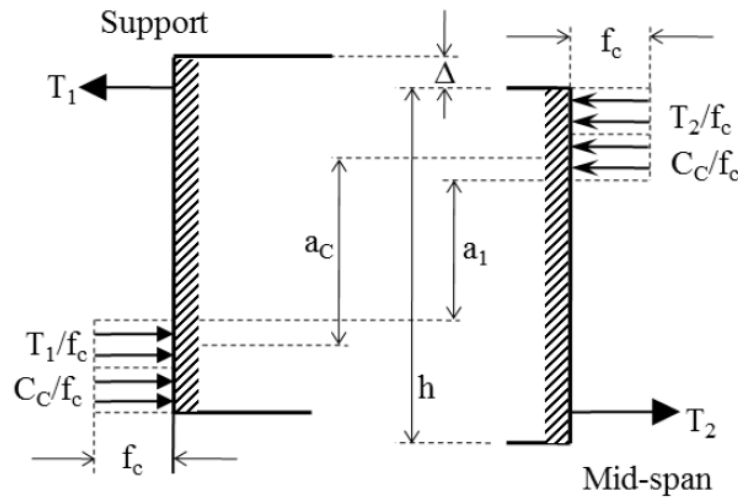


Figure 6-2: internal forces at support and at mid-span, Christiansen (1963)

The distribution of compressive stress in the concrete at the hinges is assumed to be uniform with a constant average stress, $f_c$. The depth of the compression becomes $(T_1 + C_c)/f_c$ at the supporting region and $(T_2 + C_c)/f_c$ at the mid-span region, where $T_1$ and $T_2$ are equal to the force per unit width in the reinforcements and $C_c$ is the additional compressive force due to arching, and $a_1$ is the arching depth.

(McDowell et al., 1956) developed an arching theory of masonry walls based on the observation from testing a masonry brick beam. The researchers assumed that the beam was constrained between two rigid supports and the contact areas at the ends and mid-span are equal and decrease with increased deflection and cracking. They derived an equation to obtain the load-deflection curve for masonry brick beam. Due to some similarities in the material properties of masonry and concrete, Rankin and Long (1997) modified this theory to predict the arching resistance and load capacity of restrained RC slabs.

The method was extended to predict the ultimate load capacity in RC slab strips by employing an elastic-plastic constitutive law as well as a polynomial expression for the plastic strain in concrete. Also, for the prediction of ultimate load, it can be assumed that the maximum arching moment develops after yielding of the reinforcement and the bending deformations necessary to cause yield can be neglected (Rankin and Long, 1997).

Taylor et al. (2001) modified Rankin's model to predict the maximum capacity of slabs with high concrete compressive strength. Based on the stress-strain model proposed by the Concrete Society (1998) for high strength concrete, Taylor et al. developed an equation to calculate the ultimate and plastic strains for concrete:

$$\varepsilon_{cu} = 0.0042 - [(f_{cu} - 60)x2.5 \; x \; 10^{-5}] \tag{6 - 2}$$

$$\varepsilon_{co} = 2\varepsilon_{cu}(1 - \beta) \tag{6 - 3}$$

$$\beta = 1 - 0.003f_{cu} \tag{6 - 4}$$

Where:

$\varepsilon_{cu}$, is the ultimate concrete strain.

$\varepsilon_{co}$, is the plastic concrete strain.

$f_{cu}$, is the cube concrete compressive strength.

(Park, 1964a) developed an approach to include the effect of the arching action in load carrying capacity calculations which are based on rigid-perfectly plastic analysis. Later Park and Gamble (1980) extended this approach into a set of equations that were more easily manipulated and applied. Park and Gamble considered a slab strip partially restrained against horizontal movement with a stiffness *S*, and fully restrained against rotation and vertical deflection at the ends.

They assumed that after applying the load and after formation of plastic hinges, the deflected shape of the strip will be as shown in Figure 6-3. At each plastic hinge shown in Figure 6-3 it is assumed that the tension steel has yielded and compressed concrete has reached its strength. Also, the tensile strength of concrete is neglected and no strain hardening of the steel occurs. It is also assumed that the slab strip has a uniform cross section with a constant area of top and bottom steel reinforcements along the entire length.
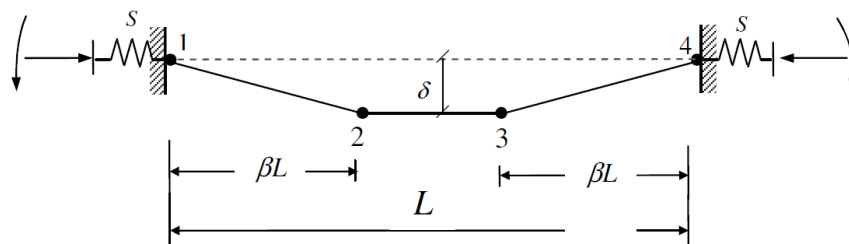


Figure 6-3: Collapse mechanism of a slab with ends restrained, Park and Gamble (2000)

In order to take into account, the effect of elasticity, creep and shrinkage, the component of strain, $\varepsilon$ was assumed to be constant across the entire length as the axial force was constant. The shortening of the strip between the two yield points 2 and 3 in Figure 6-3, will be equal to $\varepsilon(1 - 2\beta)L$, and each end of the central section will move by $0.5\varepsilon(1 - 2\beta)L$ towards the mid-span. The horizontal movement of the supports at the ends will be assumed as $t$. Figure 6-4 shows the changes in length of the left part of the strip.
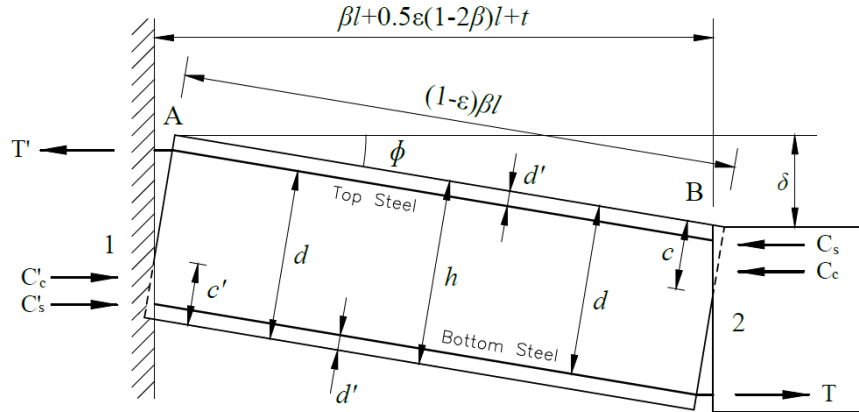


Figure 6-4: Internal forces of end portion of a strip, Park and Gamble (2000)

Since $\theta$ and $\varepsilon$ are small, it can therefore be assumed that:

$$\sin(\theta) = \theta = \frac{\delta}{\beta L} \qquad \text{And} \quad \cos(\theta) = 1 \ , \tan(\theta) = \sin(\theta)$$

From geometry, they derive the following equation:

$$c' + c = h - \frac{\delta}{2} - \frac{\beta L^2}{2\delta}\left(\varepsilon + \frac{2t}{L}\right) \qquad\qquad (6 - 5)$$

Where:

$c'$, is the compression depth zone at section 1

$c$ , is the compression depth zone at section 2

From equilibrium of internal forces:

$$C_c' + C_s' - T' = C_c + C_s - T \qquad\qquad (6 - 6)$$

Where:

$C_c'$ , $C_c$, are the concrete compressive forces at sections 1 and 2, respectively.

$C_s'$ , $C_s$, are the steel compressive forces at section 1 and 2, respectively.

$T', T$, are the steel tensile forces at section 1 and 2, respectively.

Park and Gamble adopted the ACI 318-77 concrete compressive stress block. Therefore, the forces $C'_c$ and $C_c$ are calculated as follows:

$$C'_c = 0.85 f'_c \beta_1 c' b \qquad\qquad (6 - 7)$$

$$C_c = 0.85 f'_c \beta_1 c b \qquad\qquad (6 - 8)$$

Where:

$f'_c$, is the compressive strength of concrete.

$\beta_1$, is the ratio of compression depth to the neutral axis depth.

*b,* is the width of the strip.

By substituting equations 6-7 and 6-8 into equation 6-6, the equilibrium equation will be:

$$c' - c = \frac{T' - T - C'_s + C_s}{0.85 f'_c \beta_1 b} \qquad\qquad (6 - 9)$$

By solving equations 6-5 and 6-9 simultaneously gives:

$$c' = \frac{h}{2} - \frac{\delta}{4} - \frac{\beta L^2}{4\delta}\left(\varepsilon + \frac{2t}{L}\right) + \frac{T' - T - C'_s + C_s}{1.7 f'_c \beta_1 b} \qquad\qquad (6 - 10)$$

$$c = \frac{h}{2} - \frac{\delta}{4} - \frac{\beta L^2}{4\delta}\left(\varepsilon + \frac{2t}{L}\right) - \frac{T' - T - C'_s + C_s}{1.7 f'_c \beta_1 b} \qquad\qquad (6 - 11)$$

They pointed out that the use of geometry of deformation and the equilibrium requirements have enabled the neutral axis depths at the critical sections to be determined. They concluded that these equations apply only when the deflection of the slab is significant. If the deflection is very small ($\delta \rightarrow 0$), and if $\varepsilon > 0$ and $t > 0$, the neutral axis depths tend to ($\infty$) because of the third term on the right hand side of those equations.

There are many drawbacks in Park and Gamble's model, such as it does not consider the actual state of stress of compressive steel reinforcement. Also, there is no consideration for bar fracture and reduction of slab thickness due to concrete crushing at the extreme fibre. Later, Park's model was modified by (Merola, 2009).

(Regan, 1975) derived an equation to evaluate the catenary behaviour of reinforced concrete element under CRS. The static equilibrium equation for the beam shown in Figure 6-5 is:

$$Ha = \frac{qL^2}{2} \qquad\qquad (6 - 12)$$

From geometry, the axial extension of the element is:

$$\frac{\Delta L}{L} = \frac{1}{2}(\frac{a}{L})^2 \qquad\qquad (6 - 13)$$

Where
$\Delta L$, is the axial extension of the beam.
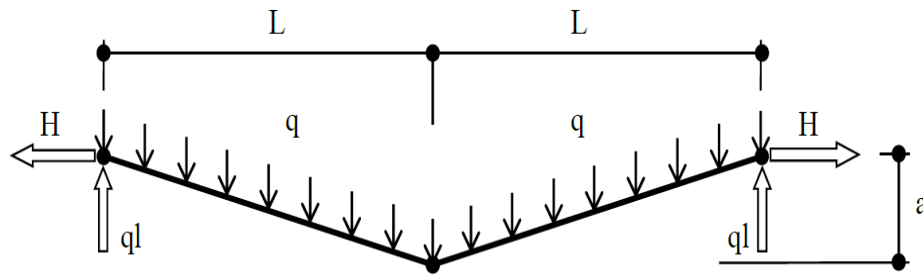


Figure 6-5: Free body diagram of Regan's Model (Regan, 1975)

Regan concluded that the reinforcement detailing has a great effect on the axial tension force (H) and axial extension of the beam ($\Delta L$), therefore, he defined the slip of reinforcement at the joint $(N_{slip})$ as varying between 0 and maximum extension at the joint $(\Delta L)_u$, this gives an estimated load, axial force, deflection relationship of:

$$a = \frac{qL^2}{2N_{slip}} \qquad For \quad 0 < a < L\sqrt{2\frac{\Delta L_u}{L}} \qquad (6 - 14)$$

It was difficult to predict the ultimate load due to difficulty in predicting the ultimate extension of the joint$(\Delta L)_u$.

(Izzuddin and Elghazouli, 2004) proposed an analytical equation for axially restrained and lightly reinforced concrete members to capture catenary action response under elevated temperature. The model accounts for compressive arch phase, bond-slip, yielding, and rupture of steel reinforcement.

They concluded that the compressive arch phase was followed by catenary phase at a deflection equal to the depth of the beam. They also pointed out that the extent of the catenary effect is dependent on the stiffness of axial support and the beam depth. However, this model cannot be applied to reinforced concrete members with moderate or high reinforcement ratios.

Merola (2009) conducted research to investigate the validity of the tying rules required by the UK and European RC design codes which intend to prevent or reduce the likelihood of progressive collapse. He designed a series of RC framed structures and examined their structural behaviour under CRS. The research included developing an analytical model to predict the structural behaviour at both compressive arch action and catenary action. Based on Park's model which is developed for membrane action in slabs, Merola pointed out that Park's model can be used for beams and he modified the model by adopting the EC2 (2004) stress block instead of ACI-318 (1977) which was adopted by Park and Gamble (1980). The model takes into account the steel fracture criterion at both compressive and catenary actions.

The model was then validated by comparing the results against test data despite there being limited reliable experimental test results available. From a parametric study, he conducted, the study confirmed other researcher's conclusions that the span-depth ratio, axial restraint stiffness and concrete compressive strength are the main key factors that affect the RC compressive membrane action under CRS. In addition, steel reinforcement area and steel properties are the main key factors that affect RC behaviour at catenary action.

Although Merola's model is capable of predicting the load and deflection at the point of reinforcement fracture, it was only used to predict the peak load, because, in the tests under consideration, reinforcement fracture did not occur prior to the attainment of the peak load. The model considers that the compression steel has reached its yield strength, which is not accurate and will lead to an error in predicting CAA capacity. Also, there is no consideration for the reduction of the beam depth due to concrete crushing at the extreme fibre.

An analysis model was created by Orton (2007) to understand the mechanisms governing catenary action. A system of equations was developed to characterise the load and deflection relationship of a reinforced concrete beam in catenary action. The equations were based on the fundamental concepts of equilibrium, compatibility, and material characteristics. With the knowledge of the load-deflection relationship of a catenary and the axial tension expected, the effect of the catenary action on the rest of the structure can be determined. The analysis model was based on the results of the continuity tests.

These results were broken into two cases. Case 1 was based on test results of specimen retrofitted with CFRP in negative moment region, while case 2 based on test results of the specimen with no retrofit. Both cases involved solving equations for equilibrium and compatibility.

(Jian and Zheng, 2014) developed a simplified model to assess progressive collapse of RC structures under CRS. The proposed static model comprised of three stages, beam action stage, transient stage and catenary action stage. The model takes into account the effect of the span-depth ratio, beam section dimensions and longitudinal steel reinforcement ratio on progressive collapse capacity. Progressive collapse-resisting capacity curves of substructures are established based on the energy conservation principle, which creates a foundation for progressive collapse assessment of RC frame structures. The proposed model was validated by available experimental results.

The shortcomings of this model did not consider the effect of sudden drops in the response curves resulting from bar fractures. Also, not considering beam elongation especially in large middle joint displacement a parameter which cannot be ignored.

(Mitchell and Cook, 1984) investigated the response of slab structures after initial failures due to punching shear and flexure. They presented analytical models for predicting post-failure response of slabs and the predictions were compared with existing experimental results. These models along with the experimental investigation enabled the development of simple design and detailing guidelines for bottom steel reinforcement which are capable of hanging the slab from the columns after failure. They concluded that the bottom bars which are well anchored and effectively continuous provide not only a means of preventing progressive collapse but also provide a means of preventing initiation of punching shear failure.

(Dat et al., 2015) developed a simplified approach for progressive collapse assessment of RC building structures subjected to a penultimate column loss. The structural behaviour is considered as an elastic–plastic static response, which is constructed with (i) ultimate flexural capacity of the beam-slab structure that is determined by the yield line method of analysis and (ii) displacement ductility at the removed column position that is established based on curvature ductility of a critical connection touching on the affected area. They validated the idealised static response by comparing an experimental result of 12 beam-slab sub-assemblage tests with the simplified model.

(Yu and Guo, 2015) proposed a non-linear single degree of freedom (SDOF) model with a tri-linear resistance function to predict the transient dynamic response of substructure subjected to a CRS. The model takes into account the effect of gravity load, column removal time ($t_r$), nonzero initial boundary condition and stiffness of the plastic stage (hardening).

(Sucuoglu et al., 1994) investigated the redistribution paths of released forces resulting from column loss in framed structures. Column loss caused by a steam boiler explosion in a building was considered and implemented in a multi-storey and multi-bay frame structure. The internal forces developed due to the redistribution of forces were calculated by performing a three dimensional structural analyses.

They concluded that the monolithic building frames possess inherent structural capacity to resist progressive collapse by the nonstructural infill partitions. The linear elastic analysis is fully justified due to the fact that, if a building has sufficient reserve strength, deformations and cracking are observed to be small within the elastic limits.

(Li et al., 2011) investigated the adequacy of current tie force (TF) method to reduce progressive collapse which is adopted in many practical codes such as BS 8110-1:1997. They conducted a numerical study on two RC frame structures which showed the inadequacy of current TF method in increasing progressive collapse resistance. They concluded that the current TF method does not take into account such important factors such as load redistribution in three dimensions, dynamic effects, and internal force correction. In the same study, they proposed a modification to the current TF method by taking into account dynamic effects, load redistribution in three dimensions and internal force correction.

The reliability of the improved TF method is verified by designing an 8-story frame building according to the improved TF method. New designs using the improved TF method have been found to satisfy the requirement of progressive collapse resistance. Also, they found that the improved TF method is also reliable for improving progressive collapse resistance for frames designed under different seismic intensities.

(Li et al., 2014) proposed an energy based theoretical framework to predict the structural and elemental demands of RC frame structures subjected to a column loss at the catenary action stage. The theoretical framework can predict the relationship between nonlinear static and nonlinear dynamic demands and obtain the dynamic load amplification factor at both structural

(DLAFs) and elemental (DLAFe) levels. The two DLAFs are validated through a series of numerical models with varying parameters.

They concluded that the DLAFs and DLAFe are identical for regular frame structures, while for irregular frame structures, the two values may not be identical. Also, they concluded that for structures designed with seismic consideration, progressive collapse capacity increases due to the noticeable contribution of the energy dissipation of the beam mechanism.

(Yu and Tan 2013) proposed an analytical model to predict the structural behaviour and progressive collapse capacity of RC sub-assemblages at CAA under CRS. The proposed model takes into account the combined effects of the actual stress state of compression reinforcement and imperfect boundary conditions on CAA.

The model was verified by comparing the analytical results with the experimental results available in the literature. Another comparison has been made with Park's model which showed the necessity of considering the actual stress state of compression reinforcement instead of assuming it as at yield strength or zero.

Yu and Tan found that the CAA capacity and axial compression forces are greatly affected by the boundary conditions. Also, they concluded that the span to depth and steel reinforcement ratios are the main two parameters which affect the CAA capacity for given boundary conditions.

(Deputy and Story, 2015) carried out an analytical investigation on the effect of nonlinearity of static and dynamic analysis on the structural behaviour of a catenary system. The aim of their research was to examine the amplification factors resulting from geometrically nonlinear static and dynamic analysis of a modified catenary system.

A modified catenary system refers to the case when a beam subjected to a point load, and the deflected beam final shape is in the form of straight legs. They concluded that the amplification factors for geometric nonlinear analysis are less than or equal to unity, and when deflections increase, amplification factors for the static and dynamic cases tend to unity and 2.0, respectively.

(Mohajeri Nav et al., 2016) developed a theoretical method to compute the dynamic resistance of RC structures against progressive collapse. The proposed method calculates the arching and catenary capacities under CRS.

The effect of high strain rate due to dynamic behaviour of RC members was considered in this method. A dynamic increase factor (DIF) was utilized to consider the effect of high strain rates on the material properties and their effects on the capacity of RC structure against progressive collapse. In their study, a blast was taken as an example of dynamic loading. Neglecting the effect of failure modes such as bar fracture and concrete crushing was the main limitation of the proposed method.

## SUMMARY AND CONCLUSION

Review of the theoretical studies on the progressive collapse in RC structures has shown that most studies were related to CMA and TMA in slabs and less attention has been paid to CAA and CTA in RC beams under middle CRS. Investigation of the developed models has revealed that these models are not capable of capturing the real behaviour of concrete after attaining its ultimate strain. A reduction in compression zone depth due to concrete crushing has not been addressed in these models until now.

All previous models and approaches assumed that the ultimate concrete strain remains constant as the deflection increases, which in fact is not the actual state according to the experimental tests. It is noticed from experimental tests that after the specimen attained its ultimate capacity and the crushing of concrete has occurred, the compression zone depth decreases. Thereafter, the effective beam depth changes and the lever arm decreases.

Apart from Merola (2009), other researchers assumed that the top and bottom reinforcement bars remained intact after the section has attained its maximum capacity at CAA stage. This is not the case as observed from current and previous experimental studies. Bar fracture could occur at any stage of deflection after the peak load capacity has been attained by the beam.

Despite that Merola's model can predict the fracture of steel reinforcement, but the calculation of steel strains was based on a questionable assumption, which states that the ultimate compressive strain of concrete $\varepsilon_{cu}$ remains constant. In fact, when concrete attains its ultimate strain, the crushed part of concrete will no longer contribute to the compressive force and should be neglected. Neglecting the crushed concrete part requires the beam depth to be modified at each increment of the deflection.

The aim of the model in this study is to propose a new approach to obtain a reasonable solution to predict the behaviour of a RC sub-assemblage which includes bar fracture and the reduction in beam depth due to concrete crushing.

## 6.3 THE PROPOSED ANALYTICAL MODEL

In this section, the proposed model will be introduced and developed. The model will include two main sections, the first part for the CAA model and the second part for the CTA model. A system of equations will be developed in order to predict the load-deflection curve of a reinforced concrete beam at CAA and catenary action. The equations will be based on the fundamental concepts of equilibrium, compatibility, and material characteristics. In addition, simplifying assumptions will be proposed to overcome the complexity of developing the equations without compromising validity.

## 6.3.1 ASSUMPTIONS AND SIMPLIFICATION

There are two main categories of assumptions, firstly, the assumptions related to the material behaviour and secondly, the assumptions related to the methods or approaches used for analysis. In terms of analysis methods, the structural members subjected to column loss can be classified into two systems, rigid-plastic and elastic-plastic systems (Eyre, 1997). Figure 6-6 shows these systems for RC sub-assemblage under CRS. Many researchers have assumed a rigid-plastic system for restrained concrete members considering zero elastic deformation along the length of the member. For the elastic-plastic system, the elastic deformation in restrained concrete members is taken into account in the model.
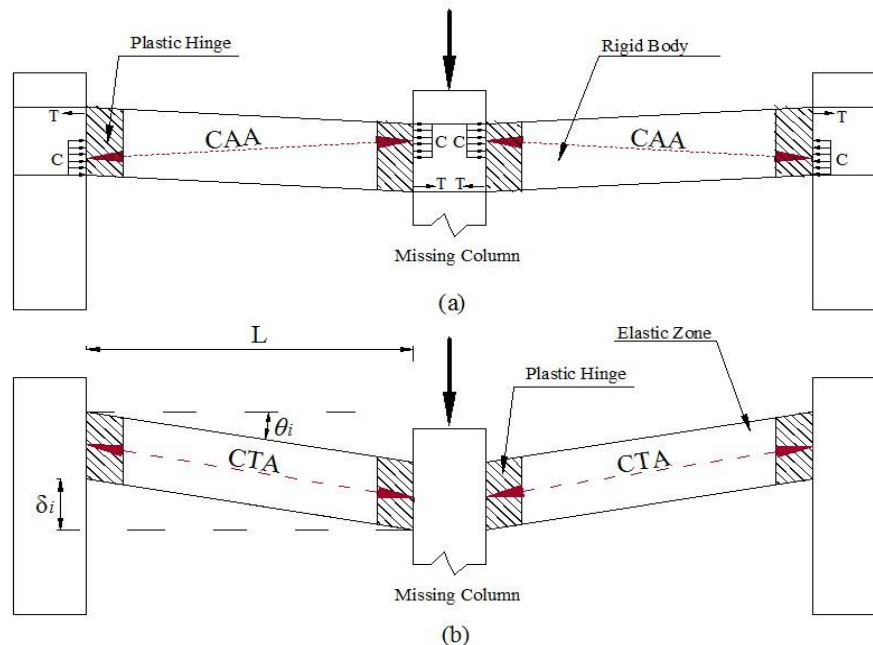


Figure 6-6: RC sub-assemblage under CRS. (a) Rigid-Plastic. (b) Elastic-Plastic

From experimental observations, the following assumptions can be made: The rigid-plastic system will be used for developing the CAA model, and an elastic-plastic system will be used for developing the CTA model.

In addition to the aforementioned assumption above, further assumptions related to the approach are made in order to simplify the development of the equations:

1- For calculation of strains across the section, it is assumed that plane sections before bending remain plane after bending. This assumption will not be valid for the whole depth of the section after concrete crushing. Therefore, a new procedure to calculate the strains after the crushing of concrete will be presented in the next section.
2- Perfect bond between steel and concrete, which dictates that the steel strain is equal to the concrete strain at the same point.
3- No support rotation will occur.

Furthermore, the properties of concrete and steel are considered as follows:

1- Concrete tensile strength is neglected.
2- Crushed concrete should be neglected, and this assumption will be explained later.
3- Maximum concrete strain at crushing is 0.0035 as shown in Figure 6-7(b).
4- The stress-strain relationship of the reinforcing steel is assumed to be bilinear. This relationship is valid for both reinforcements in tension and compression, as shown in Figure 6-7(a).
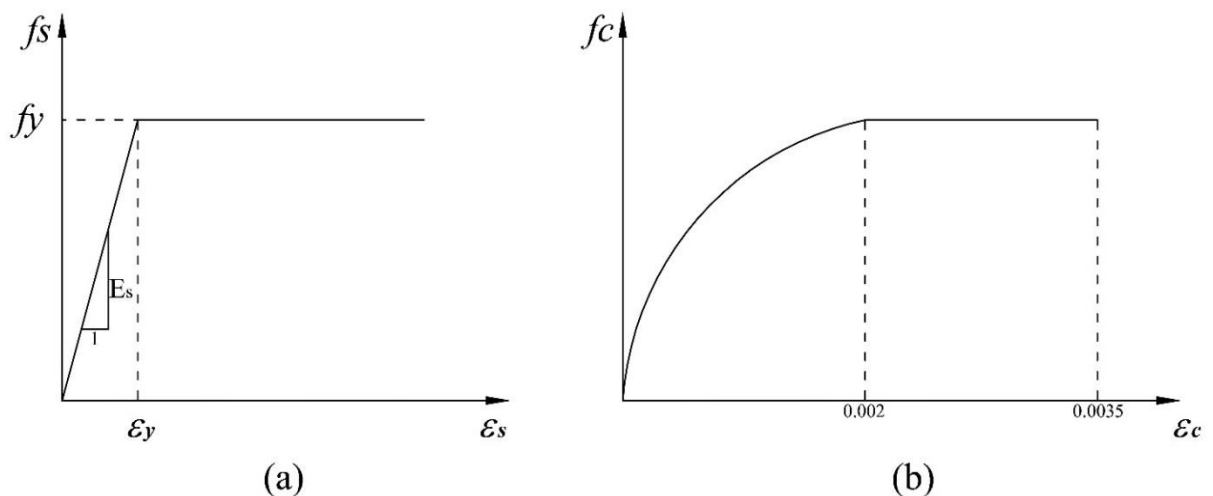


Figure 6-7: Assumed stress-strain relationship, (a) Steel, (b) Concrete

## 6.3.2 PROPOSED PROCEDURE FOR STRAIN CALCULATION

The main limitation of the existing models is the assumption of constant ultimate concrete strain $\varepsilon_{cu}$ at the extreme fibre after concrete crushing. Crushing of concrete beyond the level of ultimate strain will reduce the effective depth of the beam (*d*). Assuming a constant effective depth of the beam for different levels of loading and deflection after concrete crushing can lead to overestimation of the load capacity of the RC beams under CRS. Figure 6-8 shows the strain distribution for different levels of deflection based on constant ultimate concrete strain.
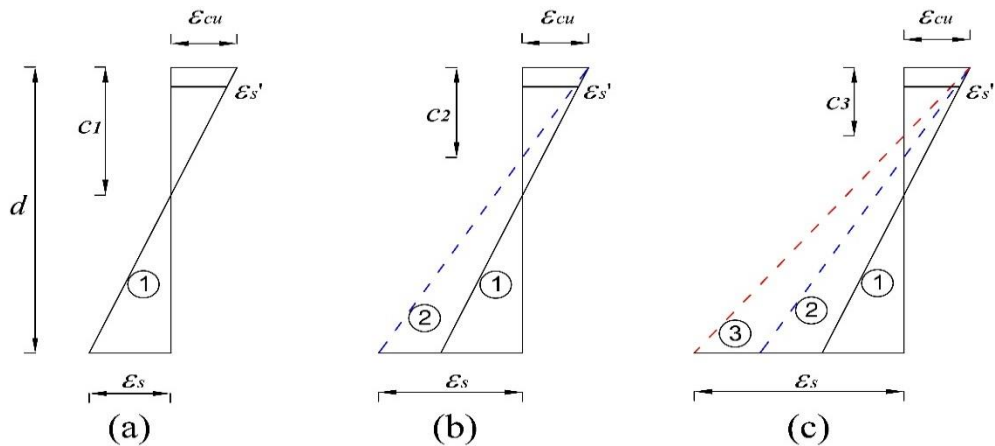


Figure 6-8: Strain distribution with constant $\varepsilon_{cu}$, (a) at $\delta_1$ (b) at $\delta_2 > \delta_1$ (c) at $\delta_3 > \delta_2$

It can be seen from Figure 6-8 that when the beam deflection increases, the strain profile steps from 1 to 3. It shows that the strain of compression reinforcement decreases from profile 1 to 3. In fact, the strain of compression reinforcement increases with the increase of deflection until the point where axial compressive forces decrease as shown in Figure 6-9(b). At that point, the strain of these bars starts to decrease marking the onset of catenary action.
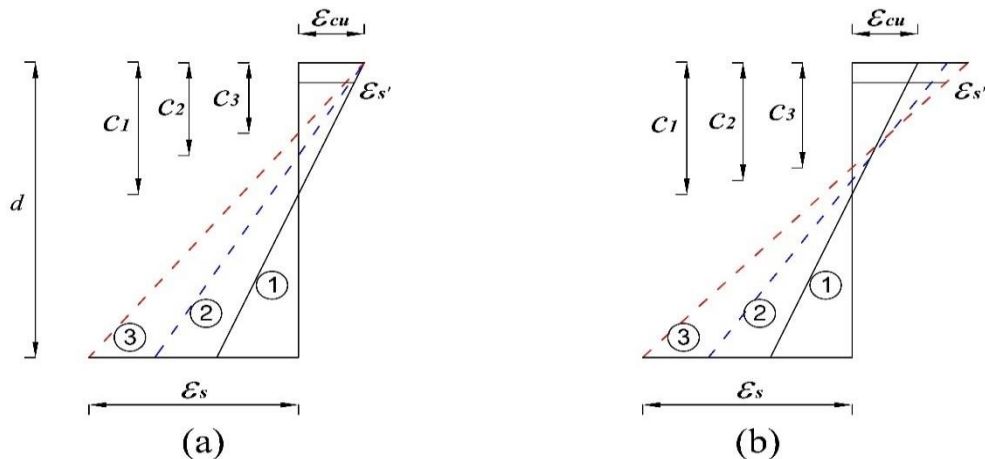


Figure 6-9: Strain distribution (a) with constant $\varepsilon_{cu}$ , (b) actual distribution

In Figure 6-9, $c_1$ represents the compression depth in the beam section corresponding to $\delta_1$, while $c_2$ and $c_3$ represent compression depth corresponding to $\delta_2$ and $\delta_3$ respectively, where crushing of concrete was not considered.

Compression depths for profiles 2 and 3 need to be modified because their values include a thickness of crushed concrete. This thickness should be neglected and subtracted from the compression zone depth. Consequently, the beam effective depth should be reduced by the same value of crushed concrete.

Figure 6-10 shows the deflected beam shape after column loss subjected to different values of deflection. The relationship between deflection and beam rotation angle can be obtained as follows:

$$\tan(\theta_i) = \frac{\delta_i}{L} \qquad\qquad (6 - 15)$$
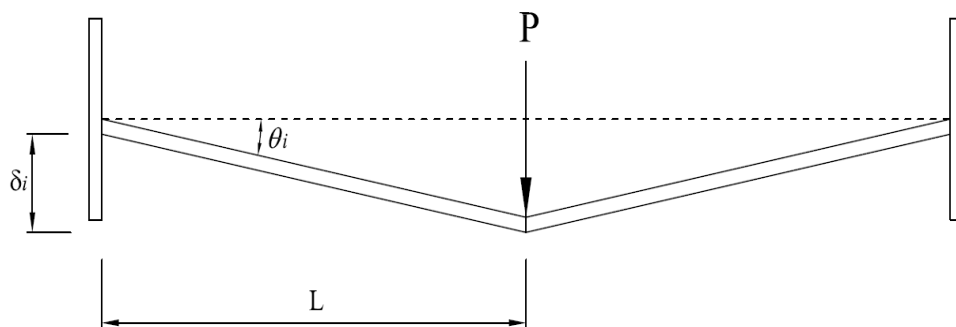


Figure 6-10: Deflected shape of RC beam at CAA stage

Figure 6-11 shows the strain profile with the crushed concrete layer. The proposed approach to calculate concrete and steel strains for each value of deflection after concrete crushing is based on dividing the concrete compression zone into small layers as shown in Figure 6-11(c).

When the strain of the top layer exceeds the ultimate concrete strain, the layer is neglected and the effective depth of the beam section is modified according to the triangular geometry and compatibility conditions.
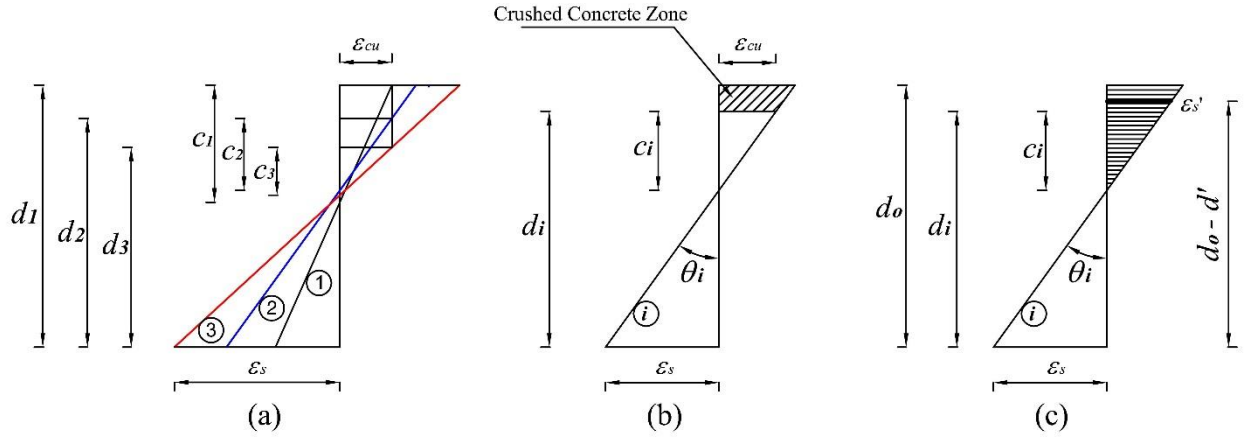
Figure 6-11: Proposed strain distribution profiles at different deflection values

In order to obtain the thickness of the crushed concrete, a relationship between the deflection and the effective depth should be derived. In addition, the strain of compression steel should be calculated dependent on tension steel strain. From Figure 6-11(b), the relationship between the effective depth and the concrete compression zone can be derived as follows:

$$\frac{\varepsilon_{cu}}{c_i} = \frac{\varepsilon_{si}}{d_i - c_i}$$

(6 - 16)

According to (Haskett et al., 2009), the length of strain penetration over the extreme compression fibre is equal to $d_i$, therefore:

$$tan(\theta_i) = \frac{\varepsilon_{cu}}{c_i} d_i$$

(6 - 17)

From equating equations (6-15) and (6-17), $c_i$ $and$ $c_{i+1}$ can be obtained as follows:

$$c_i = \frac{L\,\varepsilon_{cu} d_i}{\delta_i} \quad , \quad c_{i+1} = \frac{L\,\varepsilon_{cu} d_{i+1}}{\delta_{i+1}}$$

(6 - 18)

For each value of $\delta$, there is a layer of concrete that should be neglected and the effective beam depth should be modified.

To simplify the calculation of the crushed concrete thickness, the depth of neutral axis is assumed to be constant. Therefore, the crushed concrete thickness ($t_i$) will be equal to only ($c_i -$ $c_{i+1}$) as in equation (6-19), and can be obtained from equation (6-20):

$$t_i = c_i - c_{i+1} \tag{6 - 19}$$

$$t_i = \frac{L\,\varepsilon_{cu}d_i}{\delta_i} * \frac{\delta_{i+1} - \delta_i}{\delta_{i+1} - L\,\varepsilon_{cu}} \tag{6 - 20}$$

The procedure and steps for the derivation of equation (6-20) are detailed in Appendix A. Therefore, the value of modified effective depth for each deflection or deflection increment can be calculated from equation (6-21) as follows:

$$d_{i+1\,modified} = d_i - t_i \tag{6 - 21}$$

For $i = 0$, equation (6-21) will be as follows:

$$d_1 = d_0 - t_0 \tag{6 - 22}$$

From Figure 6-11(c), and from triangular relations, the strain of compression steel reinforcement can be calculated as follows:

$$\varepsilon'_{si} = \frac{d_o - d'}{c_i}\varepsilon_{cu} - \varepsilon_{si} \tag{6 - 23}$$

From Figure 6-11(b), and from triangle relations, the strain of tension steel reinforcement can be calculated as follows:

$$\varepsilon_{si} = \frac{d_i - c_i}{c_i}\varepsilon_{cu} \tag{6 - 24}$$

## 6.3.3 DEVELOPMENT OF CAA MODEL

Figure 6-12 shows a typical load-deflection relationship of a RC slab strip or a beam subjected to a column loss scenario. The relationship curve can be divided into three parts according to the resisting mechanisms, from A to B flexural action, from B to D compressive arch action and from D to E catenary action. From A to B, the behaviour of the beam is elastic, followed by yielding at point B.

Due to the effect of CAA, the load increases from B until ultimate capacity at C. From C to D, a reduction in the capacity occurs due to concrete crushing and formation of plastic hinges at critical sections. At point D, which is the onset of CTA, a transition from axial compressive force into axial tensile force occurs and the axial force therefore is zero. From D to E, the load capacity starts to increase due to the catenary action stage.

In this section, an analytical model will be developed to predict the behaviour of RC beams for the region C to D.
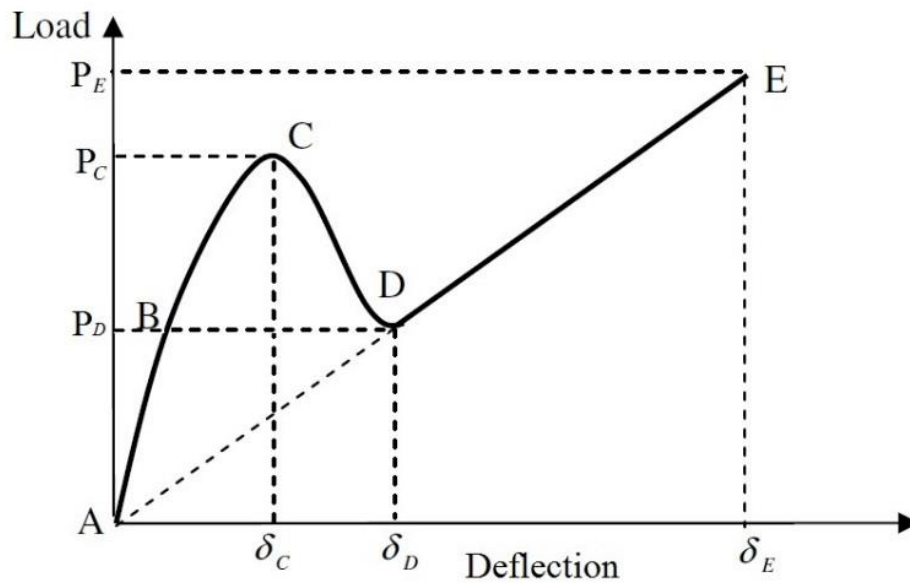


Figure 6-12: Load-Deflection relation of RC beam under CRS.

From Figure 6-6(a), which shows a RC beam sub-assemblage under CAA, a free body diagram of a single beam and the middle joint subjected to a load $P$ are shown in Figure 6-13.



(a) Single Beam                                    (b) Middle Joint
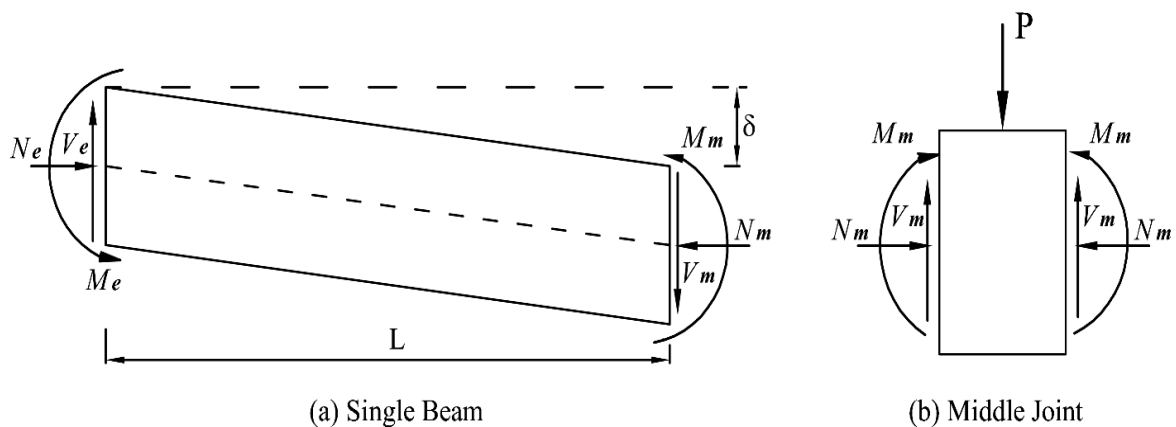
Figure 6-13: Free Body Diagram of RC Sub-Assemblage, (a) Single Beam (b) Middle Joint

From Figure 6-13 based on equilibrium, the vertical applied load capacity can be determined as follows:

$$Axial\ Force, \quad N = N_e = N_m \qquad\qquad (6\text{-}25)$$

$$Shear\ Force, \quad V = V_e = V_m \qquad\qquad (6\text{-}26)$$

$$Applied\ Load, \ P = 2V \qquad\qquad (6\text{-}27)$$

By taking moment equilibrium about the end support in Figure 6-13(a):

$$V_m L = M_e + M_m - N_m \delta \qquad\qquad (6\text{-}28)$$

By substituting equations 6-25, 6-26 and 6-27 into equation 6-28, the load capacity can be obtained:

$$P = \frac{2(M_e + M_m - N\ \delta)}{L} \qquad\qquad (6\text{-}29)$$

The values of $M_e$, $M_m$ and $N$ can be calculated based on the internal beam section forces shown in Figure 6-14.
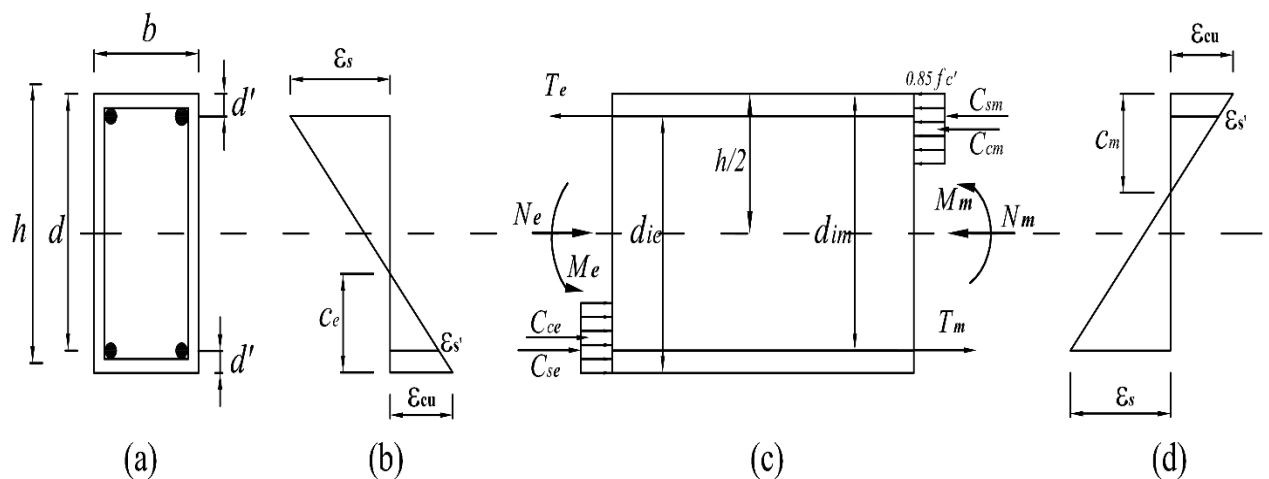


Figure 6-14: Strain and force distribution (a) Beam section, (b) Strains at beam end section, (c) Moments and forces at beam section, (d) Strains at middle joint section

Figure 6-14 shows the distribution of beam section internal forces and strains. From moment equilibrium at the beam section and by taking moments about the centre of the beam section, moments $M_e$ and $M_m$ can be obtained as follows:

$$M_e = C_{ce}\left\{d_i + d' - \frac{h}{2} - \frac{\beta c_e}{2}\right\} + C_{se}\left\{\frac{h}{2} - d'\right\} + T_e\left\{\frac{h}{2} - d'\right\} \qquad (6\text{-}30)$$

$$M_m = C_{cm}\left\{d_i + d' - \frac{h}{2} - \frac{\beta c_m}{2}\right\} + C_{sm}\left\{\frac{h}{2} - d'\right\} + T_m\left\{\frac{h}{2} - d'\right\} \qquad (6\text{-}31)$$

From the equilibrium of horizontal forces, axial forces $N_e$ and $N_m$ can be obtained as follows:

$$N_e = C_{ce} + C_{se} - T_e \qquad (6\text{-}32)$$

$$N_m = C_{cm} + C_{sm} - T_m \qquad (6\text{-}33)$$

Where

$C_c$, $C_s$ and $T$ are the concrete compressive force, steel compressive force and steel tensile force, respectively. The subscripts $e$ and $m$ refers to the beam end and middle joint, respectively. From Figure 6-14(c), $C_c$, $C_s$ and $T$ can be calculated as follows:

$$C_{ce} = 0.85f_c'b\beta c_e \qquad (6\text{-}34)$$

$$C_{cm} = 0.85f_c'b\beta c_m \qquad (6\text{-}35)$$

$$C_{se} = \varepsilon_{se}'E_sA_{se}' \qquad (6\text{-}36)$$

$$C_{sm} = \varepsilon_{sm}'E_sA_{sm}' \qquad (6\text{-}37)$$

$$T_e = f_yA_{se} \qquad (6\text{-}38)$$

$$T_m = f_yA_{sm} \qquad (6\text{-}39)$$

By substituting equations (6-32) to (6-39) into equation (6-25), the equation of equilibrium will be as follows:

$$0.85f_c'b\beta c_e + \varepsilon_{se}'E_sA_{se}' - f_yA_{se} = 0.85f_c'b\beta c_m + \varepsilon_{sm}'E_sA_{sm}' - f_yA_{sm} \qquad (6\text{-}40)$$

Equation (6-40) indicates that $c_e$ and $c_m$ are functions of each other. In order to find the values of these unknowns, another equation that can relate $c_e$ with $c_m$ is required. The other equation will be based on compatibility conditions, which can correlate both unknowns $c_e$ and $c_m$ and relate them to the vertical deflection of the middle joint ($\delta$).

Figure 6-15 shows a single bay beam subjected to a concentrated load at the middle joint. The developed axial compressive forces throughout the length of the beam will induce a lateral support movement of a value ($u$).

The value of ($u$) depends on the support stiffness termed (K) and the amount of axial compressive forces developed under CRS. According to the assumptions, no axial deformation will occur and no support rotation. Therefore, the total horizontal length of the bay beam after joint lateral movement will be equal to ($L + u$).

At the beam end, a crack of width equal to $(h - c_e)\,tan(\theta)$ occurs, and a strain elongation $l_e$ occurs at the tension steel at the top. At the middle joint of the beam, the length of the crushed concrete will be equal to ($c_m tan(\theta)$), and a strain elongation $l_m$ occurs at the tension steel at the bottom. Therefore, the total length of the bay beam will be equal to $(L + (h - c_e)\,tan(\theta) - c_m\,tan(\theta))$.
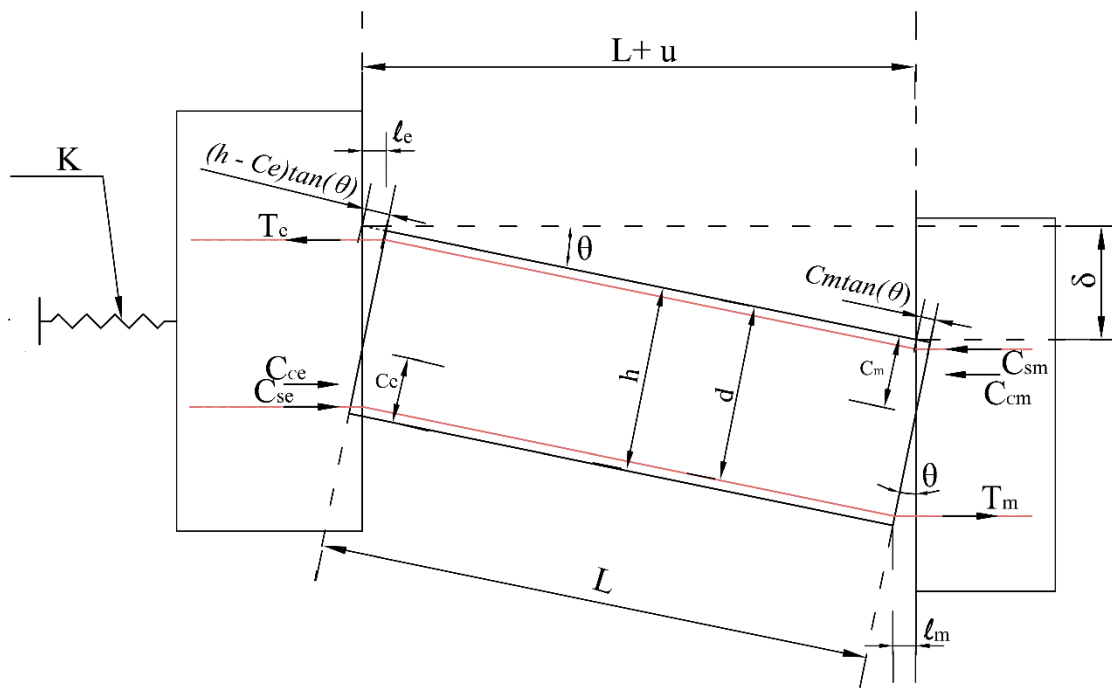
Figure 6-15: Deflected shape of single bay beam with all internal forces and deformations

Figure 6-16 shows the triangular sketch of the bay beam with all deformation and concrete crushing.
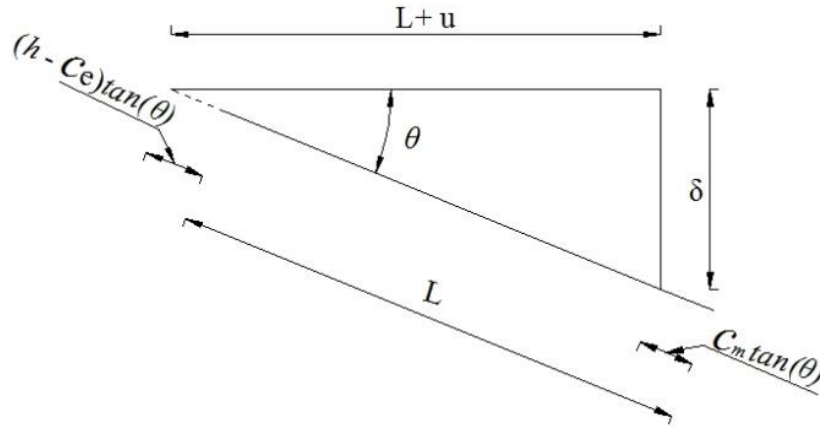


Figure 6-16: Geometry of the bay beam with all deformations

From triangluar geometry relations, the relationship between $c_e$ and $c_m$ can be derived as follows:

$$\delta^2 + (L + u)^2 = (L - c_m \tan(\theta) + (h - c_e) \tan(\theta))^2 \tag{6 - 41}$$

$$u = \frac{N}{K} \tag{6 - 42}$$

$$\tan(\theta) = \frac{\delta}{L + u} \quad , \quad \tan(\theta) = \frac{\delta}{L} \quad for\ small\ u \tag{6 - 43}$$

By substituting equations (6-42) and (6-43) into equation (6-41) and rearranging the variables, the relation between $c_e$ and $c_m$ can be obtained from the equation (6-44):

$$c_e + c_m = h - \frac{\delta}{2} - \frac{N}{K}\left(\frac{2L^2 + \delta^2}{2L\delta}\right) \tag{6 - 44}$$

The procedure and steps for the derivation of equation (6-44) are detailed in Appendix A. Examination of equation (6-44) indicates that the presence of axial forces in restrained RC beams will increase the compression depth zones. When $N = 0$ in simply supported RC beams, the value of $(c_e + c_m)$ will be equal to only $h - \delta/2$ .

The compatibility equation (6-44) indicates that for a given value of deflection $\delta$, $c_e$ and $c_m$ become a function of each other. With the equilibrium equation, which relates $c_e$ and $c_m$ with each other, the two unknowns can be obtained by solving the two equations simultaneously.

After obtaining the value of $c_e$ and $c_m$ for a given value of $\delta$, then $N$, $M_e$ and $M_m$ can be obtained consequently, and thereafter the load capacity $P$ can be obtained from equation (6-29). Equations (6-40) and (6-44) can be solved iteratively using appropriate mathematical programming software.

In this case 'Matlab' is the software of choice. Starting with a deflection $\delta$ correspond to ultimate concrete strain and yield strain of tension steel bars and increasing $\delta$ gradually, the values of $c_e$ and $c_m$ can be calculated.

The starting value of deflection $\delta$ can be calculated firstly from the compatibility equation (6-44), using maximum values for $c_e$ and $c_m$ that ensure steel yield and ultimate concrete strain. Maximum values for $c_e$ and $c_m$ can be calculated from equation (6-24) by putting $\varepsilon_s = \varepsilon_y$, as follows:

$$c_e, c_m\}_{max} = \frac{d\ \varepsilon_{cu}}{\varepsilon_y + \varepsilon_{cu}} \qquad\qquad (6 - 45)$$

It should be mentioned that the starting step of the iteration process is not the actual peak value of the load capacity at CAA. During the progress of the iteration process, the values of $c_e$ and $c_m$ take the exact values until $N_e = N_m$ and then the peak load $P$ obtained.

## 6.3.4 DETERMINATION OF BAR FRACTURE

In order to obtain the deflection $\delta$ correspond to the bar fracture, the strain of tension steel bars should be monitored for each increment of deflection $\delta$. From the experimental results and observations, the fracture of top or bottom bars during CAA causes the beam section to lose its ability to carry the loads by flexural action.

The beam section carries the load after bar fracture by pure tension either by the top or bottom bars. This indicates that the bar fracture at both sides, either at the ends or at the middle joint, will be followed by the onset of the catenary action stage.

There are two possible scenarios for the sequence of bar fracture. The first scenario is that the top steel bars at the beam end fracture first followed by the onset of catenary action and then fracture of bottom steel bars at the middle joint will occur during the catenary action stage. The second scenario is that the bottom steel bars at the middle joint fracture first followed by the onset of catenary action and then fracture of the bottom steel bars at the middle joint will occur during the catenary action stage.

In Figure (6-17), which shows the two possible scenarios, $\delta_{Ft}$ , $\delta_{Fb}$ represent the deflections at which top and bottom bars fracture, respectively, and $\delta_D$ represents the deflection at the onset of the catenary action stage.
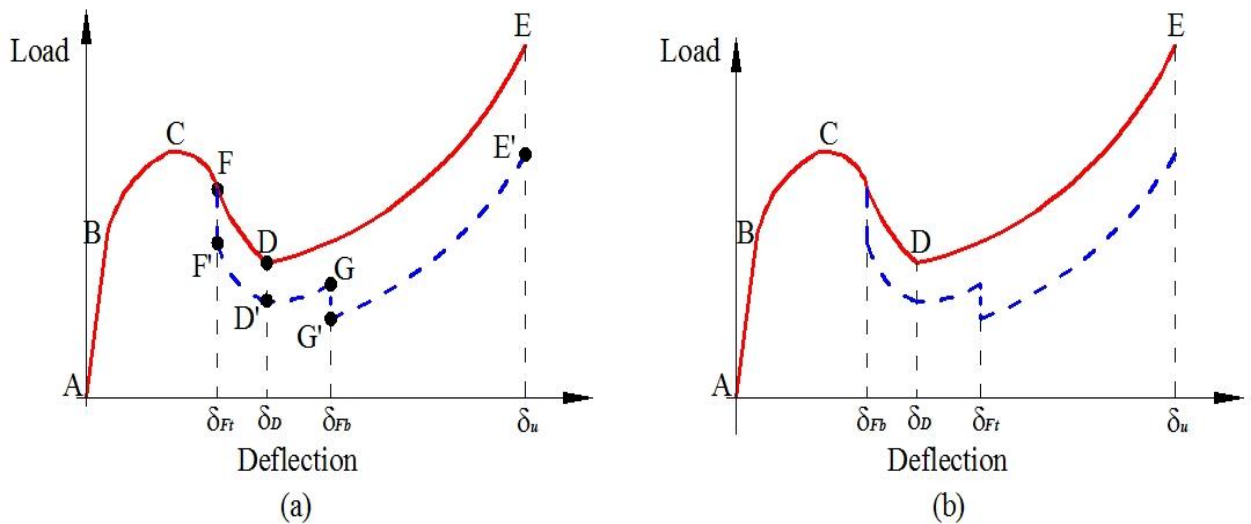


Figure 6-17: Possible Scenarios for bar fracture (a) First scenario. (b) Second scenario

From Figure (6-15) and (6-16), the steel bar elongations $l_e$ and $l_m$ can be calculated as follows:

$$\sin(\theta) = \frac{l_e}{d - c_e} = \frac{l_m}{d - c_m} \qquad (6 - 46)$$

$$\sin(\theta) = \frac{\delta}{L - c_m \tan(\theta) + (h - c_e)\tan(\theta)} \qquad (6 - 47)$$

By equating equations (6-46) and (6-47) and arranging the parameters:

$$l_e = \frac{\delta(d - c_e)L}{L^2 + \delta(h - c_e - c_m)} \tag{6 - 48}$$

$$l_m = \frac{\delta(d - c_m)L}{L^2 + \delta(h - c_e - c_m)} \tag{6 - 49}$$

It is known from the mechanics of materials that the strain is equal to the elongation divided by the original length. According to the assumption of the perfect bond between concrete and steel bars, the length that experiences the elongation is the plastic hinge length only.

Many researchers attempted to obtain the length of the plastic hinge in RC beams and columns. According to (Mattock, 1965) , the length of the plastic hinge can be obtained from the empirical formula as follows:

$$l_p = 0.5d + 0.05z \tag{6 - 50}$$

Where
z is the distance from the point of the maximum moment to the point of zero moments.

Therefore, the strain can be calculated as follows:

$$\varepsilon_{se} = \frac{l_e}{l_p} \tag{6 - 51}$$

$$\varepsilon_{sm} = \frac{l_m}{l_p} \tag{6 - 52}$$

For each deflection increment, the strains $\varepsilon_{se}$ and $\varepsilon_{sm}$ should be calculated using equations (6-48) to (6-52), then the results should be compared with the ultimate steel strain. If one of the calculated strains ($\varepsilon_{se}$ or $\varepsilon_{sm}$) equals or exceeds the ultimate steel strain this means that the steel bars at that section have fractured and the beam section carries the load by tension.

By following the steps shown in Figure 6-18, the relationship between the applied load and the middle joint deflection can be obtained. The first step in the flowchart represents the input of all material, geometry and boundary condition properties.

The ( $i$ ) loop is an iterative process to find the correct solution for values of $c_e$ and $c_m$ when $N_e = N_m$ . The ( j ) loop implements the gradual increase of the deflection. The deflection increment can be used as a percentage of the beam height such as $0.05h$ or $0.01h$ which depends on the accuracy required.

At the deflection corresponding to the steel bar fracture (Point F), the moment capacity at that section will be equal to zero. The load correspond to steel bar fracture can be calculated using equation 6-29 by taking either $M_e$ or $M_m$ a zero value, which depends on whether the fracture has occurred.
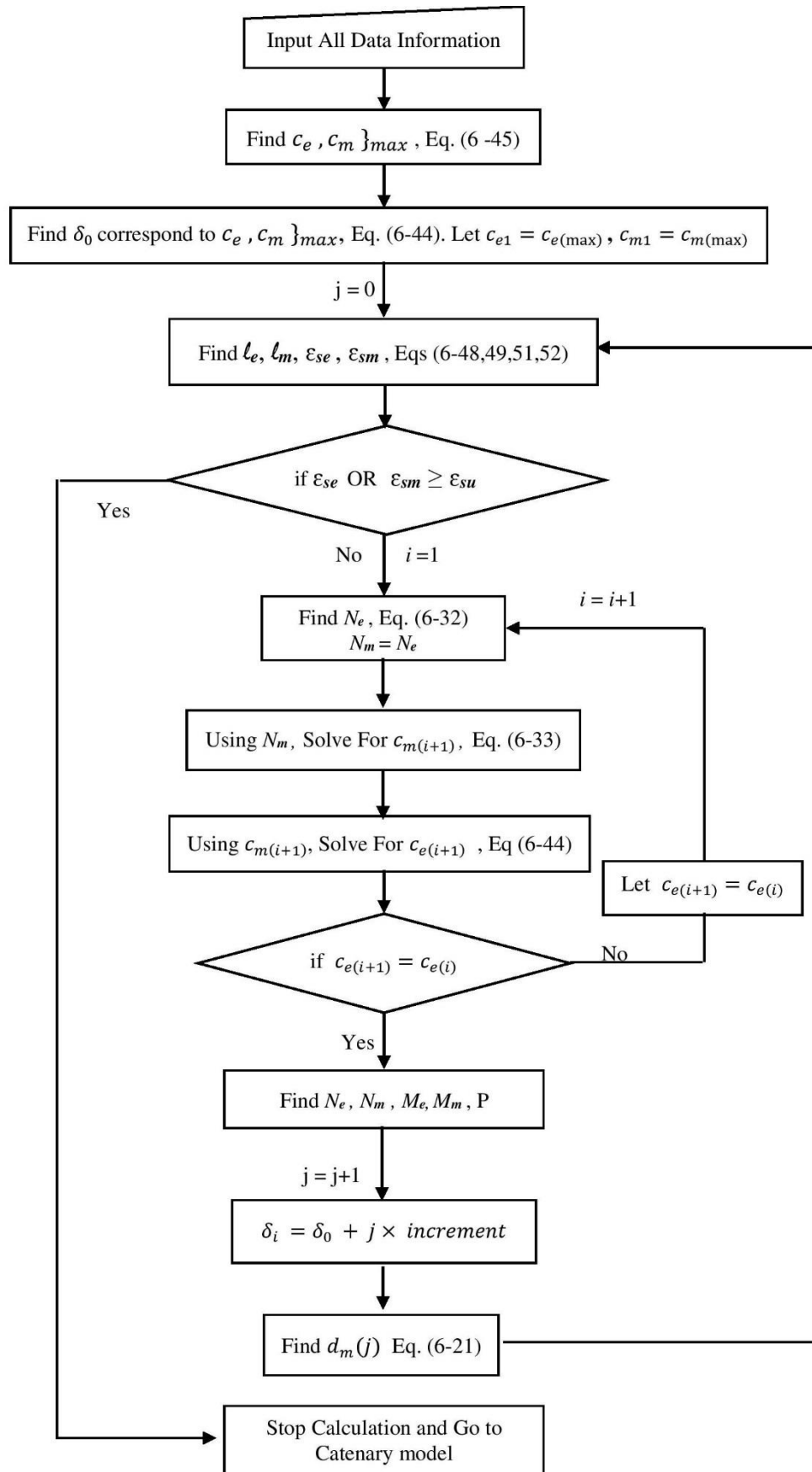
Figure 6-18: Flowchart of the Steps to implement the CAA

## 6.3.5 DEVELOPMENT OF CATENARY MODEL

As mentioned in the previous section, there are two possible scenarios for bar fracture. The first scenario is that the tension steel bars at the beam end fracture first followed by the onset of catenary action or tension steel bars at the middle joint fracture first. Both scenarios can follow the same steps to obtain the structural behaviour at catenary action stage.

After the fracture of steel bars at the middle joint or at the beam ends, at a certain point the load will be carried by the remaining steel bars by means of tensile forces, which were previously carrying the loads by means of compressive forces during CAA.

Transition from compression to tension means that there is a zero point of axial force that indicates the onset of catenary action at a deflection $\delta_D$ as shown in Figure 6-17. On the other hand, the load will be carried by means of flexure at the intact joint where no bar fracture has occurred. In Figure 6-17(a), as the deflection increases, the beam force increases in axial tension, and the tensile forces in the tension steel bars at the intact joint increase and eventually fracture at a deflection $\delta_{Fb}$. As the deflection increases beyond $\delta_{Fb}$, the load will be carried by axial tension throughout the beam length.

The tensile force at the beam end may not produce a uniform tensile stresses in all sections due to concrete confinement and formation of plastic hinges at the critical sections. In order to simplify the calculation, it is assumed a uniform axial force will be developed along the length of the beam.

During catenary action, there are three critical points, as shown in Figure 6-17, and they are; the catenary action start point D, steel bar fracture G, and ultimate load capacity E. The main goal of this section is to determine these points rather than the whole structural behaviour.

Considering the first scenario of bar fracture, Figure 6-19 shows a single bay beam after fracture of the tension steel bars at the beam end. During catenary action and under tensile axial forces, the end supports are expected to move onwards for a distance ($u$), which depends on the surrounding stiffness.
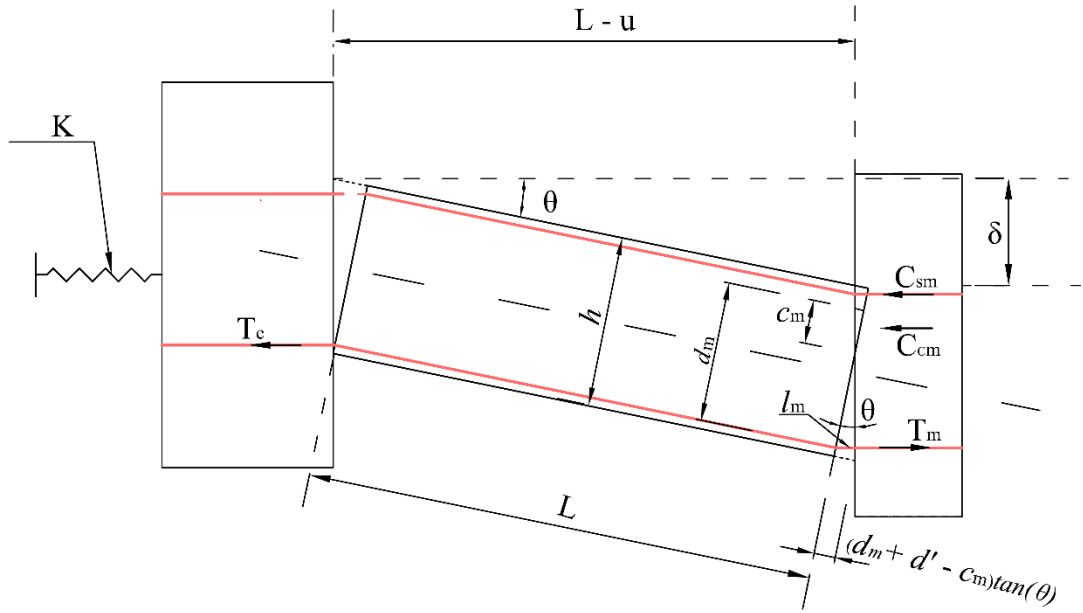
Figure 6-19: Deflected shape of single bay beam after bar fracture at the beam end.

In order to determine the catenary action start point, which occurs at a deflection $\delta$ equal to $\delta_D$, two equations are required to be developed and solved for the two unknowns $\delta_D$ and $c_m$. At the onset of catenary action, the axial force will be equal to zero, therefore, the equilibrium equation will be as follows:

$$C_{cm} + C_{sm} - T_m = 0 \tag{6 - 53}$$

Substituting equations. (6-35, 37, 39) into equation (6-53):

$$0.85 f_c' b \beta c_m + \varepsilon_{sm}' E_s A_{sm}' - f_y A_{sm} = 0 \tag{6 - 54}$$

Where:

$$\varepsilon_{sm}' = \frac{d_D - d'}{c_m} \varepsilon_{cu} - \varepsilon_{sm} \qquad \text{Equation } (6 - 23)$$

$$\varepsilon_{sm} = \frac{d_D - c_m}{c_m} \varepsilon_{cu} \qquad \text{Equation } (6 - 24)$$

$$d_D = d_o - \frac{L \, \varepsilon_{cu} d_0}{\delta_0} \times \frac{\delta_D - \delta_0}{\delta_D - L \, \varepsilon_{cu}} \qquad \text{Equation } (6 - 21)$$

Where

$d_D$, is the effective beam depth corresponding to $\delta_D$.

It is clear that equation (6-54) has two unknowns, which are; $\delta_D$ and $c_m$. From the compatibility equation, the movement of the support ($u$) at the onset of catenary action will be zero due to $N = 0$. From Figure (6-19) and triangular geometry, the relationship between $\delta_D$ and $c_m$ can be derived as follows:

$$\delta_D^2 + L^2 = (L + (d_m + d' - c_m)\tan(\theta))^2 \qquad (6\text{ - }55)$$

By rearranging equation (6-55) and substituting $\tan(\theta) = \delta_D / L$, the equation (6-55) will be as follows:

$$\delta_D = \frac{2(d_m + d' - c_m)L^2}{L^2 - (d_m + d' - c_m)^2} \qquad (6\text{ - }56)$$

By solving equations (6-54) and (6-56) simultaneously, the values of $\delta_D$ and $c_m$ can be found. Thereafter, $C_{cm}$ and $C_{sm}$ can be obtained. With these values in hand, $M_m$ can be obtained from equation (6-31). Finally, the load $P$ can be obtained from equation (6-29), with $M_e$ and $N$ equal to zero.

The second critical point in the catenary action stage is the fracture of the tension steel bars at the middle joint, which is point G in Figure 6-17(a). After the onset of catenary action and as the deflection increases, the beam picks up a tensile axial force. At the middle joint, the internal compressive forces decrease and the tensile force increases until the fracture of tension steel bars occurs. At the fracture of tension steel bars of the middle joint, the compressive forces change abruptly into tensile force.

It is expected at early stages of catenary action, the axial tension force developed is small, and the tension steel bars at the middle joint is at an advanced stage of yielding. Therefore, it is expected that the axial inward movement of the supports ($u$) is extremely small compared with $L$, and can be neglected to simplify the complex calculation.

From Figure (6-20), which shows the triangular deflected shape of the beam after the fracture of the top bars at the beam end, $\delta_{Fb}$ can be obtained as follows:
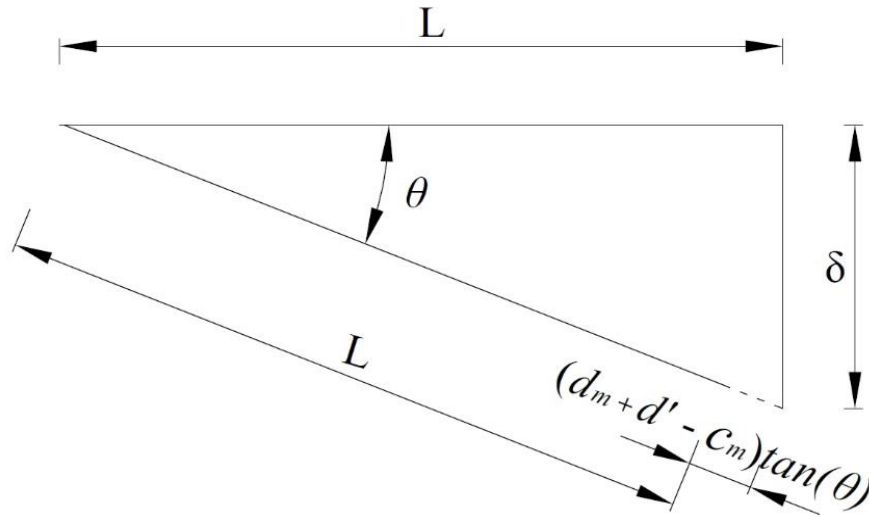
Figure 6-20: Triangular deflected beam shape after top bar fracture at the beam end

$$sin(\theta) = \frac{\delta}{L + (d_m + d' - c_m)tan(\theta)} \qquad (6\text{-}57)$$

Equating with equation (6-46) and rearranging, the relationship between $\delta$ and $c_m$ will be as follows:

$$\delta = \frac{l_m L^2}{L(d_m - c_m) - l_m(d_m + d' - c_m)} \qquad (6\text{-}58)$$

At the fracture point, the strain of the tension steel bars should equal to the ultimate steel strain. Therefore, from equation (6-52), the steel elongation $l_m$ at which bar fracture occurs can be obtained as follows:

$$l_m = \varepsilon_{su} l_p \qquad (6\text{-}59)$$

By substituting equation (6-59) into equation (6-58):

$$\delta_{Fb} = \frac{\varepsilon_{su} l_p L^2}{L(d_m - c_m) - \varepsilon_{su} l_p(d_m + d' - c_m)} \qquad (6\text{-}60)$$

Equation (6-60) relates two unknowns, $\delta_{Fb}$ and $c_m$, and another equation is required to solve them. At bar fracture, equation (6-56) can be written as follows:

$$\delta_{Fb} = \frac{2(d_m + d' - c_m)L^2}{L^2 - (d_m + d' - c_m)^2} \qquad (6\text{-}61)$$

Equations (6-60) and (6-61) can then be solved simultaneously, and the load capacity $P$ can be obtained using equation (6-29) with $M_e$ equal to zero.

Figure (6-21) shows the single bay beam snap-through of the middle joint. After this point, the load $P$ is carried only by pure tensile forces. At point $G'$ in Figure 6-17(a), the line of action of the tensile force acts at an angle $\varphi$ and magnitude $N$ (equal to the tensile force at point $G$). Therefore, the load $P$ at point $G'$ which corresponds to $\delta_{Fb}$ can be calculated as follows:

$$P = 2N\sin(\varphi) \tag{6 - 62}$$

$$\sin(\varphi) = \frac{\delta_{Fb} - (d - d')\cos(\theta)}{\sqrt{L^2 + (d - d')^2}} \tag{6 - 63}$$

$$\cos(\theta) = \frac{L - u}{\sqrt{\delta_{Fb}^2 + (L - u)^2}} \tag{6 - 64}$$
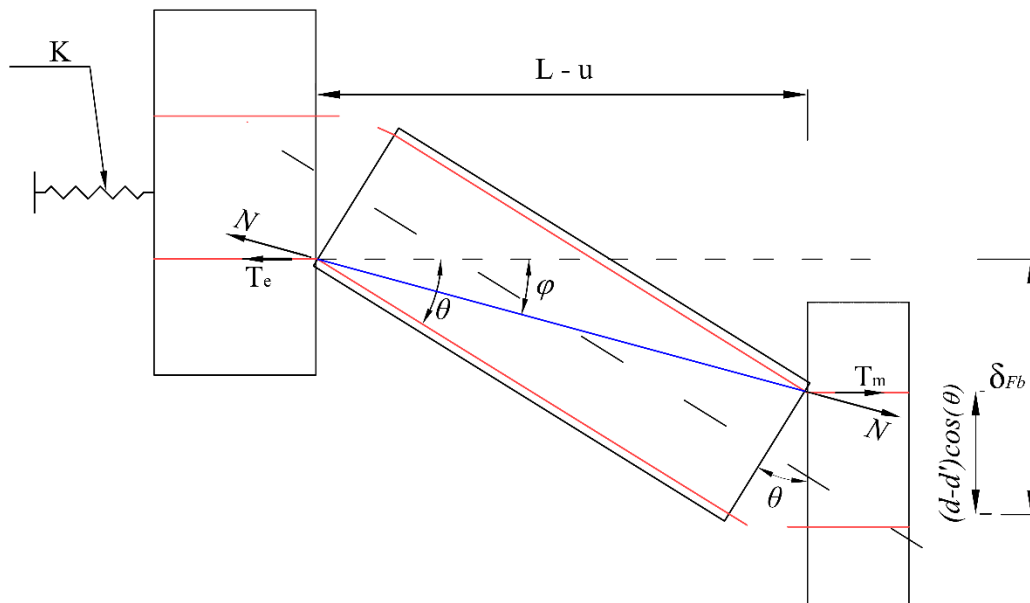


Figure 6-21: Deflected shape of single bay beam after second bar fracture.

The final critical point $(E')$ in the catenary action stage is the ultimate capacity which corresponds to the deflection $\delta_u$. As the applied load increases beyond the load corresponding to the second bar fracture, the vertical deflection increases until the longitudinal steel bars attain their full strain capacity and eventually fracture.

Figure (6-22) shows the deflected shape of the double bay beam at second bar fracture and at ultimate load state. From geometry and compatibility conditions, the ultimate deflection $\delta_u$ can be obtained as follows:

$$\delta_u = \sqrt{L_2^2 - (L - u)^2} \tag{6 - 65}$$

$$L_2 = L_1 + \Delta L \tag{6 - 66}$$

$$L_1 = \sqrt{L^2 + (d - d')^2} \tag{6 - 67}$$

Where

*ΔL,* is the maximum elongation of the beam during catenary action stage.

According to the assumptions of neglecting the tensile strength of concrete and a perfect bond between steel bars and concrete, the steel stress will be distributed uniformly over the length of plastic hinges. In addition, the failure mode is expected by bar fracture. Therefore, the maximum beam elongation during catenary action can be obtained as follows:

$$\Delta L = 2\varepsilon_{su}l_p \tag{6 - 68}$$

After obtaining the ultimate deflection $\delta_u$, the ultimate load capacity $P$ can be obtained from equilibrium conditions as follows:

$$P = 2N\sin(\theta) \tag{6 - 69}$$

$$\sin(\theta) = \frac{\delta_u}{L_2} \tag{6 - 70}$$

$$N = f_u A_s \tag{6 - 71}$$

According to the fact, that the failure will occur at the weakest section, $A_s$ in equation (6-71) should be taken as the lesser value at any section along the length of the beam.
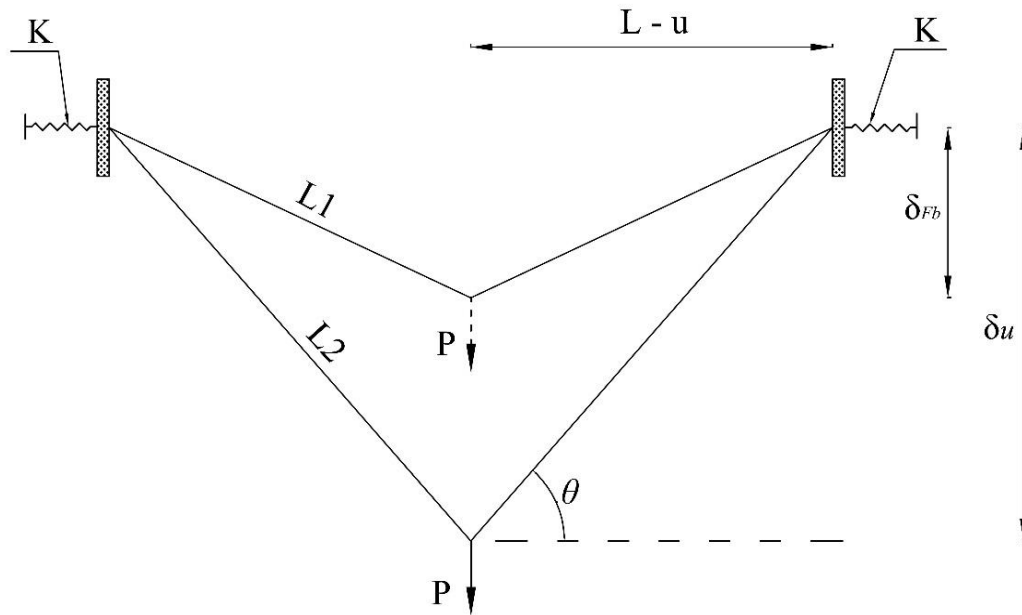
Figure 6-22: Deflected shape of the beam at second bar fracture and ultimate load state.

## 6.4 DETERMINATION OF AXIAL RESTRAINT STIFFNESS

The surrounding members are the main source of stiffness provided to any horizontal bay beams forming part of a structure, and are especially significant in the event of progressive collapse. The non-failed members can provide the structural stiffness either by axial or flexural mechanisms or both. The adjacent beams at the ends tend to provide the stiffness by an axial mechanism, while the columns provide it by a flexural mechanism.

By assuming that the surrounding members remain intact after column damage, and the damage is limited to column loss only, neglecting the contribution from slabs, the axial restraint stiffness can be obtained using one of two approaches.

The first approach is to run a numerical model simulating the building under investigation applying the following steps:

1- Remove the affected two bay beam from the building.

2- Apply a unit lateral force at the joint where the removed beam end was. Based on the symmetry assumption, the left and right end have the same lateral stiffness.

3- Calculate the lateral deflection, $\delta_l$, caused by the applied unit load using any available numerical FE software.

4- Calculate the axial lateral stiffness from equation 6-72:

$$K = \frac{1}{\delta_l}$$ (6 - 72)

The second approach is to consider that the stiffness is provided by the surrounding members such as beams and columns, as shown in Figure 6-23. The lateral stiffness provided to the beam BE at point B comes from beam BG and columns BC and AB.

The axial stiffness of the un-cracked beam BG is equal to $E_c A/L$, while the flexural stiffness of columns BC and AB are $3E_c I/H_2^3$ and $3E_c I/H_1^3$ respectively, where, $E_c$ is the modulus of elasticity of concrete. Therefore, the lateral stiffness at points B and E will be equal to:

$$K = \frac{E_c A}{L} + \frac{3E_c I}{H_1^3} + \frac{3E_c I}{H_2^3}$$ (6 - 73)
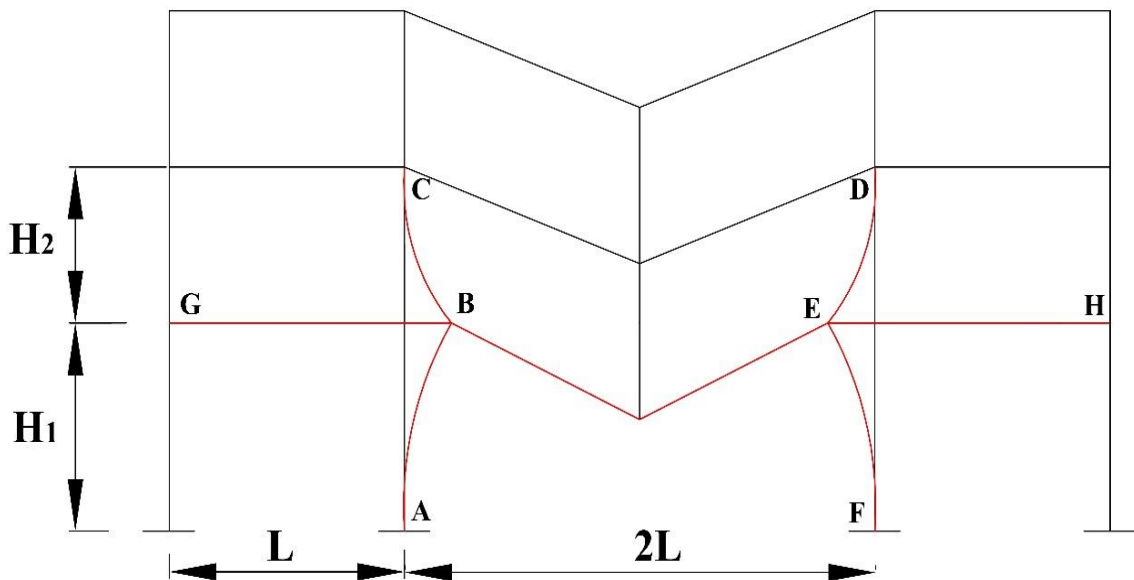


Figure 6-23: Lateral stiffness for affected in a building after column removal.

It should be mentioned that the remaining columns and beams in the building, may reduce the lateral stiffness of the affected beam BE, while members, such as slabs and walls, may increase the lateral stiffness. Therefore, adopting the second approach is reasonably accurate and time efficient.

However, for the experimental tests, the lateral stiffness was provided using two steel rods, which connect the beam end stub into the steel frame. Two 50 mm threaded steel rods of 300 mm length were connected into each beam end stub using threaded nuts with high stiffness.

By assuming infinite stiffness from the steel frame, the axial restraint stiffness from the threaded connecting steel rods can be calculated using equation, $K = E_s A/L$, where $E_s$ is the modulus of elasticity of the steel rods, and as a result, the axial lateral restraint stiffness is $2.6 \times 10^6$ kN/m.

## 6.5 COMPARISON WITH THE EXPERIMENTAL RESULTS

In order to verify the adequacy of the proposed models and equations to predict the structural behaviour of RC beams at CAA and catenary action, a comparison with the test results from the experimental study was performed. For the calculation and processing of the analytical results, Matlab was used for the CAA model, while for the catenary action model, S-math sheets were used.

The analytical and experimental results of specimen SS-1 and SS-2 are given in Figure 6-24. Only one analytical curve was obtained for SS-1 and SS-2, this is because the material and geometrical properties of specimen SS-1 and SS-2 were the same. Figure 6-25 shows the comparison between analytical and experimental results for specimen SS-3.

It should be noted that the calculation of the CAA model starts with point 'C' shown in Figures 6-24 and 6-25, which represent the ultimate load capacity at CAA. The line AC does not represent the actual elastic behaviour of the RC sub-assemblage as it was drawn to connect the origin with point 'C'.

It can be seen from Figures 6-24 and 6-25 that the general trend of both analytical and experimental structural behaviour was quite similar. It is clear from the comparison that the area under the experimental curves is greater than those under the analytical curves.

The area under the load-deflection curve represents the strain energy absorbed by a member under any applied load. This means that the analytical model prediction underestimates the progressive collapse capacity of the RC beams.
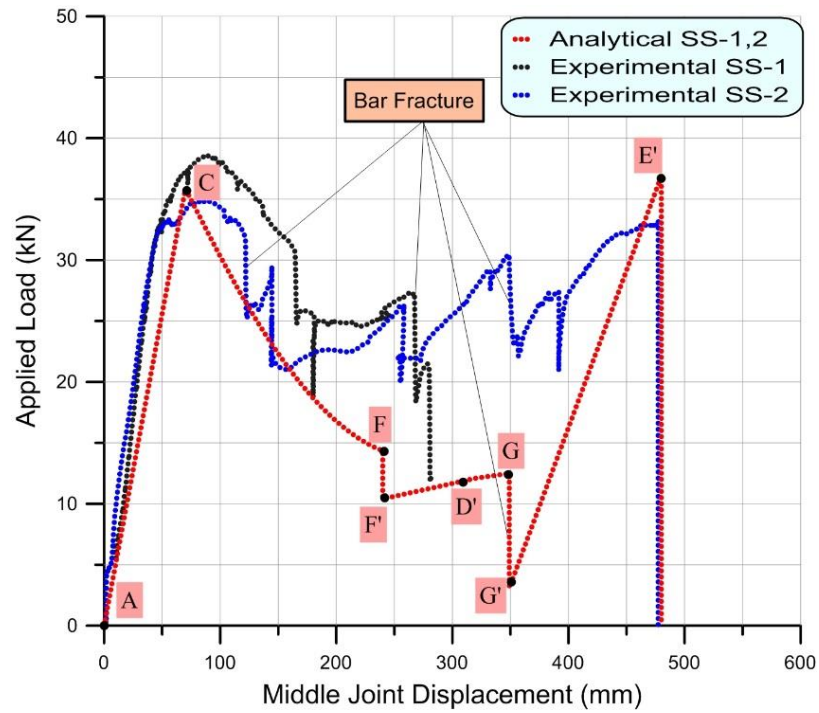
Figure 6-24: Load-MJD Comparison of Analytical vs. Experimental for SS-1 and SS-2.
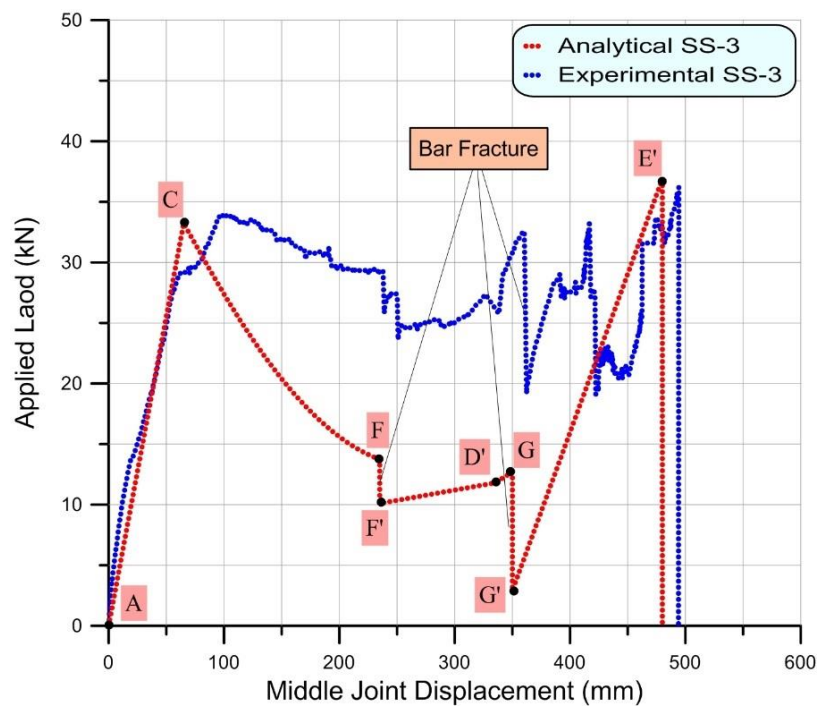


Figure 6-25: Load-MJD Comparison of Analytical vs. Experimental for SS-3

The analytical model considers that the beam material is a homogeneous material and uniform geometry, also it considers a perfect specimen fabrication. For these considerations, the model considers the fracture of all steel reinforcement within the same layer, occurs simultaneously.

Therefore, the difference between the areas under the analytical and experimental curves could be related to the non-homogeneity of the concrete, the imperfection of beam construction, steel bar manufacturing and unsymmetrical boundary conditions and loading.  These parameters clearly affect the experimental results and failure modes such as the sequence of bar fracture.

Due to the effect of these parameters, the steel bars within the same layer fractured sequentially at different stages of deflection, which is clearly observed during the experimental testing. For ideal and perfect homogeneous conditions, the fracture of all steel bars within the same layer is expected to occur at one specific deflection, which is clearly reflected by the analytical curve.

In fact, the peak demands develop during only a very short period of time in the event of progressive collapse. Based on this fact, the fracture of all steel bars at the same layer is likely to happen at the same time. Therefore, it can be concluded that the analytical results represent an accurate lower bound of the structural capacity.

Table 6-1 summarises the forces and their corresponding middle joint displacements at critical stages of load-deflection history for both experimental and analytical results.

Table 6-1: Comparison of Forces with their MJD's at Critical Stages

| Specimen | Type of Results | Max. load at CAA | | At the onset of Catenary Action | | Max. Load at Catenary Action | |
|---|---|---|---|---|---|---|---|
| | | $P_{com}$ (kN) | MJD (mm) | $P$ (kN) | MJD (mm) | $P_{cat}$ (kN) | MJD (mm) |
| SS-1 | Experimental | 38.5 | 91.1 | 26.4 | 248.3 | 12.1 | 280.0 |
| | Analytical | 35.8 | 70.2 | 12.1 | 320.0 | 36.9 | 480.0 |
| SS-2 | Experimental | 34.9 | 89.3 | 25.2 | 246.0 | 33.2 | 477.3 |
| | Analytical | 35.8 | 70.2 | 12.1 | 320.0 | 36.9 | 480.0 |
| SS-3 | Experimental | 34.0 | 101.0 | 24.9 | 272.5 | 36.2 | 494.0 |
| | Analytical | 33.2 | 64.9 | 11.8 | 335.1 | 36.9 | 480.0 |

It is clear from table 6-1 that both experimental and analytical applied loads were very close at CAA and catenary action. The large difference in load capacity during the transition stage could be related to the non-homogeneity in material and geometry as explained earlier in this section.

Also, bond slip occurrence during experimental tests could explain the larger deflection at peak load at CAA stage, compared to the deflection obtained analytically in which no consideration for bond slip was taken.

Figures 6-26 shows the comparison between analytical and experimental pseudo-static behaviour of specimen SS-2 and SS-3. The overall trend of both analytical and experimental structural behaviour was quite similar. The analytical progressive collapse capacity was less than the experimental result by about 14.7% and 18.9% for specimen SS-2 and SS-3 respectively.

As explained earlier in this section, the analytical progressive collapse represents the minimum capacity which corresponds to the worst scenario of failure mode by simultaneous bar fracture of all steel bars at the top or bottom beam section.

It is clear from Figure 6-26 that both specimens attained their maximum capacity at CAA at a deflection of 140.2 mm and 135.3 mm for specimen SS-2 and SS-3 respectively. Both experimental and analytical results show that both specimens were not able to increase their capacities at catenary action.
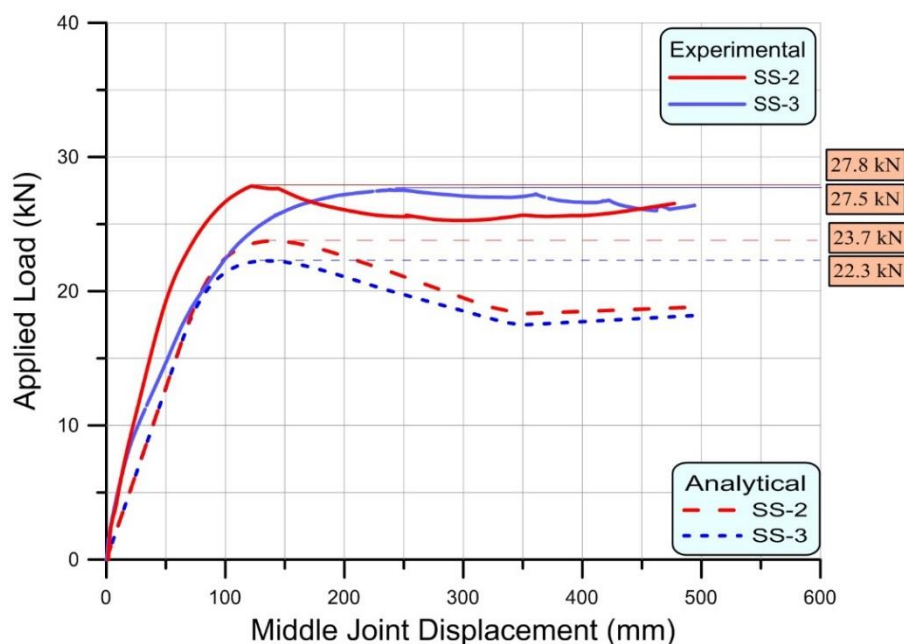


Figure 6-26: Analytical vs. experimental Pseudo-Static response of SS-2 & SS-3

Figure 6-27 shows the analytical relationship of steel strain with middle joint displacement. This Figure presents the strain in the top bars at the beam ends and strain in the bottom bars at the middle joint. It is clear from Figure 6-27 that the bottom steel bars at the middle joint were in tension and they fractured first followed by fracture of the top bars at the beam ends.

For specimen SS-1 and SS-2, the fracture of the bottom bars at the middle joint occurred at a deflection of 240.0 mm, and the fracture of the top bars at the beam ends occurred at 349.0 mm, while they were 235.0 mm and 350.0 mm for specimen SS-3. This minimal difference could be related to the small difference in concrete compressive strength.
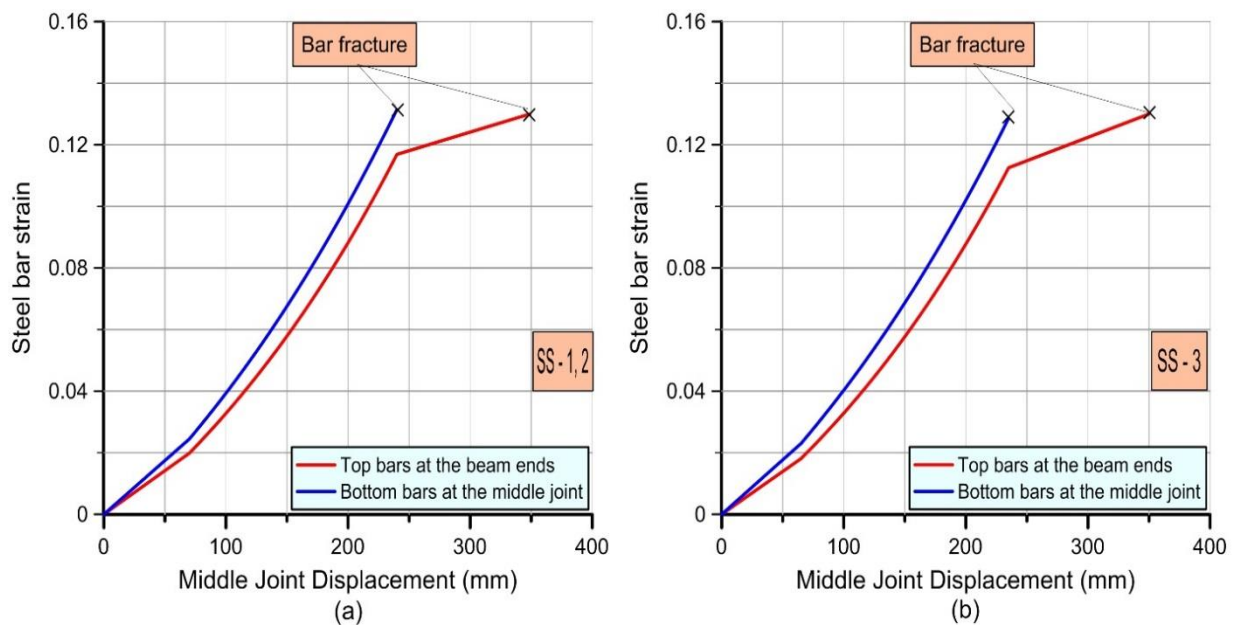
Figure 6-27: Strain distribution of top and bottom steel bars for (a) SS-1,2, (b) SS-3

## 6.6 COMPARISON AND VALIDATION

In order to verify the adequacy of the proposed models and equations to predict the structural behaviour of RC beams at CAA and CTA, another comparison with the available test results was performed. These experiments were performed by other researchers on RC sub-assemblages consisting of two bay beams and three column stubs as explained in the literature review chapter two, (Su et al., 2009, Choi and Kim, 2011, Yu and Tan, 2013, FarhangVesali et al., 2013).

In order to quantify the relationship between theoretical and experimental results, the correlation factor was obtained, which was 0.987 for the CAA model and 0.940 for the CTA model. In addition, the coefficient of variation was also calculated, which was 15.2% for CAA and 26.5 for the CTA model. The comparison in Table 6-2 shows that the proposed models at CAA and CTA were able to assess the capacity of RC beams subjected to CRS.

Figure 6-28 indicates that the CAA model slightly underestimates the capacity of RC beams, while the CTA model slightly overestimates the capacity of RC beams at CTA stage. This can be explained by the occurrence of slip between the concrete and steel reinforcements, which is not considered in the proposed model.

Slip occurrence could allow steel stresses to penetrate through a larger length of steel reinforcement in tension, which cause an increase in CAA load capacity and decrease in the final deflection, leading to a decrease in CTA load capacity.
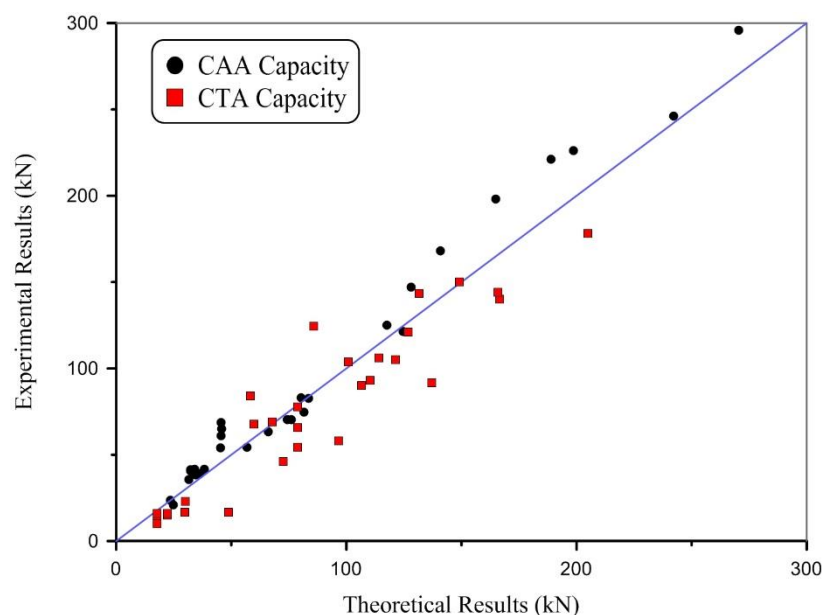


Figure 6-28: Comparison of experimental and theoretical results for CAA and CTA models.

Table 6-2: Comparison of Experimental and Theoretical results for CAA and CTA models.

| No. | Reference | $L/h$ | $f_c'$ MPa | Beam Section (mm) | | Longitudinal Rein. Ratio (%) | | Ultimate capacity (kN) | | | | | |
|---|---|---|---|---|---|---|---|---|---|---|---|---|---|
| | | | | | | | | CAA | | | CTA | | |
| | | | | Width | Depth | Top | Bott. | Exp. | Theo. | Exp./Theo. | Exp. | Theo. | Exp./Theo. |
| S1 | (Yu and Tan 2013) | 11.0 | 31.2 | 150 | 250 | 0.90 | 0.49 | 41.6 | 38.2 | 1.089 | 68.9 | 67.9 | 1.015 |
| S2 | | 11.0 | 31.2 | 150 | 250 | 0.73 | 0.49 | 38.4 | 34.5 | 1.113 | 67.6 | 59.8 | 1.13 |
| S3 | | 11.0 | 38.2 | 150 | 250 | 1.24 | 0.49 | 54.5 | 56.8 | 0.96 | 124.4 | 85.9 | 1.448 |
| S4 | | 11.0 | 38.2 | 150 | 250 | 1.24 | 0.82 | 63.2 | 66.0 | 0.958 | 103.7 | 100.8 | 1.029 |
| S5 | | 11.0 | 38.2 | 150 | 250 | 1.24 | 1.24 | 70.3 | 74.4 | 0.945 | 105.1 | 121.4 | 0.866 |
| S6 | | 11.0 | 38.2 | 150 | 250 | 1.87 | 0.82 | 70.3 | 76.1 | 0.924 | 143.3 | 131.6 | 1.089 |
| S7 | | 8.6 | 38.2 | 150 | 250 | 1.24 | 0.82 | 82.8 | 83.5 | 0.992 | 106.0 | 114.1 | 0.929 |
| S8 | | 4.6 | 38.2 | 150 | 250 | 1.24 | 0.82 | 121.3 | 124.7 | 0.973 | 91.8 | 137.0 | 0.67 |
| A1 | (Su et al. 2009) | 4.08 | 24.5 | 150 | 300 | 0.55 | 0.55 | 168.0 | 140.9 | 1.192 | 93.1 | 110.3 | 0.844 |
| A2 | | 4.08 | 26.8 | 150 | 300 | 0.83 | 0.83 | 221.0 | 189.0 | 1.169 | 140.0 | 166.6 | 0.84 |
| A3 | | 4.08 | 29.6 | 150 | 300 | 1.13 | 1.13 | 246.0 | 242.3 | 1.015 | 178.0 | 204.9 | 0.869 |
| A4 | | 4.08 | 21.9 | 150 | 300 | 0.55 | 0.38 | 147.0 | 128.1 | 1.148 | 45.9 | 72.6 | 0.632 |
| A5 | | 4.08 | 25.2 | 150 | 300 | 0.83 | 0.55 | 198.0 | 164.9 | 1.201 | 58.1 | 96.5 | 0.602 |
| A6 | | 4.08 | 27.2 | 150 | 300 | 1.13 | 0.75 | 226.0 | 198.6 | 1.138 | 144.0 | 165.8 | 0.869 |
| B1 | | 6.58 | 17.6 | 150 | 300 | 1.13 | 1.13 | 125.0 | 117.7 | 1.062 | 150.0 | 149.1 | 1.006 |
| B2 | | 9.08 | 18.3 | 150 | 300 | 1.13 | 1.13 | 82.9 | 80.4 | 1.031 | 121.0 | 126.8 | 0.954 |
| B3 | | 9.08 | 20.1 | 150 | 300 | 1.13 | 0.75 | 74.7 | 81.6 | 0.915 | 90.2 | 106.5 | 0.847 |
| C1 | | 6.12 | 15.1 | 100 | 200 | 1.30 | 1.30 | 60.9 | 45.6 | 1.336 | 65.7 | 78.8 | 0.834 |
| C2 | | 6.12 | 16.0 | 100 | 200 | 1.30 | 1.30 | 64.9 | 45.7 | 1.42 | 77.6 | 78.8 | 0.985 |
| C3 | | 6.12 | 15.5 | 100 | 200 | 1.30 | 1.30 | 68.6 | 45.6 | 1.504 | 54.4 | 78.8 | 0.69 |
| V1 | (FathangVesali al. 2013) | 11.72 | 30.5 | 180 | 180 | 0.51 | 0.51 | 40.5 | 32.4 | 1.25 | 12.0 | 17.8 | 0.674 |
| V2 | | 11.72 | 27.0 | 180 | 180 | 0.51 | 0.51 | 35.7 | 31.6 | 1.13 | 16.0 | 17.8 | 0.899 |
| V3 | | 11.72 | 30.0 | 180 | 180 | 0.51 | 0.51 | 41.4 | 32.4 | 1.278 | 10.0 | 17.8 | 0.562 |
| V4 | | 11.72 | 26.0 | 180 | 180 | 0.77 | 0.51 | 40.1 | 33.7 | 1.19 | 16.0 | 22.3 | 0.717 |
| V5 | | 11.72 | 29.5 | 180 | 180 | 0.77 | 0.51 | 41.6 | 34.0 | 1.224 | 15.0 | 22.3 | 0.673 |
| V6 | | 11.72 | 30.0 | 180 | 180 | 0.77 | 0.51 | 39.4 | 34.1 | 1.155 | 16.0 | 22.3 | 0.717 |
| 5S | (Choi and Kim 2011) | 6.94 | 17.0 | 150 | 225 | 1.16 | 0.46 | 39.0 | 36.3 | 1.074 | 16.5 | 48.9 | 0.337 |
| 5G | | 8.47 | 17.0 | 150 | 185 | 0.58 | 0.58 | 21.0 | 24.8 | 0.847 | 16.5 | 29.8 | 0.554 |
| 8S | | 8.01 | 30.0 | 140 | 195 | 1.46 | 0.87 | 54.1 | 45.2 | 1.197 | 84.0 | 58.2 | 1.443 |
| 8G | | 9.80 | 30.0 | 125 | 160 | 0.82 | 0.82 | 23.7 | 23.6 | 1.004 | 23.0 | 30.1 | 0.764 |
| Mean value of experimental to theoretical ratios | | | | | | | | | | 1.115 | | | 0.850 |
| Coefficient of Variation | | | | | | | | | | 15.2% | | | 26.5% |
| Correlation coefficient | | | | | | | | | | 0.987 | | | 0.940 |

## 6.7 PARAMETRIC STUDY

In order to better understand the resisting mechanisms of RC structures during progressive collapse and the parameters which may affect these mechanisms, a parametric study was conducted on a full scale two bay RC beam specimen.

The specimen was assumed to be extracted from a perimeter frame of a multi-storey building shown in Figure 3-2, with a height of 4.0 m for the ground storey and 3.5 m for other storeys. The clear span between column faces is 5.4 m in both directions.

The dead and live load were 15.0 kN/m and 9.0 kN/m respectively. Based on these loads, a beam with dimensions of 500 mm height and 300 mm width was used. Steel reinforcement of the beam near the supports was 3T16 and 5T16 for bottom and top respectively.

The same steel properties in the experimental study were used and a compressive concrete strength of 28.0 MPa was used with 24400 MPa specified for the modulus of elasticity. The dimensions of the supporting columns were $500 \times 500$ mm. The lateral stiffness was calculated according to equation (6-73) namely $6.7 \times 10^5$ kN/m.

Four groups with different parameters were taken in the study to investigate their effects on the structural response and progressive collapse capacity as follows:

- First and second group: Span to depth ratio ($L/d$) = 12, 15, 18. These values could be achieved either by changing the beam length or its depth. Two groups with different $L$ and $d$ values were used to investigate the effect of span/depth ratio on the structural behaviour as listed in table 6-3.

- Third group: Top reinforcement ratio = 0.5 %, 0.67 % and 1.0 % of the beam section area.

- Fourth group: Bottom reinforcement ratio = 0.4 %, 0.6 % and 0.8 % of the beam section area. Steel reinforcement areas are listed in table 6-4.

Table 6-3: Span to depth ratios for the parametric study

| Group | Specimen | $L$ (mm) | $d$ (mm) | L/d |
|-------|----------|----------|----------|-----|
| 1 | S-1 | 5400 | 450 | 12 |
|   | S-2 | 6750 | 450 | 15 |
|   | S-3 | 8100 | 450 | 18 |
| 2 | S-4 | 6750 | 560 | 12 |
|   | S-2 | 6750 | 450 | 15 |
|   | S-5 | 6750 | 375 | 18 |

Table 6-4: Steel reinforcement areas used in the parametric study

| Group | Parameter | Specimen | $A_s^{top}$ % | $A_s^{Bottom}$ % | $A_s^{top}$ mm$^2$ | $A_s^{Bottom}$ mm$^2$ |
|-------|-----------|----------|------|------|------|------|
| 3 | Top Reinforcement Ratio | S-6 | 0.5 | 0.4 | 750 | 600 |
|   |  | S-1 | 0.67 | 0.4 | 1000 | 600 |
|   |  | S-7 | 1.0 | 0.4 | 1500 | 600 |
| 4 | Bottom Reinforcement Ratio | S-1 | 0.67 | 0.4 | 1000 | 600 |
|   |  | S-8 | 0.67 | 0.6 | 1000 | 900 |
|   |  | S-9 | 0.67 | 0.8 | 1000 | 1200 |

## 6.7.1 EFFECT OF SPAN TO DEPTH RATIO

Six specimens were divided into two groups, three specimens in each group with different span to depth ratio of (12, 15, 18) were considered in this study. The effect of span to depth ratio is illustrated in Figure 6-29. As shown in Figure 6-29, the general trend of the load-deflection curve for all specimens was similar.

It is clear that the initial stiffness, ultimate load at CAA and ultimate load at catenary action decreased with an increase in the span to depth ratio. The final MJD for the specimens with same beam depth was increased with an increase in span to depth ratio as shown in Figure 6-29(a). However, the final MJD for the specimens with same beam span decreased with an increase in span to depth ratio as shown in Figure 6-29(b).

For specimens with span to depth ratios of 12 and 15, the fracture of bottom reinforcement occurred first at the middle joint during CAA followed by the fracture of top reinforcement at the beam ends during catenary action.

However, for specimens with span to depth ratios of 18, no fracture of reinforcement has occurred during CAA and both top and bottom steel reinforcement fractured during catenary action. This means that the required beam rotation for the fracture to occur is not sufficient which greatly depends on the span to depth ratio. It also indicates the ability of the CAA model to predict the structural response at catenary action stage before the fracture of steel bars, as shown in Figure 6-29 for S-3 and S-5.

Table 6-5 lists the critical values of load-displacement curves for all specimens. For the first group, the applied load at CAA decreased by 25% and 23% with an increase in span to depth ratio from (12 to 15) and (15 to 18) respectively, while it was 35% and 31% for the second group. It is clear from these values that the effect of beam depth on the applied load is greater than the effect of beam span for the same span to depth ratio.

It is clear from table 6-5 that there is no great effect of span to depth ratio on the applied load at catenary action stage because the applied load at catenary action mainly depends on the steel reinforcement. The slight difference in the applied load at catenary action was due to the difference in the final deflection, which affects the vertical component of the tensile forces developed in the beam at catenary action. It is clear from table 6-5 that the final deflection increased with the increase in the beam span and beam depth.
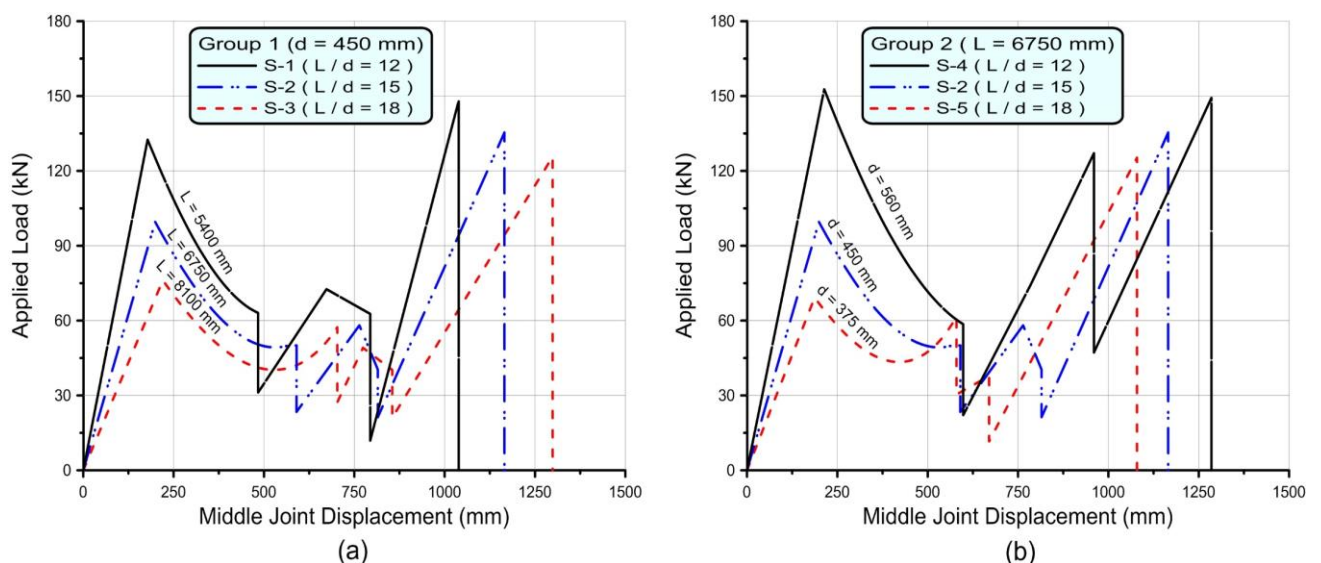


Figure 6-29: Comparison of applied load-displacement relationship, (a) Group1, (b) Group 2

Table 6-5: Critical values of load-displacement curves for group (1) and (2)

| Specimen | L/d | Max. load at CAA | | At the onset of Catenary Action | | Max. Load at Catenary Action | |
|---|---|---|---|---|---|---|---|
| | | $P_{com}$ (kN) | MJD (mm) | $P$ (kN) | MJD (mm) | $P_{cat}$ (kN) | MJD (mm) |
| S-1 | 12 | 132.5 | 178 | 72.6 | 673 | 148.2 | 1039.7 |
| S-2 | 15 | 99.6 | 199 | 49.4 | 545 | 135.4 | 1165.5 |
| S-3 | 18 | 76.2 | 220 | 40.4 | 542 | 125.7 | 1298.9 |
| S-4 | 12 | 152.7 | 214 | 74.4 | 785 | 149.3 | 1285.1 |
| S-5 | 18 | 69.2 | 187 | 437 | 437 | 125.3 | 1079.1 |

Figure 6-30 shows the progressive collapse capacity curves for all specimens, which were obtained based on energy approach proposed by Izzuddin (2008). It is clear from Figure 6-30 that the increase in the span to depth ratio causes a significant decrease in the progressive collapse capacity. Specimens with (18) span to depth ratio attained their maximum capacity at catenary action stage, while for the specimens with (12) and (15) span to depth ratios, their maximum capacities were attained during CAA.

Based on the GSA requirements, the applied load combination of (D.L. + 0.25L.L.) should be considered in the event of progressive collapse. It is clear from Figure 6-30 that all specimens were not able to provide sufficient capacity to resist the load demand.



Figure 6-30: Pseudo-static response for all specimens, (a) Group 1, (b) Group 2

Table 6-6 summarises the progressive collapse capacities for all specimens. Progressive collapse capacity of specimens with span to depth ratios of 12 are greater by about 26-36% than the capacity of specimen with span to depth ratios of 15. Progressive collapse capacities fall by about 36-38% when the span to depth ratio increases from 12 to 18. For the same span to depth ratio, i.e. 12, the progressive collapse capacity increased by 14% when the beam depth increased from 450 mm to 560 mm.

For specimens with span to depth ratios of 18, the effect of beam depth on the progressive collapse capacity can be neglected. This means that for high span to depth ratios, changing beam depth has no great effect on progressive collapse capacity.

The middle joint displacement at which the specimen attained its maximum capacity increased when span to depth ratio increased.

Table 6-6: Progressive Collapse Capacities for all specimens, group (1) and (2)

| Specimen | $L$ (mm) | $d$ (mm) | L/d | Progressive Collapse Capacity | | $\dfrac{P_{s-1} - P}{P_{s-1}}$ %|
|---|---|---|---|---|---|---|
| | | | | $P$ (kN) | MJD (mm) | |
| S-1 | 5400 | 450 | 12 | 85.5 | 331 | 0.0 |
| S-2 | 6750 | 450 | 15 | 63.4 | 365 | 26 |
| S-3 | 8100 | 450 | 18 | 55.1 | 1290 | 36 |
| S-4 | 6750 | 560 | 12 | 97.3 | 381 | -14 |
| S-5 | 6750 | 375 | 18 | 53.4 | 1079 | 38 |

## 6.7.2 EFFECT OF TOP AND BOTTOM REINFORCEMENT RATIO

In order to investigate the effect of steel reinforcement ratio on the progressive collapse capacity, an additional four specimens with different top and bottom reinforcement ratios were considered and compared with specimen S-1 in this section. The specimens were divided into two groups according to the location of the reinforcement considered as listed in table 6-4. Figure 6-31 illustrates the effect of the steel reinforcement ratio on the progressive collapse capacity.
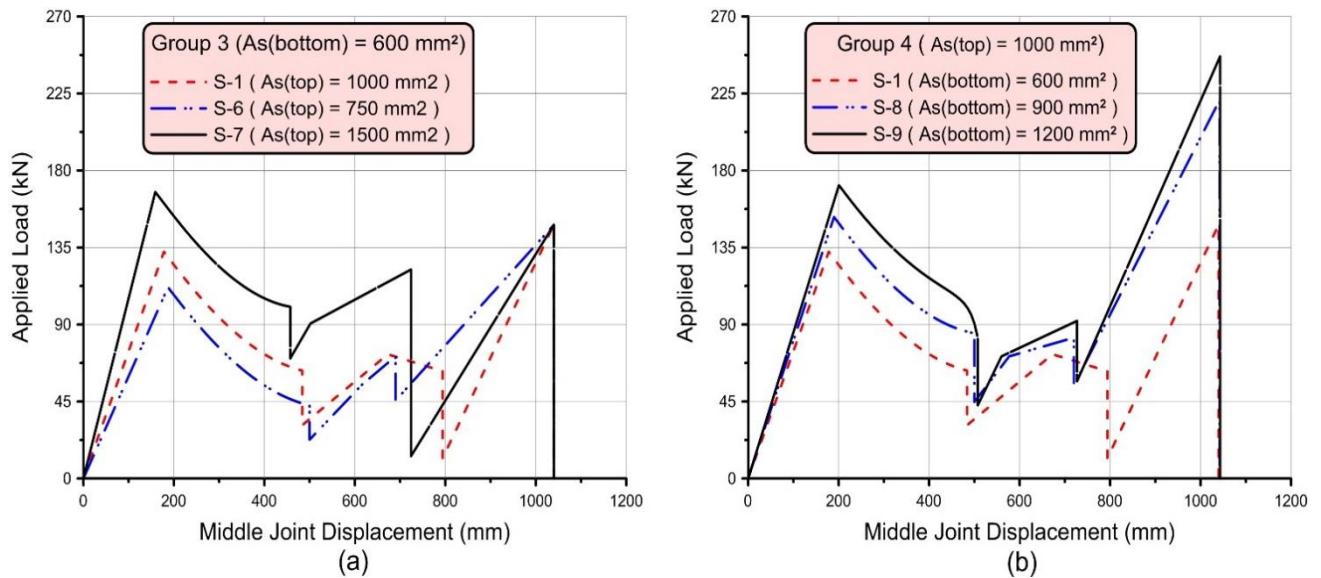
Figure 6-31: Comparison of applied load-displacement relationship, (a) Group 3, (b) Group 4

From group (3), the effect of top reinforcement ratio on the structural response was limited at CAA, while for group (4) the bottom reinforcement ratio has affected both CAA and catenary action stages. In group (3), the stiffness and ultimate load at CAA were increased when the top reinforcement content increased. However, in group (4) the ultimate load at CAA and catenary action were increased when the bottom reinforcement ratio increased.

Due to the similarity in beam dimensions and geometry, the final deflection for all specimens was nearly the same. For all specimens except S-9, the fracture of the bottom reinforcement at the middle joint occurred first during CAA followed by the fracture of the top reinforcement at the beam ends.

For specimen S-9, the top reinforcement ratio was smaller than bottom reinforcement, which caused the top reinforcement at the beam end to fracture first followed by the fracture of bottom reinforcement at the middle joint.

As shown in Figure 6-31 (a), there is a large drop in the applied load after the fracture of the top reinforcement at the beam ends for specimen S-7. This can be explained by the large ratio of steel at the top, which could cause a large load drop when fractured.

Table 6-7 lists the critical values of the load-displacement curves for all specimens. From table 6-7, for the same bottom reinforcement ratio, the applied load at CAA increased by 18% and 26% when the top reinforcement ratio increased from 0.5% to 0.67% and 0.67% to 1.0% respectively.

Table 6-7: Critical values of load-displacement curves for group (3) and (4)

| Specimen | $A_s^{top}$ % | $A_s^{Bottom}$ % | Max. load at CAA | | At the onset of Catenary Action | | Max. Load at Catenary Action | |
|---|---|---|---|---|---|---|---|---|
| | | | $P_{com}$ (kN) | MJD (mm) | $P$ (kN) | MJD (mm) | $P_{cat}$ (kN) | MJD (mm) |
| S-6 | 0.5 | 0.4 | 111.7 | 187 | 54.6 | 615 | 148.2 | 1039.7 |
| S-1 | 0.67 | 0.4 | 132.5 | 178 | 72.6 | 673 | 148.2 | 1039.7 |
| S-7 | 1.0 | 0.4 | 167.5 | 159 | 90.6 | 502 | 148.2 | 1039.7 |
| S-8 | 0.67 | 0.6 | 152.8 | 189.8 | 71.4 | 577 | 221.2 | 1042.3 |
| S-9 | 0.67 | 0.8 | 171.3 | 200.6 | 71.4 | 560 | 246.7 | 1043.2 |

For specimens with the same top reinforcement ratio, the applied load at CAA increased by about 15% when the bottom reinforcement ratio increased by 50%. At catenary action, the applied load increased by 66% when the bottom reinforcement ratio increased by 100%, and this increase was only for group (4).

Figure 6-32 shows the converted non-linear behaviour of all specimens in both group. It is clear from Figure 6-32 that the increase in top and bottom reinforcement ratio cause a significant increase in the progressive collapse capacity.

Specimens S-6, S-8 and S-9 attained their maximum capacity at catenary action stage, while for specimens S-1 and S-7, their maximum capacity was attained during CAA. The common point between S-6, S-8 and S-9 is that the top and bottom reinforcement ratios were close to each other. However, the difference between the top and bottom reinforcement ratios for S-1 and S-7 was larger than those for specimens S-6, S-8 and S-9.

Specimens S-7, S-8 and S-9 were able to provide the structure with the required progressive collapse capacity according to the applied load proposed by GSA. This confirms the need for the additional steel reinforcement in the beam section in order to increase the resistance of RC structures against progressive collapse. This conclusion is similar to the conclusion made by many researchers that seismic detailing can significantly increase the progressive collapse capacity.
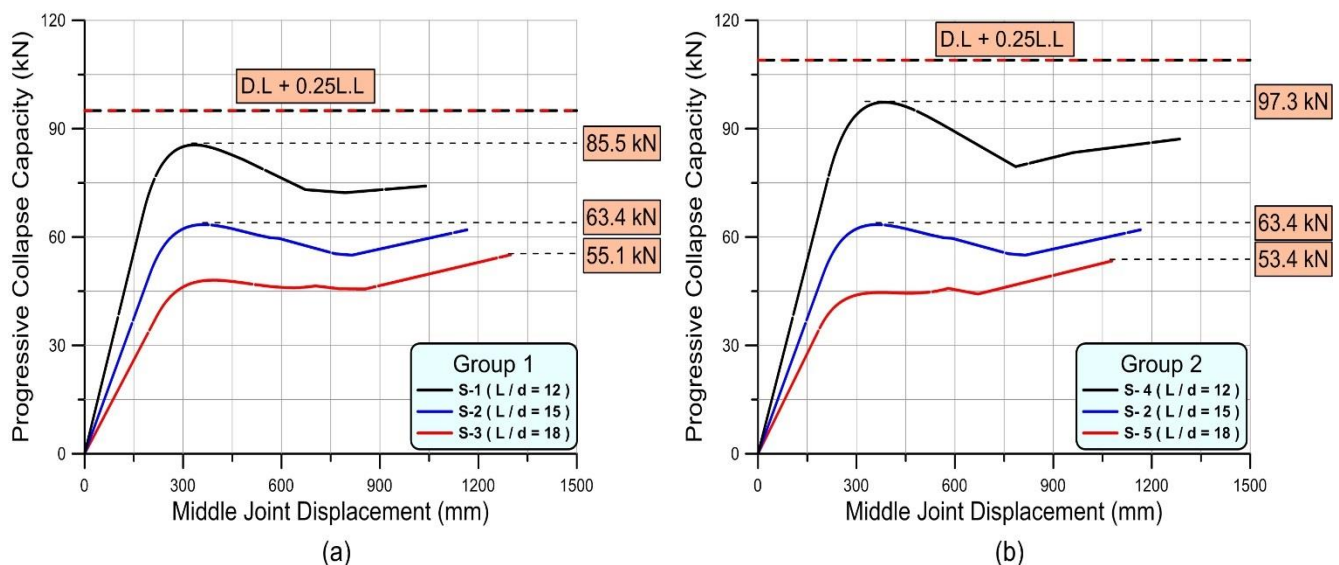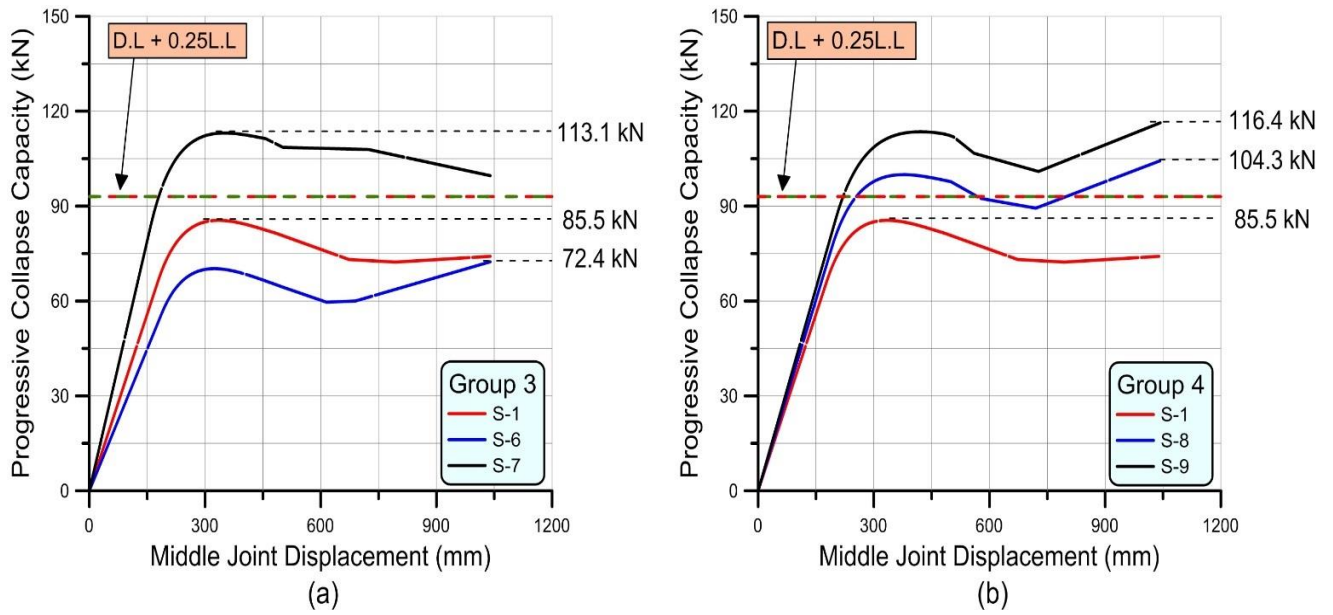
Figure 6-32: Pseudo-static response for all specimens, (a) Group 3, (b) Group 4

Table 6-8 summarises the progressive collapse capacities for all specimens. For specimens with the same bottom reinforcement ratio, the progressive collapse capacity has increased by about 56% when the top reinforcement ratio increased from 0.5% to 1.0%.

By keeping the top reinforcement ratio, the same, the increase in bottom reinforcement ratio from 0.4% to 0.8% increases the capacity by about 36%. From this significant increase, it can be concluded that the progressive collapse capacity relies significantly on the steel reinforcement ratio.

Table 6-8: Progressive Collapse Capacities for all specimens, group (3) and (4)

| Specimen | $A_s^{top}$ % | $A_s^{Bottom}$ % | Progressive Collapse Capacity | | $\dfrac{P - P_{s-1}}{P_{s-1}}$ % |
|---|---|---|---|---|---|
| | | | $P$ (kN) | MJD (mm) | |
| S-6 | 0.5 | 0.4 | 72.4 | 1040 | -15 |
| S-1 | 0.67 | 0.4 | 85.5 | 331 | 0.0 |
| S-7 | 1.0 | 0.4 | 113.1 | 347 | 32 |
| S-8 | 0.67 | 0.6 | 104.3 | 1042 | 22 |
| S-9 | 0.67 | 0.8 | 116.4 | 1043 | 36 |

## 6.8 SUMMARY AND CONCLUSION

In this chapter, an analytical model to predict the structural behaviour of RC beams subjected to column removal was proposed. Both CAA and catenary action were incorporated in this model. The development of the model equations was based on the concepts of equilibrium, compatibility, and material properties.

During the experimental tests, bar fracture at the middle joint and the beam ends occurred. Therefore, a system of equations was developed and included in this model to predict the bar fracture and their corresponding load and vertical deflection. The reduction in the effective beam depth due to concrete crushing, which occurs after the concrete has attained its maximum strain, was also included in this model.

Following on, a comparison with the experimental results was conducted. A parametric study was carried out to investigate the effect of several parameters on the structural behaviour of RC beams under the removal of the middle column.

 The following summarises the main findings of this chapter:

1.The comparison made between the experimental and analytical results showed the ability of the proposed model to evaluate and predict the structural behaviour of RC beams in the event of progressive collapse.

2. The analytical model was able to predict and evaluate the occurrence of bar fracture at both CAA and catenary action. The analytical model considers the beam under investigation as a homogenous material and geometry. Based on this, the fracture of all steel reinforcement in the same layer occurs simultaneously. Although it is a rare occurrence in the actual event, it is considered as the worst scenario possible, and the analytical prediction gives the lower bound of progressive collapse capacity.

3. Parametric studies showed that the increase in the span to depth ratio causes a decrease in the ultimate capacity, while the increase in the top and bottom reinforcement ratio increases the ultimate capacity.

4. Bar fracture could be avoided during CAA by increasing the span to depth ratio. Increasing span to depth ratio leads to a decrease in the ultimate capacity, which can be compensated by increasing the top or bottom reinforcement ratio.

5. Parametric studies showed that the beams designed with the conventional design were not able to withstand the required applied load suggested by GSA. With the increase in the longitudinal reinforcement ratio, the beams were able to resist the applied load suggested by GSA. This demonstrates the need for the additional reinforcement to prevent or reduce the probability of progressive collapse in RC structures.

## 7. CHAPTER SEVEN     CONCLUSIONS AND RECOMMENDATIONS

### 7.1 GENERAL

Progressive collapse of RC structures, which can result from a local failure of a member or column loss, has not been explicitly included in the design guidelines in the last few decades. Local failure or column loss in RC structures is usually caused by extreme loadings, such as explosions, failure of support and/or design errors. Records have shown that the progressive collapse of buildings leads to catastrophic hazards causing loss of structural integrity and human lives.

In this study, the structural behaviour of RC structures subjected to CRS has been investigated. Thereafter, a new scheme to mitigate progressive collapse was proposed and the effect of the new scheme on the progressive collapse resisting capacity was investigated. The study was divided into three main programs, experimental, numerical and analytical studies.

The experimental study comprised of testing eight RC beam-column specimens, three specimens designed and detailed in accordance with conventional rules and five specimens reinforced with modified steel detailing as proposed by the new scheme. A comparison has been made between the specimens to understand the effect of the proposed new scheme to mitigate progressive collapse and improve global structural behaviour at limit state.

The numerical study was conducted to simulate the structural behaviour of these specimens. A macro-model was developed and proposed to simulate the critical sections at which the failure occurred. Bond slip and bar fracture were included in the macro-model which was implemented in the finite element software package ANSYS 11.0.

The analytical study was presented and a model created to predict the structural behaviour of RC sub-assemblages was proposed and developed. The development of the equations for the model was based on the concepts of equilibrium, compatibility, and material properties. The model is comprised of two distinct of behaviour, CAA model and catenary action model. The novelty of the model is the ability to predict the bar fracture and the reduction in effective beam depth due to concrete crushing. Based on the theoretical models, a parametric study was conducted to understand the effect of different parameters on the structural behaviour and progressive collapse capacity of RC structures in the event of middle column loss.

## 7.2 CONCLUSIONS

The conclusions are divided into four main sections, i.e. global level behaviour, local level behaviour, numerical modelling and theoretical modelling conclusions. The global level behaviour includes the structural behaviour in terms of applied load vs. MJD relationship, axial forces vs. MJD relationship and the converted Pseudo-Static relationship. Local level behaviour includes the internal forces developed in the reinforcing steel bars during the development of different structural mechanisms under the middle CRS.

## 7.2.1 CONCLUSIONS AT GLOBAL LEVEL

1- All specimens experienced three stages of resisting mechanisms, flexural, CAA and catenary action. The behaviour was dominated by flexure in the early stages of the response. With increased vertical displacement of the centre column, resistance was provided through the development of compressive diagonal axial forces or "arching action" due to the restraint on the axial elongation of the beams by the end columns. With further increase in the vertical displacement, the tensile axial forces developed in the beams and the behaviour was dominated by catenary action.

2- There is no clear transition point from flexural to CAA due to the fact that the restraint beams can develop CAA even at early stages. The transition point from CAA to catenary action was indicated by the change in axial forces from compression to tension. The onset of catenary action stage occurred at a MJD equal to $0.98h – 1.13h$.

3- The compressive forces generated at the ends of the RC beam-column specimen, during the first stage of the response, increases the load resistance capacity of the beam by increasing the ultimate moment capacities of the beam critical sections. CAA capacity was 15.5% - 21.5 % larger than flexural capacity calculated based on the plastic hinge analysis. At catenary action stage, on the top of CAA, the resisting capacity was increased by up to 103% for specimens with the new scheme modified detailing.

4- CAA attained its capacity at a relatively small deflection compared to catenary action. At a MJD of about $0.35h$, the specimens attained their maximum capacity for CAA, while the MJD was about $1.75h – 2.23h$ for the catenary action stage.

5- The failure of all specimens was characterised by (1) Crushing of concrete at compression zones during flexural action. (2) Development of flexural cracking during flexural and CAA. (3) Bar fracture at beam-column interfaces. (4) Large slippage between concrete and steel bars accompanied by wide cracks at critical sections.

6- Compared with specimen SS-3, the capacity of specimens with the modified detailing was 5% - 12% larger at CAA, while it was larger by about 48% - 109% at catenary action. Specimen SS-4 attained the largest ratio at CAA and the largest ratio was for specimen SS-5 attained at catenary action.

7- Setting partial hinges can increase the ductility and final MJD of RC structures. This means that the rotational capacity is increased, and it increases the vertical projection of the axial force. The largest MJD at the end of the test was for specimen SS-8.

8- Pseudo-static results suggest that the presence of additional steel bars can increase progressive collapse capacity, and the maximum capacity can be attained when placing two additional steel bars at a distance of $(d - d')/4$ from the centre of the bottom reinforcement. The increase in progressive collapse capacity was 22% - 67%.

9- Pseudo-static results suggest that the presence of partial hinges can increase the progressive collapse capacity by 34% - 44%.

10- Pseudo-static results suggest that the addition of steel bars near the top reinforcement will be dangerous in the event of progressive collapse unless the specimen can provide more resistance at catenary action stage. It also suggests that the setting of partial hinges at a distance equal to the beam depth is not preferable due to the lowest enhancement at catenary action stage.

## 7.2.2 CONCLUSIONS AT LOCAL LEVEL

1- Experimental results showed that the bottom bars experienced tensile strains at the specimen ends, and yielded in tension, during the last stage of the beam tensile membrane action, despite the fact that the bottom bars fractured earlier at the middle joint interfaces. This indicates that the increasing tensile stresses at the level of the top bars (developed due to catenary action of the top bars), were transferred to the bottom bars through concrete bond and remaining anchorage.

2- The tensile forces developed during catenary action were carried mainly by steel bars, while the contribution of concrete to the compression forces at CAA was about 50%.

3- The bottom bars were more vulnerable to fracture at early stages in the event of progressive collapse due to sudden impact of gravity loads. The additional bars near the bottom bars can reduce the probability of early bottom bar fracture due to load sharing and increased tensile capacity, and then reduce the probability of progressive collapse.

4- The presence of additional steel bars enhanced the tensile capacity at catenary action stage by about 59% - 110%, and the enhancement to the CAA was very limited.

5- The presence of partial hinges enhanced the bottom bars at an early stage of loading due to additional bent bars. The contribution of partial hinges to axial tension capacity was limited because of the top bars already present from the original design.

## 7.2.3 CONCLUSIONS TO THE NUMERICAL WORK

1- Macro-models consisting of beam and spring elements can accurately predict the response characteristics of RC beam-column sub-assemblages. Furthermore, the macro-models developed in this study will be valuable in the analysis of complete structural systems for assessing the progressive collapse capacity.

2- Compared to experimental results, numerical results underestimate the applied load and axial forces throughout the beam. This can be explained by many factors related to experimental studies, such as the presence of friction due to restraints and the imperfections of the constructed specimens. experimental uncertainties in measurement are also one of the factors which contribute to the differences observed between experimental and numerical results.

## 7.2.4 CONCLUSIONS TO THE ANALYTICAL WORK

1- The ability of the proposed model to predict the structural behaviour of the RC structure under CRS was verified through the comparison between the experimental and analytical results. The model was able to predict the bar fracture during the event of progressive collapse. The model considers that the beam material is homogeneous and the geometry is uniform, also it considers perfect specimen fabrication. The model assumes the fracture of all steel reinforcement within the same layer occurs simultaneously.

2- Based on the first conclusion, the model is considered to give the lower bound value of progressive collapse capacity. This is because the situation of fracture of all steel reinforcement within the same layer is considered the worst scenario possible in the event of column loss.

3- The parametric study showed that the span to depth ratio can significantly affect the progressive collapse resistance in RC structures. An increase in span to depth ratio causes a decrease in the ultimate capacity against progressive collapse.

4- The parametric study showed that the steel ratio of the top and bottom reinforcement has a marked effect on the progressive collapse capacity of the RC structure. An increase in the top and /or the bottom reinforcement ratio can significantly increase the ability of RC structure to resist progressive collapse.

5- The parametric study showed that it is possible to avoid fracture of steel reinforcement at early stages after column loss or damage by increasing the span to depth ratio. This increase in span to depth ratio will decrease the progressive collapse capacity which can then be increased again by increasing steel reinforcement ratio. Further experimental and analytical studies are required to obtain the balance point between span to depth ratio and steel reinforcement ratio for the optimum performance of an RC structure under a column loss event.

## 7.3 RECOMMENDATIONS FOR PRACTICE

Based on the above conclusions and until the date of this research, some recommendations can be summarised for engineering practice as follows:

1- RC Structures designed according to the conventional design may not be able to withstand the structural demand of progressive collapse. This is because that the abnormal loading is not considered in the process of conventional design.

2- In order to prevent or at least reduce the probability of progressive collapse, a steel reinforcement layer of minimum two steel bars of the same size of the main reinforcement, should be placed at an elevation of $(d - d')/4$ above the bottom reinforcement. This layer can absorb any sudden redistribution of load after the fracture of the bottom reinforcement at the middle joint.

3- Additional steel reinforcement at the top quarter of the beam section should be avoided. This is because that the additional steel reinforcement in the compression zone could accelerate the bar fracture in the tension zone, which may release additional energy due to load redistribution and cause progressive collapse.

4- An economic balance between span to depth ratio and the steel reinforcement ratio should be obtained. This balance would ensure that all steel reinforcements could remain intact at the early stages of column loss, and at the same time, maintain an optimum progressive collapse capacity.

## 7.4 RECOMMENDATION FOR FUTURE STUDY

Several questions have been raised during the period of the research need to be answered and investigated. The following summarises the recommendations for future studies in both the experimental and analytical work:

1- At the beginning of this research, the plan was to test 24 specimens divided into two groups. Twelve specimens were intended to be tested under static loading and the other twelve specimens to be tested under dynamic loading. Due to limitations in lab resources, time and funding, the total number was reduced to eight specimens to be tested under static loading only.

Due to the fact that the progressive collapse is a dynamic event, it is recommended to conduct dynamic tests to better understand the structural behaviour of RC structures under column loss or damage.

2- To increase experimental data results of RC sub-assemblages reinforced with the proposed new scheme, further static tests are recommended. Extra experimental results with the data available could evaluate the enhancement of the additional steel reinforcement bars, more accurately.

3- More experimental tests are required using other different types of concrete, such as lightweight concrete and high strength concrete. This is because that many high-rise buildings were constructed from lightweight and high strength concrete.

4- Global F.E. models for the whole RC building are needed to better understand the structural behaviour under CRS. Incorporating a macro-model and the additional steel reinforcement with these models, evaluation of the structural capacity against progressive collapse can be examined.

5- Conducting numerical analysis using other different F.E. software such as DIANA and ABAQUS, and incorporating macro-model approached.

6- Development of the analytical model, proposed in this study, to incorporate the effect of the additional steel reinforcement, are required. This can be made after conducting additional experimental tests to increase the available data.

# APPENDIX

## DERIVATION OF THE COMPATIBILITY EQUATION (6 – 20)
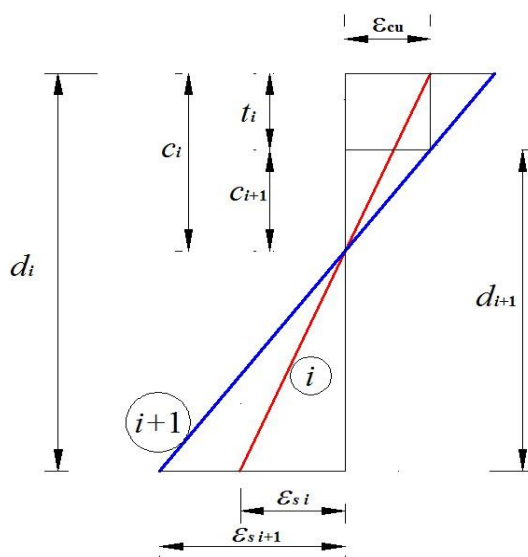


$$c_i = \frac{L\,\varepsilon_{cu}d_i}{\delta_i} \quad , \quad c_{i+1} = \frac{L\,\varepsilon_{cu}d_{i+1}}{\delta_{i+1}} \qquad\qquad (6 - 18)$$

$$t_i = c_i - c_{i+1} \qquad\qquad (6 - 19)$$

$$t_i = \frac{L\,\varepsilon_{cu}d_i}{\delta_i} - \frac{L\,\varepsilon_{cu}d_{i+1}}{\delta_{i+1}} = \frac{L\,\varepsilon_{cu}(d_i\,\delta_{i+1} - d_{i+1}\,\delta_i)}{\delta_i\,\delta_{i+1}} \;, \quad d_{i+1} = d_i - t_i$$

$$t_i = \frac{L\,\varepsilon_{cu}(d_i\,\delta_{i+1} - d_i\,\delta_i + t_i\,\delta_i)}{\delta_i\,\delta_{i+1}} = \frac{L\,\varepsilon_{cu}\,d_i(\delta_{i+1} - \delta_i)}{\delta_i\,\delta_{i+1}} + \frac{L\,\varepsilon_{cu}t_i}{\delta_{i+1}}$$

$$t_i - \frac{L\,\varepsilon_{cu}t_i}{\delta_{i+1}} = \frac{L\,\varepsilon_{cu}\,d_i(\delta_{i+1} - \delta_i)}{\delta_i\,\cancel{\delta_{i+1}}} = t_i\left(\frac{\delta_{i+1} - L\,\varepsilon_{cu}}{\cancel{\delta_{i+1}}}\right)$$

$$t_i = \frac{L\,\varepsilon_{cu}d_i}{\delta_i} * \frac{\delta_{i+1} - \delta_i}{\delta_{i+1} - L\,\varepsilon_{cu}} \qquad\qquad (6 - 20)$$

DERIVATION OF THE COMPATIBILITY EQUATION $(6 - 44)$

$$\delta^2 + (L + u)^2 = (L - c_m \tan(\theta) + (h - c_e)\tan(\theta))^2 \qquad \text{(6 - 41)}$$

$$\delta^2 + L^2 + 2Lu + u^2 = [L + (h - c_e - c_m)\tan(\theta)]^2$$

$u^2 \to 0$ *because it is very small value*

Assume $Z = h - c_e - c_m$ and replace it, we get:

$$\delta^2 + L^2 + 2Lu = [L + Z\tan(\theta)]^2$$

*By substituting* $\qquad \tan(\theta) = \dfrac{\delta}{L + u} \qquad$ *we get:*

$$\delta^2 + L^2 + 2Lu = \left[L + \frac{\delta Z}{L + u}\right]^2$$

$$\delta^2 + \cancel{L^2} + 2Lu = \cancel{L^2} + \frac{2L\delta Z}{L + u} + \frac{\delta^2 Z^2}{(L + u)^2}$$

*This value* $\dfrac{\delta^2 Z^2}{(L + u)^2}$ *is too small and can be neglected without affecting the results*

$$\delta^2 + 2Lu = \frac{2L\delta Z}{L + u}$$

$$Z = \frac{L + u}{2L\delta}(\delta^2 + 2Lu)$$

$$Z = \frac{\delta^2 L + 2L^2 u + \delta^2 u + \cancel{2Lu^2}}{2L\delta}$$

$2Lu^2$ *is a small value and can be neglected*

$$Z = \frac{\delta^2 \cancel{L}}{2 \cancel{L\delta}} + u \left( \frac{2L^2 + \delta^2}{2L\delta} \right)$$

$$Z = h - c_e - c_m = \frac{\delta}{2} + u \left( \frac{2L^2 + \delta^2}{2L\delta} \right)$$

*By substituting* $u = \dfrac{N}{K}$ *and rearranging we get:*

$$c_e + c_m = h - \frac{\delta}{2} - \frac{N}{K} \left( \frac{2L^2 + \delta^2}{2L\delta} \right) \qquad (6-44)$$

# REFERENCES

BS 8110-1:1997. Structural Use of Concrete". Part 1: Code of Practice for Design".

ABEDI, K. & PARKE, G. 1996. Progressive collapse of single-layer braced domes. *International Journal of Space Structures,* 11 (3)**,** 291-306.

ABRAMS, D. P. 1987. Scale relations for reinforced concrete beam-column joints. *ACI structural Journal,* 84 (6)**,** 502-512.

ACI-318. Building code requirements for structural concrete (ACI 318-05) and commentary (ACI 318R-05). 2002. American Concrete Institute.

AHMADI, R., RASHIDIAN, O., ABBASNIA, R., MOHAJERI NAV, F. & USEFI, N. 2016. Experimental and Numerical Evaluation of Progressive Collapse Behavior in Scaled RC Beam-Column Subassemblage. *Shock and Vibration,* 2016**,** Article ID 3748435, 17 pages.

ALATH, S. & KUNNATH, S. K. Modeling inelastic shear deformation in RC beam-column joints. Engineering Mechanics (1995), 1995. ASCE, 822-825.

ALLEN, D. E., AND SCHRIEVER, W. R. 1972. Progressive Collapse, Abnormal Loads, and Building Codes. *Proceedings ASCE National Meeting on Structural Engineering,Cleveland, Ohio***,** 21-47.

ALMUSALLAM, T., MENDIS, P., NGO, T., ELSANADEDY, H., ABBAS, H., ALSAYED, S., AL-SALLOUM, Y. & AL-HADDAD, M. 2010. Progressive Collapse Analysis of a Typical RC Building of Riyadh. *Proceedings of the IMPLAST 2010 Conference,* October 12-14 2010 Providence, Rhode Island USA.

ALSIWAT, J. M. & SAATCIOGLU, M. 1992. Reinforcement anchorage slip under monotonic loading. *Journal of Structural Engineering,* 118 (9)**,** 2421-2438.

ASCE 2005. *Minimum Design Loads for Buildings and Other Structures*, ASCE Publications.

ASTANEH-ASL, A. Progressive collapse prevention in new and existing buildings. Proc., 9th Arab Structural Engineering Conf., Abu Dhabi, UAE, Nov, 2003.

ASTM-A370 2005. Standard test methods and definitions for mechanical testing of steel products. ASTM International: West Conshohocken, PA.

BAO, Y., KUNNATH, S. K., EL-TAWIL, S. & LEW, H. 2008. Macromodel-based simulation of progressive collapse: RC frame structures. *Journal of Structural Engineering,* 134 (7)**,** 1079-1091.

BREEN, J. E. 1975. Research Workshop on Progressive Collapse of Building Structures, Held at the University of Texas at Austin. *November 18-20, 1975*.

BS1881-116 1983. Testing concrete. Method for determination of compressive strength of concrete cubes.

BS1881-118 1983. Method for determination of flexural strength.

BS1881-121 1983. Method for determination of static modulus of elasticity in compression.

BSI BS5950-1 2000. Structural Use of Steelwork in Buildings": Code of Practice for Design: Rolled and Welded Sections. *London, England, 1985.*

BYFIELD, M., DE MATTEIS, G. & DINU, F. 2007. Robust design of steel framed buildings against extreme loading. *Proc. Cost C26,* 253-267.

BYFIELD, M. & PARAMASIVAM, S. 2007. Catenary action in steel-framed buildings. *Proceedings of the ICE-Structures and Buildings,* 160 (5), 247-257.

CEB-FIP 2000. Bond of reinforcement in concrete: state-of-art report. *FIB Bulletin 10, CEB-FIP.*

CHOI, H. & KIM, J. 2010. Progressive collapse-resisting capacity of RC beam–column sub-assemblage. *magazine of concrete research,* 63 (4), 297-310.

CHOI, H. & KIM, J. 2011. Progressive collapse-resisting capacity of RC beam–column sub-assemblage. *magazine of concrete research,* 63, 297-310.

CHRISTIANSEN, K. 1963. The effect of membrane stresses on the ultimate strength of the interior panel in a reinforced concrete slab. *The Structural Engineer,* 41 (8), 261-265.

CORLEY, W. G., SR, P. F. M., SOZEN, M. A. & THORNTON, C. H. 1998. The Oklahoma City bombing: Summary and recommendations for multihazard mitigation. *Journal of Performance of Constructed Facilities,* 12 (3), 100-112.

CRAWFORD, J. E. Retrofit methods to mitigate progressive collapse. The Multihazard Mitigation Council of the National Institute of Building Sciences, Report on the July 2002 National Workshop and Recommendations for Future Effort, 2002.

DAT, P. X., HAI, T. K. & JUN, Y. 2015. A simplified approach to assess progressive collapse resistance of reinforced concrete framed structures. *Engineering Structures,* 101, 45-57.

DEPUTY, L. & STORY, B. 2015. Progressive Collapse Mitigation: Geometrically Nonlinear Catenary Behavior. *PROCEEDINGS AEI 2015,* 185-196.

DOD 2005. Design of Buildings to Resist Progressive Collapse. *Unified Facilities Criteria (UFC). Department of Defense*

ELIGEHAUSEN, R., POPOV, E. P. & BERTERO, V. V. 1982. Local bond stress-slip relationships of deformed bars under generalized excitations. *Report UCB/EERC-83/23, Earthquake Engineering Research Center. University of California, Berkeley, California, U.S.*

ELLINGWOOD, B., MARJANISHVILI, S., MLAKAR, P., SASANI, M. & WILLIAMSON, E. 2009. Disproportionate collapse research needs. *Proceedings of the Structures*, 1896-1907.

EYRE, J. 1990. Flow rule in elastically restrained one-way spanning RC slabs. *Journal of Structural Engineering,* 116 (12), 3251-3267.

EYRE, J. R. 1997. Direct assessment of safe strengths of RC slabs under membrane action. *Journal of Structural Engineering,* 123 (10), 1331-1338.

FARHANGVESALI, N., VALIPOUR, H., SAMALI, B. & FOSTER, S. 2013. Development of arching action in longitudinally-restrained reinforced concrete beams. *Construction and Building Materials,* 47, 7-19.

FEMA(277) 1996. The Oklahoma City Bombing: Improving Building Performance Through Multi-Hazard Mitigation / Mitigation Assessment Team Report. Augost 1996.

FLEURY, F., REYNOUARD, J.-M. & MERABET, O. 2000. Multicomponent model of reinforced concrete joints for cyclic loading. *Journal of engineering mechanics,* 126 (8), 804-811.

GOTO, Y. Cracks formed in concrete around deformed tension bars. ACI Journal Proceedings, 1971. ACI.

GSA 2003. Progressive Collapse Analysis and Design Guidelines. *U.S. General Services Administration.*

HADI, M. N. & ALRUDAINI, T. M. S. 2012. A new cable system to prevent progressive collapse of reinforced concrete buildings. *Structures Congress 2012 © ASCE 2012*, 257-267.

HARTMANN, D., BREIDT, M., STANGENBERG, F., HÖHLER, S., SCHWEIZERHOF, K., MATTERN, S., BLANKENHORN, G., MÖLLER, B. & LIEBSCHER, M. 2008. Structural collapse simulation under consideration of uncertainty–Fundamental concept and results. *Computers & Structures,* 86 (21), 2064-2078.

HASKETT, M., OEHLERS, D. J. & ALI, M. M. 2008. Local and global bond characteristics of steel reinforcing bars. *Engineering Structures,* 30 (2), 376-383.

HASKETT, M., OEHLERS, D. J., ALI, M. M. & WU, C. 2009. Rigid body moment–rotation mechanism for reinforced concrete beam hinges. *Engineering Structures,* 31, 1032-1041.

IZZUDDIN, B. 2005. A simplified model for axially restrained beams subject to extreme loading. *International Journal of Steel Structures,* 5 (5), 421-429.

IZZUDDIN, B. & ELGHAZOULI, A. 2004. Failure of lightly reinforced concrete members under fire. I: Analytical modeling. *Journal of Structural Engineering,* 130 (1), 3-17.

IZZUDDIN, B., VLASSIS, A., ELGHAZOULI, A. & NETHERCOT, D. 2008. Progressive collapse of multi-storey buildings due to sudden column loss—Part I: Simplified assessment framework. *Engineering Structures,* 30**,** 1308-1318.

JASPART, J.-P. 2000. General report: session on connections. *Journal of Constructional Steel Research,* 55**,** 69-89.

JIAN, H. & ZHENG, Y. 2014. Simplified Models of Progressive Collapse Response and Progressive Collapse-Resisting Capacity Curve of RC Beam-Column Substructures. *Journal of Performance of Constructed Facilities,* 28 (4)**,** 04014008.

JOHANSEN, K. 1943. Yield-Line Formulae for Slabs, Cement and Concrete Association. *London, UK.*

KIM, J. & CHOI, H. 2015. Monotonic Loading Tests of RC Beam-Column Subassemblage Strengthened to Prevent Progressive Collapse. *International Journal of Concrete Structures and Materials,* 9 (4)**,** 401-413.

KIM, J. & SHIN, W. S. 2011. Retrofit of RC frames against progressive collapse using prestressing tendons. *The Structural Design of Tall and Special Buildings,* 22 (4)**,** 349-361.

KIM, J. & YU, J. 2012. Analysis of reinforced concrete frames subjected to column loss. *Magazine of Concrete Research,* 64 (1)**,** 21-33.

KRAUTHAMMER, T., HALL, R. L., WOODSON, S. C., BAYLOT, J. T., HAYES, J. R. & SOHN, Y. 2002. Development of progressive collapse analysis procedure and condition assessment for structures. DTIC Document.

LI, Y., LU, X., GUAN, H. & REN, P. 2016. Numerical investigation of progressive collapse resistance of reinforced concrete frames subject to column removals from different stories. *Advances in Structural Engineering,* 19 (2)**,** 314-326.

LI, Y., LU, X., GUAN, H. & YE, L. 2011. An improved tie force method for progressive collapse resistance design of reinforced concrete frame structures. *Engineering Structures,* 33 (10)**,** 2931-2942.

LI, Y., LU, X., GUAN, H. & YE, L. 2014. Progressive Collapse Resistance Demand of Reinforced Concrete Frames under Catenary Mechanism. *ACI Structural Journal,* 111 (5).

LONG, X. 2013. *Numerical study on reinforced concrete beam-column frames in progressive collapse.* NANYANG TECHNOLOGICAL UNIVERSITY.

LOWES, L. N., ALTOONTASH, A. & MITRA, N. 2003a. "Modeling Reinforced-Concrete Beam-Column Joints Subjected to Cyclic Loading" by Laura N. Lowes and Arash Altoontash. *Journal of Structural Engineering,* 131 (6)**,** 993-994.

LOWES, L. N., MITRA, N. & ALTOONTASH, A. 2003b. *A beam-column joint model for simulating the earthquake response of reinforced concrete frames*, Pacific Earthquake Engineering Research Center, College of Engineering, University of California.

MATTOCK, A. H. 1965. Rotational capacity of hinging regions in reinforced concrete beams. *Special Publication,* 12**,** 143-181.

MCDOWELL, E., MCKEE, K. & SEVIN, E. 1956. Arching action theory of masonry walls. *Journal of the Structural Division,* 82 (2)**,** 1-8.

MEROLA, R. 2009. *Ductility and robustness of concrete structures under accidental and malicious load cases, PhD Thesis.* The University of Birmingham.

MINISTER, O. O. T. D. P. 2004. The Building Regulations 2000, Approved Document A Structure. *NBS, pp. 39.*

MITCHELL, D. & COOK, W. D. 1984. Preventing progressive collapse of slab structures. *Journal of Structural Engineering,* 110 (7)**,** 1513-1532.

MITRA, N. 2007. An analytical study of reinforced concrete beam-column joint behavior under seismic loading. *PhD dissertation, University of Washington.*

MOHAJERI NAV, F., ABBASNIA, R., RASHIDIAN, O. & USEFI, N. 2016. Theoretical Resistance of RC Frames under the Column Removal Scenario Considering High Strain Rates. *Journal of Performance of Constructed Facilities,* 30 (5)**,** 1-12.

MOHAMED, O. A. 2006. Progressive collapse of structures: annotated bibliography and comparison of codes and standards. *Journal of performance of constructed facilities,* 20 (4)**,** 418-425.

MOHAMED, O. A. 2009. Assessment of progressive collapse potential in corner floor panels of reinforced concrete buildings. *Engineering Structures,* 31 (3)**,** 749-757.

NAIR, R. S. 2004. Progressive collapse basics. *Modern steel construction,* 44 (3)**,** 37-44.

NIST 2007. Best Practices for Reducing the Potential for Progressive Collapse in Buildings.". *National Institute of Standards and Technology*.

OCKLESTON, A. 1958. Arching action in reinforced concrete slabs. *The Structural Engineer,* 36 (6)**,** 197-201.

ORTON, S. 2007. Development of a CFRP System to Provide Continuity in Existing Reinforced Concrete Structures Vulnerable to Progressive Collapse. PhD thesis, Austin, Texas: The University of Texas at Austin.

PARK, R. 1964a. The ultimate strength and long-term behaviour of uniformly loaded, two-way concrete slabs with partial lateral restraint at all edges. *Magazine of concrete Research,* 16 (48)**,** 139-152.

PARK, R. & GAMBLE, W. L. 1980. *Reinforced concrete slabs*, John Wiley & Sons.

POUR, H. V., VESSALI, N., FOSTER, S. & SAMALI, B. 2015. Influence of Concrete Compressive Strength on the Arching Behaviour of Reinforced Concrete Beam Assemblages. *Advances in Structural Engineering,* 18 (8)**,** 1199-1214.

RANKIN, G. & LONG, A. 1997. Arching action strength enhancement in laterally-restrained slab strips. *Proceedings of the Institution of Civil Engineers. Structures and buildings,* 122 (4)**,** 461-467.

REGAN, P. 1975. Catenary Action in Damage Concrete Structures. *ACI Special Publication,* 48.

REN, P., LI, Y., LU, X., GUAN, H. & ZHOU, Y. 2016. Experimental investigation of progressive collapse resistance of one-way reinforced concrete beam–slab substructures under a middle-column-removal scenario. *Engineering Structures,* 118**,** 28-40.

SADEK, F., MAIN, J. A., LEW, H. & BAO, Y. 2011. Testing and analysis of steel and concrete beam-column assemblies under a column removal scenario. *Journal of Structural Engineering,* 137 (9)**,** 881-892.

SALEM, H., EL-FOULY, A. & TAGEL-DIN, H. 2011. Toward an economic design of reinforced concrete structures against progressive collapse. *Engineering Structures,* 33 (12)**,** 3341-3350.

SASANI, M. & KROPELNICKI, J. 2007. Progressive collapse analysis of an RC structure. *The Structural Design of Tall and Special Buildings,* 17 (4)**,** 757-771.

SEZEN, H. & SETZLER, E. J. 2008. Reinforcement slip in reinforced concrete columns. *ACI Structural Journal,* 105 (3).

SOZEN, M. A. & MOEHLE, J. P. 1990. Development and lap-splice lengths for deformed reinforcing bars in concrete. *Portland Cement Association, Skokie, IL, Serial,* (1891).

SU, Y., TIAN, Y. & SONG, X. 2009. Progressive Collapse Resistance of Axially-Restrained Frame Beams. *ACI Structural Journal,* 106 (5)**,** 600-607.

SUCUOGLU, H., ÇITIPITIOGLU, E. & ALTIN, S. 1994. Resistance mechanisms in RC building frames subjected to column failure. *Journal of structural engineering,* 120 (3)**,** 765-782.

TAYLOR, S., RANKIN, G. & CLELAND, D. 2001. Arching action in high-strength concrete slabs. *Proceedings of the Institution of Civil Engineers-Structures and Buildings,* 146 (4)**,** 353-362.

TIAN, Y. & SU, Y. 2011. Dynamic Response of Reinforced Concrete Beams Following Instantaneous Removal of a Bearing Column. *International Journal of Concrete Structures and Materials,* 5 (1)**,** 19-28.

TSAI, M.-H. 2010. An analytical methodology for the dynamic amplification factor in progressive collapse evaluation of building structures. *Mechanics Research Communications,* 37 (1)**,** 61-66.

WEI-JIAN, H. Q. Y. 2008. Experimental study of the collapse-resistant behavior of RC beam-column sub-structures considering catenary action [J]. *China Civil Engineering Journal,* 4**,** 010.

YI, W.-J., HE, Q.-F., XIAO, Y. & KUNNATH, S. K. 2008. Experimental study on progressive collapse-resistant behavior of reinforced concrete frame structures. *ACI Structural Journal,* 105 (4)**,** 433-439.

YIN, Y. & WANG, Y. 2005. Analysis of catenary action in steel beams using a simplified hand calculation method, Part 1: theory and validation for uniform temperature distribution. *Journal of Constructional Steel Research,* 61 (2)**,** 183-211.

YOUSSEF, M. & GHOBARAH, A. 2001. Modelling of RC beam-column joints and structural walls. *Journal of Earthquake Engineering,* 5 (01)**,** 93-111.

YU, J. & GUO, Y. 2015. Nonlinear SDOF Model for Dynamic Response of Structures under Progressive Collapse. *Journal of Engineering Mechanics,* 142 (3)**,** 04015103.

YU, J., RINDER, T., STOLZ, A., TAN, K.-H. & RIEDEL, W. 2014. Dynamic Progressive Collapse of an RC Assemblage Induced by Contact Detonation. *Journal of Structural Engineering,* 140 (6).

YU, J. & TAN, K. H. 2013. Structural behavior of RC beam-column subassemblages under a middle column removal scenario. *Journal of Structural Engineering,* 139 (2)**,** 233-250.

YU, J. & TAN, K. H. 2014. Special Detailing Techniques to Improve Structural Resistance against Progressive Collapse. *Journal of Structural Engineering*.

ZHAO, J. & SRITHARAN, S. 2007. Modeling of Strain Penetration Effects in Fiber-Based Analysis of Reinforced Concrete StructuresConcrete Structures. *ACI structural journal,* 104 (2).